Terms and Conditions of Use of Digitised Theses from Trinity College Library Dublin

Copyright statement

All material supplied by Trinity College Library is protected by copyright (under the Copyright and Related Rights Act, 2000 as amended) and other relevant Intellectual Property Rights. By accessing and using a Digitised Thesis from Trinity College Library you acknowledge that all Intellectual Property Rights in any Works supplied are the sole and exclusive property of the copyright and/or other IPR holder. Specific copyright holders may not be explicitly identified. Use of materials from other sources within a thesis should not be construed as a claim over them.

A non-exclusive, non-transferable licence is hereby granted to those using or reproducing, in whole or in part, the material for valid purposes, providing the copyright owners are acknowledged using the normal conventions. Where specific permission to use material is required, this is identified and such permission must be sought from the copyright holder or agency cited.

Liability statement

By using a Digitised Thesis, I accept that Trinity College Dublin bears no legal responsibility for the accuracy, legality or comprehensiveness of materials contained within the thesis, and that Trinity College Dublin accepts no liability for indirect, consequential, or incidental, damages or losses arising from use of the thesis for whatever reason. Information located in a thesis may be subject to specific use constraints, details of which may not be explicitly described. It is the responsibility of potential and actual users to be aware of such constraints and to abide by them. By making use of material from a digitised thesis, you accept these copyright and disclaimer provisions. Where it is brought to the attention of Trinity College Library that there may be a breach of copyright or other restraint, it is the policy to withdraw or take down access to a thesis while the issue is being resolved.

Access Agreement

By using a Digitised Thesis from Trinity College Library you are bound by the following Terms & Conditions. Please read them carefully.

I have read and I understand the following statement: All material supplied via a Digitised Thesis from Trinity College Library is protected by copyright and other intellectual property rights, and duplication or sale of all or part of any of a thesis is not permitted, except that material may be duplicated by you for your research use or for educational purposes in electronic or print form providing the copyright owners are acknowledged using the normal conventions. You must obtain permission for any other use. Electronic or print copies may not be offered, whether for sale or otherwise to anyone. This copy has been supplied on the understanding that it is copyright material and that no quotation from the thesis may be published without proper acknowledgement.

Investigation of interactions of nanoparticles with components of the human vascular microenvironment: platelets, plasma and endothelial cells

by

Stephen Paul Samuel

Being a dissertation submitted for the degree of
Doctor of Philosophy

at

University of Dublin
Trinity College

Under the supervision and direction of
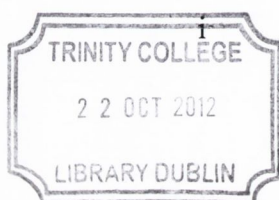
Professor Yuri Volkov, MD, PhD

Department of Clinical Medicine

Trinity College Dublin

2012

TABLE OF CONTENTS

LIST OF FIGURES

LIST OF TABLES

DECLARATION

I hereby declare that this thesis has not been previously submitted as an exercise for a degree at this or any other university. I have carried out all the practical work except where duly acknowledged. I agree to deposit this thesis in the University's open access institutional repository or allow the library to do so on my behalf, subject to Irish Copyright Legislation and Trinity College Library conditions of use and acknowledgement.

Stephen Paul Samuel

ACKNOWLEDGEMENTS

I would like to express my sincere gratitude to my supervisor **Professor Yuri Volkov** for giving me this great opportunity to launch my career in Nanomedicine. I am deeply thankful for taking me as a PhD student and for the expert direction, inspiration and encouragement from the beginning to the end of this research. He has made available his support in a number of ways throughout my thesis with his patience and knowledge. I attribute this entire achievement to his intellectual abilities and without whom this entire endeavour would not exist, and I cannot thank enough for this opportunity. In addition, he was always approachable and inclined to help. Thanks Professor Volkov.

I would also whole-heartedly like to thank Dr. Maria and Dr. Carlos for the expert teaching, help, advice and suggestions whenever needed. Their continuous guidance complemented my work. Thanks to Professor Marek Radomski, for the support and valuable suggestions during this study. I also thank Dr. Jose and Dr. Shona for their support in the lab.

I thank Professor Louri Gounko, Dr. Gemma and Ms. Valerie for synthesising and characterising the nanoparticles for this research.

I thank the Cellix team, Mr. Dimitry, Mr. Frank, Ms. Jenifer and Mr. Toby for their technical support.

I thank Dr. Catherine Botting for carrying out mass spectrometry analysis.

I thank Dr. Cormac for acquiring beautiful TEM images.

I thank Dr. Anthony Davies and Mr. Connla for much assistance in HCA work.

In my daily lab work I have been blessed with a friendly and cheerful group of postdoctoral scientists and fellow students. Dr. Peter and Dr. Eugene provided good ideas for steering my thesis. Ms. Jennifer gave useful guidance in the use of microscopic techniques. Dr. Navin helped me throughout my project.

My special thanks to the entire nanogroup, Dr. Adriele, Dr. Yuvonne, Dr. Bashir, Dr. Kieran, Dr. Tatsiana, Dr. Omar, Dr. Gareth and Dr. Namrata, who have encouraged and supported me over the years. The Monday meetings have always been informative and motivating. Thank you all.

ABBREVIATIONS

AC	Adenyl cyclase
ADP	Adenosine diphosphate
ATP	Adenosine triphosphate
COX	Cyclooxygenase
DAG	Diacylglycerol
EC	Endothelial cell (s)
EDTA	Ethylenediaminetetraacetate
FBS	Foetal bovine serum
FITC	Fluorescein isothiocyanate
GPIb	Glycoprotein Ib
GPV	Glycoprotein V
GPIX	Glycoprotein IX
GPIIb-IIIa	Glycoprotein IIb-IIIa
HUVEC	Human umbilical vein endothelial cell(s)
ICAM	Intercellular adhesion molecules
IP$_3$	Inositol triphosphate
mAb	Monoclonal antibody
MMP	Matrix metalloproteinase
NP	Nanoparticle(s)
PAGE	Polyacrylamide gel electrophoresis
PAF	Platelet activating factor
PBS	Phosphate buffered saline
PDMS	Polydimethylsiloxane
PECAM	Platelet endothelial cell adhesion molecule
PFA	ParaformaldehydE
PG	Prostaglandin

PGH2   Prostaglandin H2

PGI2   Prostacyclin

PI3-K   phosphatidylinositol 3-kinase

PLC   Phospolipase C

PKC   Protein kinase C

QD   Quantum dot(s)

SDS   Sodium dodecyl sulfate

TIMP   Tissue inhibitor of matrix metalloproteinases

TNF-α   Tumour necrosis factor-α

TXA2   Thromboxane A2

vWF   von Willebrand Factor

VCAM-1   Vascular-cell adhesion molecule 1

°C – degree(s) Celsius

g – gram

μg – microgram

h – hour(s)

l – litre(s)

μl – microlitre(s)

μm – micrometer(s)

μM – micromolar

M – molar

min – minute(s)

Rpm – revolutions per minutes

w/v – weight per volume

v/v - volume per volume

COMMUNICATIONS FROM THIS THESIS

Peer reviewed publications

Santos-Martinez, M.J., Medina, C., Prina-Mello, A., Conroy, J., **Samuel, S.P.,** Volkov, Y., Radomski, M.W. (2010). **"A nanoscale resolution assay of flow-induced platelet microaggregation."** Polish Journal of Cardio-Thoracic Surgery. 7 (4): 365–375**.**

Stephen Paul Samuel, Namrata Jain, Frank O'Dowd, Toby Paul, Dmitry Kashanin, Valerie A. Gerard, Yuri Gunko, Adriele Prina-Mello, Yuri Volkov. (2012). **"Multi-factorial determinants governing the nanoparticles uptake by human endothelial cells under flow."** International Journal of Nanomedicine (In press).

Oral presentations

Stephen, S.P. Investigation of interactions of engineered nanoparticles with human platelets and endothelial cells. BioNanoInteract site-visit training meeting, August 10, 2010, Conway institute, UCD, Ireland.

Stephen, S.P. Quantum Dots Interactions with vascular microenvironmemt: human plasma, platelets and endothelial cells. School of Medicine Postgraduate Research Day, September 19, 2011, Biomedical Sciences Institute, Trinity College Dublin, Ireland.

Poster presentations

Stephen, S.P. Investigation of interactions of engineered nanoparticles with human endothelial cells. BioNanoInteract Governance Board meeting, August 26, 2010, Conway Institute, UCD, Ireland.

Stephen, S.P. CdTe quantum dots interactions with human platelets and endothelial cells. 13th Annual Meeting of the Institute of Molecular Medicine, November 12th & 13th, 2010, Trinity Centre for Health Sciences, St James Hospital, Dublin, Ireland.

Stephen, S.P. Quantum dots interactions with vascular microenvironment: the influence of particle size, human plasma and shear forces. MMI Clinician Scientist Annual meeting, July 1, 2011, Science Gallery, Trinity College Dublin, Ireland.

Stephen, S.P. Quantum dots interactions with human microvascular components: platelets and endothelial cells. TCD Medical School Tercentenary Symposium, November 4, 2011, Trinity Biomedical Sciences Institute, Trinity College Dublin, Ireland.

ABSTRACT

Nanotechnology is defined as 'the understanding and control of matter at dimensions less than 100 nanometers', and exploits the novel physical, chemical and biological properties of materials. Nanomedicine, application of nanotechnology in medicine, has the potential for early detection, improved diagnosis, treatment and follow-up of diseases. Nanotechnology-enabled constructs based on for example, silica (Lee et al., 2010), magnetite (Wu et al., 2008b), and quantum dots (QDs) (Biswas et al., 2011) are rapidly emerging as potential candidates for diagnostic and drug delivery applications, or both (called theranostics). The systemic delivery of nanoparticle based pharmacological, therapeutic, biosensor, imaging and diagnostic agents implies the interactions of nanoparticles (NPs) with the components of the vascular microenvironment (Winter et al., 2003, Buxton et al., 2003, Martin and Kohli, 2003). Therefore, the aim of this thesis is to study the interactions of engineered nanoparticles with human plasma, platelets and endothelial cells.

Blood plasma is the yellow liquid component of blood and contains dissolved proteins, glucose, clotting factors, mineral ions, hormones and carbon dioxide. Platelets in blood are small, discoid shaped, anucleate cell elements of size between 1.5 to 3 micrometers. Platelets are involved physiologically in primary haemostasis, and pathologically in thrombosis. Endothelial cells line the interior of the entire vascular system and provide the phospholipid surface for coagulation reactions (Davie et al., 1991, Esmon, 2005). Endothelial cells recognize shear stress as a mechanical stimulus and respond through a variety of cellular responses that involve alterations in cell morphology, cell function, and gene expression (Ando and Yamamoto, 2011).

Human platelets and platelet rich plasma were isolated from peripheral blood and their interactions with NPs were analysed under static conditions by aggregometry, flow cytometry, immunofluorescence, gelatin zymography and transmission electron microscopy. The influence of QDs on flow induced platelet adhesion was analysed by utilizing the Cellix™ microfluidic platform, quartz crystal microbalance and atomic force microscopy. The proteins associated with QD were investigated by native gel electrophoresis and mass spectrometry analysis. The interaction of nanoparticles with

human umbilical vein endothelial cells (HUVEC) under shear stress was investigated using the Cellix^{TM} microfluidic platform and immunofluorescence imaging. Shear stress-induced alterations in endothelial cell morphology were studied using confocal and atomic force microscopy. In addition, the cytotoxic effect of NPs was investigated by high content analysis.

In static conditions, silica and magnetite-based NP were well tolerated by platelets. However, QDs were found to induce significant activation of platelets which was abrogated in the presence of plasma. The proteins associated with two different sized and negatively charged (cadmium telluride) CdTe particles have approximately 50% homology between them suggesting that the size and charge are more important than the particle composition. QDs activated platelets in the absence of plasma and caused increased surface expression of P-selectin and GPIIb-IIIa receptors on platelets, and release of a pro-coagulant enzyme matrix metalloproteinase-2. The QDs did not have a significant effect on flow induced platelet adhesion in whole blood samples. However, QDs increased platelet activation and adhesion under flow conditions in the presence of plasma. QDs bound to various plasma proteins including proteins involved in coagulation. The results demonstrated that shear stress is critical in both inflamed and non-inflamed endothelial cells for uptake of NPs. Activation of endothelial cells with tumour necrosis factor-α did not cause significant difference in the uptake of QDs. However, a maximum uptake was observed at lower shear stress rates. Shear stress induced cell membrane ruffling and was critical for cellular uptake of QDs which were localized in the cytoplasm. Our cytotoxicity data indicates that silica- and magnetite-based NPs were well tolerated by endothelial cells, and smaller QDs did not induce marked toxicity post nanoparticle exposure for up to 8 hours.

In conclusion, this study has demonstrated that the silica and magnetite-based NPs are compatible with platelets and endothelial cells. In addition, this study has contributed to understanding the mechanism of QD-associated platelet activation. QDs induce activation of platelets by binding to surface integrin GPIIb-IIIa, thereby initiating the "outside-in" signalling. This study demonstrates that the presence of plasma inhibits QD-induced platelet aggregation due to the adsorption of plasma proteins on the surface of QDs. Understanding the mechanisms of nanoparticle interaction with the body milieu could be instrumental in designing strategies to prevent the toxicity and premature clearance of novel

nano-drugs. This is the first study to demonstrate that shear stress is critical in both the normal and artificially-inflamed endothelial cells for uptake of QDs and silica NPs. The findings suggest that membrane ruffle formation aids in the endocytosis of particles. The NPs may be potentially used for short term targeting of endothelial plasma membrane or the cytoplasm provided the shear stress is maintained at 0.5 dynes/cm^2. The understanding and knowledge of nanoparticle interactions with living cells will enable researchers with tools for rational design of nanomedicines.

Chapter 1

Introduction

Introduction

1.1 Nanomedicine

Nano, the Greek word for "dwarf", is the name given to values of 10^{-9}. Nanotechnology can be defined as the techniques aimed at characterizing and producing materials on the nanometre (a nanometre is ~6 carbon atoms wide) scale (L'Azou et al., 2008). A NP is a tiny particle with at least one dimension less than 100 nm. Engineered NPs exhibit behaviours different from bulk materials with identical chemical compositions, such as ultra-small size, large surface area to mass ratio, and high reactivity (Chen et al., 2011). Some of the most widely used NP types are colloidal gold (Chen et al., 2005), superparamagnetic iron-oxide crystals (Weissleder et al., 1990), silicon dioxide (Kneuer et al., 2000a), dendrimers (Kobayashi et al., 2005), liposomes (Hofheinz et al., 2005), nanotubes (Negri et al., 2010), and QDs (Gao and Nie, 2003). Nanomedicine is an interdisciplinary research field incorporating nanotechnology, biology and medicine (Chun and Webster, 2009, Klostranec and Chan, 2006). Nanomedicine raises high expectations for millions of patients for better, more efficient and affordable healthcare and has the potential of delivering promising solutions to many illnesses. Research in nanomedicine will allow for a better understanding of the functioning of the human body at molecular level. There is a burgeoning interest in the medical applications of nanotechnology. Most broadly, nanomedicine in all its forms, i.e. nanodiagnostics and imaging, targeted drug delivery and controlled release, and regenerative medicine, has the potential to revolutionize our ability to prevent disease, accurately diagnose early in pathogenesis, effectively treat with superior nano-pharmaceuticals, monitor disease progression, and improve human health (Freitas, 2005a, Robert, 1999). In the relatively short term, nanomedicine can address many important medical problems by using nanoscale-structured materials and simple nanodevices that can be manufactured today, including the interaction of nanostructured materials with biological systems. In the mid-term, biotechnology will make possible even more remarkable advances in molecular medicine, including microbiological biorobots or engineered organisms. In the longer term, the earliest molecular machine systems and nanorobots may join the medical armamentarium, finally giving physicians the most potent tools imaginable to conquer human disease, ill-health, and aging (Freitas, 2005b). Current hurdles for a wider application of NPs are the issues related to their potential toxicity, their

long-term secondary effects or their biodegradability and environmental impact of nanoscale materials.

1.2 Nanoparticles and biomedical applications

The size of NPs is similar to that of biomolecules such as antibodies, proteins and lipids. Viruses and subcellular organelles are also in the nano-range (Figure 1.1). Hence, nanotechnology has a significant role in biology as living matter is composed basically of nanomachines and nanostructures (Kralj and Pavelic, 2003). The EU Community Research and Development Information Service (CORDIS) has described that the application of nanotechnology could lead to better, more efficient and affordable healthcare and has the potential of delivering promising solutions to many illnesses. Thus engineered NPs are found in an increasing number of biological applications (http://cordis.europa.eu/nanotechnology).
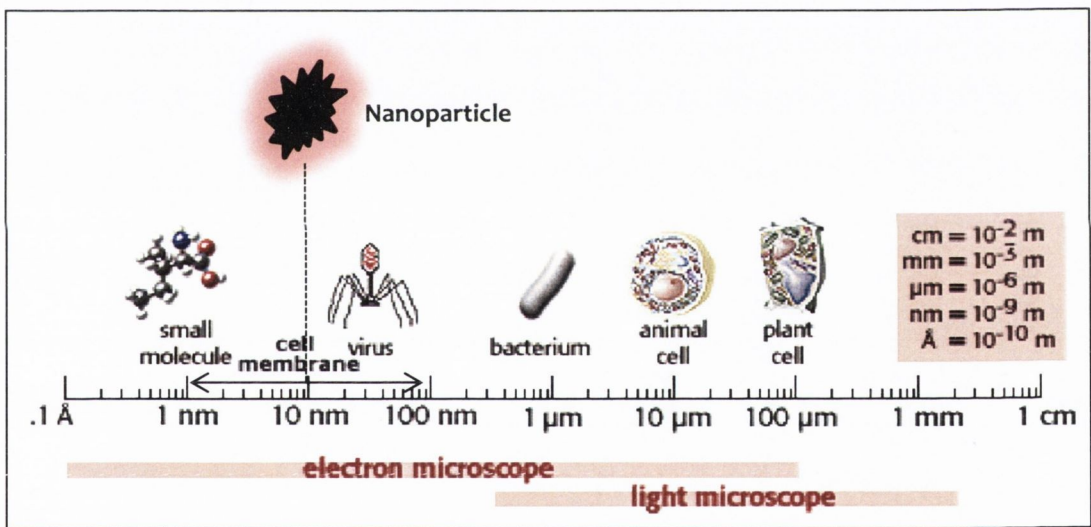
Figure 1.1: Nanoparticle size in relation to biomolecules, microorganisms and cells
Size comparison of nanoparticle with biological objects (http://click4biology.info/c4b/2/Pic2.1/size.gif)

Techniques such as atomic force microscopy (AFM), scanning electron microscopy (SEM), transition electron microscopy (TEM), confocal microscopy and quartz crystal microbalance techniques have enabled detailed analysis at the nano-scale. From the ever expanding list of NPs, the properties and biomedical applications of QDs, silica and magnetite NPs, which are relevant to my thesis, are discussed below.

3

Introduction

1.2.1 Quantum dots

1.2.1.1 Physicochemical properties

Quantum dots are semiconductor nanocrystals between 2 to 10 nm in diameter. They are usually 10-50 atoms wide (The hydrogen atom is approximately 1 Angstrom (Å) or 1×10^{-10} m), and can be considered an artificial atom (Alivisatos, 2004). Quantum confinement is the change of electronic and optical properties when the diameter of the particle is of the same magnitude as the wavelength of the electron wave function (typically $\leq$ 10 nanometres). The electrons are kept in quantum confinement within the confines of the Bohr radius (the most probable distance between the proton and electron in a hydrogen atom in its ground state). This in turn gives rise to new physical properties non-existent in the bulk material (Bentolila et al., 2009). The term "band gap" (Figure 1.2) refers to the energy difference between the top of the valence band (highest range of electron energies in which electrons are normally present at absolute zero temperature) and the bottom of the conduction band (higher electron energies than valence band, sufficient to free an electron from binding with its individual atom). The band gap increases as the size of the nanostructure decreases. Specifically, the phenomenon results from electrons and holes being squeezed into a dimension that approaches the Bohr radius. However, in order for an electron to jump from a valence band to a conduction band, it requires a specific minimum amount of energy for the transition. The required energy differs with different materials. Electrons can gain enough energy to jump to the conduction band by absorbing either a phonon (heat) or a photon (light).
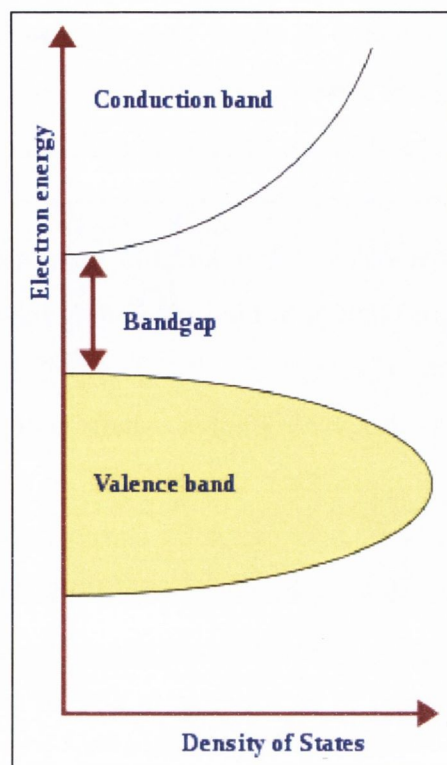
Figure 1.2: Semiconductor band structure

Schematic representation of electron band gap (http://en.wikipedia.org/wiki/Band_gap).

As the electrons become more confined, by decreasing the size of the dot, the emitting wavelengths become smaller and smaller. The most vivid demonstration of quantum confinement is the relationship between emission colour of QDs and their size (Bentolila et al., 2009).

Semiconductors are synthesized from elements within Periodic Table Group II and Group VI; Group III and Group V; and Group IV and Group VI. The hard metal core of a QD is usually made of Cadmium (Group II), and Selenium or Tellurium or Sulphur (Group VI), or Indium phosphate (Group III–V) (Alivisatos et al., 2005). A huge interest in research into these particles was led by the capacity to synthesise these QDs in solution (Alivisatos, 2004). The first step in the process of QD core synthesis involves injection of liquid precursors into solvents at high temperatures of 300 °C, and then an inorganic shell is grown to protect the optical properties of the core. This increases the quantum yield of

fluorescence to approximately 80% (Alivisatos et al., 2005, Smith et al., 2006). The QDs are non-polar and therefore insoluble in water. They have to be rendered water soluble in order to be utilised in biological systems (Yin and Alivisatos, 2005). The surface of the nanoparticle is coated with solubilisation ligands to make them water soluble and suitable for use in cell biology. Various solubilisation ligands such as thiol-containing molecules, peptides and polymerised silica shells with polar groups are used (Maysinger et al., 2007). The resulting charge of QDs in relation to the surrounding medium is referred as the "zeta potential" i.e. the electrokinetic potential in colloidal systems. The particles can be made biocompatible by replacing the hydrophobic shell with hydrophilic ligands like dihydrolipoic acid (Clapp et al., 2006). In addition to ligand exchange, NPs with hydrophobic surface ligands can be solubilized by encapsulation in amphiphilic polymers (Gao et al., 2004, Wu et al., 2003) and phospholipid micelles (Dubertret et al., 2002). Further functionalization can be done with the addition of bioactive groups e.g. antibodies, drugs, peptides etc. without much of an increase in size of QD (Maysinger et al., 2007) (Figure 1.3).
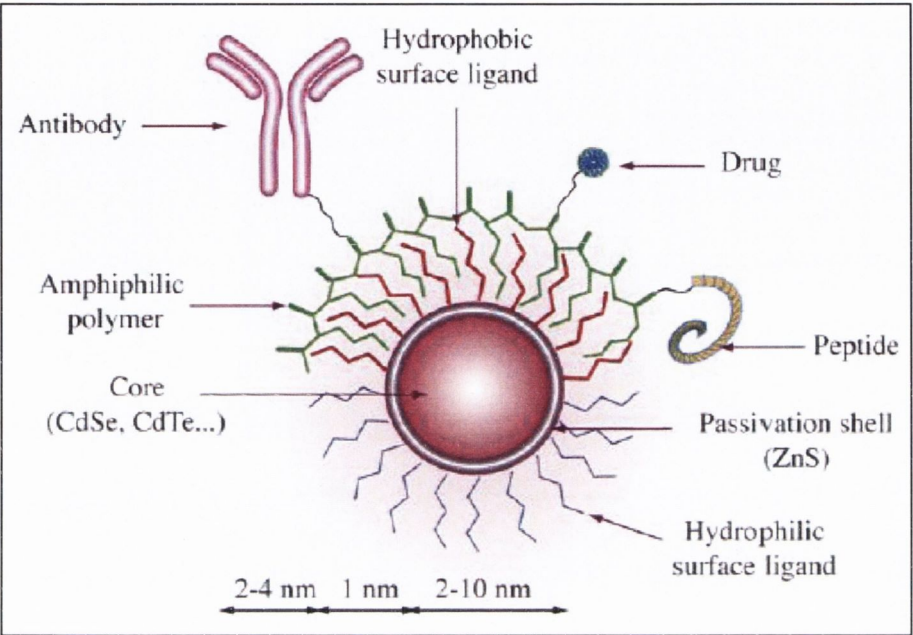
Figure 1.3: Structure of a QD

Figure demonstrates the possible surface modifications (Maysinger *et al*, 2007).

1.2.1.2 Optical properties

QDs are tiny light-emitting inorganic nanocrystals, and are emerging as a new class of fluorescent probes for biomolecular and cellular imaging. In comparison with organic dyes and fluorescent proteins, they have distinct optical properties, with narrow emission bands (Jain, 2007), resistance to photo bleaching (Alivisatos et al., 2005), broad absorption spectra for simultaneous excitation of multiple fluorescence colours (Azzazy et al., 2007), and size-tunable light emission (Goldman et al., 2006). For the same material, the size of the quantum dot determines the colour of the emitted light. Large dots emit red (lower energy) light. Conversely, smaller dots emit bluer (higher energy) light (Figure 1.4). QDs also provide a versatile nanoscale scaffold for designing multifunctional NPs with both imaging and therapeutic functions (Smith et al., 2008).
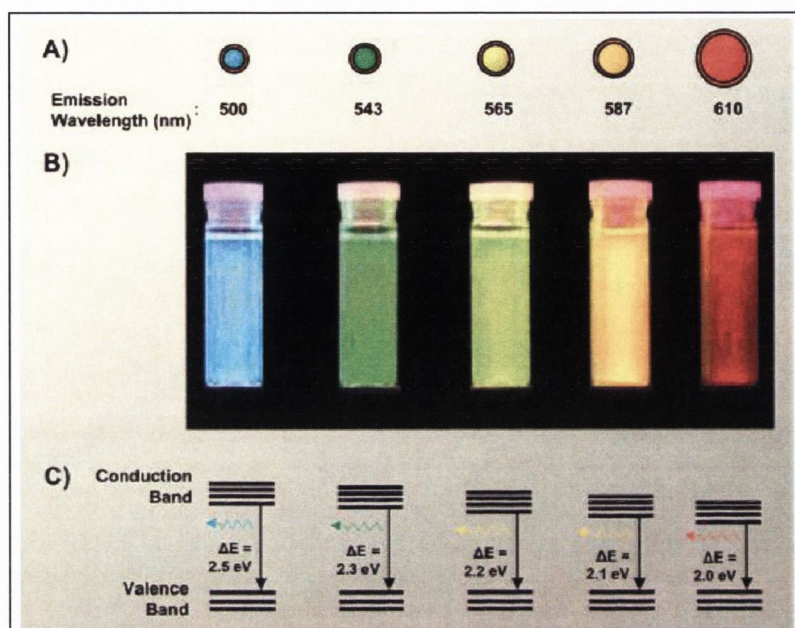
Figure 1.4: Tunable optical properties of QD
A) Schematic of the size-dependent optical properties of QD (not drawn to scale). The optical emission shifts from blue to red as the QD becomes larger. The size range of the QD is 2–10 nm. B) Corresponding real-color emission. C) Band gap energies. *(Klostanec et al 2006).*

1.2.1.3 Bioapplications

Bio-functionalization allows for improved stability and biocompatibility of nanocrystals enabling them to be used for specific in vitro biological targeting. Avidin (Goldman et al., 2002), serotonin (Rosenthal et al., 2002), and chitosan (Xie et al., 2005) have been used to date to target specific cell proteins and receptors. Wu *et al.* described that QDs linked to immunoglobulin G and streptavidin can be used to label breast cancer marker Her2 on the surface of fixed and live cancer cells, to stain actin and microtubule fibers in the cytoplasm, and to detect nuclear antigens inside the nucleus (Wu et al., 2003). Peptide coated CdSe/ZnS semiconductor nanocrystals were used to specifically target chimeric proteins expressed on the membranes of live HeLa cells (Pinaud et al., 2004). Williams *et al.* studied the compartmentalization of size-tuned

luminescent semiconductor nanocrystal QDs in four distinctive cell lines and found that each cell line displays its own cut off size threshold, reflecting cell-type-determined cytoplasmic and nuclear pore penetration specificity (Williams et al., 2009). QDs have also been used as probes to monitor individual synaptic receptors in living neural circuits (De Koninck et al., 2007). Nabiev *et al.* systematically studied the mechanism of interaction of nonfunctionalized QDs with live human blood monocyte-derived primary macrophages and cell lines of phagocytic, epithelial, and endothelial nature and demonstrated that nonfunctionalized QDs exploit the cell's active transport machineries for delivery to specific intranuclear destinations (Nabiev et al., 2007). Goa *et al.* showed that optically encoded beads using mesoporous polystyrene beads and surfactant-coated semiconductor QDs could be identified with a standard flow cytometer at 1000 beads/s (Gao and Nie, 2004). Bio-functionalized QDs can be utilized for detection of genomic aberrations of cancer genes by fluorescence in situ hybridization (FISH) (Azzazy and Mansour, 2009). Pathak *et al.* demonstrated the use of hydroxylated QDs as luminescent probes for FISH (Pathak et al., 2001). Zhu *et al.* developed semiconductor quantum dot-conjugated antibodies to label Cryptosporidium parvum and Giardia lamblia (Zhu et al., 2004). Bacterial strains that are slow growing (e.g., Mycobacterium), or highly infectious (e.g., Bacillus anthracis) could be detected using phage conjugated streptavidin-coated QDs (Edgar et al., 2006). Han *et al.* achieved multicolor optical coding for biological assays by embedding different-sized CdSe/ZnS QDs into polymeric microbeads at precisely controlled ratios and utilized it in DNA hybridization studies (Han et al., 2001). Antibody conjugated CdSe/ZnS core-shell QDs were utilized to perform multiplexed fluoroimmunoassays for the simultaneous detection of cholera toxin, ricin, shiga-like toxin 1, and staphylococcal enterotoxin B (Goldman et al., 2004). Medintz *et al.* reported the design, formation and testing of QD-protein assemblies that function as chemical sensors based on quantum dot fluorescence resonance energy transfer (FRET) donors (Medintz et al., 2003). The optical properties of ZnS-capped CdSe quantum dots were shown to be sensitive to environmental factors such as pH and divalent cations, leading to the potential use of quantum dots in molecular sensing (Gao et al., 2002). Sukhanova *et al.* demonstrated the first application of nanocrystal-encoded microbeads to clinical proteomics in the

detection of circulating autoantibodies, markers of systemic sclerosis (Sukhanova et al., 2007).

Application of QDs as a contrast agent for *in vivo* imaging is an exciting area of research. Organic fluorophores and chemiluminescence probes are currently the most commonly used optical probes for animal imaging (Contag and Ross, 2002, Klostranec and Chan, 2006, Weissleder, 2002). The near-infra red (NIR) emitting window (> 650 nm) is appealing for biological optical imaging because of the low tissue absorption and scattering effects in this emission range (Jiang et al., 2004, Weissleder, 2001). Since the optical properties of QDs can be tuned by size and composition, CdTe, CdTeSe, InPAs, PbS, and PbSe have been successfully synthesized with NIR emission (Bailey and Nie, 2003, Kim et al., 2004, Kim et al., 2005, Klostranec and Chan, 2006). There are a few manuscripts demonstrating QDs as *in vivo* contrast agents. Alloyed semiconductor QDs have been successfully synthesized to achieve red-shifted light emission up to 850 nm and quantum yields up to 60% without changing the particle size (Bailey and Nie, 2003). QDs were tuned to NIR fluorescence emission (emitting at 850 nm) and utilized in major cancer surgery for mapping sentinel lymph node up to 1cm deep (Frangioni et al., 2007) (Kim et al., 2004, Kim et al., 2005). Protease-activated NIR fluorescent probes were developed to image tumour-associated lysosomal protease activity in a xenograft mouse model to detect early stage tumours *in vivo* and to probe for specific enzyme activity (Weissleder et al., 1999). Akerman *et al.* coated ZnS-capped CdSe QDs with peptides that can target tumours or blood vessels or lymphatic vessels in tumor-bearing mice and they observed tumour-tissue sections stained with QDs under epifluorescence microscopy (Akerman et al., 2002). QD-labelled tumour cells and fluorescence emission-scanning microscopy were used to track the extravasation of tumour cells into lung tissue after they were intravenously injected into mice (Voura et al., 2004). So *et al.* presented quantum dot conjugates that luminesce by bioluminescence resonance energy transfer in the absence of external excitation and showed that the conjugates emit long-wavelength (from red to near-infrared) bioluminescent light in cells and, even in deep tissues of animals, and are suitable for multiplexed *in vivo* imaging (So et al., 2006).

1.2.2 Silica nanoparticles

1.2.2.1 Physicochemical properties

Silicon dioxide, also known as silica, is an oxide of silicon with the chemical formula SiO_2. Silica is most commonly found in nature as sand or quartz, clays and soils. Silica is used primarily in the production of glass for windows, drinking glasses, beverage bottles, and many other uses. The majority of optical fibers for telecommunications are also made from silica. Silica is a common additive in the production of foods, where it is used primarily as a flow agent in powdered foods, or to absorb water in hygroscopic applications. Amorphous silica NPs are one of the most important engineered nanomaterials. The preparation of this colloidal nanoparticle was firstly reported by Stöber in 1968. These particles are highly hydrophilic with good biocompatibility. Several attractive features of silica have been described previously (Tallury et al., 2008). Silica is an excellent host material for encapsulating a variety of agents, such as fluorescent dyes, metal ions, metal NPs and drugs. The silica matrix is optically transparent, enabling excitation and emission light to pass through the silica matrix efficiently in the case of optical material-encapsulated NPs. Moreover, silica encapsulation also provides a protective layer around encapsulated optical agents, thus improving photostability. The spectral properties of the contained dye molecules remain intact (Santra et al., 2001a, Santra et al., 2001b). Silica is water dispersible and also resistant to microbial attack. Amorphous silica NPs appear to be a biocompatible and nontoxic (Tallury et al., 2008). Furthermore, silica particles can be modified easily to attach biomolecules, such as proteins, peptides, sugars, antibodies and oligonucleotides, using conventional saline-based chemistry (Qhobosheane et al., 2004, Tallury et al., 2008). All these excellent features make silica NPs widely applied in biomedical and biotechnology fields, including: bioanalysis, medical imaging, labelling and so on (Lu et al., 2007, Nakamura et al., 2007, Ow et al., 2005). Studies have shown that encapsulating QD/magnetite NPs with silica has made them water soluble and biocompatible (Okuda et al., 2009).

1.2.2.2 Bioapplications

Various silica based NPs have been developed for biomedical applications. Silica based NP surfaces were biofunctionalized with various molecules such as enzymes, antibodies, and

DNA molecules for potential bioanalyzing, biosensing and bioimaging applications (Tan et al., 2004, Qhobosheane et al., 2001, Tallury et al., 2008). Organic dye-doped silica NPs were surface modified for biosensor and bioanalysis applications (Tapec et al., 2002). Dye-doped silica NPs have also been successfully used for bacteria and DNA detection (Zhao et al., 2007). Human leukaemia cells have been successfully stained with surface modified luminophore-doped silica NPs (Santra et al., 2001a, Santra et al., 2001b). Silica based nanomaterials were tested for the detection of a neurotransmitter protein, glutamate (Qhobosheane et al., 2004). Human breast cancer cells (*in vitro*) and mouse tissues (*ex vivo*) were imaged using arginine-glycine-aspartic acid (RGD) peptide-labelled fluorescent silica NPs (Wu et al., 2008a). Lipid coated silica NPs with a quantum dot core were used to specifically target endothelial cells in vitro (Koole et al., 2008). A novel electrochemical immunosensor using functionalised silica NPs as protein tracer has been developed for the detection of prostate specific antigen in human serum (Qu et al., 2008). Foraker *et al.* showed that microfabricated porous silicon particles enhanced paracellular delivery of insulin across intestinal Caco-2 cell monolayers (Foraker et al., 2003). Kneuer *et al.* demonstrated that surface modified silica NPs could be utilized as DNA carriers for gene delivery (Kneuer et al., 2000b). Porous hollow silica NPs could be utilized for controlled drug delivery applications (Li et al., 2004). Surface-functionalised mesoporous silica (form of silica with pores, which allows the particles to be filled with compounds of interest) NPs were used for site-specific and intracellular controlled release of drugs, genes and therapeutic agents (Foraker et al., 2003, He et al., 2010, Kneuer et al., 2000a, Kneuer et al., 2000b, Li et al., 2004, Simovic et al., 2010, Slowing et al., 2008). Anticancer drugs loaded surfactant-templated mesoporous silica NPs showed long-term anticancer efficacy in *in vitro* studies (He et al., 2010). Simovic *et al.* showed that silica-lipid hybrid microcapsules could be used as an oral delivery system in rat models (Simovic et al., 2010). Multifunctional nanocomposites could be utilized for simultaneous enhanced magnetic resonance imaging, fluorescence imaging, and drug delivery (Kim et al., 2008, Lee et al., 2010, Patel et al., 2010).

1.2.3 Magnetite nanoparticles

1.2.3.1 Physicochemical properties

Superparamagnetic NPs are one of the most widely studied types of nanoparticle because of their immense importance in the emerging area of nanomedicine. They normally consist of iron oxides, magnetite (Fe_3O_4), maghemite (γFe_2O_3) or other ferrites, which are insoluble in water and have no magnetic properties outside an external magnetic field (Corot et al., 2006). Magnetite is superparamagnetic, when its particle size is 10 nm or below. The magnetic moments of such small particles have the ability to rotate along the gradient of the applied field and to increase the overall magnetic strength. Superparamagnetism means that the magnetite particle is attracted to a magnetic field but retains no residual magnetism after the field is removed. Superparamagnetic NPs do not interact with each other. In recent years numerous biomedical applications have emerged for superparamagnetic iron oxide NPs dispersed in an aqueous medium (Halbreich et al., 1998).

1.2.3.2 Bioapplications

The combination of the nanometer size with superparamagnetic properties led to their use in labelling and sorting cells or organelles (Perrin-Cocon et al., 1999), magnetic resonance imaging (MRI) as contrast agents (Kim et al., 2001), targeted drug delivery (Kohler et al., 2005) and magnetically mediated hyperthermia (MMH) therapy for cancers (Ito et al., 2006, Ito et al., 2003, Moroz et al., 2002). MMH consists of the localization of magnetic particles or seeds within tumour tissue followed by exposure to an externally applied alternating magnetic field to cause them to heat. Since this concept was introduced (over 40 years ago), MMH has evolved into four general sub-classes: arterial embolization hyperthermia, direct injection hyperthermia, intracellular hyperthermia and interstitial implant hyperthermia (Moroz et al., 2002). The addition of fluorescence properties to these magnetic NPs offers new potential for *in vitro* and *in vivo* imaging (Mikhaylova et al., 2004, Levy et al., 2002, Bertorelle et al., 2006, Lu et al., 2004, Gu et al., 2005). Superparamagnetic NPs can be applied in immunoassays for detection of C-reactive protein, an acute phase protein (Azzazy and Mansour, 2009). Biopolymer coated (beta-glucagon) magnetite colloidal suspensions were stable and exhibit enhancement of MRI contrasts in vitro (Cho et al., 2009). Guo *et al.* reported high loading capacity and favourable release property for a typical anticancer drug "Doxorubicin" with the use of

monodisperse mesoporous superparamagnetic single-crystal NPs (Guo et al., 2009). Yi *et al.* developed silica-coated nanocomposites of magnetic NPs and QDs which were biocompatible and more water soluble (Okuda et al., 2009). Ito *et al.* investigated the possibility of using magnetite NPs and magnetic force to construct and deliver cultured retinal epithelial cell sheets in vitro, termed "magnetic force-based tissue engineering", as a possible treatment for choroidal neovascularisation (the most severe form of age-related macular degeneration) (Ito et al., 2005). Block copolymer-coated magnetite NPs were developed for enhanced pancreatic cancer magnetic resonance imaging in mice (Kumagai et al., 2009). Mesoporous dye-doped silica NPs decorated with multiple magnetite nanocrystals were synthesized for simultaneous enhanced magnetic resonance imaging, fluorescence imaging, and anticancer drug delivery (Lee et al., 2010). Osaka *et al.* demonstrated that the magnetic NPs with positive charge showed higher internalization into human breast cancer cells than the negative charged ones, while the degree of internalization of the positively and negatively charged NPs into HUVEC was almost the same (Osaka et al., 2009). Racuciu *et al.* developed citric acid stabilized magnetite NPs for biological applications (Racuciu et al., 2006). Shimizu *et al.* indicated an effective cell-seeding technique using magnetite NPs and magnetic force for vascular tissue engineering (Shimizu et al., 2007). Hydrophilic multi-walled carbon nanotubes decorated with magnetite NPs were described as lymphatic targeted drug delivery vehicles (Yang et al., 2009).

1.3 Biological barriers

A living organism should have the capacity to uptake nutrients and dispose waste material for survival. However, infectious agents could exploit such permeability, and therefore it is essential there are biological barriers set in place to prevent any detrimental invasions (Sanhai et al., 2008). NPs are being investigated for numerous medical applications and are showing potential as an emerging class of carriers for drug delivery. The physicochemical properties (e.g., size, surface charge, shape, and density of targeting ligands) of NPs should be able to overcome the biological barriers to reach designated cellular destinations. A biological barrier is anything that stops pharmaceutical agents, biomolecules, NPs and any other foreign agent (e.g. Pathogens) from reaching their target site (Sanhai et al., 2008). The bio distribution of administered agents is generally governed by their ability to

negotiate and bypass biological barriers (Sanhai et al., 2008). Any agent of natural or engineered origin, introduced into the living system must first overcome the physical barrier consisting of skin, endothelium, or mucous membranes, depending on whether the foreign agent is administered parentally, ingested or inhaled (Stern and McNeil, 2008).

The *epidermal barrier* resides within the most superficial layer of the skin, the stratum corneum. A mature epidermis is a protective barrier which prevents dehydration from the loss of body water, poisoning from the absorption of toxins (pesticides, benzene etc.), and systemic infection from invading surface microorganisms. The desmosome (major adhesion complex in epidermis, anchoring keratin intermediate filaments to the cell membrane and bridging adjacent keratinocytes) has a characteristic ultrastructure, in which the cell membrane of two adjacent cells forms a symmetrical junction with a central intercellular space. Pores in the skin are normally 0.3 nm wide and can be opened without major skin damage to 20–40 nm at most (Cevc et al., 2002). The squamous cells of the skin is invaded by physical puncturing, while the mucosal layer of the lungs and guts are designed to protect the underlying tissue from damage and yet allow the regulated passage of gases, nutrients, and fluids between the exterior and the internal milieu. The surface of the cells has specific receptors to recognize certain molecules in a process known as transcytosis, and alternatively some substances may pass between the cells (Stenbeck and Horton, 2004).

The *endothelium* lining the blood vessels has been classified as continuous, fenestrated (60 nm pores), or discontinuous (fenestrea of 50–100 nm), depending on the morphological features of the endothelium (Alexis et al., 2008). The vascular system and lungs have continuous endothelia. In contrast, kidney, digestive mucosa, and glands are lined by fenestrated endothelium. Liver and bone marrow are characterized by discontinuous endothelia.

The *blood brain barrier (BBB)* maintains brain homeostasis by selectively transporting nutrients and beneficial endogenous substances into the brain and excluding toxic metabolite from the brain. The endothelial cell monolayer fused by tight junctions is the pivotal component of the BBB. Recent evidence suggests that the physiologic upper limit of pore size in the capillary walls of most non-sinusoidal blood capillaries ranges between 5 and 12 nm (Sarin, 2010).

The *pulmonary barrier* is composed of the alveolar epithelium, capillary endothelium, and the extracellular matrix consisting of basement membranes of the two cell layers. A continuous epithelium comprising of Type I and Type II alveolar epithelial cells, joined by tight junctions, line the distal air spaces (alveolus). Type I cells have a pore size of 0.6-1.0 nm and the Type II cells have a pore size of 4-5.8 nm (Proud, 2008).

The *gastrointestinal barrier* is governed by the epithelial cells and the digestive enzymes. Studies have shown that gastrointestinal passage of particles could be achieved if they were below 200 nm in diameter (Almeida et al., 2011). In addition, the same size range favoured escape from splenic filtration effects thereby enhancing the particle half-life.

The *phagocytic barrier* consists of specialized cells for recognizing and removing foreign matter into the reticuloendothelial system. Macrophages and monocytes internalize particles mainly by phagocytosis and present to the immune system via the lymph nodes, or alternatively they can fuse with lysosomes leading to the degradation and disposal of the particle via the excretory system (Desjardins, 2003). Thus, if the particles were required for the purpose of drug delivery or diagnostic imaging, phagocytosis would need to be avoided.

Inflammatory barriers, comprising of a potent cocktail of cytokines, antibodies, and complement that can disable infectious agents, or speed up the process of their destruction (Han and Ulevitch, 2005).

Further barriers are due to chemico-physical alterations in response to infectious agents or particles, abnormal blood flow, interstitial pressure gradients, digestive enzymes and extremes of pH (stomach vs. small intestine). For example, the increase of body temperature in response to infection affects the fluidity of the membranes. The low pH in the stomach can alter charged functional groups affecting the ability to attach to cells. Similarly, molecular and ionic pumps can expel particles away from cells (Sanhai et al., 2008). Certain mucus producing cells also prevent foreign agents gaining access to the cell (Behrens et al., 2002). In the case of certain diseases such as cancer, abnormal tumour vasculature and interstitial matrix creates an extra barrier which inhibits the delivery of therapeutic agents and immune cells to the tumour (Jain and Stylianopoulos, 2010). For certain nanoparticle carriers, transport into the intracellular regions of the cell such as the nucleus is essential (Belting et al., 2005, Escoffre et al., 2010). This creates more barriers

such as the nuclear envelope, receptors, vesicles, lysosomes, peroxisomes, microfilaments and cytoskeletal structures and enzymes. Each of these barriers has unique properties which must be considered when synthesizing specific NPs for targeted delivery.

Since nuclear transport and renal clearance plays a critical role in nanoparticle based targeted therapy, it is explained in detail below. *Nuclear pores* extend through both membranes of the nuclear envelope and provide direct contact between cytoplasm and nucleoplasm. The pores are 100 nm in total diameter; however, studies have shown that the gap through which molecules freely diffuse is only about 9 nm wide, due to the presence of regulatory systems within the centre of the pore. It has been suggested that the pore diameter can be dilated to around 26 nm to allow molecular passage. *The nephron*, the functional unit of renal system, consists of the renal corpuscle and tubule system. The renal corpuscle contains a tuft of blood capillaries and support tissue (the mesangium) called the glomerulus. The glomerulus filters the blood plasma to produce an ultra-filtrate, which will be collected by the tubule system and ultimately, processed into urine. The glomerular endothelium is the first component, with pores that have been reported to be in the range of 80–100 nm in diameter (Luft et al., 1982). Next is the glomerular basement membrane (GBM), a 300- to 350-nm-thick basal lamina rich in heparin sulphate (Kanwar and Farquhar, 1979) and charged proteoglycans with an average pore size of 3 nm (Ogawa et al., 1999), which filters small molecules by size and charge. The podocytes, cells with interdigitating foot processes, lie behind the GBM to form filtration slits that are 32 nm wide (Lahdenkari et al., 2004). Studies have shown that prolonged residency of NPs in the kidney induces toxicity in the form of cell shrinkage because of excessive nanoparticle uptake by renal cells (Chen et al., 2006, L'Azou et al., 2008). The glomerular filtration apparatus, taken in its entirety, possesses an effective size cut-off of 10 nm, and it is responsible for the rapid renal clearance of small NPs (Choi et al., 2011). These are by no means all of the biological barriers present in the body but they are some of the most challenging and complex and which must be overcome if the potential of nanodrugs are to be fully realized.

Many researchers have shown the role of nanoscale barriers in nanoparticle transport and localization. Nanoparticle size, along with shape and charge, plays an important part in its interaction with any biological system (Williams et al., 2009).

Engineered NPs are proving to be useful tools in probing size-related barriers (Nabiev et al., 2007). Studies have shown that NPs with size greater than 6 nm will accumulate in the liver, lungs, and reticuloendothelial system, while smaller ones accumulate directly into the kidneys and bladder (Williams et al., 2009). Choi *et al.* have showed that kidneys could not clear NPs with a hydrodynamic diameter greater than 15 nm, but anything under 5 nm can be cleared quite rapidly (Choi et al., 2007). It has also been shown that small (20-200 nm) particles will travel straight to the lymph nodes, whereas particles of 500-2000 nm size were taken by dendritic cells before being processed in the lymph nodes (Manolova et al., 2008). The immune response, another barrier, could be potentially stimulated by any foreign particle. A cell-mediated or an antibody-mediated response could be induced depending on the particle size (Xiang et al., 2006). The nanoparticle uptake mechanism by living cells is largely unknown (Dobrovolskaia and McNeil, 2007). However, it is believed that receptor-mediated endocytosis is the most likely scenario (Xiang et al., 2006). Studies have shown that 2-3nm QDs target histones in the nucleoli of macrophages in a process involving endocytosis, active cytoplasmic transport, and nucleocytoplasmic exchange via the nuclear pore complex (Conroy et al., 2008, Nabiev et al., 2007).

1.4 Nanoparticle endocytosis

The plasma membrane provides a protective layer between the cell and the environment outside. The process of internalizing macromolecules and particles through the plasma membrane is called endocytosis (Figure 1.5). While small molecules passively diffuse through the cell membrane (Unfried et al., 2008), macromolecules are internalized by endocytosis. The endocytic process plays a crucial role in cell development, the immune response, neurotransmission, intercellular communication, signal transduction, and both cellular and organismal homeostasis (Conner and Schmid, 2003). The mechanisms of endocytosis vary depending on the endocytic cargo and the cell type (Mayor and Pagano, 2007). Two main internalization pathways may occur: either phagocytosis or other

endocytic pathways (i.e. clathrin- and caveolae-mediated endocytosis, macropinocytosis and other clathrin-and caveolae-independent endocytosis) (Hillaireau and Couvreur, 2009).
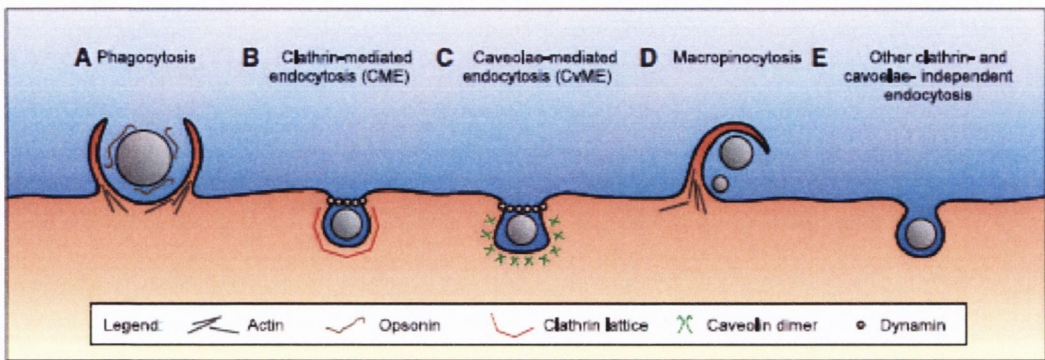
Figure 1.5: Endocytic pathways in mammalian cells.

Figure shows principal internalization pathways. (A) Phagocytosis is an actin based mechanism occurring primarily in professional phagocytes. (B) Clathrin-mediated pathway is associated with formation of clathrin lattice. (C) Caveolae-mediated endocytosis occurs in typical flask shaped invaginations of the membrane coated with caveolin dimers. (D) Macropinocytosis is an actin-based pathway, engulfing the extracellular milieu. (E) Other endocytosis pathways are independent of both clathrin and caveolae (e.g. lipid rafts). *Hillaireau, H. et al. (2009).*

1.4.1 Phagocytosis pathway

Phagocytosis is usually limited to specialised cells such as macrophages, neutrophils, monocytes and dendritic cells (Maxfield and McGraw, 2004). Other types of cells (fibroblasts, epithelial and endothelial cells), may display some phagocytic activity, but to a lesser extent (Aderem and Underhill, 1999, Rabinovitch, 1995) . The phagocytic pathway of entry into the cells happens through three distinct steps: recognition by opsonization in the blood stream; adhesion of opsonized particles to macrophages; ingestion of particles (Hillaireau and Couvreur, 2009). Phagocytes have receptors on their cell surface that recognise and attach to foreign particles, thus stimulating the formation of pseudopods to wrap around the particle. Endosomes from within the cytoplasm fuse with the cell membrane, and recruit the endoplasmic reticulum (ER), internalizing the particle forming the phagosome, from where they are processed and presented to the immune system via the lymph nodes.

1.4.2 Non-phagocytosis pathway

Non-phagocytic endocytosis has been traditionally referred to as pinocytosis, literally 'cell drinking,' i.e., uptake of fluids and solutes. Unlike phagocytosis, which is restricted to specialized cells, other endocytic pathways occur in virtually all cells by four main mechanisms: clathrin-mediated endocytosis, caveolae-mediated endocytosis, macropinocytosis and other clathrin- and caveolae-independent endocytosis (Hillaireau and Couvreur, 2009). *Clathrin-mediated endocytosis*, is the dominant endocytosis mechanism in most mammalian cells, and fulfils crucial physiological roles, including nutrient uptake and intracellular communication. The endocytosis typically occurs in a membrane region enriched in clathrin. Formation of the endocytosis vacuole is driven by assembly of a basket-like structure (Kanaseki and Kadota, 1969) formed by polymerization of clathrin units. Clathrin is a three-legged structure called triskelion. These triskelia assemble in a polyhedral lattice just on the cytosolic surface of the cell membrane, which helps to deform the membrane into a coated pit of ~150 nm. Notably, clathrin-mediated endocytosis causes the endocytosed material to end up in degradative lysosomes or in the Golgi apparatus (Mayor and Pagano, 2007). *Caveolae-mediated endocytosis* is one of the major alternative pathways other than clathrin-mediated endocytosis. The caveolae are characteristic flask-shaped membrane invaginations, having a size generally reported in the lower end of the 50–100 nm range, typically 50–80 nm (Hillaireau and Couvreur, 2009). Caveolae are particularly abundant in endothelial cells, where they can constitute 10–20% of the cell surface (Conner and Schmid, 2003), but also smooth muscle cells and fibroblasts. GTPase dynamin mediates fission of the caveolae from the membrane, then generates the cytosolic caveolar vesicle (caveosomes), which does not contain any enzymatic cocktail (many pathogens employ this pathway to escape degradation by lysosomal enzymes).These vesicles can directly connect to the ER or to the Golgi (Marsh and Helenius, 2006). Another type of clathrin-independent endocytosis pathway, known as *macropinocytosis* (Swanson and Watts, 1995), occurs in many cells including macrophages (Mukherjee et al., 1997). Actin-driven membrane protrusions form similar to phagocytosis. However, they collapse onto and fuse with the plasma membrane. This generates large endocytic vesicles, macropinosomes, which sample the extracellular milieu and have a size generally bigger than 1 μm. The intracellular fate of macropinosomes may vary depending on the cell type,

but in most cases, they acidify and shrink. Macropinocytosis is a form of endocytosis related to cell surface ruffling and provides a route for non-selective endocytosis of solute macromolecules (Zhang and Monteiro-Riviere, 2009). Cholesterol-rich microdomains called 'rafts,' having a 40–50 nm diameter have been described to be involved in pathways similar to caveolae-mediated endocytosis (Conner and Schmid, 2003).

Nanoparticle uptake by cells may occur through one of the different mechanisms described above. It is possible that nanoparticle may be taken up by cells via their size selectivity that may match that of endocytic pits. It has been demonstrated that nanoparticle endocytosis by cells not only depends on the size of the particle, but also the surface coating and charge. The amount of carboxyl groups on the surface of superparamagnetic iron oxide NPs was correlated with the efficiency of uptake by human mesenchymal stem cells (Mailander et al., 2008). Cationic D,L-polylactide NPs entered Hela cells in greater amounts than anionic PLA- NPs (Dausend et al., 2008, Harush-Frenkel et al., 2007). Internalization studies performed with QDs have demonstrated that carboxylic acid surface coating of QDs was recognized by lipid rafts but not by clathrin or caveolae in human epidermal keratinocytes (Zhang and Monteiro-Riviere, 2009). QDs were then internalized into early endosomes and then transferred to late endosomes or lysosomes. However, the specific endocytic mechanisms by which various NPs are internalized by cells remains largely unknown but the mechanism of cellular uptake is important in the field of nanomedicine.

1.5 Nanoparticle protein interactions

As potential applications of nanotechnology and NPs increase, so too does the likelihood of human exposure to NPs. On parenteral introduction of the nanoparticle systems, the host cells and tissues interact with them, from the initial contact with blood/plasma to when the NPs end up in the cells and tissues. These interactions could be (a) an immediate association with plasma proteins, platelets and blood cells; (b) time-dependent changes in the protein and cell association pattern during residence in the blood stream; (c) activation of signalling cascades; (d) recognition of the nanocarriers by the immune cells/macrophages; (e) deposition of the nanocarriers in non-macrophage cells including tumour cells and healthy tissues; (f) intracellular processing and activation of signalling

pathways/apoptosis (Karmali and Simberg, 2011). Blood plasma is the yellow liquid component of blood in which the blood cells in whole blood are normally suspended. It is the intravascular fluid part of extracellular fluid and makes up about 55% of the total blood volume. It is mostly water (93% by volume) and contains dissolved proteins, glucose, clotting factors, mineral ions, hormones and carbon dioxide (plasma being the main medium for excretory product transportation). Blood proteins are proteins found in blood plasma. Total serum protein content in the blood is 7g/dl. Some of the most important blood proteins are presented below (Table 1.1). 60% of plasma proteins are albumin, which is a major contributor to the osmotic pressure of plasma which assists in the transport of lipids and steroid hormones. Globulins make up 35% of plasma proteins and are used in the transport of ions, hormones and lipids assisting in immune function. 4% is fibrinogen which is essential in the clotting of blood and can be converted into insoluble fibrin. Regulatory proteins, which make up less than 1% of plasma proteins, are proteins such as enzymes, proenzymes and hormones. Other types of blood proteins include: prealbumin, alpha 1 antitrypsin, alpha 1 acid glycoprotein, alpha 1 fetoprotein, haptoglobin, alpha 2 macroglobulin, ceruloplasmin, transferrin, C3/C4, beta 2 microglobulin, beta lipoprotein, gamma globulin proteins, C-reactive protein (CRP), lipoproteins (chylomicrons, VLDL, LDL, HDL), transferrin and prothrombin. According to the estimates, plasma proteome is an extremely complex system consisting of ~ 100,000 protein types and variants (Anderson et al., 2004, Karmali and Simberg, 2011). This poses an enormous problem for characterization of proteins that adhere to NPs during their contact with blood. The highly abundant proteins include carrier/adaptor proteins such as albumin, transferrin and immunoglobulins. Intermediate and low-abundance proteins include receptor ligands and cytokines, tissue and cell leakage products and secretions.

Table 1.1: Abundance of different proteins

Blood protein	Serum concentration	Abundance
Albumin	35-50 mg/ml	High
Immunoglobulins	1.0-1.5 g/dl	High
Fibrinogens	1.8-3.5 mg/ml	High
Transferrin	2-4 mg/ml	High
Alpha-2-macroglobulin	1-3.1 mg/ml	High
C5 complement	0.9-1.7 mg/ml	High
Apolipoprotein A-1	0.8-1.7 mg/ml	High
Haptoglobulin	0.2-1.9 mg/ml	High
Ceruloplasmin	170-480 µg/ml	Moderate
Plasminogen	70-170 µg/ml	Moderate
IgD	<80 µg/ml	Moderate
Myoglobin	<60 µg/ml	Low
TNF-α	<20 pg/ml	Low
Interleukin-10	15.6 pg/ml	Trace

Table 1.1 shows most important blood proteins and their abundance levels (*Karmali et al. 2011*).

1.5.1 Evolution of protein corona

When NPs enter a biological fluid, proteins and other biomolecules compete for the nanoparticle surface, thus leading to the formation of a protein corona that defines the biological identity of the particle (Cedervall et al., 2007b). Continuous protein association and dissociation event make the corona dynamic in nature and vary its composition over time. Eventually, equilibrium is established, at which point the free and bound protein concentrations are such that for each protein the association and dissociation rates have become equal and the continued exchange will not affect the composition of the corona. However, the corona will again change composition if the nanoparticle moves to another compartment or fluid (Dell'Orco et al., 2010). The term ''hard corona'' defines the long-lived equilibrium state, representing a fingerprint of a nanoparticle in a certain environment. Ultimately, it is this corona of proteins, 'expressed' at the surface of

the particle that is 'read' by living cells (Dell'Orco et al., 2010). What the biological cell, organ, or barrier actually "sees" when interacting with a nanoparticle dispersed in a biological medium matters more than the bare material properties of the particle itself (Walczyk et al., 2010). Protein adsorption may result in the exposure of amino acid residues at the surface that are normally buried in the core of the native protein, which are recognized by the cells as "cryptic epitopes" (Lynch et al., 2006b). These cryptic epitopes may trigger inappropriate cellular signalling events (as opposed to being rejected by the cells as foreign bodies) (Lynch et al., 2007, Lynch et al., 2006a). The nature of the organization of the adsorbed proteins on the surface of NPs, and any subsequent colloidal instability of either the NPs (e.g. particle aggregation, flocculation, precipitation, etc.) or the adsorbed proteins (such as protein aggregation, clustering, fibrillation, etc.) determines the initial biological responses to the presence of NPs. The effect of different nanoparticle surface compositions on the nature and conformation of the adsorbed protein may disrupt downstream signalling pathways. For example, if a tightly bound protein loses much of its conformational identity, it will no longer function as it should. This would lead to disruption of essential cellular processes or functions. Additionally, downstream signalling pathways would be disrupted due to the inactivation of proteins that the adsorbed protein normally interacts with. Thus, it is not the nanoparticle per se which is biologically relevant, but instead the nanoparticle-protein complex (Lynch et al., 2007). The exceptional case of particles becoming so small that they cannot support such a 'coating', but are partially ligated was acknowledged to be of importance (Cedervall et al., 2007b, Lynch et al., 2006a).

1.5.2 Methods used to characterize protein corona

Study of the nanoparticle corona involves incubation of NPs with complex mixtures of proteins (e.g., plasma or serum) for various periods of time (often between 10 min and a few hours) and washing the unbound proteins using ultracentrifugation, column chromatography or density gradient purification (Karmali and Simberg, 2011). The proteins that adsorb on NPs following washing/enrichment steps are eluted and analysed. One- or two-dimensional gel electrophoresis is used for separating proteins. Two-dimensional gel electrophoresis (2D-GE) is often used (Gessner et al., 2002, Rabilloud, 2002), and specific antibodies are then used to identify the proteins (Chonn et al., 1992). Advances in

proteomics and mass spectrometry have facilitated the identification of many nanoparticle-binding proteins in one experiment. The protein band is excised from the gel, digested and identified by liquid chromatography-coupled mass spectrometry (LC-MS). Hellstrand *et al.* used size exclusion chromatography and NMR spectroscopy to show that copolymer NPs bind cholesterol, triglycerides and phospholipids from human plasma (Hellstrand et al., 2009). Recently, plasma proteins bound to dextran-coated iron oxide NPs have been analysed using a two-dimensional LC-MS/MS proteomics approach (Simberg et al., 2009). Cederval et al. applied methods which have not been used before for studying nanoparticle–protein affinity but, are nonetheless based on established techniques, including size-exclusion chromatography (SEC), isothermal titration calorimetry (ITC), and surface plasmon resonance (SPR), which should make them widely accessible (Cedervall et al., 2007b). A new approach based on SEC-gel filtration that can yield both the identity of the proteins on the NP and the rates of exchange with plasma proteins was introduced (Cedervall et al., 2007b), which was less perturbing of protein–particle complexes than centrifugation and other approaches (Klein, 2007). Cedervall *et al.* also showed that ITC can be used to assess the stoichiometry and affinity of protein binding, and SPR studies (in which NPs are linked to gold by a thiol anchor) yield additional data on protein association/dissociation from NPs (Cedervall et al., 2007b).

1.5.3 Factors influencing protein corona formation

The very large natural variation in protein composition and expression in different individuals, even amongst healthy individuals, is a complicating factor in studies of this nature. For example, the protein composition of blood (serum) has been shown to vary significantly between individuals, with many of the proteins that are considered wild-type not being the ones present in the majority of individuals (Lynch et al., 2007, Muthusamy et al., 2005). Also the concentrations of particles as well as bodily fluid will influence the outcome of identification experiments. The total protein concentration in bodily fluids and intracellular environments can be up to 35% (0.35 g/ml) representing several thousand different proteins spanning a wide range of concentrations (Lynch et al., 2007). A number of factors have been found to play a significant role in determining the composition of the corona (Figure 1.6) (Nel et al., 2009).
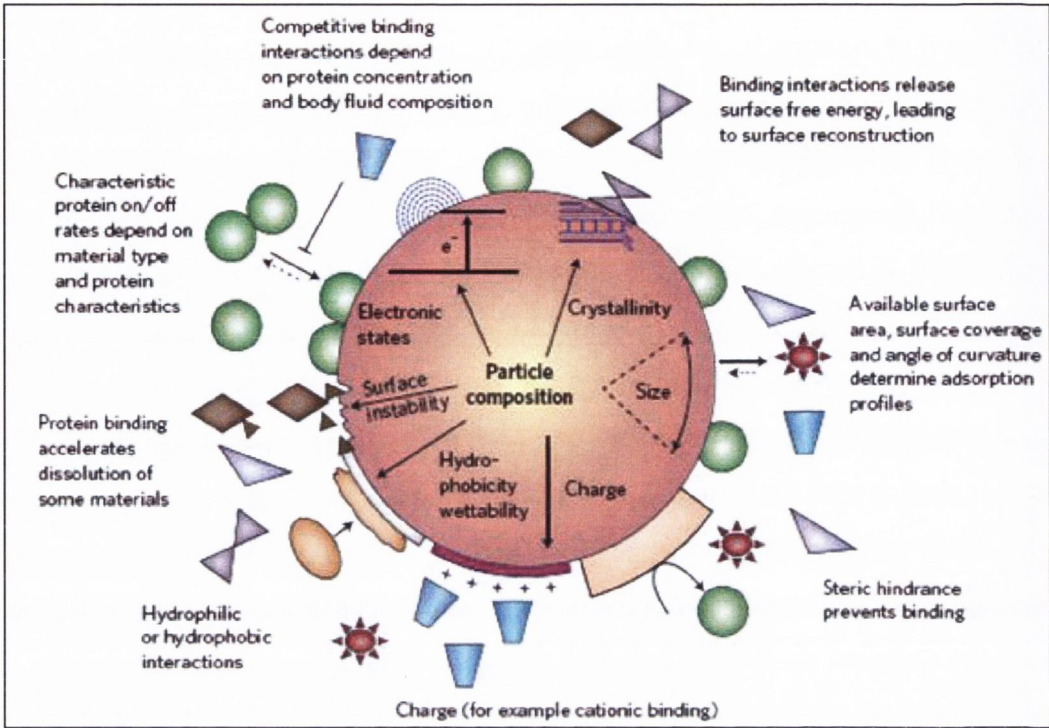
Figure 1.6: Factors influencing protein corona formation.
The image shows the various factors involved and their role in protein corona formation *(Nel, A. E., L. Madler, et al. 2009)*.

1.5.3.1 Nanoparticle size

NPs have distinct properties compared to the bulk form of the same materials. An important aspect of NPs is their small size, and extremely high surface to volume ratios, which means that the importance of the surface cannot be overemphasized. For example, nanoparticles with a diameter of 70 nm at a concentration of 0.01 mg/ml provide a total surface area of 0.8 m^2/l, whereas particles with a diameter of 200 nm at the same concentration (0.01 mg/ml) have a total surface area of 0.3 m^2/l, illustrating the dramatic increase in surface area with decreasing particle size, at constant weight fraction. The number of binding sites on a nanoparticle will be determined by the size of the particle as well as of the protein (Dell'Orco et al., 2010). Many researchers have studied the influence of size on protein adsorption. It has been shown that dextran particles in the size range of ~ 250 nm were more efficient in classical immunoglobulin-M (IgM)-dependent complement activation (Pedersen et al., 2010), whereas larger particles do not attract as much IgM and therefore do

not activate to the same extent. Size-dependent activation of complement was also observed for liposomes (Karmali and Simberg, 2011). A significant adsorption of protein was observed on 30 nm than on 50 nm gold particles (Dobrovolskaia et al., 2009b). Lynch *et al.* (Lynch et al., 2007) studied NIPAM/BAM (50:50) copolymer NPs varying in size between 70 and 700 nm. They demonstrated that the amount of bound plasma proteins increased with increasing available surface area. At a constant weight fraction of NPs, the surface area available for protein binding increases with decreasing particle size.

1.5.3.2 Nanoparticle surface characteristics

Nanoparticle *surface chemistry* may control the number of possible binding sites, and is expected to affect both the competition between different proteins for the same nanoparticle and the maximum level of coverage of the nanoparticle surface by each specific protein (Dell'Orco et al., 2010). Cederval *et al.* found a strong dependence of protein adsorption on particle surface characteristics (Cedervall et al., 2007b). Apolipoproteins are the main type of proteins which coat liposomes and polymeric NPs, but not inorganic NPs (Karmali and Simberg, 2011). Some proteins specifically bind to defined chemical groups on the nanoparticle surface. For example, hydroxyl groups (e.g., dextran and sugars) could promote the binding of C3 complement through its thiol ester group (Arima et al., 2009). Mannose-binding lectins (MBLs) were shown to bind to sugar moieties of dextran-coated NPs (Simberg et al., 2009). Specific binding of serum mannose binding protein (MBP) to phosphatidylinositol (PI) liposomes was demonstrated by Kuroki et al (Kuroki et al., 1997).

Nanoparticle *surface charge* is another important factor in protein interaction. Anionic liposomes (liposomes having surface charge imparted by anionic phospholipids), including those containing phosphatidylserine, were found to adsorb significantly more serum proteins such as apolipoprotein E than their neutral counterparts (Chonn et al., 1992, Cullis et al., 1998), (Kamps and Scherphof, 1998). Binding of complement (C1q) to anionic liposomes has been reported (Bradley et al., 1998). Oku *et al.* found significant binding of plasma proteins to liposomes containing cationic lipids (Oku et al., 1996). Cationic lipoplexes and polyplexes show strong albumin binding (Karmali and Simberg, 2011). This could be due to the electrostatic interactions between the cationic lipids and most of the negatively charged plasma proteins. An increase in plasma protein adsorption with

increasing surface charge density (-3.7 to -8.2 $\mu C/cm^2$) was observed with negatively charged polymeric NPs (Gessner et al., 2002).

1.5.3.3 Nanoparticle hydrophobicity/hydrophilicity

The nanoparticle surface hydrophobicity was found to strongly influence both the amount and the profile of the proteins adsorbed to NPs. Several studies have demonstrated the role of nanoparticle hydrophobicity (Cedervall et al., 2007a, Cedervall et al., 2007b, Gessner et al., 2000). A common observation has been that hydrophobic particles bind more plasma proteins than their hydrophilic counterparts (Karmali and Simberg, 2011). Furthermore, studies with less hydrophobic copolymer particles revealed virtually no proteins, whereas significant amounts of six different proteins were consistently bound to the hydrophobic particles (Lindman et al., 2007, Lynch et al., 2007). Lynch *et al.* observed that albumin and fibrinogen dissociated faster from the more hydrophobic compared to the more hydrophilic particles (Lynch et al., 2007). Gessner *et al.* (Gessner et al., 2000), using model polymer particles with decreasing hydrophobicity, demonstrated that apolipoproteins gradually disappear from the surface with decreasing hydrophobicity of the nanoparticle, whereas absorption of IgG and albumin does not change to the same extent. In contrast to NPs with hydrophobic surface components, a different category of proteins are attracted to hydrophilic inorganic NPs, which could be defined as adaptor and carrier proteins, such as transferrin, haptoglobin, kininogen, histidine-rich glycoprotein, and contact (intrinsic) clotting pathway factors FXI and FXII. The presence of positively charged domains in most of these proteins enables them to adhere to the anionic and metal surfaces (Karmali and Simberg, 2011).

1.5.3.4 Affinity/ exchange ratio

The association and dissociation rate of different proteins from NPs, i.e., the rate at which particle-associated proteins exchange with free proteins, are other critical parameters determining their interaction with receptors, and biological effects. If the particle endocytose from the extracellular fluid into an intracellular location, a tightly associated protein that exchanges slowly may follow the particle, whereas a protein with fast exchange will be replaced by an intracellular protein during or after such transfer. The relative protein exchange rates between NPs and cellular receptors may also impact the biological outcome.

The rates of association and dissociation are likely to vary quite considerably with protein and particle type. Most kinetic studies of adsorbed proteins report time scales of exchange of adsorbed proteins from silica, polymer and TiO_2 NPs ranging from 100 s to many hours (Cedervall et al., 2007b). Higher rates of association and dissociation were found for both albumin and fibrinogen, than apolipoprotein A-I and many other plasma proteins (Cedervall et al., 2007b, Lynch et al., 2007). Studies with 200 nm Nisopropylacrylamide (NIPAM) and N-tert-butylacrylamide (BAM) copolymer NPs with different compositions implied that the rates of association/dissociation are very different from protein to protein, depending on the nanoparticle composition. Thus, human serum albumin had a longer residence time on 85:15, 65:35 and 50:50 NIPAM: BAM NPs, and fibrinogen dissociated at a lower rate on 65:35 NIPAM:BAM NPs (Lynch et al., 2007). In addition, Lynch and co-workers also suggested that at short times albumin and fibrinogen may dominate on the particle surface, but will subsequently be displaced by lower abundance proteins with higher affinity and slower kinetics, for example apolipoprotein A-I. In contrast, when the available NP surface area is in excess over the total protein concentration, lower affinity proteins like albumin may also be found in isolation experiments.

1.5.3.5 Experimental procedure and times

In centrifugation experiments, different sets of proteins may be identified as part of the particle-protein corona, depending on the experimental procedure and times of the different steps in the protocol. Cedervall *et al.* reported that the quickly dissociating proteins like albumin and fibrinogen were found in lower fraction with longer incubation and wash times used. They have also shown that loosely bound components of the protein corona detach from the nanoparticle surface during relatively mild washes (Cedervall et al., 2007b). Another report suggested that the protein corona and the nanoparticle morphology are stable even after multiple centrifugation and washing steps (Walczyk et al., 2010). Most of the kinetic studies have proven that the length of incubation and the protein/ nanoparticle ratio are important determinants of the type and amount of adsorbed protein (Cedervall et al., 2007a, Cedervall et al., 2007b, Chonn et al., 1992). The change in total amount and the repertoire of adsorbed proteins over time seems to be the overall trend in protein adsorption (Cedervall et al., 2007a, Cedervall et al., 2007b, Goppert and Muller, 2005a). It should be noted that serum or plasma are used in the majority of protein corona studies, and the

presence of blood cells, platelets and microparticles was not taken into account. The cells and cellular elements can affect the interaction between NPs and proteins in unpredictable ways (Karmali and Simberg, 2011).

1.5.4 Proteins identified in nanoparticle corona

Vroman *et al.* (Vroman et al., 1980) first predicted the behaviour of proteins adsorbing on artificial surfaces. The major serum proteins albumin, IgG and fibrinogen have been identified as being associated with a wide range of particles of distinct composition, by the preferred method to-date of centrifugation (Allemann et al., 1997, Blunk et al., 1993, Diederichs, 1996, Gessner et al., 2003, Gessner et al., 2000, Goppert and Muller, 2005b, Gref et al., 2000) (Muller et al., 1997, Salvador-Morales et al., 2006, Sun et al., 2003). Albumin, due to its high abundance, is almost always observed on particles and may be detected even if it has relatively low affinity. Other proteins observed with several particle types in these centrifugation assays are immunoglobulins, apolipoproteins and alpha-1-antitrypsin (Cedervall et al., 2007b). Human serum albumin, high density lipoprotein (HDL) and fibrinogen have been found to be major biological macromolecules in the corona around the NIPAM: BAM copolymer particles (Cedervall et al., 2007b, Hellstrand et al., 2009). Albumin and fibrinogen adsorbs to polystyrene and poly-L-lactic NPs at earlier stages but are gradually displaced by lower abundance proteins with higher affinity, such as apolipoproteins and immunoglobulins (Cedervall et al., 2007b). In contrast, when the available nanoparticle surface area is in excess over the total available protein, lower-affinity proteins such as albumin also may be found in isolation experiments. Studies have shown that the corona around the copolymer particles contains the apolipoproteins that build up HDL (Cedervall et al., 2007a, Cedervall et al., 2007b). HDL is a complex composed of different proteins, phospholipids, cholesterol and triglycerides. Hellstrand *et al.* implied that copolymer NPs bind complete HDL complexes and may be recognized by living systems as HDL complexes. Apolipoproteins have been identified as binding to many other NPs, suggesting that lipid and lipoprotein binding to NP is a general feature under physiological conditions (Hellstrand et al., 2009). A time-dependent increase in the coating of C3 complement and IgG, but not albumin, with a maximum absorption at 2 h was observed by incubation of lecithin-coated polystyrene NPs with serum (Nagayama et al., 2007). Lundqvist *et al.* (Lundqvist et al., 2008) performed systematic studies on the

long-lived ("hard") protein corona formed from human plasma for six different polystyrene NPs: three different surface chemistries (plain PS, carboxyl-modified, and amine-modified) and two sizes of each (50 and 100 nm). The proteins identified were grouped according to their function. Immunoglobulins (IgGs) have been identified as a part of the hard-protein corona around the different particles, and great variability due to size and charge was noticed. The types identified (alpha, gamma, lambda, Kappa, mu and J chains) are involved in many processes like immune response (from allergic reaction to anaphylactic shock), transport across the placenta, as well as the general process of opsonisation for presentation to macrophages (Jefferis and Kumararatne, 1990). Apolipoproteins were the second group of proteins identified, and are involved in the transportation of cholesterol and lipids in the bloodstream (Anderson and Anderson, 2002). They are expected to greatly affect the intracellular trafficking, fate, and transport of NPs in cells. The third group identified was complement pathway proteins, a key part of the innate immune response. The plain particles bound most proteins compared to the rest. The next group identified was acute-phase proteins, and they closely followed the results for the complement-pathway proteins. Proteins involved in coagulation processes constituted the last group identified. Several proteins were detected in all of the particle coronas. In conclusion, the local chemical property determines the nature of proteins in the corona. However, the size of the particle, and its surface modification are able to entirely change the nature of the biologically active proteins in the corona, even for a fixed material type, and thereby possibly also the biological impact.

1.6 Haemostasis

Systemically administered nanoparticle-based formulations have the potential to interact with the haemostatic system. Haemostasis is a complex physiologic process that provides an important defence mechanism against bleeding when injury occurs to a blood vessel. It is subdivided into a primary and secondary cascade. The first refers to processes relating to platelet activation; the second, to processes of coagulation. Both processes are intertwined and occur to varying degrees in the arterial and venous circulation. The vascular endothelium, the intraluminal lining of the blood vessels, provides an anticoagulant surface to prevent clots from occurring. The coagulation system responds by the formation of the haemostatic plug that occludes the bleeding vessel. This includes platelets, but also fibrin,

fibrinogen, and other inflammatory cells including neutrophils. The coagulation cascade comprises a series of proteolytic reactions that convert zymogens into active enzymes, which then promotes the activation of zymogens further down the cascade resulting in the formation of thrombin and finally fibrin. Thrombosis, formation of a blood clot inside the blood vessel, involves the activation of three interconnected regulatory systems, the coagulation cascade, the complement cascade and the cellular components of the blood such as leukocytes and platelets (McGuigan and Sefton, 2007b). Thrombosis occurs only if the activated clotting factors are above a certain threshold in localized regions. In addition to flow, several positive [e.g. thrombin, tissue factor (TF)] and negative [e.g. thrombomodulin (TM), TF pathway inhibitor (TFPI)] feedback molecular factors determine whether the "cascade switch" is on or off (Jesty et al., 1993). Cellular components, such as platelets and leukocytes, take part in the maintenance of vessel integrity, and initiate wound healing. Once activated, they promote further amplification of the thrombosis response by generation of various factors. The complement system facilitates communication between the blood and the body's immune system. Various components of the complement cascade amplify inflammation and coagulation. For example, leukocytes can be activated by low amounts of C5b-9. Some coagulation factors (e.g. thrombin) also activate complement (McGuigan and Sefton, 2007a). Flow decreases the localized concentration of some factors and removes activated material by dilution into a larger volume, thus offering a negative feedback. Removal of fibrin plug after an injury (fibrinolysis) is mediated by molecules such as tissue plasminogen activator, and plasminogen activator inhibitor (McGuigan and Sefton, 2007a).

1.6.1 Components of coagulation system

1.6.1.1 Platelets

Platelets are anucleate cell elements derived from megakaryocytes. They play a critical role in haemostasis and thrombosis. Platelets circulate in a quiescent discoid shape in the absence of any activating stimulus. However, in response to an activating stimulus such as a damaged vessel wall, they interact with different sub endothelial proteins leading to a cascade of events resulting in a haemostatic plug to repair the vascular damage that occurs in daily life. The platelet cytoskeleton contains two actin filament-based components (Fox, 1993b). One is the cytoplasmic actin which fills the cytoplasm mediating contractile events

and the other is the membrane skeleton which coats the plasma membrane, regulating its contours and stability (Fox, 1993a). Only 30-40% of actin is polymerized into filaments in an unstimulated platelet. However, when activated, there is a rapid increase in actin polymerization, with new filaments filling the extending filopodia, forming a network at the periphery of the platelet (Fox, 1993a). The major signalling pathways are summarized in Figure 1.7.
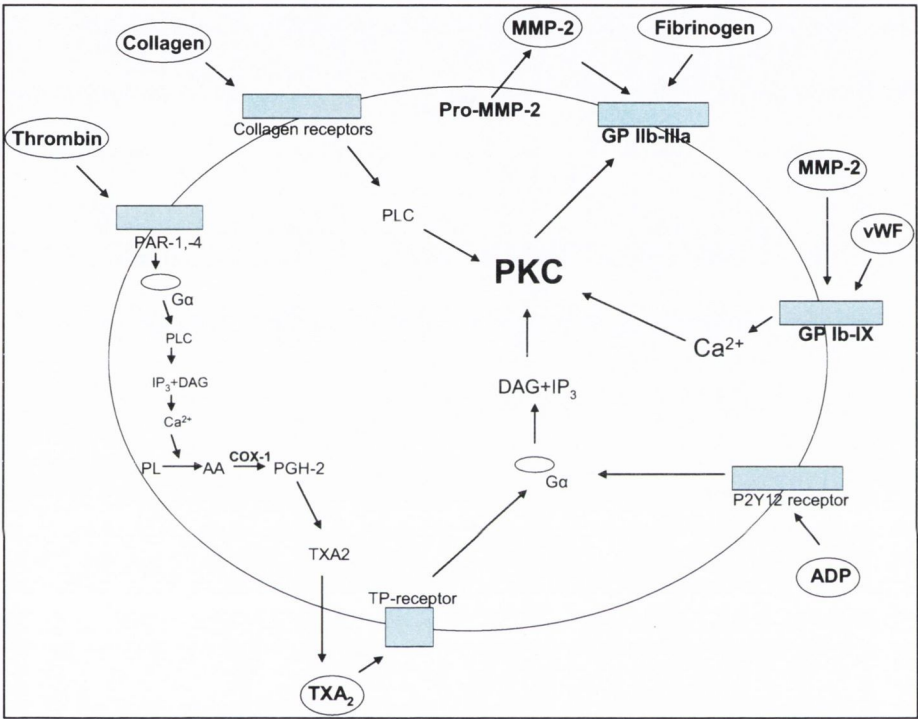
Figure 1.7: A summary of major platelet reactions and intracellular signalling pathways.
Receptors are boxes and ligands are circled. Matrix metalloproteinase-2, MMP-2; Adenosine diphosphate, ADP; von Willebrand factor, vWF; ThromboxaneA$_2$, TXA$_2$; Alpha subunit of a G-protein, Gα; arachidonic acid, AA; adenylate cyclase, AC; glycoportein, GP; prostacyclin receptor, IP-receptor; thromboxane receptor, TP-receptor; membrane phospholipids, PL; protease activated receptor, PAR. Other abbreviations are defined in the list of abbreviations.

Platelets contain alpha (containing GPIIb-IIIa, P-selectin, fibrinogen, von Willebrand factor (vWF), coagulation factors V & XIII, platelet-derived growth factor, platelet factor 4 and transforming growth factor-β1) and dense granules (containing ADP or ATP, calcium and serotonin). Activated platelets excrete the contents of these granules into surrounding blood through its canalicular systems. As platelets aggregate, GPIIb-IIIa associates with adhesive ligand in a platelet aggregate resulting in the association of GPIIb-IIIa, membrane skeleton proteins, and signalling molecules with cytoplasmic actin (Fox, 1993a, Fox, 1993b). The GPIIb-IIIa stored mainly in the α-granules is cardinal for platelet aggregation, since it allows binding fibrinogen to the receptors of adjacent platelets (Cramer et al., 1990). GPIIb-IIIa is the integrin that mediates platelet aggregation, and its ability to form a stable thrombus *in vivo* depends upon both the inside-out and outside-in signalling (Plow and Ma, 2007). The activated conformation of the extracellular domain of GPIIb-IIIa engages fibrinogen or vWF, an event necessary for platelet aggregation, is the consequence of inside-out signalling. As platelets aggregate, there is clustering of GPIIb-IIIa integrins, triggering an outside-in signalling that stabilizes the aggregate and supports responses, including platelet spreading and clot retraction. Therefore, inside-out and outside-in signalling constitute the two elements of the bidirectional signalling across GPIIb-IIIa.

Platelet adhesion and aggregation is mediated initially by different proteins in the plasma and sub endothelium, such as, collagen, von Willebrand factor and fibrinogen. High concentrations of fibrillar collagen types I and III are present in human adult arterial subendothelium, along with collagen types IV, V, and VI. Type III collagen dominates the relatively pristine childhood subendothelium. Both collagen types I and III increase in the thickened subendothelium of atherosclerotic arteries; however, most of the accumulating collagen is type I. Collagen types I, 111, and VI bind to vWF (Kroll et al., 1996). vWF is a large multimeric glycoprotein present in blood plasma and produced constitutively in endothelium (in Weibel-Palade bodies), megakaryocytes (α-granules of platelets), and subendothelial connective tissue (Sadler, 1998). Shear forces play a critical role in rapid platelet attachment. Under flow conditions, insoluble vWF derived from endothelial cells may be more active in initiating platelet adhesion than plasma derived soluble vWF multimers (Baruch et al., 1991). Both GPIbα and GPIIb-IIIa are involved in shear stress-dependent platelet adhesion onto vWF (Baruch et al., 1991, Olson et al., 1989). Monomeric

vWF contains two binding sites for collagen types I and III. The vWF binding site for type VI collagen is uncertain (Kroll et al., 1996). Fibrinogen is a soluble plasma glycoprotein, synthesized by the liver. Thrombin cleaves plasma fibrinogen to fibrin monomers that polymerizes and is subsequently cross-linked by a transglutaminase (factor XIII). Platelet aggregation requires binding of fibrinogen to GPIIb-IIIa receptors. Although GPIIb-IIIa complex is present on the surface of unstimulated platelets, it binds fibrinogen only after platelet activation (Isenberg et al., 1987). Studies have shown that platelets deposit on to fibrin-coated coverslips under flow conditions (Endenburg et al., 1995, Hantgan et al., 1992, Hantgan et al., 1990). vWF and GPIbα were involved at higher shear stresses and GPIIb-IIIa was involved at lower shear stresses (Hantgan et al., 1990).

Platelet collagen receptors, GPVI and GPIbα (the vWF-binding subunit of the GPIb/V/IX complex) (Ginsberg et al., 1988, Ginsberg et al., 1993) mediates platelet adhesion to the endothelium (Andrews and Berndt, 2004). GPIbα also contains binding sites for P-selectin expressed on activated platelets or endothelial cells. P-selectin is also mobilized from α-granules to the platelet membrane upon activation, mediating platelet-leukocyte aggregation and clot stabilization (Hamburger and McEver, 1990, Larsen et al., 1989). GPVI and GPIb/V/IX are physically associated on the platelet surface (Andrews and Berndt, 2004). Following platelet activation, platelets undergo a dramatic change in their shape due to cytoskeleton reorganization leading to a cascade of events mediated by thromboxane A2 (Needleman et al., 1976), adenosine diphosphate (Born, 1966) and matrix metalloproteinase-2 (MMP-2) (Sawicki et al., 1997), resulting in platelet aggregation. MMPs are a family of zinc and calcium-dependent proteinases that are involved in the turnover of the extracellular matrix of the connective tissue. MMPs get translocated to the platelet surface from the cytoplasm upon aggregation, interacting with the cell surface proteins and receptors (Sawicki et al., 1998, Sheu et al., 2004). MMP-2 facilitates modification of GPIIb-IIIa and GPIb/V/IX (Radomski et al., 2001), and release of platelet MMP-2 is associated with activation of GPIIb-IIIa receptor (Martinez et al., 2001). MMP-2 amplifies the pro-aggregatory effects of different agonists at the level of second messenger system and it has been shown that MMP-2 may prime platelet activation via stimulation of PLC, PKC, calcium mobilization and PI3K) (Falcinelli et al., 2005).

1.6.1.2 Endothelial cells

The vascular endothelium is the thin layer of cells that lines the interior surface of blood vessels, forming an interface between circulating blood in the lumen and the rest of the vessel wall. These cells are called endothelial cells (EC). EC line the entire circulatory system, from the heart to the smallest capillary. These cells reduce turbulence of the flow of blood, allowing the fluid to be pumped further. EC play a critical role in vascular homeostasis function by the expression of various mediator proteins and molecules, which regulate the coagulation cascade and by providing the phospholipid surface for many coagulation reactions (Davie et al., 1991, Esmon, 2005). They sense and integrate hemodynamic and hormonal stimuli (Vanhoutte, 1989). Tissue factor, the key initiation molecule, is present in intracellular pools and are released if the integrity of the EC is disrupted (e.g. TNF α), and expressed on the surface of activated EC (McGuigan and Sefton, 2007a, Slupsky et al., 1998). EC also provide three major negative feedback mechanisms which regulate the coagulation cascade; thrombomodulin is expressed constitutively (at a constant rate irrespective of the demand) on the surface of un-activated EC (Esmon, 2000); tissue factor pathway inhibitor (TFPI) is predominantly synthesized in the EC and both secreted into the plasma and also constitutively bound to the EC surface; and heparin sulphate molecules bound to the EC surface support antithrombin III binding (McGuigan and Sefton, 2007a). EC communicate with both platelets and leukocytes. EC synthesize platelet activating factor (PAF) and vWF to promote interactions with platelets (Jaffe et al., 1974, McIntyre et al., 1985). Even though platelets contain some vWF, virtually all plasma vWF is derived from the endothelium (Pearson, 1999). Leukocyte adhesion to EC is mediated by PAF and cell adhesion molecules such as PECAM, ICAM-1, P-selectin and VCAM-1 on the EC surface (Andrews and Berndt, 2004, Garlanda and Dejana, 1997, Zimmerman et al., 1990). EC also express molecules involved in complement system and receptors for a number of complement system proteins (Hamilton et al., 1990, McGuigan and Sefton, 2007a, Tedesco et al., 1999). Vascular tone controls vessel diameter and influences flow is an important factor in the regulation of thrombosis. EC releases a combination of vasodilators, such as nitric oxide (NO) and prostacyclin (PGI2) (Luscher and Barton, 1997, Palmer et al., 1988), and vasoconstrictors, such as endothelins and PAF, which regulates vascular tone by interacting with the underlying

smooth muscle layer (Bhatt, 1997, Furchgott and Zawadzki, 1980, Lopes-Martins et al., 1996, Ortega Mateo and de Artinano, 1997). NO and PGI2 are constitutively secreted by EC at low levels to maintain basal tone but secretion is increased transiently in response to agonists such as ATP and ADP secreted from activated platelets. PAF and endothelins are secreted only in response to agonists (McGuigan and Sefton, 2007a). EC play an important role in fibrinolysis, an essential event associated with thrombosis. It is the removal of a thrombus once formed, to facilitate wound healing. EC secrete both tissue plasminogen activator (tPA) and plasminogen activator inhibitor (PAI-1) to control fibrinolysis (Hajjar, 1995). The relative balance of tPA and PAI-1 is altered in activated EC during thrombosis to initiate thrombus dissolution and wound healing (Schleef et al., 1988). In normal, unactivated, confluent EC, secretion of PAI-1 is several fold higher than tPA (McGuigan and Sefton, 2007a).

1.7 Overview of hemodynamic forces

The mechanical forces created by flowing blood will have a profound effect on the bio-distribution of the systemically administered NPs. During left ventricular ejection, the blood expelled into the arterial system exerts hemodynamic forces on the artery wall. EC, which lines the interior of blood vessels experience three primary mechanical forces: (a) pressure, created by the hydrostatic forces of blood within the blood vessel. This represents the tensile stress (dilating force), which is a measure of the percent change in vessel circumference generated by the expansion and contraction of the luminal diameter; (b) circumferential stretch or tension, created as a result of defined intercellular connections between the endothelial cells that exert longitudinal forces on the cell during vasomotion; and (c) shear stress, defined as "the force per unit area between laminae". Blood flow can be described as an "infinite number of infinitesimal laminae sliding across one another, each lamina suffering some frictional interaction with its neighbours." Liquid shear stress (in dynes per square centimetre) in a tubular blood vessel is the force applied per unit area within the flowing stream. Wall shear stress is the dragging frictional force created by blood flow on the endothelial surface of the vessel wall (Figure 1.8). It can be

estimated as the product of wall shear stress rate (WSR) and local blood viscosity, WSR being defined as the radial derivative of blood flow velocity distribution at the wall (Reneman and Hoeks, 2008).
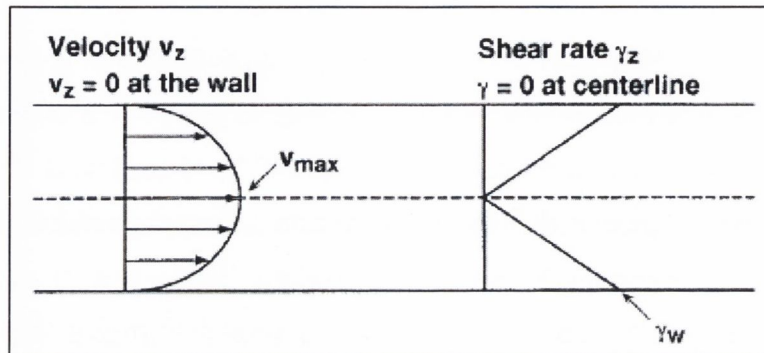
Figure 1.8: Schematic representation of shear forces
Diagram shows the wall shear stress rate and velocity in a blood vessel (*Kroll et al. 1996*).

Blood flow in a tubular chamber generates a parabolic flow velocity profile. This results in maximal velocity and minimal shear stress at the centre of the blood flow stream, and minimal velocity and maximal shear stress at the vessel wall. It is the difference in velocity between laminae of flowing blood that generates shearing forces. This means that shear stress (τ) in a tubular chamber having radius r and flow direction z can be represented by the mathematical formula: $\tau = -\mu \, (dv_z/dr)$, with dv_z/dr being the local velocity gradient (or shear rate) and viscosity (μ) the proportionality constant. In Fig 8, the shear rate dv_z/dr is designated as γ. As illustrated in figure 8, the shear rate (and hence, the shear stress) varies continuously through the fluid from zero at the centreline to a maximum at the wall. For a Newtonian fluid, the relationship between shear stress and shear rate $[\tau = -\mu(dv_z/dr)]$ allows one to convert simply from shear stress to shear rate: shear rate (in cm/s per cm or s^{-1}) = shear stress/viscosity (Kroll et al., 1996). Wall shear stress of Newtonian fluids for flow in tubular vessels can be calculated as a function of volumetric flow rate: $\tau w = 4\mu Q/\pi r^3$, where Q is the volumetric flow rate. This formula has been used to calculate shear forces *in vivo,* assuming that the viscosity of whole blood is 0.038 Poise (Kroll et al., 1996).

1.7.1 Normal physiological range of wall shear rates and shear stresses

It is a generally accepted phenomenon that the arterial system remodels itself within a narrow range to maintain constant wall shear stress throuhout (Giddens et al., 1993, Kamiya et al., 1984) based on Murray's law. Murray's law utilizes the principle of minimum work and states that the cube of the radius of the parent vessel is the same as the sum of the cubes of the radii of the daughter vessels (Murray, 1926). The assumption regarding a uniform shear stress, however, was based on the studies of steady flow of a Newtonian fluid in straight vessels described by Poiseuille's law (Stroev et al., 2007). Murray's law is consistent with a constant shear rate in the vascular system, because in steady flow the shear stress on the tube wall is proportional to the flow rate and inversely proportional to the cube of the radius of the tube (Zamir, 2000). However, blood flow in the human arterial system is pulsatile. Although segmental pressure drop and resistance in large arteries could be estimated using the models designed for steady flow (Simon et al., 1990), they fail to describe pulsatile flow taking place in the human systemic circulation up to the arteriolar level. Studies have shown different WSR in different parts of the arterial tree. For example, mean WSR was about 200 second^{-1} in the common carotid artery (CCA) (Hoeks et al., 1995), while mean WSR of about 100 second^{-1} both in the brachial artery (BA) (Simon et al., 1990) and in the femoral artery (SFA) were reported (Kornet et al., 1999). *In vivo* studies have shown that mean WSS measurements are neither constant along the arterial tree in a particular species, nor the same in a particular artery across species (Table 1.2) (Reneman and Hoeks, 2008) (Bakker et al., 2003, Lipowsky et al., 1978, Pries et al., 1995). The wall shear rate and shear stresses in different parts of circulatory system are summarized in Table 1.3.

Introduction

Table 1.2: Wall shear stress across species

	Man	Rat	Mouse
Infrarenal aorta	5	70	88
Common carotid artery	12	40	70

Table 1.2 shows the differences in mean wall shear stress (Dynes/cm^2) in a particular artery across species *(Derived from Reneman et al 2008).*

Table 1.3: Wall shear rate and shear stress values across major vessels

	Wall shear rate (/s)		Wall shear stress (Dynes/cm2)		
Veins	20-200	*(Kroll et al 1996)*	0.76-7.6		*(Kroll et al 1996)*
CA	Mean 165-403 Peak 588-1640	*(Wu et al 2004, stroev et al 2007)*	**Men** *Young* Mean 13±2.7 *Old* Mean 12±2 Peak 43±13 Peak 26±3 **Women** *Young* Mean 12±2 *Old* Mean 11±2 Peak 33±7 Peak 25±4		*(Reneman et al 2006)*
BA	Mean 84.5-194.2 Peak 770-908	*(Wu et al 2004, stroev et al 2007)*	**Men** *Young* Mean 5±1 *Old* Mean 5±3 Peak 33±7 Peak 33±5 **Women** *Young* Mean 4±2 *Old* Mean 5±2 Peak 27±6 Peak 29±12		*(Reneman et al 2006)*
CFA	134.2-1251	*(Stroev et al 2007)*	*Young* Mean 4±3 *Old* Mean 3±1 Peak 40±13 Peak 38±12		*(Reneman et al 2006)*
SFA	Mean 36-130.3 Peak 356-735.8	*(Wu et al 2004, stroev et al 2007)*	*Young* Mean 5±1 *Old* Mean 5±2 Peak 34±6 Peak 40±1		*(Reneman et al 2006)*
Stenotic vessels	800-10000	*(Kroll et al 1996)*	30.4-380		*(Kroll et al 1996)*

Table 1.3 displays the mean and peak wall shear rate, and the mean and peak shear stress values assessed in the veins, carotid artery (CA), brachial artery (BA), common (CFA) and superficial femoral arteries (SFA), and stenotic vessels (Kroll et al., 1996), (Wu et al., 2004), (Stroev et al., 2007), (Reneman et al., 2006).

Results clearly show that, at rest, mean WSS and WSR are far from constant along the arterial tree as predicted by the theory of minimal energy expenditure, neither in man, nor in animals. In humans, the carotid artery was found to have higher mean WSS than in the femoral and brachial arteries. Brachial and femoral arteries supply vascular beds with a high variation in blood demand (factor 20–30), depending on the level of exercise and associated variation in peripheral resistance (Stroev et al., 2007). During exercise, after all, the arteries may have to accommodate ten times higher blood flows, because arteries can dilate maximally 20%, which would lead to too high WSS levels. The lower mean WSS allows for an increase in mean WSS during exercise without reaching high levels that could be damaging to endothelial cells. So the arteries in the extremities must have a substantially lower mean shear stress at rest (de Groot et al., 2004, Schmidt-Trucksass et al., 2000) to accommodate the high blood flow in exercise without endothelial damage. It was also been shown that, across species, WSS in a particular artery is substantially different and will be higher, the smaller the animal is. Mean WSS will be higher in the absence of reflections, as in the brain circulation, and lower when reflections are dominantly present as in the arm and leg circulations at rest. Mean WSS was found to be not significantly different in men and women, either in the common carotid artery (Samijo et al., 1998) or in the brachial artery (Dammers et al., 2003).

1.8 Effect of shear stress on platelets

The mechanical force most relevant to platelet-mediated haemostasis and thrombosis is shear stress. In a steady Newtonian flow through a cylinder, liquid components (e.g., platelets) at the periphery of the cylinder (the wall) are subjected to maximal shear stress and liquid components at the centre of the cylinder are subjected to zero shear stress (ref to figure 8) (Kroll et al., 1996). However, blood flow *in vivo* is far more complicated under many physiologic and pathologic conditions. Surfaces of blood cells and blood vessels experience fluid shear stresses in circulation. Freely moving particles rotate in the shear field within a liquid stream, and are therefore subjected to time-varying (sinusoidal) shear stress. However, since the platelets have an irregular shape (unactivated platelets are discoid and activated platelets become rounded with many irregular tendrils), the time-average of shear stresses sensed by platelets is not identical to that sensed by an ideal spherical particle. The irregular surfaces of platelets are subjected to tangential shearing

forces even near the centre of a flowing stream at some distance from the vessel wall. The precise level of shear stress on platelets in flowing blood is not known. However, it is known that platelets in whole blood are pushed toward the periphery of flow nearer to the maximal shear stresses generated at the vessel wall (Kroll et al., 1996).

1.8.1 Shear stress affects platelet function – the concept

The study of platelet reactions became simple, routine and widespread after the invention of the "platelet aggregometer" by Born in 1962 (Born, 1962). The method involves recording changes in light transmission of a stirred platelet suspension as platelet aggregates are forming. Because platelets are stirred to maintain a suspension, platelet-platelet interactions in the platelet aggregometer take place under the influence of fluid mechanical shear stress. However, the aggregometer is inadequate for studying platelet responses within the context of Virchow's triad (i.e. hypercoagulability, haemodynamic changes and endothelial injury/dysfunction) since the shear stress is low and variable throughout platelet suspension. The imbalance between a complex network of procoagulant and anticoagulant factors results in clinical bleeding and thrombosis. This network involves three primary interactions, between blood (soluble and cellular constituents), the blood vessel (including fixed and dynamic responses), and blood flow was first described by the eminent pathologist Rudolph Virchow. The direct effect of shear stress was first reported in a cone-plate viscometer by Brown et al. in 1975 (Brown et al., 1975). These investigators observed that pathologic levels of shear stress (>50 dynes/cm^2) applied to platelet-rich plasma (PRP) induced changes in platelet morphology, along with secretion and aggregation. They were uncertain about the causes of those changes, although lysis was minimal at shear stresses below 250 dynes/cm^2. Based on these early experiments, it was concluded that the threshold stress for any specific response depends on two factors: (1) platelet solid surface interactions, and (2) the duration that platelets are subjected to the shear stress (Kroll et al., 1996). A rotational viscometer became the instrument of choice for experiments to investigate the importance of bulk shear stress versus surface effects. The two most used designs are (1) a stationary bob placed within a rotating outer cylindrical (the Couette viscometer); and (2) a rotating cone whose centre is placed in proximity (25 μm) to the centre of a flat plate (the cone-plate viscometer) (Figure 1.9). A constant and uniform shear stress constant and uniform shear stress is generated by both designs (Kroll et al., 1996).
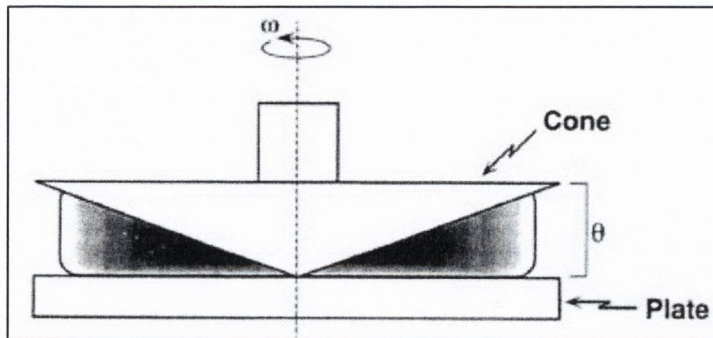
Figure 1.9: Cone-plate viscometer
The level of shear stress proportional to the cone angle (θ) and the rotation rate (ω). In this device, the shear stress within a suspension of platelets, or at the plate surface is constant and uniform *(Kroll et al 1996)*.

The shear stress generated by a rotational viscometer ranges from less than 2 dynes/cm^2 (venous level) to 20 to 30 dynes/cm^2 (arterial) to greater than 200 dynes/ cm^2 (as occurs in stenosed coronary, peripheral, or cerebral arteries).

1.8.2 Shear stress induced platelet adhesion

Human arterial mean shear stress levels reach 20 to 30 dynes/cm^2 (shear rates of whole blood equal to 500 to 750 S^{-1}) physiologically, and may reach >350 dynes/cm^2 (shear rate of 8,750 S^{-1}) in pathological conditions (ie, as in a stenosed coronary artery) (Strony et al., 1993, Strony et al., 1990, Tangelder et al., 1988). Pathologic stenosis can directly lead to shear-induced aggregation of platelets from the blood in constricted arteries. In all cases (1 to 200 dynes/cm^2), platelets adhere, change shape ("spread"), and aggregate ("thrombus formation"). These responses depend on mechanical shear forces. Studies have shown that fibrinogen may be the bridging ligand effecting platelet aggregation at shear stresses below 12 dynes/cm^2 (Ikeda et al., 1991, Weiss et al., 1973); however, within the range of elevated shear stresses (>80 dynes/cm^2), platelet thrombus production depends on vWF binding to platelet GPIb/IX/V and GPIIb-IIIa (Ikeda et al., 1991, Moake et al., 1988, Peterson et al., 1987).

The source of vWF can be plasma (Weiss et al., 1978a, Weiss et al., 1978b), platelet alpha granules (Sakariassen et al., 1986, Weiss et al., 1986) or the subendothelial extracellular matrix (Stel et al., 1985). Studies have proven that platelet GPIb/IX/V is involved in the initiation of platelet-subendothelial interactions under arterial level shear stress (>30 dynes/cm^2), and vWF attachment to GPIIb-IIIa is required for subsequent aggregation and thrombus propagation (Sakariassen et al., 1986). In perfusion experiments, larger vWF multimers are more effective than smaller vWF multimers at promoting platelet thrombus formation (Sixma et al., 1984). Studies have suggested that under pathologically elevated shear stress conditions (>350 dynes/cm^2), direct binding of GPIIb-IIIa to fibrin "slows down" the passing platelets, but that vWF bridging to GPIbα "locks" the platelets into a stable thrombus capable of remaining attached under high shear stresses (Endenburg et al., 1995, Hantgan et al., 1990).

1.9 Effect of shear stress on endothelial cells

1.9.1 Vascular mechanobiology

Blood vessels are not just part of the circulatory system that transports blood throughout the body, but are active organs with a variety of functions that maintain the homeostasis of the circulatory system. Biochemical mediators, including hormones, cytokines, and neurotransmitters control vascular function. However, it has recently become apparent that the biomechanical forces generated by blood flow and blood pressure regulate vascular function. Mechanotransduction refers to the process by which cells convert mechanical stimuli into a chemical response. The endothelium is a key mechanotransduction interface between blood and vessel wall. Mechanical forces are important modulators of endothelial cells. The endothelium can detect changes in the physiological conditions and respond rapidly and sensitively not only to humoral factors in the circulation but also to the mechanical conditions created by blood flow (Davies, 1995, Frangos et al., 1985, Rubanyi et al., 1986). The fact that EC respond to shear stress indicates that they have the ability to sense shear stress as a signal and transmit it into the interior of the cell.

1.9.2 Receptors and pathways associated with mechanotransduction

A variety of membrane molecules and cellular microdomains, including ion channels, G protein, growth factor receptors, tyrosine kinase receptors, adhesive proteins, caveolae, the cytoskeleton, the glycocalyx, and primary cilia have been shown to be involved in shear stress induced signal transduction pathways (Ando and Yamamoto, 2009). Based on the demonstrated importance of shear stress to endothelial cell function and integrity, it is likely that each of these putative mechanoreceptors activates intracellular signalling pathways to affect endothelial response to shear stress (Traub and Berk, 1998). Plasma membrane fluidity has been shown to increase in response to shear stress (Butler et al., 2001, Dangaria and Butler, 2007, Haidekker et al., 2000). It has also been demonstrated that depleting cholesterol from the plasma membrane abolishes EC responses to shear stress, including ERK activation and endothelial nitric oxide synthase activation (eNOS) (Lungu et al., 2004, Park et al., 1998).

1.9.3 Endothelial cell responses to shear stress

Cytoskeletal components that include an interconnected network of microfilaments, microtubules, and intermediate filaments stabilize cellular structure and shape. *In vivo* studies have shown that EC experiencing rapid and unidirectional blood flow were spindle-shaped and aligned with their long axis parallel to the direction of blood flow, whereas EC lining segments in which blood flow was turbulent or stagnant were much rounder in shape without a uniform orientation (Langille and Adamson, 1981, Nerem et al., 1998). *In vitro* experiments on cultured EC showed elongated cells with a net cellular movement in the direction of the shear stress. This morphological change was accompanied by cytoskeletal reorganization, with actin filaments becoming rearranged into bundles of stress fibers and aligned in the direction of the shear stress (Girard and Nerem, 1995, Langille et al., 1991, Malek and Izumo, 1996, Masuda et al., 1985, Wechezak et al., 1985, Wong et al., 1983). The cytoskeletal reorganization in response to flow is associated with an increase in cell stiffness (Sato et al., 1987). Studies have suggested that close interactions between the cytoskeleton and the cell membrane play a key role in cell shape rearrangement during flow (Wang et al., 1993). Because of these findings, shear stress is thought to determine the shape and orientation of EC. The cytoskeleton has been shown to play an important role in

shear-stress-induced gene expression by EC (Imberti et al., 2000, Kakisis et al., 2004, Resnick et al., 1993). Shear stress stimulates the release of powerful antithrombotic agents from endothelial cells like prostacyclin, NO, thrombomodulin and tissue plasminogen activator, and reduce secretion of plasminogen activator inhibitor type-1 (Diamond et al., 1990, Frangos et al., 1985, Grabowski et al., 1985, Helmlinger et al., 1995, Kawai et al., 1997, Malek et al., 1994, Stamler et al., 1989, Takada et al., 1994, Vanhoutte, 1989). Endothelial cells regulate leukocyte adhesion and migration of monocytes and leukocytes into the blood vessel wall by secretion of chemotactic factors and expression of cell surface molecules like ICAM-1 and VCAM-1 (mediates adhesion of monocytes to the endothelium). High shear stress inhibits leukocyte binding and chemo attractant protein expression while low shear stress and flow reversal promote leukocyte binding and transmigration (Cybulsky and Gimbrone, 1991, Traub and Berk, 1998). Low shear stress increases smooth muscle proliferation by increased expression of endothelial cell factors such as platelet-derived growth factor-A mRNA and endothelin-1 levels, and reduces angiotensin-converting enzyme mRNA (Buga et al., 1991, Kraiss et al., 1993, Ohno et al., 1995, Sharefkin et al., 1991, Traub and Berk, 1998). Low shear stress conditions results in an increased rate of lipid infiltration into the blood vessel (Berceli et al., 1990, Deng et al., 1995, Fry et al., 1993, Schwenke and Carew, 1988, Sprague et al., 1987, Weinbaum and Chien, 1993, Wiklund et al., 1985). Studies performed earlier have demonstrated increased endothelial cell turnover in turbulent conditions (Davies et al., 1986), and apoptosis in the absence of shear stress (Dimmeler et al., 1996, Kaiser et al., 1997). Thus, it appears that shear stress acts as an endothelial cell "survival" factor rather than as a "growth" factor (Traub and Berk, 1998). Shear stress is a potent physiological stimulus for NO production in endothelial cells (Berk et al., 1995, Corson et al., 1996, Fleming et al., 1997, Kuchan and Frangos, 1994). NO is produced by a unique enzyme present in the endothelium, termed eNOS (Janssens et al., 1992, Nishida et al., 1992, Sessa et al., 1992) and appears to be a key mediator of the atheroprotective effects of shear stress on the blood vessel wall. NO has been reported to play a role in platelet aggregation and leukocyte binding to the endothelium, in inhibition of vascular smooth muscle tone, and in alteration of lipoprotein metabolism (Vanhoutte, 1989). Shear stress plays a critical role in blood-flow-dependent phenomena, including angiogenesis (Ando and Yamamoto, 2009), vascular tone (Olesen et

al., 1988, Pohl et al., 1986), vascular remodelling (Kamiya and Togawa, 1980), and atherosclerosis (Cunningham and Gotlieb, 2005). Shear stress also stimulates cell adhesion to the substratum (Dardik et al., 1999), and generates dramatic increase in cytoplasmic viscosity and cell membrane rigidity (Lee et al., 2006).

Certain areas of the arterial tree, such as branch points, show manifestations of dysfunctional endothelium in response to low mean shear stress and flow reversal (Ku et al., 1985). These sites demonstrate increased uptake of lipoproteins, appearance of leukocyte adhesion molecules on the surface of the endothelial cells, and leukocyte transmigration (Traub and Berk, 1998). Impairment of these endothelial cell–mediated processes has been postulated to play a central role in the pathogenesis of atherosclerosis (Ross, 1993). Impaired EC responses to shear stress and cyclic strain lead to vascular diseases, including hypertension, thrombosis, and atherosclerosis (Ando and Yamamoto, 2011).

1.10 Nanoparticle toxicity and limitations

Humans have been exposed to NPs throughout their evolutionary phases; however, this exposure has been increased to a great extent in because of the industrial revolution. The growing use of nanotechnology in high-tech industries is likely to become another way for humans to be exposed to engineered NPs. Nanomedicine, the application of nanotechnology in medicine, may contribute to the toxicological profile of NPs in biological system. However, like most new technologies, including all nascent medicine and medical devices, there is a rising debate concerning the possible side effects derived from the use of particles at the nano-level.

The often very high surface area to volume ratio of NPs makes them more active, both chemically and biologically. The greater chemical reactivity of nanomaterials can result in increased production of reactive oxygen species (ROS), including free radicals (Cho et al., 2007, Lovric et al., 2005). ROS and free radical production are the primary mechanisms of nanoparticle toxicity; they result in oxidative stress, inflammation, damaged cell organelles, ruptured lysosomes, deformed nucleus and can also cause lipid peroxidation of the cell membrane resulting in apoptosis (Maysinger et al., 2007, Nel et al., 2006). While cytotoxic effects of NPs could be preferred in targeted cancer therapy (Barua and Rege, 2009), specificity remains a problem. Inappropriately activated immune response could

also result in toxic effects (Dobrovolskaia et al., 2009a). The accidental release of NPs into the environment during biomedical applications is a possibility, and very little is known or understood about their potential hazards (Hardman, 2006, Nel et al., 2006). Limitations of NPs include insolubility, aggregation (which may also have a cytotoxic affect) and presently, the difficulty in synthesising large amounts of NPs with reproducible characteristics and stability (Alivisatos, 2000, Maysinger et al., 2007). The cytotoxic effects observed in various studies performed with NPs on the coagulation system components and endothelial cells are described below.

1.10.1 Effect of nanoparticles on the coagulation system

Nanoparticles have been shown to induce platelet activation and microthrombosis in peripheral vasculature. Many types of inorganic nanomaterial, including negatively and positively charged QDs, induce platelet aggregation *in vitro* and microthrombi in vital organs (Geys et al., 2008). *In vitro* platelet aggregation and activation has also been observed with carbon nanotubes (Radomski et al., 2005). Thrombogenic iron oxide NPs have been used to induce targeted tumour infarction (Agemy et al., 2010). On binding of clotting factors, antibodies and complement, there is activation of contact defence responses, including clotting and complement cascade (Cullis et al., 1998). Interaction of NPs with blood proteins can cause contact toxicity in the form of thrombosis and hypersensitivity (Dobrovolskaia and McNeil, 2007, Moghimi et al., 2001, Nemmar et al., 2002b, Radomski et al., 2005). Studies have proved that intratracheal instillation of silica particles could enhance peripheral thrombosis (Nemmar et al., 2005). Stevens *et al.* showed that silver NP-coated indwelling vascular catheters accelerated the coagulation of contacting blood (Stevens et al., 2009a). Results have also shown that 9 nm sized gold NPs aggregated platelets in whole blood. On the other hand, Dobrovolskaia and co-workers (Dobrovolskaia et al., 2009b) showed that 30 and 50 nm colloidal gold NPs did not induce platelet activation and thrombosis, and concluded that the thrombogenicity of NPs is surface dependent. Surface-triggered thrombosis could be explained by several mechanisms. Factor FXII, Factor FXI, prekallikrein and kininogen adsorbs on the negatively charged surface to initiate the intrinsic (contact) clotting pathway, but the role of the intrinsic clotting pathway in nanoparticle-induced thrombosis has not been conclusively proven (Gorbet and Sefton, 2004).

1.10.2 Effect of nanoparticles on endothelial cells

Investigators have demonstrated that there were no cytotoxic effects for up to 72 hours with unmodified CdTe QDs on monocyte, epithelial and endothelial cell lines (Nabiev et al., 2007). However, they have indicated that there could be unknown delayed effects in the long term. Yan *et al.* showed that mercaptosuccinic acid (MSA)-capped CdTe QDs caused a dose dependent toxicity of endothelial cells through activation of mitochondrial death pathway and induction of endothelial apoptosis (Yan et al., 2011). Investigators have demonstrated cytotoxic injury and inhibition of cell growth with carbon black (Yamawaki and Iwai, 2006b) and 100 nm MgO NPs (Ge et al., 2011). Previous studies with silica NPs (diameters of 14-, 15-, 16-, 19-, 60-, 104-, or 335-nm) have demonstrated that smaller silica particles were more toxic on endothelial cells than bigger ones (Napierska et al., 2009). Cell viability assays performed with citrate-stabilized iron oxide particles have proven that the cell viability decreased with increasing iron concentration (Wu et al., 2010). Cytotoxic studies performed with various metal oxides (20-70 nm ZnO, 20-60 nm Y_2O_3 and 45 nm Fe_2O_3) on vascular endothelial cells Fe_2O_3 did not have any cytotoxic effects (Gojova et al., 2007). However, ZnO caused considerable cell death at concentrations above 10µg/ml.

1.11 Rationale and aims of this study

The development of nanotechnology has greatly increased the potential of engineered nanomaterials (1–100 nm in size). Nanotechnologies exploit the specific properties that arise from structuring matter at a nanoscale. NPs have vast applications in the electronics, aerospace, computer industries, consumer products (e.g. cosmetics, house cleaning products, paints, food, and textile) and, more recently, biomedical applications (e.g., "lab-on-a-chip", biosensors, medical imaging, prostheses and implants, drug delivery devices) (European, 2006). The National Institutes of Health (Bethesda, MD, USA), reviewing the applications of nanotechnology in monitoring, diagnosis and treatment of human diseases, introduced the term 'nanomedicine' to describe these applications (Moghimi et al., 2005). Studies carried out in animal models have shown that nanotechnology based constructs such as silica NPs (Lee et al., 2010), magnetite NPs (Wu et al., 2008b), and QDs (Biswas et al., 2011) are rapidly emerging as potential candidates for nanoparticle based bioapplications. Various silica-based NPs have been developed for bioimaging and

biosensing applications. The biocompatible and nontoxic nature of silica particles along with properties such as optical transparency, water dispersity, resistance to microbial attack and swelling, and easily modifiable surface makes them an attractive candidate for nanomedicine (Tallury et al., 2008). The use of paramagnetic iron oxide particles in magnetic resonance imaging (MRI) was one of the earliest applications of nanotechnology in medicine; when taken up by healthy hepatocytes, these particles could help to distinguish between normal and cancerous liver cells (Saini et al., 1995). The superparamagnetic properties of iron oxide particles less than 10 nm makes them attractive candidates for magnetically mediated hyperthermia in treatment of cancers (Moroz et al., 2002). Semiconductor QDs are becoming a useful diagnostic tool for discerning cellular function at the molecular level. Their small size, exceptionally high brightness, long-lasting fluorescence, size-tunable light emission, and narrow luminescence set them apart from conventional fluorescence dyes (Rosenthal et al., 2011). QDs are being developed for a variety of biologically oriented applications, including fluorescent assays for drug discovery, disease detection, bioimaging, single protein tracking, and intracellular reporting (Zrazhevskiy et al., 2010, Chang and Rosenthal, 2011). Many nanometre-sized constructs (e.g. QDs, dendrimers, nanoshells, nanotubes etc.) developed as noninvasive probes have moved from *in vitro* to *in vivo* applications such as targeting overexpressed folate receptors (biomarker) on cancer cells, human growth factor receptors (HER2) on tumours, or integrins crucial to angiogenesis around tumours and atherosclerotic vessels (Caruthers et al., 2007). The overall goal of nanomedicine is to diagnose as accurately and early as possible, to treat as effectively as possible without side effects, and to evaluate the efficacy of treatment non-invasively. Nanotechnology promises improvements to current techniques and permits control over characteristics of drugs or agents such as solubility, blood pool retention times or controlled release over short or long durations (Caruthers et al., 2007). Furthermore, by using nanometre-sized particles, the increased functional surface area per unit volume can be exploited for bio-functionalization.

The major routes of human exposure to NPs are transcutaneous, oral (enteric), or parenteral. The systemic delivery of nanoparticle based pharmacological, therapeutic, biosensor, imaging and diagnostic agents implies the interactions of NPs with blood and its elements (Winter et al., 2003, Buxton et al., 2003, Martin and Kohli, 2003). It has been

reported that inhaled NPs reach the blood and may reach other target sites such as the liver or heart (Kreyling et al., 2002, Oberdorster et al., 2002). As the circulation half-life of the particles in blood is increased, the question of possible adverse interactions with components of the coagulation system arises. Therefore, the aim of this study is to investigate the interactions of engineered NPs with blood plasma, platelets, and the vascular endothelial cells.

Chapter 3 of this thesis deals with the investigation of interaction of CdTe QDs and silica- and magnetite- based NPs with human platelets. Light transmission aggregometry, flow cytometry, zymography, quartz crystal microbalance, microfluidic platform and advanced microscopic techniques such as confocal, atomic force and transmission electron microscopic techniques have been utilized for platelet function studies.

Chapter 4 of this thesis deals with the interaction of CdTe QDs with human plasma. The proteins adsorbed on the surface of negatively charged CdTe QDs following incubation with human plasma were detected. Native gel electrophoresis was used to resolve the QD-associated proteins and mass spectrometry was used to identify the proteins.

Chapter 5 of this thesis deals with the interaction of CdTe QDs and silica-based NPs on human endothelial cells under static and shear stress conditions. The uptake and localization of NPs, cytoskeletal reorganization in response to shear stress, and cytotoxic effect of NPs were studied using microfluidic platform, high content analysis, confocal and atomic force microscopy techniques.

Chapter 2

Materials and Methods

2.1 Materials

Thioglycolic acid (TGA) stabilized CdTe QDs with a negative or positive surface charge were synthesised and characterized by Valerie Gerard, School of Chemistry, Trinity College Dublin. TGA provides a negative surface charge and cysteamine provides a positive surface charge to the QDs. Hereinafter, they will be referred to as negatively and positively charged CdTe QDs. Silica, silica coated magnetite and citrate stabilized magnetite particles were synthesised and characterized by Gemma Davies, School of Chemistry, Trinity College Dublin. A Shimadzu UV-1601 UV - Visible Spectrophotometer was used to measure QD and metallic nanoparticle's absorption. The concentration of particles was determined using Beer's law and the Brus equation. A Varian - Cary Eclipse Fluorescence Spectrophotometer was used to determine the fluorescence emission/photoluminescence (PL) spectra of QDs. The excitation wavelength was 480 nm and the emission was detected in the range 490-700 nm. The Quantum Yields (QY) were calculated from the PL spectra using Rhodamine 6G as a reference. Zeta potential of nanoparticles was measured on a Malvern Zetasizer Nano Series V5.10. The concentration of samples used for these measurements was typically corresponding to an absorbance around 0.2 in the plasmon band. Three measurements were usually taken for each sample, each made of 10 to 20 accumulations as optimised by the machine. Negatively charged 50 nm fluorescent silica nanoparticles were purchased from Postnova Analytics GmbH (Landsberg/Lech, Germany). The sample characteristics of all the NPs are presented in tables 2.1 to 2.3 below.

All reagents were purchased from Sigma-Aldrich (Dublin, Ireland) unless otherwise indicated. Collagen was obtained from Chrono-log (Labmedics Ltd, UK). Alexa Fluor® 546 phalloidin and Alexa Fluor® 488 phalloidin were purchased from Molecular probes (Invitrogen, CA, USA). P-selectin and PAC1 (GPIIb-IIIa) antibodies were purchased from BD Biosciences (Oxford, UK). Dulbecco's Modified Eagle Medium (DMEM), heat-inactivated foetal bovine serum (FBS), Gentamycin and Amphotericin B were from Gibco (Invitrogen Ltd., Bio-Sciences, Co Dublin, Ireland). Tyrode's salt solution was purchased from Sigma-Aldrich (Dublin, Ireland) Aqueous mounting medium was purchased from DakoCytomation (Dako, Glostrup, Denmark). All plastic wares were from Nunc

(Thermofisher scientific, NY, USA). vWF was kindly donated by Prof. James O'Donnel of the Thrombosis and Haemostasis group, IMM, Trinity College, Dublin.

Table 2.1: Sample characteristics of negatively charged TGA capped CdTe QDs

Chemical structure	TGA CdTe	TGA CdTe	TGA CdTe	TGA CdTe	TGA CdTe	TGA CdTe	TGA CdTe
Size (nm)	2.5 ± 0.1	2.6 ± 0.1	2.7 ± 0.1	2.9 ± 0.1	4.6 ± 0.1	4.9 ± 0.1	5 ± 0.1
Concentration (M)	2.3×10^{-4}	6.6×10^{-5}	5.7×10^{-5}	5.7×10^{-5}	1.6×10^{-4}	1.0×10^{-4}	2.4×10^{-4}
Zeta potential (mV)	-20 ± 5	-22 ± 1	-20 ± 1	-32 ± 1	-60 ± 1	-40 ± 1	-26 ± 9
Excitation wavelength (nm)	519	522	524	531	584	592	602
Emission wavelength (nm)	544	565	557	558	626	620	609
Quantum yield (%)	25	4	20	20	20	25	30
Shell/ligand	TGA	TGA	TGA	TGA	TGA	TGA	TGA
No of particles/mL	1.4×10^{17}	4.0×10^{16}	3.4×10^{16}	3.4×10^{16}	9.6×10^{16}	6.2×10^{16}	1.4×10^{17}
Solvent	Water	Water	Water	Water	Water	Water	Water

Table 2.2: Sample characteristics of positively charged TGA capped CdTe QDs

Chemical structure	Cyteamine stabilized CdTe
Size (nm)	~2.8nm
Concentration (M)	2.3×10^{-4}
Zeta potential	+ 30 mV
Excitation wavelength (nm)	534
Emission wavelength (nm)	564
Quantum yield (%)	5%
Shell/ligand	Cysteamine
Solvent	Water

Table 2.3: Sample characteristics of negatively charged silica, silica coated magnetite and citrate stabilized magnetite nanoparticles

Chemical structure	SiO_2	SiO_2 coated Fe_3O_4	Citrate stabilized Fe_3O_4
Shape and size	Spherical NP; 5 ± 1 nm	Spherical NP; coated 51 ± 8 nm	9 ± 2 nm
Concentration (M)	0.035 M	0.0171 M	0.00023 M
Zeta potential (mV)	-38 ± 2 mV	-41 ± 6 mV	48 ± 6 mV
Solvent	Water	Water	Water

2.2 Platelet aggregation

Blood was collected (tri-sodium citrate 3.15%, 9:1 v/v) from fully consented healthy volunteers who had not taken any drugs (for example, non-steroidal anti-inflammatory drugs such as aspirin and brufen, anti-histamines such as loratadine, GPIIb-IIIa inhibitors such as tirofiban and abciximab, ADP inhibitors such as clopidogrel and ticlopidine, antibiotics such as penicillins and cephalosporins, anti-depressants, β-blockers, calcium antagonists such as verapamil and diltiazem, nitrates, and herbal medicines such as ginkgo biloba and ginseng) known to affect platelet function for at least 14 days prior to study. The study was approved by Trinity College Dublin Ethics Committee. Platelet rich plasma (PRP) was obtained by centrifugation at 240g for 20 min (with gentle acceleration and deceleration) at room temperature. At this point PRP, which had separated from white blood cells and red blood cells, was gently removed. When washed platelets (WP) were required, this PRP was centrifuged at 900g for 10 min (with gentle acceleration and deceleration) at room temperature (Radomski and Moncada, 1983) in the presence of prostacyclin. The platelet poor plasma was removed and platelet pellet was washed three times with Tyrode's salt solution, before being re-suspended in the same. Platelets were counted using a coulter counter (Beckmann, USA). Afterwards, the final platelet number (2.5×10^8 platelets/ml) in PRP/WP was adjusted using Tyrode's salt solution

Aggregation was measured by using a four-channel Chrono-log whole blood Lumi-Aggregometer (Chrono-log Corporation, Havertown, USA) linked to Aggro-link data-reduction systems (Radomski et al., 2005). The ability of NPs to stimulate platelet aggregation of unstimulated (resting) platelets was studied. In these experiments, platelet samples were incubated in the presence or absence of NPs (0.1 - 5µM with CdTe QDs, silica, magnetite, or silica coated magnetite NPs) for 20 min and effects of particles were recorded. Collagen treated or untreated PRP/WP was taken as positive and negative controls respectively. The results were expressed as percentage of light transmission where 100% transmission (platelet-poor plasma) was taken as maximal aggregation and are given as mean values of four or five replicates (indicated in text).

2.3 Flow cytometry

Activated platelets express P-selectin on surface of the platelets. In order to analyse the receptor expression on the surface of activated platelets, PRP and washed platelets were treated with various concentrations of negatively charged 2.5 or 5 nm CdTe QDs in the aggregometer. PRP samples were treated with 3µM or washed platelet samples were treated with 0.1µM or 1µM or 5µM concentration of QDs. 10 µl of samples were taken from the cuvettes when the collagen induced platelet aggregation reached 50%. Untreated (resting) and collagen treated platelets were taken as negative and positive controls respectively. After collection, samples were incubated in the presence of equal volume (10 µl) of P-selectin antibody (CD62P-APC (Allophycocyanin) from BD Biosciences, UK/Ireland) in the dark for 5 minutes at room temperature. Following incubation, samples were diluted in FACS flow fluid and analysed within 5 minutes using BD FACSArray (BD Biosciences, Oxford, UK). The instrument was set up to measure the size (forward scatter), granularity (side scatter) and cell fluorescence. Antibody binding was measured by analysing activated platelets for fluorescence.

2.4 Zymography

Samples of washed platelets were treated with 1, 3 or 5 µM concentrations of negatively and positively charged CdTe QDs in the aggregometer. After aggregation in the aggregometry, platelet releasates were separated from platelet aggregates by centrifugation (1400g for 5 minutes) and then stored at -80 $^{\circ}$C until assayed. Releasates from HT1080

(fibrosarcoma) cells was used as a loading control. Releasates from untreated and collagen treated platelets were taken as negative and positive controls respectively. The presence of MMP-2 was detected by zymography as described previously (Sawicki et al., 1997; 1998, Jurasz et al., 2001). Briefly, platelet releasates were subjected to 8% sodium dodecyl sulphate-polyacrylamide gel electrophoresis (SDS-PAGE) in which the separating gels were copolymerized with 2 mg/ml gelatin. Following electrophoresis, the gels were washed with 2.5% Triton X-100 to remove SDS and then incubated in incubation buffer (0.15 M NaCl, 5 mM $CaCl_2$, 0.05% NaN_3 and 50 mM TRIS-HCl buffer, pH 7.5) for 5 days to determine the activity of the secreted enzymes. After incubation, the gels were stained with 0.05% Coomassie brilliant blue and de-stained in de-staining solution (refer Appendix 4). The gelatinolytic activities were detected as transparent bands against the background of Coomassie blue-stained gel under UV light using ChemiDoc MP System (Bio-Rad, UK). MMP-2 was identified by its molecular weight when compared to standards.

2.5 Zeta potential measurements

Samples of PRP and washed platelets were treated with various concentrations of negatively charged CdTe QDs in the aggregometer. The samples were collected after the platelet aggregation had reached a plateau and the zeta potential was measured using Malvern Zetasizer Nano Series V5.10 (Malvern Instruments Ltd, Worcestershire, UK) at 37 °C. The protocol is shown in Figure 11. Untreated platelet samples and collagen induced aggregates were taken as negative and positive controls respectively. The zeta potential of plasma, collagen, stock QDs, and QDs resuspended in Tyrode's salt solution (used for dilution of PRP and washed platelets) to a final concentration of 0.1, 1, 3, or 5 µM was also measured for comparison.

2.6 Native gel electrophoresis

8% gel was made without SDS. Human plasma or albumin was incubated with 2.5 or 5nm negatively charged CdTe QDs at a concentration of 3 µM for 20 minutes at roomn temperature. The reaction was stopped with 1X loading buffer (Appendix 4). 20ul (24 µl plasma/ albumin sample + 6 µl of 5X loading buffer) of the samples were loaded in each well and electrophoresis performed. The procedure was optimized with various dilutions of plasma starting from undiluted plasma to 10x, 20x and 50x dilutions to get well resolved

protein bands in the gel. 10% human serum albumin was used as a control and run in parallel with the same dilutions. Immediately after electrophoresis, the gels were imaged under ultra violet light (Biospectrum® Imaging System, Upland, CA, USA) to confirm the electrophoretic migration of QDs. The gels were then fixed with fixation solution (Appendix 4) overnight at room temperature. After treating the gels with incubation solution (Appendix 4) for 1 hour at room temperature, the gels were stained with colloidal Coomassie blue. The gel was then placed in a clean clear plastic bag, photographed and stored at 4 °C prior to analysis of the desired bands by mass spectrometry.

2.7. Mass spectrometry analysis

The mass spectrometry analysis and identification of the peptides were performed by the collaborating research group at the BMS Mass Spectrometry and Proteomics Facility, Centre for Biomolecular Sciences, University of St Andrews, Scotland, UK.

2.7.1. In-gel digestion of proteins

The Coomassie stained gel was placed on the bench and the desired bands were excised with a clean scalpel. The gel pieces were placed into the tube and stored at 4 °C for further processing. The proteins in each slice were digested *in-gel* with trypsin (Promega) after reduction and alkylation, using a Investigator Progest digestion robot (Genomic Solutions Ltd., UK) using standard protocols (Shevchenko et al., 1996). Samples were desalted and concentrated using a micro C18 column (0.2 µl ZipTip, Millipore) according to the manufacturer's instructions. The peptides were eluted directly from the tip onto the target in 1.5 µl alpha-cyano-4-hydroxycinnamic acid (saturated stock prepared in 50:50 acetonitrile: 0.2% TFA, diluted 1/5 in 60:40 acetonitrile: 0.2% TFA).

2.7.2. nLC-ESI-MS/MS

The resultant peptides were separated on an UltiMate nanoLC (LC Packings, Amsterdam) equipped with a PepMap C18 trap & column, with a 60 min gradient of increasing acetonitrile concentration, containing 0.1 % formic acid. The eluent was sprayed into a Q-Star XL tandem mass spectrometer (Applied Biosystems, CA) and analysed in Information Dependent Acquisition (IDA) mode, (1 sec of MS followed by 2 × 3 sec MS/MS of the 2

most intense peaks seen by MS. These masses are then excluded from analysis for the next 60 sec.

2.7.3. Database searches

MS/MS data for doubly and triply charged precursor ions was converted to centroid data, without smoothing, using the Analyst QS1.1 mascot.dll data import filter with default settings. The MS/MS data file generated was analysed using the Mascot 2.1 search engine (Matrix Science, London, UK) against MSDB May 2006. The data was searched with tolerances of 0.2 Da for the precursor and fragment ions, trypsin as the cleavage enzyme, one missed cleavage. The functions of all the detected proteins were identified using UniProt. UniProt is a comprehensive, high-quality and freely accessible resource of protein sequence and functional information. The proteins were then grouped according to their function.

2.8 Quartz Crystal Microbalance with Dissipation

The Quartz Crystal Microbalance with Dissipation (QCM-D) from Q-Sense (Q-Sense^{TM} E$_4$ system, Q-Sense AB, Sweden) has four temperature and flow-controlled modules set up in parallel configuration (Figure 2.1). The heart of the system is a quartz crystal sensor that is placed in a chamber inside the module. Samples are perfused using a peristaltic microflow system (ISMATEC, IMS 935). When molecules adsorb to the surface the frequency (f) decreases. The formation of a soft molecular layer increases the dissipation (D). The dissipation (damping) is the sum of all energy losses in the system per oscillation cycle. A soft film attached to the quartz crystal is deformed during oscillation, which gives high dissipation. In contrast; a rigid material gives low dissipation. The chamber temperature was maintained at 37 $^{\circ}$C throughout the experiment. Untreated PRP or protein poor plasma (PPP) was taken as controls. The 'frequency' decreases when molecules (platelets/platelet aggregates) adsorb to the surface of the sensor crystals, and the 'dissipation' increases with the formation of a soft molecular layer (platelets/platelet aggregates) on the crystals.

For the study of platelet aggregation, polystyrene-coated (PC) quartz crystals (sensors) were used as sensors following coating with fibrinogen. For fibrinogen coating, sensors were placed in fibrinogen dissolved in PBS (100 µg/ml) for one hour at room temperature. Samples of PRP (250,000 platelets/ µl) or platelet poor plasma (PPP) obtained

from healthy volunteers were treated with CdTe QDs and perfused over the sensors at a speed of 100µl/minute for 30 minutes. PRP or PPP, not treated with QDs was taken as controls. Platelet aggregation was monitored for 30 minutes in real time at 37 °C by the acquisition Q-Sense software (QSoft$_{401}$) and measured as f and D.

(A)
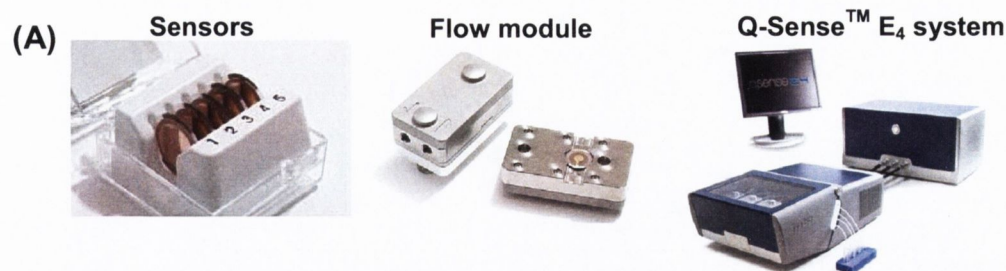
(B) Two parameters – frequency (Δf) and dissipation (ΔD) – are monitored simultaneously, in real-time, as molecular layers form on the sensor surface.
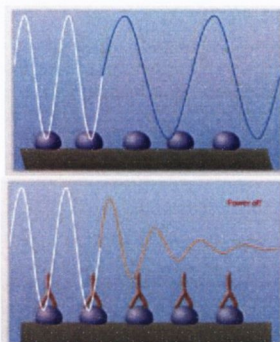
When molecules adsorb to the surface, the frequency (f) decreases

The formation of soft molecular layer increases the dissipation (D)

(C)
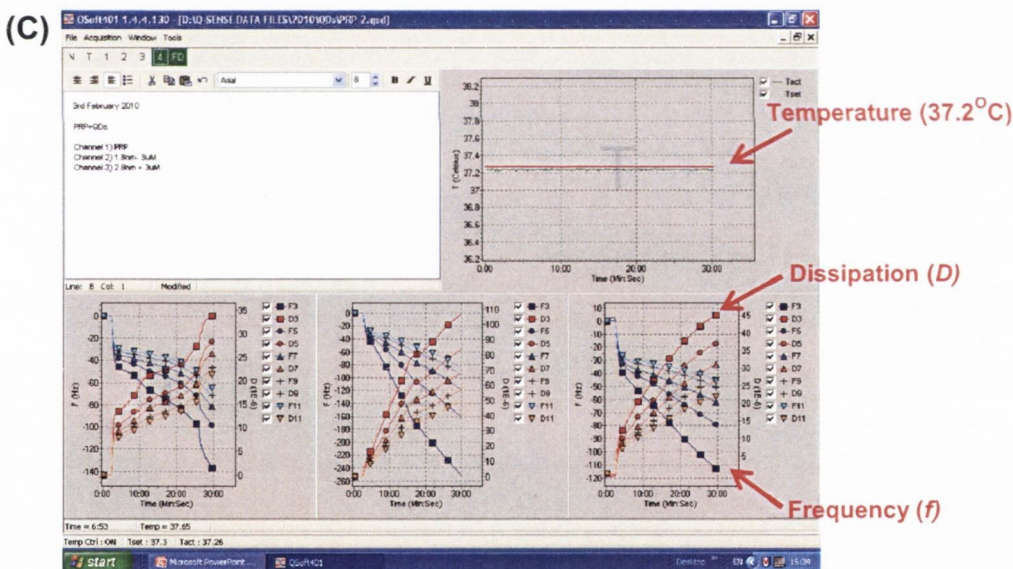
Figure 2.1: Quartz Crystal Microbalance (Q-Sense^{TM} E$_4$ system).
(A): Components of Q-Sense^{TM} E$_4$ system. (B): Schematic diagram showing the decrease the frequency (f) and the increase the dissipation (D) following formation of a soft molecular layer. (C): Representative graph shows temperature control, decrease in frequency (f) and increase in dissipation (D).

2.9 Phase contrast Optical microscopy

The formation of platelet aggregates on the crystal surface was studied using a Zeiss microscope (Axiovert 200M, UK). Briefly, PRP and PPP suspensions were perfused on fibrinogen-coated PC-quartz crystal for 30 minutes in the Q-Sense device. Thereafter, the crystals were taken for phase-contrast microscopy examination using a 20x objective. Photomicrographs were captured using a digital camera and Zeiss software (Axiovision 4.7).

2.10 Cell culture and treatments

Human umbilical vein cells (HUVEC) (ATCC CRL-1730, ATCC-LGC standards, Middlesex, UK), were kindly provided by Cellix Ltd, Dublin, Ireland. Cells were cultured in DMEM medium supplemented with heat-inactivated foetal bovine serum FBS (10% v/v), Gentamycin (0.5% v/v), Amphotericin B (1% v/v) and 5% CO_2 content at 37 $^{\circ}C$ in a humidified incubator. For experimentation, cells were seeded in 96-well plates at the density of 2000 cell/well and allowed to grow overnight to reach 80% confluence. All the NPs were dispersed in cell culture medium prior to administration to the cells. Serial dilutions were established by mixing equal volumes of particle suspension and cell culture medium followed by vigorous vortexing, and applied to the cell immediately. Untreated cells were taken as controls.

2.11 Cellix microfluidic platform

The Cellix Venaflux^{TM} platform (Figure 2.2) allows performing *in vitro* assays mimicking *in vivo* conditions of the blood vessel. Vena8 Fluoro+™ biochip was used for studying the influence of QDs on flow induced platelet adhesion and VenaEC ^{TM} was used to investigate the uptake and localization of nanoparticle under controlled shear stress conditions. Cell suspensions (e.g. whole blood) or NPs suspended in medium/PBS may be injected through the channels using the Mirus^{TM} Nanopump and FlowAssay^{TM} software which supports a range of shear stresses for dynamic flow based assays.
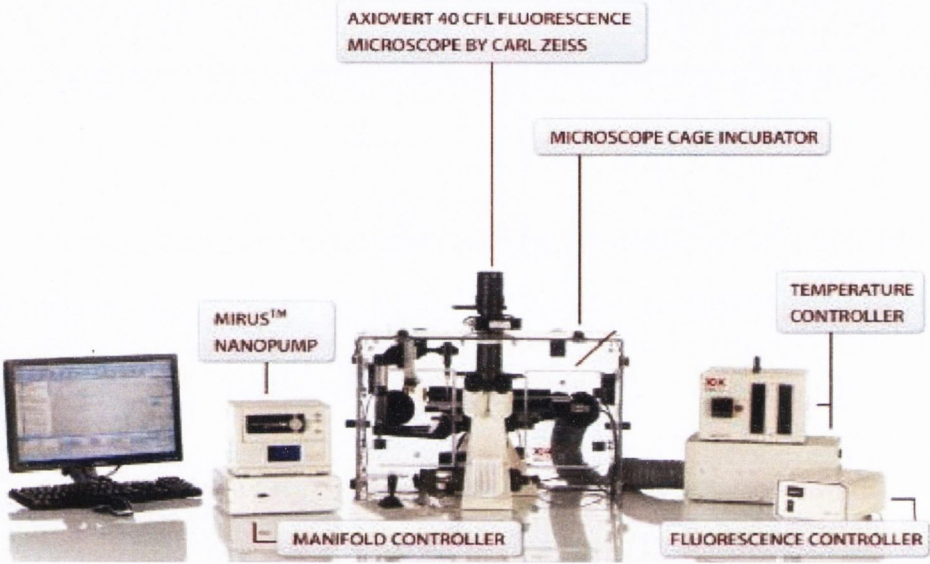
Figure 2.2: Venaflux^{TM} Platform.

Image shows the various components of the Cellix Venaflux^{TM} microfluidic platform.

2.11.1 Flow induced platelet adhesion on pro-coagulant protein coated channels

Blood was collected in vacutainers (0.9% sodium citrate) from healthy volunteers who had not taken any drugs known to affect platelet function for at least 14 days prior to study. PPACK (Calbiochem, EMD biosciences, Germany), a thrombin inhibitor was added immediately to the whole blood at a final concentration of 10µM. 3,3'-Dihexyloxacarbocyanine Iodide (DiOC6) (Invitrogen, USA), a live membrane staining, was added to the whole blood at a final concentration of 1µM to stain the platelets. Vena8 Fluoro+™ biochip (Cellix Ltd) channels were loaded with 10 µl of fibrillar collagen (Kollagenreagens Horm, Nycomed, Austria) (200µg/ml) or fibrinogen (200µg/ml) or vWf (200µg/ml) and placed in humidified box and sealed for 2 hours at room temperature or, alternatively overnight at 4 °C. The channels were then washed with PBS. The biochip was then clamped on customized aluminium frame (Figure 2.3).

After treating the whole blood with CdTe QDs, the collagen and fibrinogen coated channels were exposed to shear stress of 0.5, 5, 30, 45, 60 or 90 dynes/cm^2 for two minutes and since vWF play a critical role in high shear stress rates, Vwf coated channels were exposed to shear stress of 15, 30, 60 or 90 dynes/cm^2. Only the platelets activated by the flow adhered to the pro-coagulant proteins in the channel. Untreated whole blood was run under similar shear stress conditions with each donor, and was taken as controls. The whole experiment was performed in temperature controlled (37 $^\circ$C) microscope cage. 20x images were taken in three to five fields per channel using inverted fluorescence microscope, and the images were then analysed using Image-Pro software. An example of analysis of platelets adhered on collagen is shown in Figure 2.4. The results were expressed as area covered (sum) by adhered platelets and total number of aggregates (samples).

Dimensions of each channel 400 μm (W) × 100 μm (D) × 20 μm (L)

Vena8Fluoro™ biochip

Vena8Fluoro™ biochip

Al frame

Whole blood samples were run into channels under various shear stress conditions
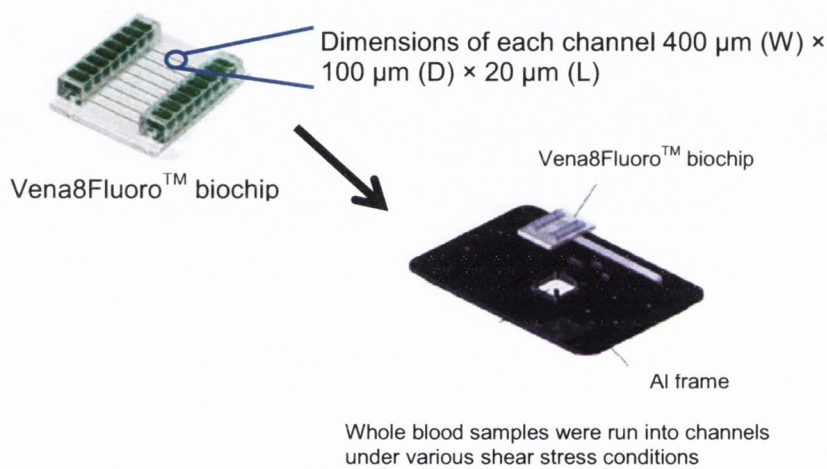
Figure 2.3: Assembly of Vena8 Fluoro+™ biochip on microfluidic platform.
Image shows dimensions and assembly of Vena8 Fluoro+™ biochip.
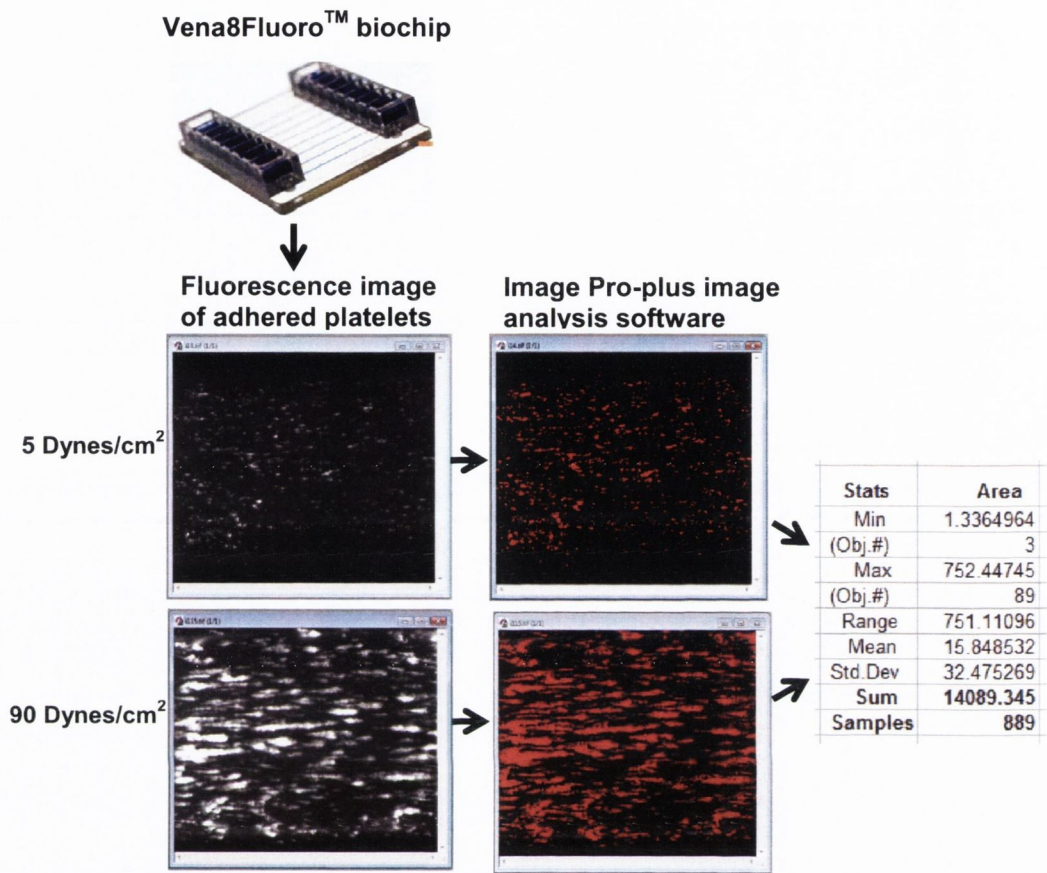
Figure 2.4: Quantification of platelets adhered on collagen in the channel.
Image shows quantification of platelets adhered on collagen coated channels using Image-Pro Plus analysis software.

2.11.2 Nanoparticle uptake and localization in human endothelial cells

VenaEC [TM] Biochips contain tissue culture treated substrates which enable the seeding and culturing of endothelial cells. The optically transparent polydimethylsiloxane (PDMS) chip comprised of two open channels were then clamped on top of EC monolayer with customized frames. This creates two parallel channels imitating human micro-capillaries (Figure 2.5).
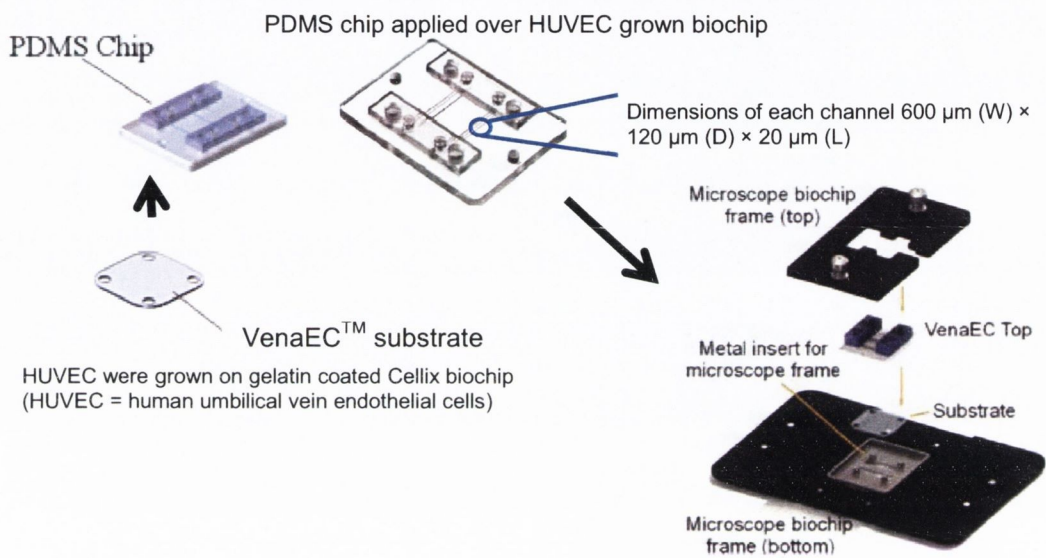
Figure 2.5: Assembly of VenaEC™ biochip on microfluidic platform.
Image shows dimensions and assembly of VenaEC™ biochip.

For nanoparticle uptake study, the HUVEC were activated with TNF-α at a final concentration of 10 ng/ml for 12 h. Before the start of the experiment, the nucleus was stained with Hoechst (1: 1000 from stock of 1mg/ml) for 5 minutes. After washing the cells with medium, endothelial monolayer was exposed to NPs suspended in PBS under 0.5, 1 or 5 dynes/cm^2 shear stress for 20 minutes using a Mirus[TM] Nanopump. Cells not treated with TNF-α were taken as control. Live images of endothelial cells were taken with 20x objective from at least three fields in each channel. Afterwards, the images were integrated to high content analysis platform using *IN Cell Translator Software* (GE Heathcare, UK). Briefly, the software converts the images taken from "each field" to simulate as if they were taken from "each well" of a 96 well plate. The QD-uptake in HUVEC was then

quantified using *IN Cell investigator software* (GE Heathcare, UK). An example is shown in Figure 2.6.
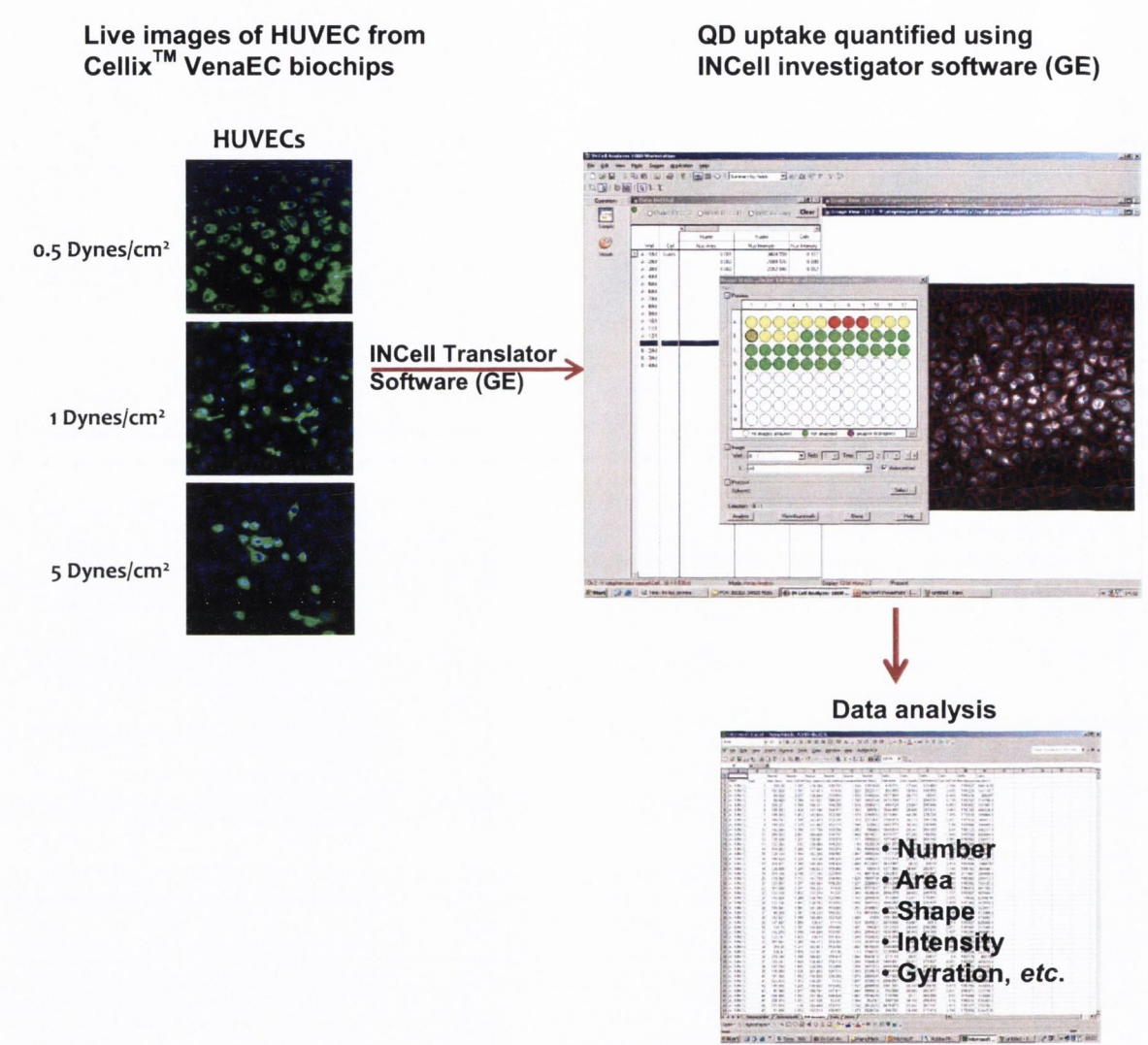
Figure 2.6: Quantification of nanoparticle uptake in live HUVEC under flow by high content analysis.
Left panel show live images taken from channels in Cellix™ chips. The images were converted to 'image. xdce' file format by INCell translator software (GE Health care) and then the nanoparticle uptake quantified using INCell investigator software (GE Health care). Images in the right panel display an example of the analysis procedure.

2.12 Confocal microscopy

2.12.1 Staining protocol for the visualization of platelet activation markers P-selectin and GPIIb-IIIa on platelet aggregates from aggregometry

For the study of surface expression of platelet activation markers, QDs induced washed platelet aggregates were taken from the aggregometer at 50% aggregation. After removal of the releasates by centrifugation, the aggregates were washed with PBS and then treated with fluorescein isothiocyanate (FITC) or APC conjugated P-selectin antibody, or FITC or APC conjugated PAC-1 antibody (against GPIIb-IIIa receptors) for 30 minutes at room temperature in the dark. The aggregates were then fixed with 2% paraformaldehyde (PFA) for 30 minutes at room temperature, stained with Alexa Fluor® 546 phalloidin actin (red) or Alexa Fluor® 488 phalloidin actin (green) (1:200 dilution) for 1 hour at room temperature, and allowed to air dry on a glass slide. Samples on the glass slide were then covered with a cover slip using mounting medium. For the study of resting platelets, platelets were treated in suspension and mounted on a glass slide afterwards. In both cases, confocal images were taken using a 63x oil immersion objective, with a numerical aperture (Numerical aperture of an optical system is a number that characterizes the range of angles over which the system can accept or emit light) of 1.4, on a Zeiss LSM 510 Meta system (Carl Zeiss, Jena, Germany). The samples were excited using 488nm and 561nm and emission filters of band-pass 505-550nm and long-pass 575nm, respectively.

2.12.2 Staining protocol for the platelets adhered on Q-Sense™ E$_4$ crystals

For the study of activated platelets, PRP was perfused on fibrinogen-coated PC-quartz crystals for 30 minutes. Afterwards the crystals were placed in 24-well plate and washed three times with PBS. The aggregates were then fixed with 2% PFA for 30 minutes at room temperature. Samples were then stained with Alexa Fluor® 546 phalloidin actin or Alexa Fluor® 488 phalloidin actin (1:200 dilution) for 1 hour at room temperature. Crystals were then mounted on glass slides (with the platelets facing upwards) using mounting medium. The platelets were covered with a cover slip using mounting medium and left at 4 °C overnight before imaging. Confocal images were taken using a 63x oil immersion objective, with a numerical aperture of 1.4, on a Zeiss LSM 510 Meta system (Carl Zeiss,

Jena, Germany). The samples were excited using 488nm and 561nm and emission filters of band-pass 505-550nm and long-pass 575nm, respectively.

2.12.3 Staining protocol for endothelial cells cultured on acrylic substrates

For the study of localization of NPs in HUVEC under static and shear stress conditions, HUVEC were seeded on 0.2% gelatin coated acrylic substrates (Cellix Ltd) at a concentration of 433,000 cells per substrate. After the cells have reached at least 80% confluence (in 24 hours), they were exposed to NPs under controlled shear stress conditions. The cells were then fixed with 3% paraformaldehyde for 30 minutes at room temperature. After washing the cells with PBS for three times, cells were stained with Alexa Fluor® 546 phalloidin actin or Alexa Fluor® 488 phalloidin actin (1:200 dilution) and Hoechst (1:800 of 1μg/ml stock) for 1 hour at room temperature. Substrates were then mounted onto glass slides (with cells facing upwards) and covered with glass cover slips using mounting medium. After leaving the samples at 4 °C for 24 h, confocal images were taken using a 63x oil immersion objective, with a numerical aperture of 1.4, on a Zeiss LSM 510 Meta system (Carl Zeiss, Jena, Germany). The samples were excited using 488nm and 561nm and emission filters of band-pass 505-550nm and long-pass 575nm, respectively.

2.13 Atomic Force Microscopy (AFM)

AFM is a highly sensitive technology and is not limited by diffraction limit of light. It is a non-invasive technique and does not use fluorescence. It can be used to visualize details of sample surface and underlying cytoskeleton. It consists of an AFM probe, laser beam and XYZ scanning stage. The trajectory of the scanning tip corresponds to the topography of the sample.

2.13.1 Protocol for analysis of platelets adhered on Q-Sense™ E₄ crystals

For the analysis of adhered platelets on quartz crystals, PRP was perfused through the Q-Sense device for 30 minutes. Afterwards, samples were fixed using pre-warmed 2.5% gluteraldehyde for 30 minutes at 37 °C. Platelets were then dehydrated through ascending grades of ethanol (60% for 20 minutes, 80% for 20 minutes, 90% for 20 minutes and finally 100% for 30 minutes repeated once). Crystals were then mounted onto glass slides with the

platelets facing upwards. The crystal-on-slide was mounted onto the microscope and clipped down to ensure no movement during acquisition. Images were then taken using an Ntegra Spectra (NT-MDT, Russia) AFM/Raman system. Imaging was carried out in dry-phase, semi-contact AFM with a silicon-nitride tip (NSG10, Golden silicon probes). The resonance frequency of the tip was found to be 280 KHz. Height AFM images were taken around the central area of the crystal, at 0.55Hz. Image analysis was carried out on the height images using the Nova software.

2.13.2 Protocol for analysis of endothelial cells on acrylic substrates

For investigating the effect of shear stress on nanoparticle uptake and endothelial cell topography, HUVEC were seeded on 0.2% gelatin coated acrylic substrates (Cellix Ltd) at a concentration of 85,000 cells per substrate. After the cells have reached 50% confluence in 24 hours, the cells were exposed to NPs under controlled shear stress conditions. Cells were then fixed with pre-warmed 2.5% glutaraldehyde for 30 minutes at 37 °C. After washing the samples with PBS for three times, the cells were left in DH_2O for liquid phase imaging or dehydrated through ascending grades of ethanol, (60% for 20 minutes, 80% for 20 minutes, 90% for 20 minutes and finally 100% for 30 minutes repeated once) for dry phase imaging. The substrates were mounted on glass slides with the cells facing upwards. AFM images were taken using an Ntegra Spectra (NT-MDT, Russia), AFM/Raman system. The substrate-on-slide was mounted onto the microscope and clipped down to ensure no movement during acquisition. Imaging was carried out in dry-phase or liquid-phase, semi-contact AFM with a silicon-nitride tip (NSG10, Golden silicon probes). The resonance frequency of the tip was found to be 280 KHz. Height AFM images were taken around the central area of the crystal, at 0.55Hz. Image analysis was carried out on the height images using the Nova software.

2.14 Transmission electron microscopy

Samples of washed platelets were treated with 3µM concentration of negatively charged 2.7 or 4.6 nm QDs. The aggregatory reaction was stopped with pre-warmed 2.5% glutaraldehyde when platelets reached 20% aggregation and left for 30 minutes at 37 °C Platelet aggregates were centrifuged and processed for transmission electron microscopy. Untreated (resting) platelets and platelets treated with collagen were taken as controls.

71

After removal of the releasates by centrifugation, the platelet pellets were washed with PBS and left in same for TEM imaging later.

2.15 High Content Analysis

HUVEC cells were seeded in 96-well plates (2000cells/well), exposed to various concentrations of NPs at 37 °C and 5% CO_2, washed with PBS and fixed in 3% paraformaldehyde. Cells were fluorescently stained with Alexa Fluor 488 phalloidin or Alexa Fluor® 546 phalloidin to visualize the cellular morphology and Hoechst to visualize the nuclei. Plates were scanned (five randomly selected fields/well) using an automated microscope IN Cell Analyzer 1000 (GE Healthcare, UK). Quantitative estimations of cell number and fluorescence intensity of the acquired images were performed with IN Cell Investigator software using multi-parameter cytotoxicity bio-application module (GE Healthcare, UK). The workflow is shown in Figure 2.7.
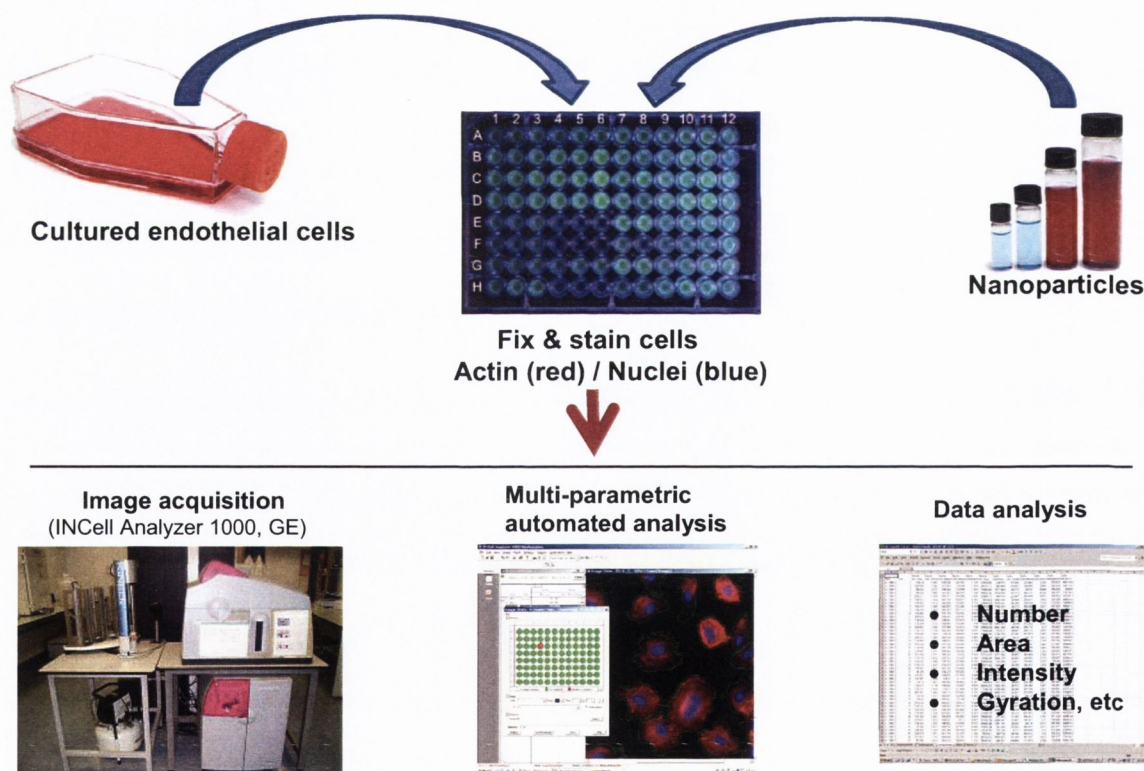
Figure 2.7: High content analysis platform.
The upper pane shows the treatment of HUVEC with NPs and lower panel shows multi-parametric analysis using high content analysis platform.

2.16 Statistical analysis

Statistical significance was performed using analysis of variance (ANOVA) technique using GraphPad Prism 5 software. Dunnett's or Tukey-Kramer's or Bonferroni multiple comparisons post-test were performed, where appropriate. Statistical significance was considered when $P < 0.05$. All data points represent mean values of at least three experimental replicates±SEM.

Chapter 3

Interaction of nanoparticles with human platelets

Chapter 3

3.1 Introduction

Nanoparticle based therapeutic applications has the potential to interact with platelets. Platelets are small, discoid shaped, anucleate cell elements of size between 1.5 to 3 micrometers. On activation, they become more spherical with pseudopodia, and releases pro-coagulant mediators from α-granules (GPIIb-IIIa, P-selectin, fibrinogen, vWF, etc.) and dense granules (ADP or ATP, calcium etc.). GPIIb-IIIa and P-selectin, expressed on the surface of platelets, represent important platelet activation markers (Joseph et al., 1998). Platelet activation causes the translocation of MMP-2, a pro-coagulant gelatinase, from the cytosol to the extracellular space (Sawicki et al., 1998). Platelets are involved physiologically in primary haemostasis, and pathologically in thrombosis. Although platelets serve an important role in control of bleeding, hyperactivity would lead to thrombosis and disease (Shrivastava et al., 2009).

The effect of NPs on the human body, in particular the physiological responses of platelets to NPs, has been less well-studied (Koziara et al., 2005a, Nemmar et al., 2005, Nemmar et al., 2003c, Radomski et al., 2005, Seaton et al., 1999, Shrivastava et al., 2009, Stevens et al., 2009a). No comprehensive systematic study evaluating the effects of engineered silica, magnetite, and QDs on human platelets has been conducted so far. Therefore, the effects of NPs on human platelet function were investigated *in vitro*. For this study, NPs with a range of size, charge and chemical composition was selected. Negatively charged silica (5 nm), magnetite (9 nm), silica coated magnetite (51 nm) NPs, and negatively or positively charged CdTe QDs (2.5, 2.8, 5) were used.

The aim of this part of the study was to investigate the influence of NPs on platelet function under static and flow conditions. To achieve this aim, the specific objectives were:

1. Investigation of interaction of QD and silica- or magnetite- based NPs on human platelets with platelet rich plasma and washed platelets by optical aggregometry.

2. Examination of QD-induced GPIIb-IIIa and P-selectin expression on platelet surface by flow cytometry and confocal microscopy.

3. Detection of QD-induced MMP-2 release from activated platelets by gelatin zymography.

4. Investigation of the influence of QD surface charge on platelet activation.

5. Ultra-structural (TEM) study of QD-induced platelet aggregates for localization of QDs.

6. Investigation of the influence of QDs on flow induced platelet adhesion using Cellix[TM] microfluidic platform and Q-Sense Quartz Crystal Microbalance system.

3.2 Results

3.2.1 Effect of nanoparticles on platelet function

Light aggregometry is the gold standard assay for platelet function studies (Born, 1962). The method records changes in the light transmission of a stirred platelet suspension as platelet aggregates are forming. The influence of NPs on the aggregation processes in platelet rich plasma (PRP) and washed platelets was assessed by optical aggregometry for 20 minutes. Aggregation was determined based on changes in the light transmission through the sample.

Incubation of negatively charged 5 nm silica (Figure 3.1), 51 nm silica coated magnetite (Figure 3.2), or 9 nm citrate stabilized magnetite (Figure 3.3) NPs did not induce platelet activation in PRP (a) or washed platelets (b).

The ability of positively charged 2.8 nm CdTe QDs to induce aggregation in human platelets was studied (Figure 3.4). The QDs did not cause significant activation of platelets in PRP (a) with 0.1, 1, 3, and 5μM concentrations. However, in washed platelets (b) a significant increase in aggregation was observed with 1, 3 and 5 μM concentrations compared to untreated platelets.

Resting platelets were incubated with negatively charged 2.5 or 5 nm CdTe QDs up to 5μM concentration (Figure 3.5). Negatively charged 2.5 and 5 nm CdTe QDs did not show significant effect on platelets in PRP (a) with 0.1, 1, 3, and 5μM concentrations. However, with washed platelets (b) 1, 3, and 5μM concentrations induced significant platelet aggregation compared to resting platelets.

The observed data showed that the silica and magnetite-based NPs did not induce aggregation of platelets. However, the examination of platelet function with CdTe QDs showed that both the positively and negatively charged QDs caused activation of platelets in the absence of plasma proteins. In contrast, the presence of plasma abrogates activation of platelets
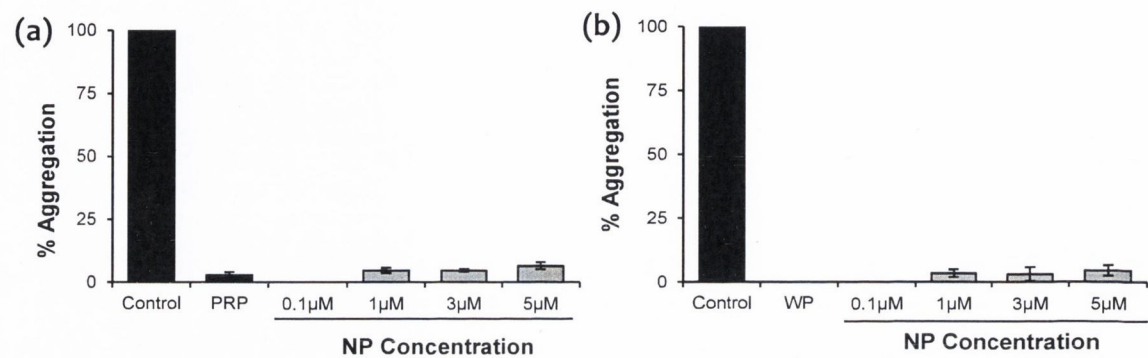
Figure 3.1: Effect of negatively charged (-33 mV) 5 nm size silica NPs on platelet function. Platelet rich plasma (PRP) and washed platelets (WP) were treated with various concentrations of the negative charged 5nm silica NPs in the optical aggregometer. Collagen treated platelets were taken as positive control (Control) and untreated platelets were taken as negative control (PRP/WP). Platelet aggregation with PRP **(a)** or WP **(b)** was recorded. Experiments were repeated with five healthy donors. Data are mean ± SEM of five independent experiments.
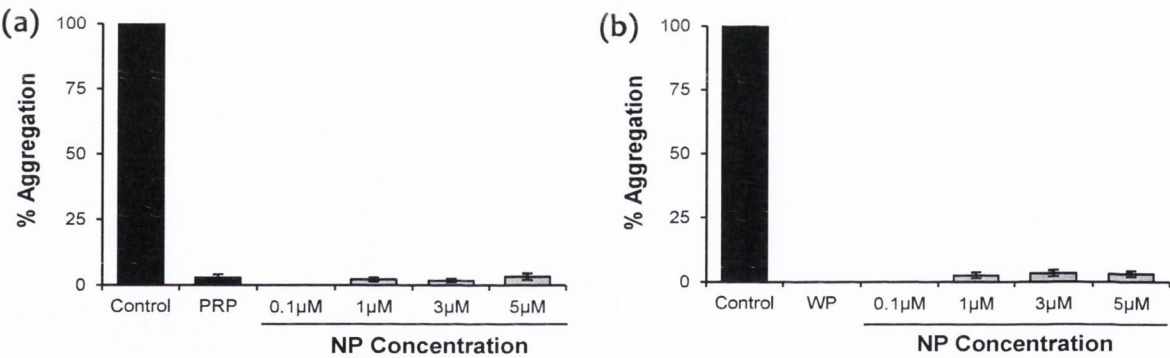
Figure 3.2: Effect of negatively charged (-40.5 mV) 51 nm size silica coated magnetite NPs on platelet function. Platelet rich plasma (PRP) and washed platelets (WP) were treated with various concentrations of the negative charged 51 nm size silica coated magnetite NPs in the optical aggregometer. Collagen treated platelets were taken as positive control (Control) and untreated platelets were taken as negative control (PRP/WP). Platelet aggregation with PRP **(a)** or WP **(b)** was recorded. Experiments were repeated with five healthy donors. Data are mean ± SEM of five independent experiments.
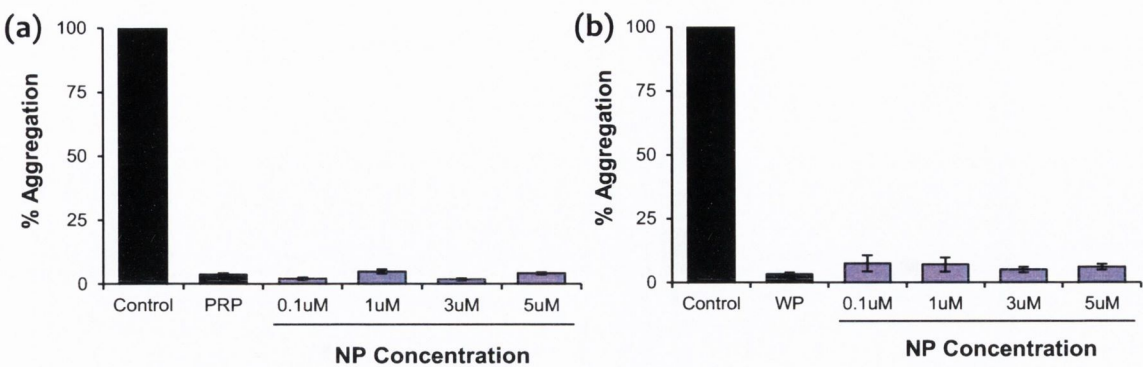
Figure 3.3: Effect of negatively charged (-48.2 mV) 9 nm size citrate stabilized magnetite NPs on platelet function. Platelet rich plasma (PRP) and washed platelets (WP) were treated with various concentrations of the negative charged 9 nm size citrate stabilized magnetite NPs in the optical aggregometer. Collagen treated platelets were taken as positive control (Control) and untreated platelets were taken as negative control (PRP/WP). Platelet aggregation with PRP **(a)** or WP **(b)** was recorded. Experiments were repeated with five healthy donors. Data are mean ± SEM of five independent experiments.
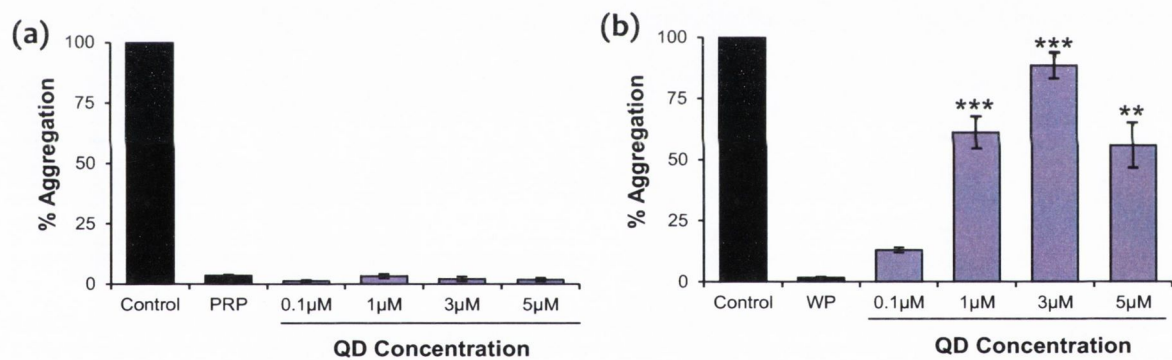
Figure 3.4: Effect of positively charged (+30 mV) 2.8 nm size CdTe QDs on platelet function. Platelet rich plasma (PRP) and washed platelets (WP) were treated with various concentrations of the positively charged 2.8 nm CdTe QDs in the optical aggregometer. Collagen treated platelets were taken as positive control (Control) and untreated platelets were taken as negative control (PRP/WP). Platelet aggregation with PRP (a) or WP (b) was recorded. Experiments were repeated with five healthy donors. Data are mean ± SEM of five independent experiments. ** p < 0.01, and ***p < 0.001 vs WP (ANOVA with Dunnett's) .
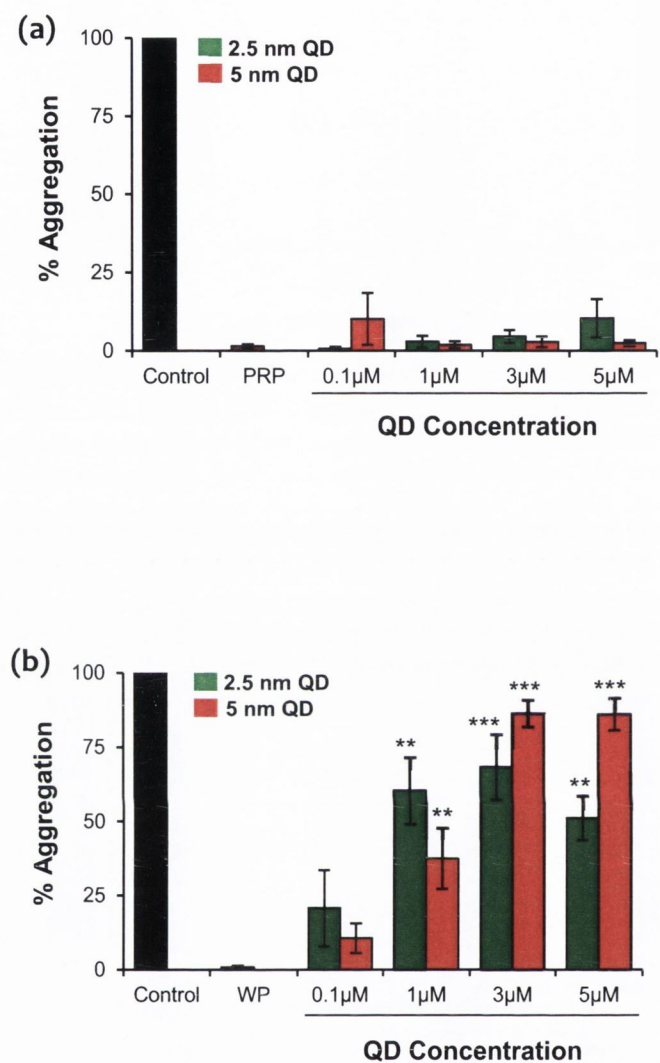
Figure 3.5: Effect of negatively charged 2.5 (-20±5 mV) and 5 (-26±10 mV) nm size CdTe QDs on platelet function. Platelet rich plasma (PRP) and washed platelets (WP) were treated with various concentrations of the negatively charged 2.5 and 5 nm size CdTe QDs in the optical aggregometer. Collagen treated platelets were taken as positive control (Control) and untreated platelets were taken as negative control (PRP/WP). Platelet aggregation with PRP **(a)** or WP **(b)** was recorded. Experiments were repeated with five healthy donors. Data are mean ± SEM of five independent experiments. ** $p < 0.01$ and ***$p < 0.001$ vs WP (ANOVA with Dunnett's).

3.2.2 Effect of QDs on platelet receptors

Platelet activation is associated with the surface abundance of receptors that play an important role in adhesion, aggregation and platelet-leukocyte aggregation. Flow cytometry and confocal microscopy were used to study the surface expression of these receptors on QD-treated platelets in samples of PRP and washed platelets.

Flow cytometry results are shown in Figure 3.6. Treatment of PRP samples (a) with QDs did not show significant increase in P-selectin expression compared to untreated platelets. However, samples of washed platelets (b) showed a significant increase in P-selectin expression when treated with 1 and 5μM concentrations of QDs. QDs are exceptionally bright and photostable. Hence, platelet aggregates were studied by confocal microscopy to visualize the QDs and platelet activation markers (GPIIb-IIIa and P-selectin). Samples of platelet aggregates were taken from aggregometry and treated with respective antibodies. After fixing and staining the actin, samples were mounted on glass slides and subjected to confocal microscopy. Untreated and collagen treated platelets (stained for actin) were taken as negative and positive controls respectively. Actin fibers were not stained in QD-induced platelet aggregates. The confocal images (maximal projection) demonstrating the expressions of P-selectin and GPIIb-IIIa receptors are shown in Figure 3.7 and Figure 3.8respectively. The Resting platelets did not express P-selectin receptors (Figure 3.7). However, minimal expression of GPIIb-IIIa (Figure 3.8) receptors was observed. Confocal images (maximal projection) demonstrate that collagen, and both 2.5 and 5 nm CdTe QD-induced platelet aggregates resulted in increased expression of P-selectin (Figure 3.7) and GPIIb-IIIa (Figure 3.8) receptors.
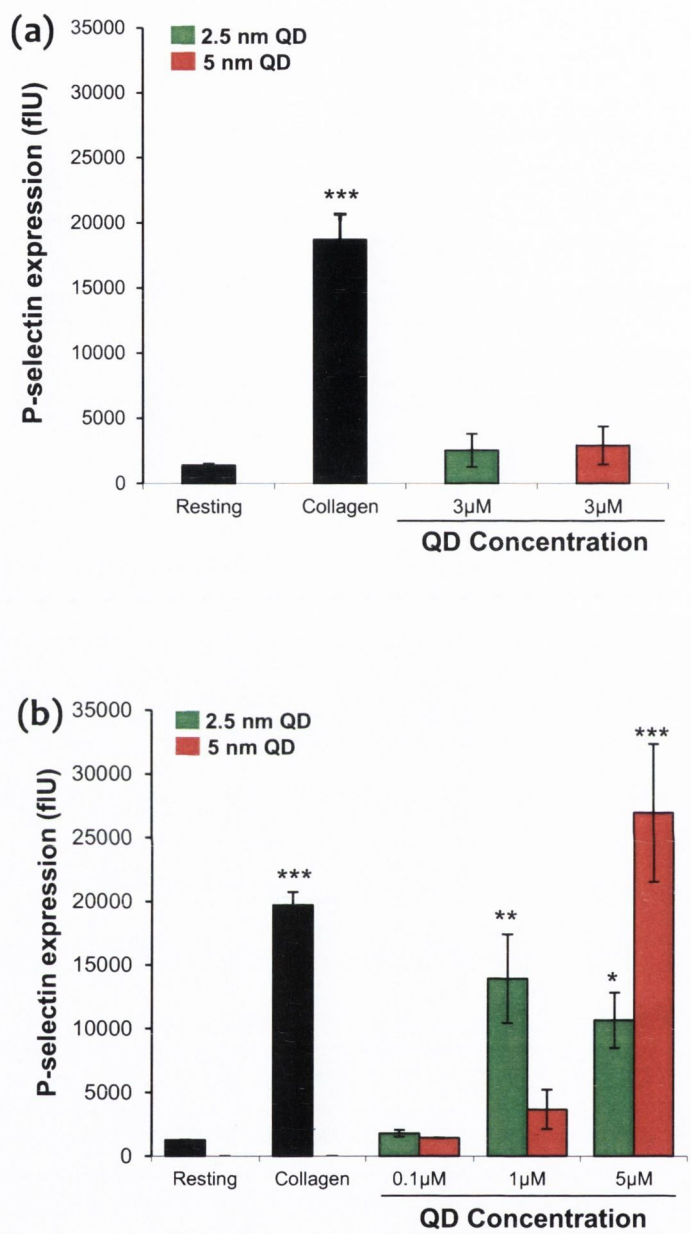
Figure 3.6: Effect of negatively charged 2.5 and 5 nm size CdTe QDs on P-selectin adhesion receptor. Platelet rich plasma (PRP) and washed platelets (WP) were treated with various concentrations of the negatively charged 2.5 and 5 nm size CdTe QDs in the optical aggregometer. Samples from aggregometer were treated with P-selectin antibodies, and the P-selectin expression was measured by flow cytometry. Collagen treated platelets were taken as positive control (Collagen) and untreated platelets were taken as negative control (Resting). Data are mean ± SEM of three independent experiments. * $p < 0.05$, **$p < 0.01$ and ***$p < 0.001$, treatments versus resting platelets (ANOVA with Dunnett's).
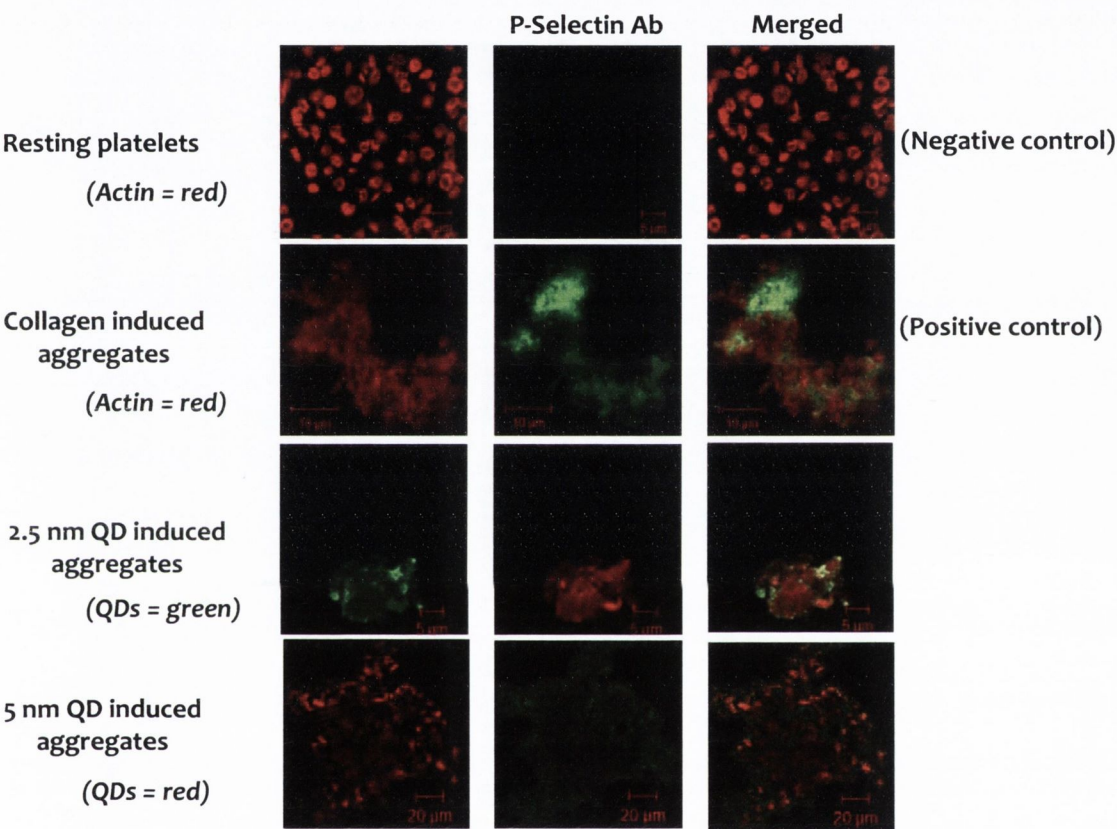
Figure 3.7: Effect of negatively charged 2.5 and 5 nm size CdTe QDs on on P-selectin receptors. Washed platelets (WP) were treated with 3μM concentration of the negatively charged 2.5 and 5 nm size CdTe QDs in the optical aggregometer. Samples from aggregometer were treated with P-selectin antibodies, and the P-selectin expression visualized by confocal microscopy. Collagen induced aggregation was taken as positive control and untreated (Resting) WP were taken as negative control. Images are representative of three independent experiments.
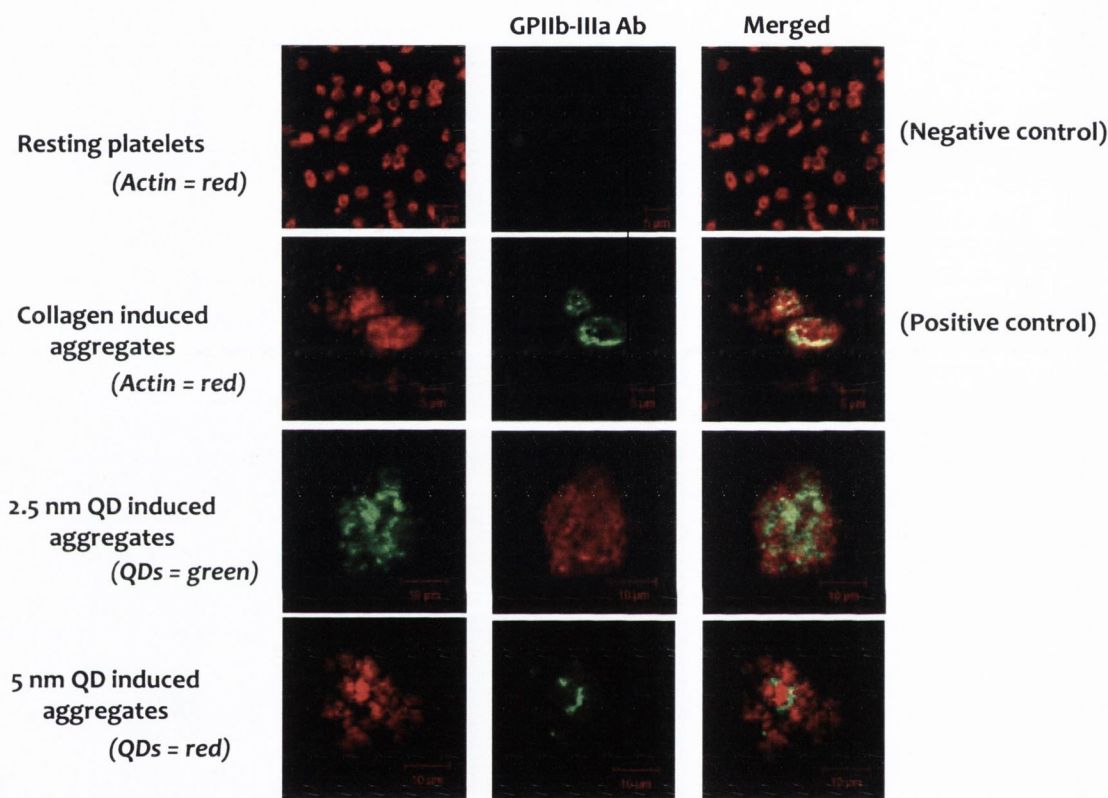
Figure 3.8: Effect of negatively charged 2.5 and 5 nm size CdTe QDs on on GPIIb-IIIa receptors. Washed platelets (WP) were treated with 3µM concentration of the negatively charged 2.5 and 5 nm size CdTe QDs in the optical aggregometer. Samples from aggregometer were treated with GPIIb-IIIa antibodies, and the GPIIb-IIIa expression visualized by confocal microscopy. Collagen induced aggregation was taken as positive control and untreated (resting) WP were taken as negative control. Images are representative of three independent experiments.

3.2.3 Effect of QDs on matrix metalloproteinase (MMP-2) release

Platelets contain and release MMP-2, a gelatinase which acts as stimulator of aggregation. Zymography was used to detect the release of MMP-2 by negatively and positively charged CdTe QDs activated platelets. The zymograms obtained with QD-induced platelet releasates are shown in Figure 3.9.

Zymograms showed gelatinolytic bands due to the presence of MMP-2 in platelet releasates. Releasates obtained from samples of washed platelets treated with negatively charged 2.5 or 5 nm QDs (a), and 2.8 nm positively charged QDs (b) showed increased gelatinolytic activity when compared to releasates from untreated platelets.
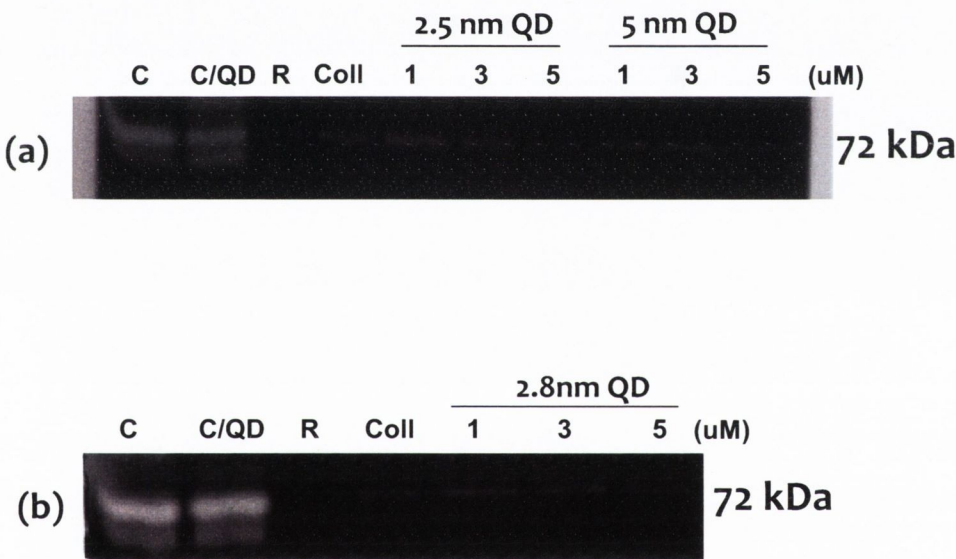
Figure 3.9: Zymography of releasates form negatively charged 2.5 and 5 nm CdTe QDs and positively charged 2.8 nm CdTe QDs . MMP-2 gelatinase activity in the releasates of negatively charged QDs (a), and positively charged QDs (b). **Lanes** (C): Releasates from HT1080 cells was used as a loading control; (C/QD): Loading control with 3μM QD; (R): Unaggregated resting platelets were considered as controls; (Coll) Releasate from collagen induced platelet aggregates; 1: releasate from platelets treated with 1μM QD; 3: releasate from platelets treated with 3μM QD; 5: releasate from platelets treated with 5μM QD. Zymograms are representative of zymography experiments carried out with samples from three different donors.

3.2.4 Effect of surface charge of QDs on platelet activation

The surface charge influences the nanoparticle's interaction with cells and biomolecules. There is evidence that the surface charge may be critical in determining the degree and the mechanism of platelet activation (Koziara et al., 2005a, Li et al., 2009, McGuinnes et al., 2011, Miyamoto et al., 1989, Miyamoto et al., 1990). Therefore, the influence of the negative charge on the surface of negatively charged CdTe QDs was studied on samples of human PRP and washed platelets.

For this study, samples of PRP and washed platelets were treated with 0.1, 1, 3, or 5 μM concentrations of negatively charged 2.7 (-20 mV) or 4.9 (-40 mV) nm CdTe QDs in the aggregometer. The samples were collected after the platelet aggregation had reached a plateau and the zeta potential was measured. Untreated platelet samples and collagen induced aggregates were taken as negative and positive controls respectively. The zeta potential of plasma, collagen, stock QDs, and QDs resuspended in Tyrode's salt solution (used for dilution of PRP and washed platelets) to a final concentration of 0.1, 1, 3, or 5 μM was also measured for comparison. The average zeta potential measurements of three different donors are shown. With samples of PRP (Figure 3.10), no significant difference was observed between untreated and collagen treated PRP. However, a significant reduction in the zeta potential of the plasma was observed compared to untreated PRP. No significant difference was observed in the zeta potential of PRP samples treated with 0.1 or 1 μM CdTe QDs compared to untreated sample. However, there was a significant reduction in the zeta potential of PRP samples treated with 3 or 5 μM of 4.9 nm CdTe QDs compared to untreated PRP. Zeta potential of PRP treated with QDs was significantly lower than the zeta potential of Tyrode's salt solution treated with QDs in all the concentrations used. With samples of washed platelets (Figure 3.11), no significant difference was observed between untreated and collagen treated samples. With both the QDs types used, no significant difference was observed between untreated and QD-treated washed platelets. However, the zeta potential of washed platelets treated with QDs was significantly lower than the zeta potential of Tyrode's salt solution treated with QDs in all the concentrations used, similar to the PRP samples.
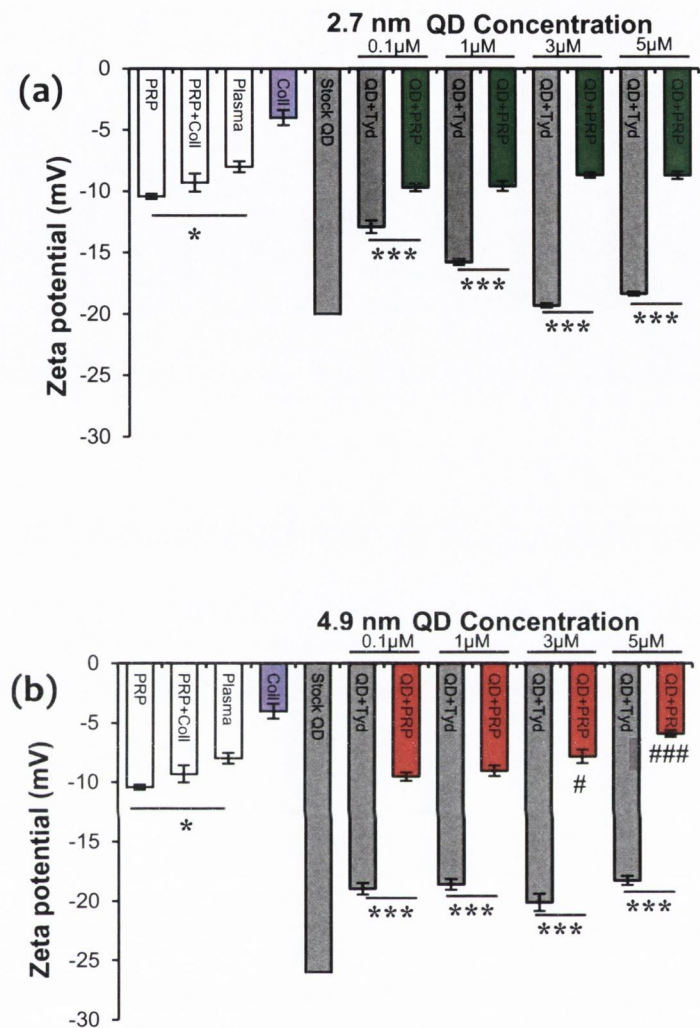
Figure 3.10: Effect of surface charge of negatively charged 2.7 (-20 mV) and 4.9 (-40 mV) nm size CdTe QDs on platelet function in PRP samples. Platelet rich plasma (PRP) samples were treated with various concentrations of the negatively charged 2.7 (a) and 4.9 (b) nm size CdTe QDs in the optical aggregometer. Collagen treated platelets were taken as positive control (PRP+Coll) and untreated platelets were taken as negative control (PRP). Zeta potential of Collagen (Coll), plasma, stock QD, QD suspended in Tyrode's salt solution (QD+Tyd) were also measured. Zeta potential of PRP and WP treated with QDs were recorded. Experiments were repeated with three healthy donors. Data are mean ± SEM of three independent experiments. *p < 0.5, ***p<0.01(ANOVA with Tukey's); #p < 0.05, ###p < 0.001 vs PRP (ANOVA with Dunnett's).
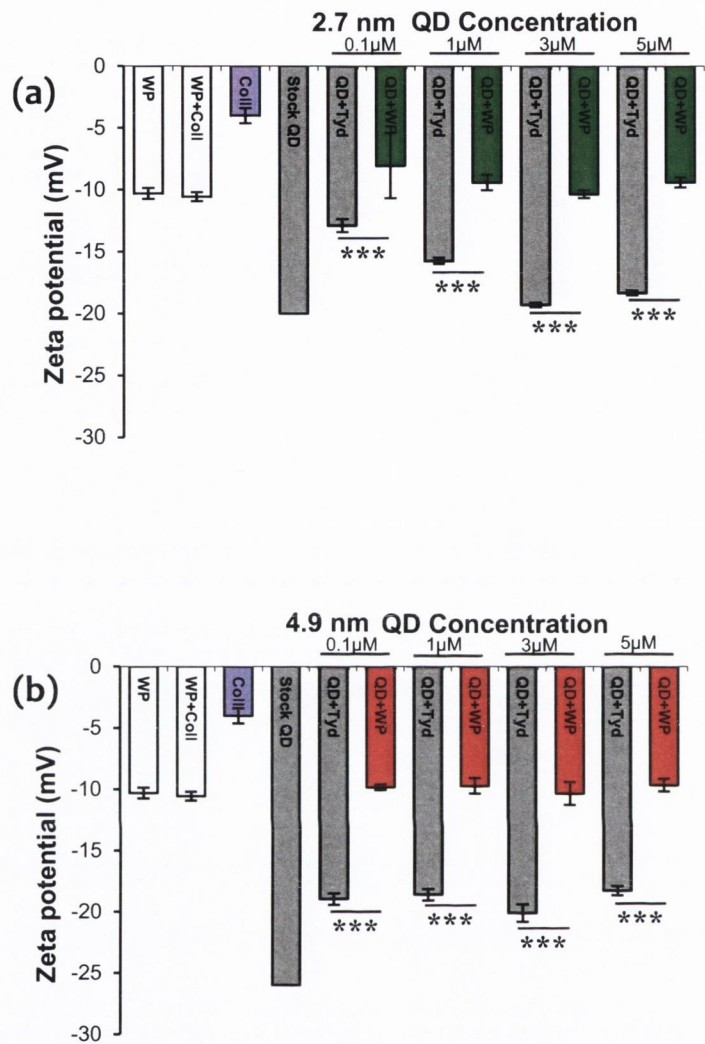
Figure 3.11: Effect of surface charge of negatively charged 2.7 (-20 mV) and 4.9 (-40 mV) nm size CdTe QDs on platelet function in washed platelets. Washed platelet (WP) samples were treated with various concentrations of the negatively charged 2.7 (a) and 4.9(b) nm size CdTe QDs in the optical aggregometer. Collagen treated platelets were taken as positive control (WP+Coll) and untreated platelets were taken as negative control (WP). Zeta potential of Collagen (Coll), plasma, stock QD, QD suspended in Tyrodes buffer (QD+Tyd) were also measured. Zeta potential of PRP and WP treated with QDs were recorded. Experiments were repeated with three healthy donors. Data are mean ± SEM of three independent experiments. ***p<0.01 (ANOVA with Tukey's).

3.2.5 Ultramicroscopic study of QD-induced platelet-platelet interactions

NPs are beyond the diffraction limit of resolution for conventional optical microscopy (~200 nm) (Gibbs-Flournoy et al., 2011). Therefore, to study closely the structure of QD-induced platelet-platelet interactions, transmission electron microscopy (TEM) was used.

TEM images of platelets are shown in Figure 3.12. Resting platelets (a) did not show any pseudopodia, and the organelles were found to be dispersed throughout the cytoplasm. The microtubules in the resting platelets are localized in the periphery of the platelet. However, collagen treated platelets (b) showed the formation of pseudopodia, and the organelles were concentrated in the centre of the platelet. Both 2.7 nm (c) and 4.6 nm (d) QD-treated platelets showed degranulated intracellular granules and pseudopodia formation, and the QDs were associated with the outer membrane of the activated platelets.
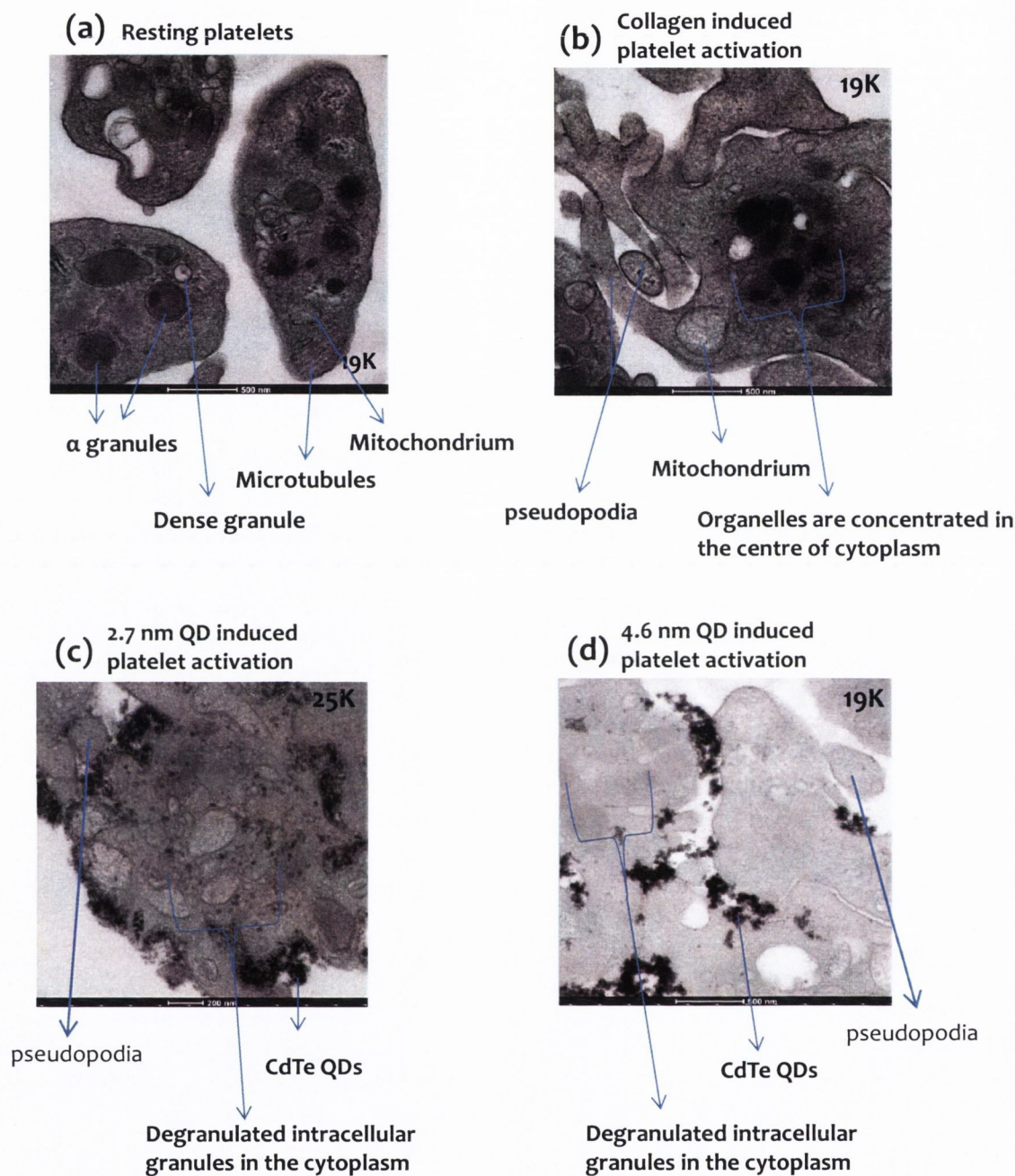
Figure 3.12: Electron microscopy QD-induced platelet aggregates. Washed platelets were treated with 3μM concentration of the negatively charged 2.7 and 4.6 nm size CdTe QDs in the optical aggregometer. Samples were fixed with glutaraldehyde at 20% aggregation in the aggregometer. After washing the platelet aggregates with PBS, the samples were processed and subjected to electron microscopy studies. Untreated resting platelets (a) were taken as negative control and collagen induced aggregates (b) was taken as positive control. 2.7 nm (c) and 4.6 nm (d) QD induced platelet aggregates were shown. Images are representative of three independent experiments.

3.2.6 Effect of QDs on flow induced platelet adhesion

Aggregometry is the gold standard instrument for studying platelet function, but it measures platelet aggregation only under static conditions, and the shear stress is not uniform throughout the glass cuvette. Hence, the platelets experience various levels of shear stress. Aggregometry studies done previously (Section 3.2.1) with various NPs including QDs did not show platelet aggregation in the presence of plasma. Studies have demonstrated nanoparticle-induced platelet activation (Radomski et al., 2005, Stevens et al., 2009a), and thrombus formation in animal models (Nemmar et al., 2005, Radomski et al., 2005). Hence, a more sensitive method is needed to detect the activation of platelets in PRP at the nano scale. Therefore, we investigated the influence of negatively charged 2.5 or 4.9 nm CdTe QDs on flow induced platelet adhesion using PRP or whole blood samples. Since the concentration of 3µM QDs induced maximal aggregation of washed platelets in aggregometry studies, the same concentration was used with PRP and whole blood to study platelet response under flow conditions.

3.2.6.1 Effect of QDs on flow induced platelet microaggregates using a commercially available Quartz Crystal Microbalance

The influence of negatively charged 2.5 nm CdTe QDs on flow-induced platelet micro-aggregation was studied using a commercially available Q-E4 SenseTM system. The results obtained are shown in Figure 3.13. PPP samples treated with QDs did not cause a significant difference in F or D when compared to untreated PPP (a). However, PRP samples treated with QDs caused a significant reduction in frequency and a significant increase in dissipation compared to untreated PRP (b).
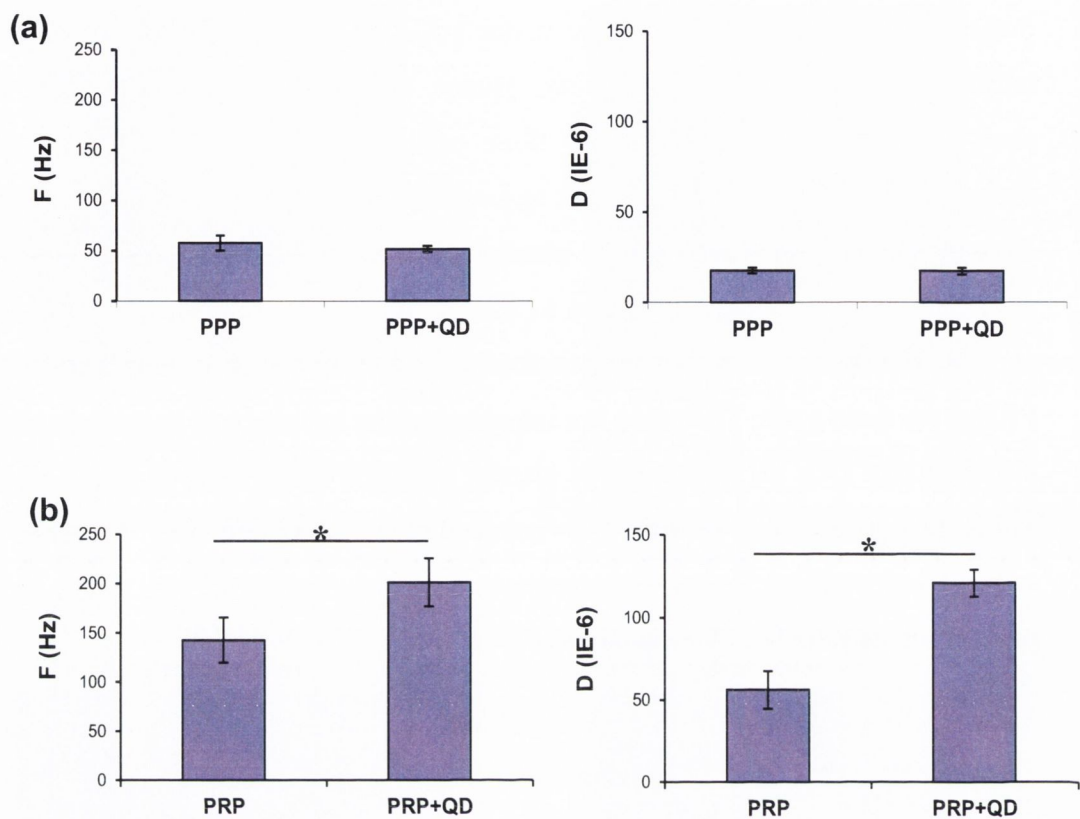
Figure 3.13: Effect of negatively charged 2.5 nm CdTe QDs on flow induced platelet microaggregation. Human platelet rich plasma (PRP) or platelet poor plasma (PPP) was treated with $3\mu M$ concentration of the negatively charged 2.5 nm CdTe QDs and perfused over fibrinogen coated sensors. Frequency (F) and dissipation (D) were recorded in real time. Untreated PRP or PPP were taken as negative control. Frequency and dissipation values obtained from PPP (a) and PRP (b) were shown. Experiments were repeated with four healthy donors. Data are mean $\pm$ SEM of four independent experiments. *$p < 0.05$ vs. PRP (student's t test).

Phase-contrast and atomic force microscopy (AFM) were used to visualize the morphology of flow-induced platelet micro-aggregates formed on the surface of fibrinogen-coated crystals. Phase-contrast images of the platelets adhered on crystals are shown in Figure 3.14 (a). Images showed large platelet aggregates in PRP samples treated with QDs compared to untreated PRP.

For AFM studies, the crystals with platelet micro-aggregates were fixed with glutaraldehyde and dehydrated with ascending grades of ethanol. Dry phase images taken by AFM are shown in Figure 3.14 (b). Image analysis demonstrated the presence of platelet aggregates on crystals perfused with QD-treated PRP samples compared to discrete platelets in crystals perfused with untreated PRP.

(a) Phase contrast microscopy

Platelet rich plasma (PRP)

PRP treated with CdTe QD

Individual platelets

Platelet aggregates

(b) Atomic force microscopy

Platelet rich plasma (PRP)

PRP treated with CdTe QD

Individual platelets

Platelet aggregates

3D

3D
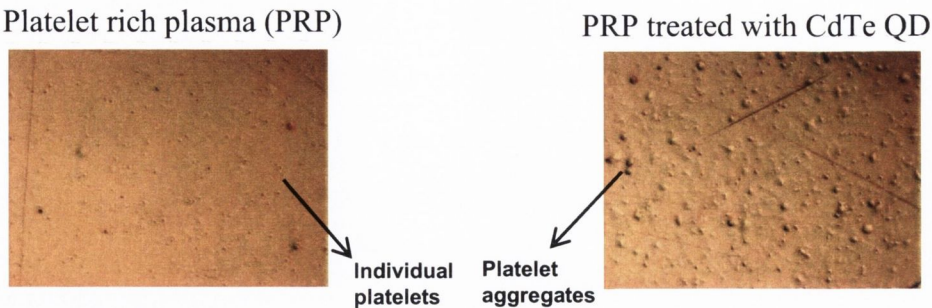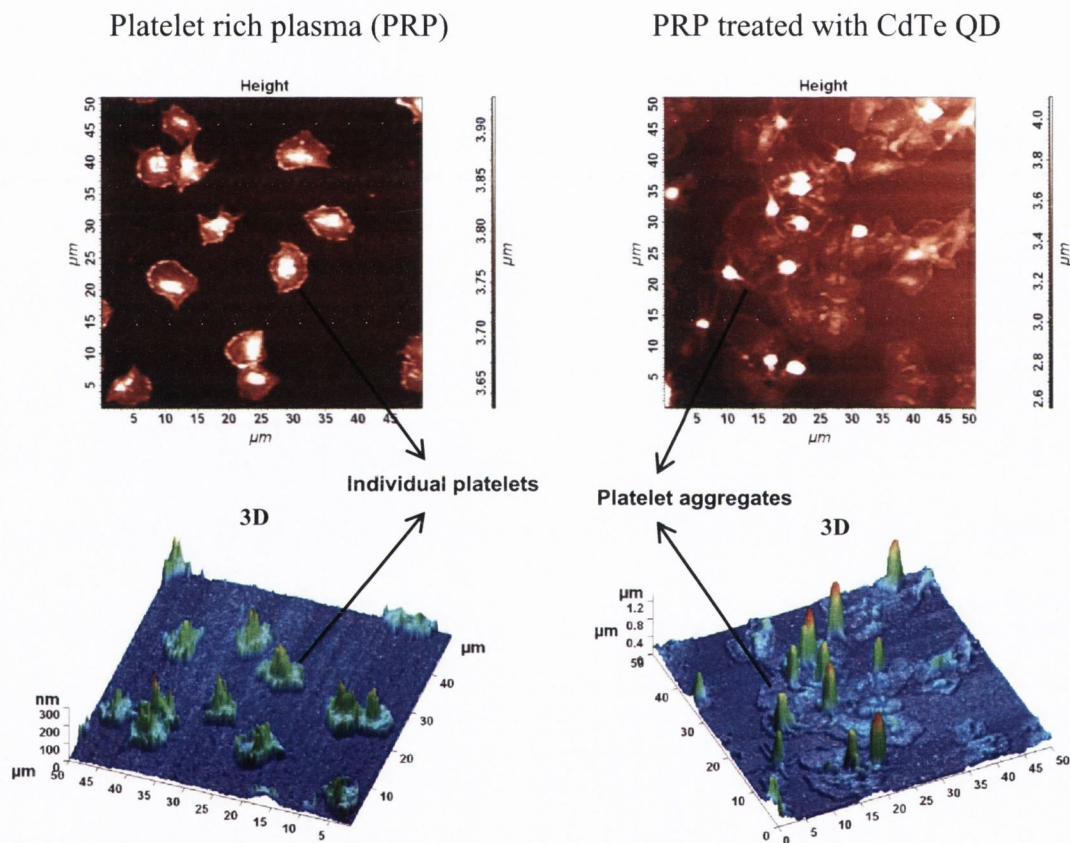
Figure 3.14: Phase-contrast and atomic force microscopic study of negatively charged 2.5 nm CdTe QDs on flow induced platelet micro-aggregates on fibrinogen coated crystals. After measuring the frequency and dissipation, the quartz crystals with adhered platelet micro-aggregates were subjected to phase-contrast (A) or atomic force microscopy (B). Platelet aggregates on crystals perfused with untreated PRP samples were taken as controls. Individual platelets and platelet aggregates were shown (arrows). Three dimensional (3D) images corresponding to height images were shown. Images shown are representative of three independent experiments.

3.2.6.2 Effect of QDs on flow induced platelet adhesion (Whole blood) using Cellix^{TM} microfluidic platform

Platelets are exposed to various hemodynamic forces in the vascular system. The mechanical force most relevant to platelet-mediated haemostasis and thrombosis is shear stress. A physical model that features the flow of whole blood in micro channels coated with proteins of interest resembles a realistic model of the human vascular system. Therefore, the effect of CdTe QDs on flow induced platelet adhesion on channels coated with biologically functional proteins which are involved in primary haemostasis such as collagen, fibrinogen and vWF was studied using Cellix^{TM} microfluidic platforms under various controlled shear stress conditions. For this study, whole blood was treated with 4.9 nm CdTe QDs at a final concentration of $3\mu M$ and perfused through collagen, fibrinogen or vWF coated channels under various shear stress rates.

Figure 3.15 shows the average percentage area covered by platelets (a) and the number of aggregates (b) adhered on collagen coated channels. In shear stress rates of 30 and 45 dynes/cm^2, the platelet adhesion was significantly lower in samples of whole blood treated with QDs compared to untreated samples. There was a significant increase in the percentage area covered by platelets in untreated whole blood with shear stress rates of 30 and 45 dynes/cm^2 compared to 0.5 dynes/cm^2. However, a significant reduction in platelet adhesion was observed in shear stress rates above 45 dynes/cm^2. In results obtained with whole blood samples treated with QDs, the platelet adhesion significantly increased with increasing shear stress rates. However, the platelet adhesion did not significantly reduce with shear stress above 45 dynes/cm^2 as observed in untreated whole blood. An increase in the average number of aggregates was observed with increasing shear stress rates in both the samples studied. However, a significant increase in the number of aggregates was observed with 60 and 90 dynes/cm^2 compared to 45 dynes/cm^2.

The average percentage area covered by platelets (a) and the number of aggregates (b) adhered on fibrinogen coated channels are shown in Figure 3.16. No significant difference in platelet adhesion and number of aggregates was observed with samples of whole blood treated with QDs compared to untreated samples. In experiments done with both untreated or QD- treated whole blood, a significant increase in the adhesion of platelets was observed with shear stress rates of 60 and 90 dynes/cm^2 compared to 0.5

dynes/cm^2. There was no significant difference in the number of aggregates in both the untreated and QD-treated samples.

Figure 3.17 shows the average percentage area covered by platelets (a) and the number of aggregates (b) adhered on vWF coated channels. A significant reduction in platelet adhesion and number of aggregates was observed in samples of whole blood treated with QDs compared to untreated samples. In experiments with untreated whole blood, no significant differences were observed in the area covered by platelets and number of aggregates at higher shear stress rates compared to 15 dynes/cm^2. However, with QD-treated whole blood, a significant increase in platelet adhesion and number of aggregates was observed with shear stress rates of 60 and 90 dynes/cm^2 compared to 15 dynes/cm^2.

Figure 3.15: Platelet adhesion on collagen coated channels under flow conditions. Human whole blood with anticoagulants (citrate and thrombin inhibitors) was treated with 3μM concentration of the negatively charged 4.9 nm CdTe QDs and perfused through coallgen coated Cellix biochips under controlled shear conditions. Platelet adhesion in the channels was imaged in real time. Untreated whole blood was run in parallel for comparison. Platelet adhesion (% area of channels covered by platelets) (a) and number of aggregates (b) obtained from untreated and QD treated whole blood were shown. Experiments were repeated with three healthy donors. Data are mean ± SEM of three independent experiments.***p < 0.001 vs. 0.5 Dynes/cm^2; ##p <0.01 ###p <0.001 vs 45 Dynes/cm^2 (ANOVA with Dunnett's), +++p<0.001(ANOVA with Bonferronis).
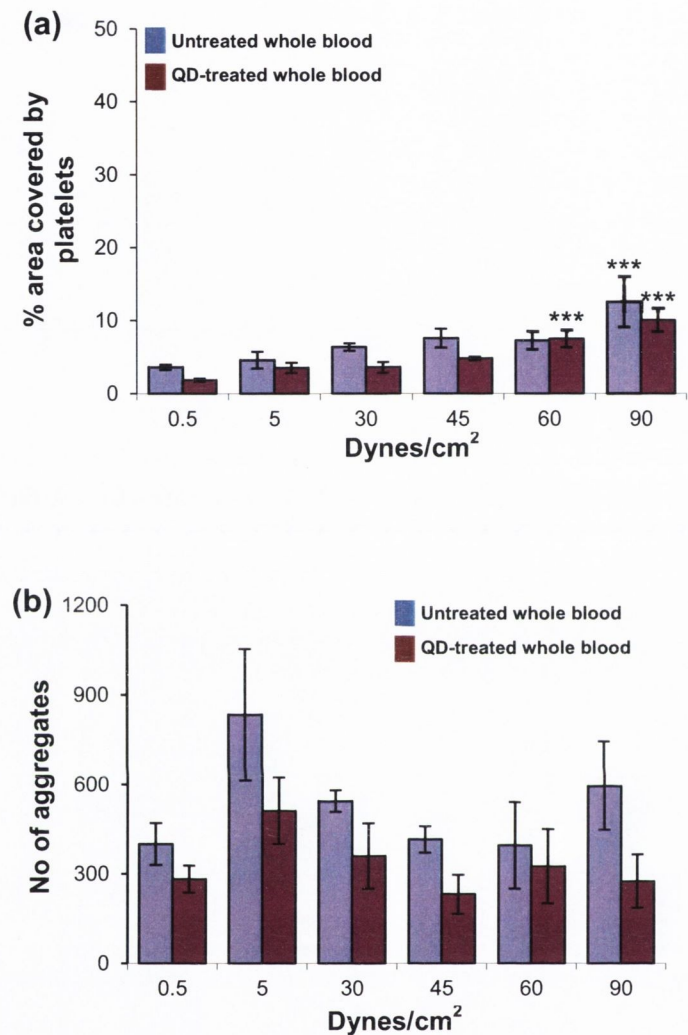
Figure 3.16: Platelet adhesion on fibrinogen coated channels under flow conditions. Human whole blood with anticoagulants (citrate and thrombin inhibitors) was treated with 3μM concentration of the negatively charged 4.9 nm CdTe QDs and perfused through fibrinogen coated Cellix biochips under controlled shear conditions. Platelet adhesion in the channels was imaged in real time. Untreated whole blood was run in parallel for comparison. Platelet adhesion (% area of channels covered by platelets) (a) and number of aggregates (b) obtained from untreated and QD treated whole blood were shown. Experiments were repeated with three healthy donors. Data are mean ± SEM of three independent experiments. ***$p < 0.001$ vs. 0.5 Dynes/cm^2 (ANOVA with Dunnett's).
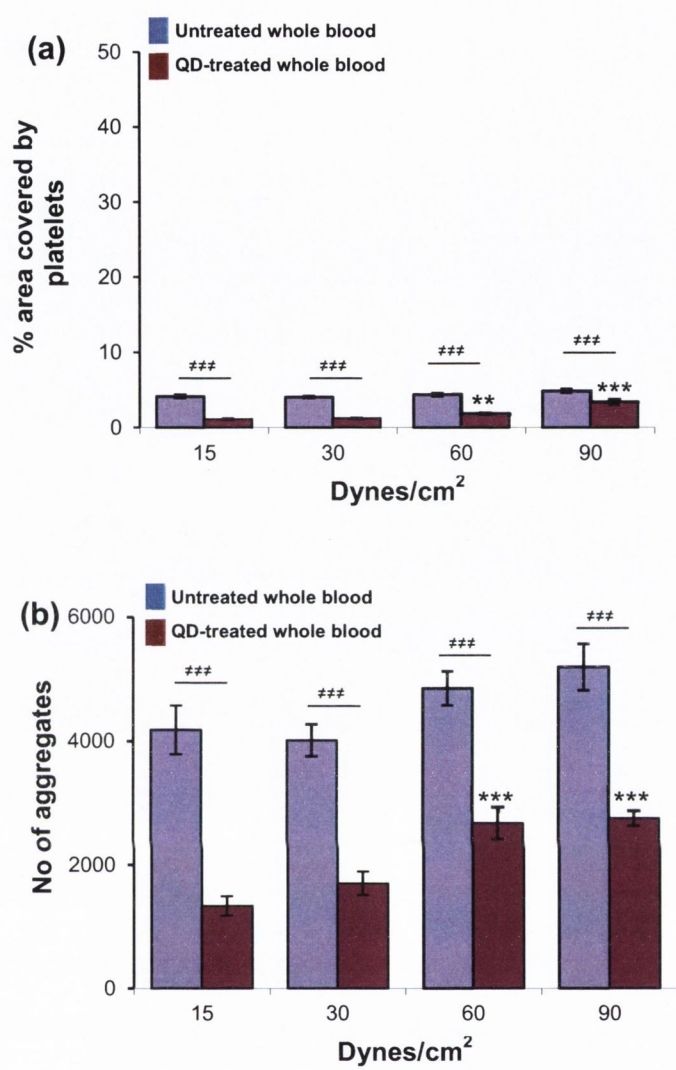
Figure 3.17: Platelet adhesion on vWF coated channels under flow conditions. Human whole blood with anticoagulants (citrate and thrombin inhibitors) was treated with 3μM concentration of the negatively charged 4.9 nm CdTe QDs and perfused through vWF coated Cellix biochips under controlled shear conditions. Platelet adhesion in the channels was imaged in real time. Untreated whole blood was run in parallel for comparison. Platelet adhesion (% area of channels covered by platelets) (a) and number of aggregates (b) obtained from untreated and QD treated whole blood were shown. Experiments were repeated with three healthy donors. Data are mean ± SEM of three independent experiments. **$p < 0.01$, ***$p < 0.001$ vs. 15 Dynes/cm^2 (ANOVA with Dunnett's), ###$p < 0.001$(ANOVA with Bonferroni).

3.3 Discussion

The biological and medical research communities have exploited nanomaterials for various nanomedicine applications. The rapidly developing field of nanomedicine pursues the use of NPs in biomedical applications (e.g., as medical devices, diagnostic devices, contrast agents, components of vaccine formulations, or drug carriers for therapeutic intervention of malignant, inflammatory, viral, neurodegenerative and other types of disorders) (Dobrovolskaia et al., 2008, Kauf et al., 2001). Nanoenabled drug delivery systems are gaining application in the pharmaceutical industry, since nanoparticle-based drugs may have improved solubility, pharmacokinetics, and bio-distribution compared to small molecule drugs (Dobrovolskaia et al., 2008). Nanoparticle-carried drugs can be efficacious at lower doses, may have fewer side effects, and may be used for targeted therapy. Nanomedicine approaches, many of which are designed for systemic administration, has caused concerns regarding their biocompatibility (Koziara et al., 2005b). However, the kinetics and the efficacy of nanoparticle-based intravenous drug delivery platforms may depend on the interactions of the vascular microenvironment with the particles. The NPs, after entering the blood stream, encounter a complex environment of plasma proteins and the cellular components of haemostasis. Thrombogenicity, the propensity of a material to induce blood clotting (a mixture of red blood cells, aggregated platelets, fibrin and other cellular elements), is relevant to the bio-distribution of the NPs. Furthermore, as the circulation half-life of the particles in blood increases, the potential for platelet-nanoparticle interactions will also be increased (Sahli et al., 1997). These interactions may affect the intended application of the nanoparticle, and thus effectively reducing the efficacy of a nanomedicine. As such, understanding nanoparticle haematocompatibility is an important step during the initial characterization of nanomaterials. Also, the potentially different physicochemical properties of NPs pose novel methodological and regulatory challenges. The above effects confer increased importance to the preclinical testing of nanoparticle interaction with the coagulation system.

The influence of silica, magnetite, silica coated magnetite NPs, and negatively and positively charged CdTe QDs on human platelet function in vitro was examined with light aggregometry. With all the particles examined, none of them caused significant aggregation in the PRP. The finding is similar to a previous study done by Geys *et al*. They studied the

prothrombotic effects of negatively charged carboxyl (-35.2mV)- and amine (-14.2 mV)-CdSe/ZnS QDs on mouse using a wide range of doses (3.6 nmol down to 1.44 pmol) (Geys et al., 2008). They speculated that QDs caused pulmonary vascular thrombosis by activating coagulation cascade via contact activation. In addition, they also found that the QDs by themselves did not activate platelets in human PRP samples. This may be due to the adsorption of plasma protein complexes with the NPs in a biological environment resulting in a protein "corona" which determines the biological identity of the nanoparticle (Cedervall et al., 2007a, Cedervall et al., 2007b, Lynch et al., 2007). This dynamic layer of proteins (and other biomolecules) adsorbs to nanoparticle surfaces immediately upon contact with living systems. Studies have demonstrated that the major serum proteins albumin, IgG and fibrinogen were associated with a wide range of particles of seemingly disparate molecular composition (Allemann et al., 1997, Blunk et al., 1993, Diederichs, 1996, Gessner et al., 2003, Gessner et al., 2000, Goppert and Muller, 2005b, Gref et al., 2000, Kasche et al., 2003, Labarre et al., 2005, Luck et al., 1998, Muller et al., 1997, Salvador-Morales et al., 2006, Sun et al., 2003). Other proteins observed with several particle types are immunoglobulins, apolipoproteins and alpha-1-antitrypsin (Cedervall et al., 2007b). On the other hand, the small dimension of QDs might also contribute to the instability of the classical components of "protein corona". A more detailed study of the interaction of QDs with human plasma was carried out and the results are presented in chapter 4 of this thesis. With the washed platelets, QDs were found to cause significant aggregation. This response may be attributed to the absence of plasma proteins, which were washed off the platelet pellet with Tyrode's salt solution during platelet preparation. The extremely small size of QDs could allow for their direct interference with platelet surface receptors, causing significant functional response. 2.5 nm QDs were found to cause more aggregation in lower concentration when compared to 5 nm QDs. This effect could be attributed to the large surface to volume ratio available for its interaction with the suspended platelets (Klein, 2007). A reduction in aggregatory response was observed with concentrations above 3μM. This pattern could be due to competitive blockade of GPIIb-IIIa, or the occlusion of the open canalicular system (Escolar et al., 1989) of platelets thereby interfering with the release of major mediators of platelet activation (Born, 1966, Needleman et al., 1976, Sawicki et al., 1997). The positively charged CdTe QDs

demonstrate a similar pattern of platelet aggregation as that of the negatively charged 2.5nm QDs. However, silica and magnetite based NPs did not cause significant aggregation in the absence of plasma. This could be attributed to the chemically inert, biocompatible, non-toxic, and non-corrosive nature of silica NPs (Tallury et al., 2008, Niessen et al., 2010). The observed effect with magnetite NPs on platelets is in agreement with a recent study performed with ferromagnetic NPs on platelets (Blair and Flaumenhaft, 2009).

Platelet activation is associated with the surface abundance of receptors that play an important role in adhesion, aggregation and platelet-leukocyte aggregation. The glycoprotein integrin receptor GPIIb-IIIa (Cramer et al., 1990) and P-selectin (Hamburger and McEver, 1990, Larsen et al., 1989) are established platelet activation markers which are translocated form the α-granules to the platelet membrane upon platelet activation mediating. The activation (a change from the low-to high-affinity conformation) of GPIIb-IIIa is crucial for platelet aggregation to occur (Coller, 1995). In addition, changes in the abundance of P-selectin on the platelet surface membrane underlie platelet–leukocyte aggregation (Radomski et al., 2005). Flow cytometry assays for GPIIb-IIIa expression showed that the QDs interfered with the fluorescence measurement from the antibodies (This could be due to the binding of the primary or the secondary antibody used, which has to be investigated further). This caused technical problems in gating, one of the important part of the analysis of flow cytometry data. Therefore, the expression of P-selectin receptors was measured in samples of PRP and washed platelets using flow cytometry. Data showed a significantly increased expression of P-selectin in washed platelets. The results observed by flow cytometry confirmed that the plasma inhibits the activation of platelets under static conditions. Since QDs interfered with the fluorescence measurements of GPIIb-IIIa antibodies, confocal imaging was used to visualize the expression of platelet activation markers at the molecular level. Confocal images showed expression of platelet activation markers in the platelet aggregates. Low level of expression in resting platelets was probably because of slight platelet activation during platelet preparation (Estebanell et al., 1998).

Gelatinases act as stimulators (MMP-2) (Sawicki et al., 1997, Sawicki et al., 1998, Radomski et al., 2001) or inhibitors (MMP-9) (Fernandez-Patron et al., 1999, Sheu et al., 2004) of aggregation and their sequential release correlates with stimulation/inhibition of

aggregation (Fernandez-Patron et al., 1999). MMP-2 has been proven to promote platelet adhesion to fibrinogen (Martinez et al., 2001). Therefore, the gelatinolytic activity of the MMP-2 released during QD-induced platelet aggregation was studied. Zymography results showed gelatinolytic bands in the gelatin incorporated SDS-page gels, in agreement with previous studies (Falcinelli et al., 2005, Radomski et al., 2002, Sawicki et al., 1998).

Results demonstrate that QDs activate human platelets in the absence of plasma. Investigators have studied the influence of NPs on platelets. An early study by Movat *et al.* have shown that the addition of latex particles to native (no anticoagulant) or citrated human platelet-rich plasma (PRP), or to a once-washed platelet suspension caused platelet aggregation, and the aggregation was associated with phagocytosis of the latex particles by the platelets (Movat et al., 1965). This same study clearly demonstrated that platelet activation and aggregation was preceded by phagocytosis of NPs by platelets themselves, thus suggesting another potential mechanism for nanoparticle removal from the circulation, i.e. redistribution to a blood clot. There is some evidence that carbon micro-scale particles can affect vascular haemostasis and precipitate thrombosis (Radomski et al., 2005). Radomski and co-workers studied the effects of engineered carbon multiwalled and single-walled nanotubes, C_{60} fullerenes and mixed carbon black NPs on human platelet aggregation in vitro and rat vascular thrombosis in vivo. They found that nanotubes and carbon black particles, but not fullerenes, induced platelet aggregation and influenced the rate of vascular thrombosis in rats (Radomski et al., 2005). Indeed, personal exposure to ambient airborne particulate matter 10 μm or less in aerodynamic size diameter increased plasma fibrinogen levels (Seaton et al., 1999). Furthermore, Nemmar *et al.* detected peripheral thrombosis following tracheal instillation of diesel exhaust particles to experimental animals (Nemmar et al., 2003a). Studies have also shown that tracheal instillation of 2 μm sized silica NPs predisposed platelets to initiate thrombotic events on mildly damaged vasculature (Nemmar et al., 2005). Shrivastava *et al.* showed that nanosilver has an innate antiplatelet property and effectively prevents integrin-mediated platelet responses, both *in vivo* and *in vitro*, in a concentration-dependent manner (Shrivastava et al., 2009). In contrast, studies performed with indwelling vascular catheters coated with silver NPs observed activation of blood platelets (Stevens et al., 2009a).

Koziara *et al.* showed that pegylated and nonpegylated cetyl alcohol/polysorbate NPs did not activate human platelets *in vitro* (Koziara et al., 2005a).

The platelet activation observed in this study is in agreement with a number of previous studies with various NPs made of biodegradable poly lactic acid (PLA) and poly lactic acid-co-ethylene oxide (PLA-PEO) (Sahli et al., 1997), carbon (Radomski et al., 2005), silver (Stevens et al., 2009b, Stevens et al., 2009c), gold (Wiwanitkit et al., 2009), latex (Glynn et al., 1965, Miyamoto et al., 1989, Miyamoto et al., 1990), cadmium selenide (Geys et al., 2008) and particulate matter (Brook et al., 2004, Nemmar et al., 2003a, Nemmar et al., 2004, Nemmar et al., 2003b, Nemmar et al., 2003c, Salvi et al., 1999, Suwa et al., 2002). The results obtained in this study also confirmed that QDs induce surface expression of GPIIb-IIIa and P-selectin receptors and release of a pro-coagulant enzyme MMP-2 during platelet activation as described earlier (Fox, 1994, Fox et al., 1993, Li et al., 2009, Radomski et al., 2005, Sawicki et al., 1998).

There is some evidence that nanoparticle *surface charge* influences the response of platelets. Studies have demonstrated that more hydrophobic and higher negatively charged particles, having a diameter of about 0.3 micron, induced platelet aggregation most easily compared to hydrophilic particles without a high negative surface potential (Miyamoto et al., 1989). Miyamoto *et al.* established that latex particles with highly negative or positive charges shortened the clotting time of whole blood and platelet-rich plasma. They also attributed the blood coagulation by positively-charged particles to platelet activation (Miyamoto et al., 1990). Koziara *et al.* have shown that decreasing particle surface charge with a PEG coating decreases platelet aggregation and activation (Koziara et al., 2005a). Li *et al.* studied the effect of biodegradable NPs containing biomaterials such as poly (D,L-lactide-co-glycolide) (PLGA) and PLGA-chitosan (CS) with sizes ranging from 580 ± 230 nm (PLGA) to 640 ± 150 nm (CS) and negative surface charge of -17.4 ± 0.6 mV (PLGA) and -5.7 ± 0.8 mV (CS). They found that the NPs did not induce platelet activation (Li et al., 2009). A recent study with polystyrene latex NPs (PLNP) [unmodified (umPLNP), aminated (aPLNP), and carboxylated (cPLNP)] of the same size but with different surface charge showed that both the cPLNPs and the aPLNPs caused platelet aggregation, whereas the umPLNPs did not. They also found that cPLNPs caused aggregation by classical upregulation of adhesion receptors, aPLNPs did not upregulate adhesion receptors and

appeared to act by perturbation of the platelet membrane, revealing anionic phospholipids (McGuinnes et al., 2011). These studies highlight the fundamental role of surface chemistry on bioactivity of nanoparticle induced platelet activation. In this study, the influence of the negative charge on the surface of CdTe QDs on platelets was examined. The zeta potential of the QD-treated platelet rich plasma and washed platelets samples was measured. The observed results were then compared with zeta potential values of plasma, untreated or collagen treated platelets. With platelet rich plasma, the zeta potential was low in collagen induced platelet aggregates compared to untreated platelets. However, the zeta potential was significantly lower in platelet poor plasma compared to untreated platelets. This could mean that the plasma and the suspended platelets, and not platelet aggregates, contribute significantly to the negative charge of platelet rich plasma. Also, a decrease in zeta potential was observed in platelets treated with increasing concentration of QDs when compared to untreated platelets. This could be explained by two reasons. Firstly, it could be due to the increased surface area available (with increased number of QDs) for the plasma proteins to interact with, thereby influencing the charge of platelet suspension. Secondly, there could be an increase in QD-induced micro- or nano-aggregates of platelets, thereby decreasing the negative charge of the platelet suspension, similar to zeta potential of collagen induced platelet aggregates. With washed platelets, the zeta potential was high in collagen induced aggregates compared to untreated washed platelets. This is in contrast to the results obtained in platelet rich plasma. This gives two impressions. Firstly, the negative charge of platelet aggregates increases in the absence of plasma proteins. Secondly, plasma proteins determine the charge of platelet suspension irrespective of the presence of platelet aggregates (Zeta potential of collagen induced platelet aggregates was low in PRP samples). The zeta potential of QD-induced platelet aggregates had a non-significant increase in their negative charges compared to untreated washed platelets. The pattern of measured zeta potentials of QD-induced platelet aggregates is similar to the percentage of platelet aggregation obtained from aggregometry (refer Figure 3.5, chapter 3.2.1). This suggests that the negative surface charge of QDs was not involved in the mechanism of activation of washed platelets. Interestingly, previous studies have demonstrated that the binding of GPIIb-IIIa integrin to its protein ligand involved multiple electrostatic interactions (Kauf et al., 2001). Further studies with carbon based NPs have suggested that

the carbon nanotube surface charge could have played a role in direct interactions with these particles and GPIIb-IIIa (Radomski et al., 2005).

The mechanisms through which NPs induce platelet aggregation are largely unknown. Radomski *et al.* compared five types of carbon-based NPs: $C_{60}CS$ (a water soluble fullerene derivative), SWCT (single-walled carbon nanotubes), and MWCT (multi-walled carbon nanotubes), mixed carbon NPs, and a standardized mixture of particulate matter from an urban environment. They demonstrated that all those particles required activation of glycoprotein integrin receptor GPIIb-IIIa in order to cause platelet aggregation. However, the size of the particles determined the pathways leading to this receptor. For instance, protein kinase C was required for micron sized particles, while activation of GPIIb-IIIa by NPs was PKC independent (Radomski et al., 2005). It was also suggested that carbon-based NPs differentially affected the release of platelet granules, as well as the activity of thromboxane-, ADP- and matrix metalloproteinase- dependent pathways of aggregation. The increased surface area of nanoparticles can act as a carrier for co-pollutants, specifically transition metals (including chromium) that could form a coat on the particle surfaces during particle formation (Niekerk and Fourie, 2004). The increased generation of reactive oxygen species by the transition metals through Fenton reaction (iron catalysed hydrogen peroxide) on the surface of particles has been implicated in the activation of platelets (Donaldson et al., 2001). Studies have also suggested that carbon nanotubes may mimic molecular bridges involved in platelet-platelet interactions, thus stimulating aggregation (Radomski et al., 2005). A recent study have demonstrated that negatively charged CdSe/ZnS QDs caused pulmonary vascular thrombosis by activating coagulation cascade and not via activating platelets (Geys et al., 2008).

To study closely the QD-induced platelet–platelet interactions at the ultrastructural level, TEM was used. Platelets are replete with secretory granules, α granules, dense granules, and lysosomes. Among the three types, the α–granule is the most abundant. Upon activation of platelets, the granules fuse with the plasma membrane, releasing their cargo (degranulation) and increasing platelet surface area (Blair and Flaumenhaft, 2009). Studies have demonstrated that, following stimulation by aggregating agents or foreign surfaces, platelets lose their discoid form, extend pseudopods, and undergo a process of internal reorganization. Randomly dispersed cytoplasmic organelles become concentrated in the cell

centre within rings of microtubules and masses of microfilaments (White and Burris, 1984). Results in this study showed that positively and negatively charged CdTe QDs caused activation and aggregation of human platelets *in vitro*. Indeed, engineered silica, magnetite, and silica coated magnetite NPs did not activate platelets. CdTe QDs caused maximal aggregatory response with degranulation of platelet granules; while silica, magnetite, and silica coated magnetite NPs (with higher concentrations than QDs) did not show detectable changes in platelet ultrastructure as compared to unstimulated platelets, with no granular release. In this respect, the effects of QDs were similar to those of potent agonists such as large concentrations of collagen (5µg/ml). The ultrastructural examination of collagen and QD treated platelet aggregates showed organelles concentrated in the centre of platelets compared to resting (unstimulated) platelets, and agglomerates of QDs are associated with the outer surface (membrane) of the platelets.

In this study, the effect of NPs on platelet aggregation was measured by light aggregometry, which detected aggregatory responses in washed platelets with various concentrations of QDs. In contrast, there was no significant increase in platelet aggregation in the presence of plasma. Using more sensitive methods such as flow cytometry (measuring P-selectin expression), confocal microscopy (visualizing P-Selectin and activated GPIIb-IIIa expression) and zymography (MMP-2), indices of QD-induced platelet activation were detected. These findings demonstrate that human platelets are susceptible to the aggregating effects of QDs in static conditions. However, no significant increase in platelet aggregation was observed in the presence of plasma (PRP) in static conditions. Also, the zeta potential measurements of QD-treated platelet rich plasma and washed platelets indicated that the light aggregometry may not detect micro or nano aggregates. Therefore, the influence of QDs on platelets under flow conditions was studied. The influence of QDs on platelets in whole blood and platelet rich plasma were studied using Cellix microfluidic platform and Q-Sense quartz crystal microbalance respectively.

Physically, platelet accumulation represents an imbalance between platelet adhesion and detachment. This study describes platelet adhesion on collagen, fibrinogen, and vWF coated microfluidic channels under various controlled shear stress conditions. Platelets adhered after 2 minutes' perfusion of treated (QD) or untreated anticoagulated whole blood at different shear stress rates was quantified. Perfusion of untreated whole blood on fibrillar

collagen coated channels showed increased platelet adhesion and decreased the number of aggregates when collagen was exposed to shear stress rates of 0.5 to 45 dynes/cm^2. This could be due to the formation of large aggregates in low shear stress conditions. However, the area covered by platelets was decreased and the number of aggregates increased in shear stress rates above 45 dynes/cm^2. The reason for this could be due to the detachment of platelets from the collagen and inability to form larger aggregates (hence increased number of smaller aggregates) at high shear stress conditions. This could be due to the fact that collagen, a major component of subendothelial matrix, mediates platelet attachment only at low shear stress rates through GP VI and integrin $\alpha_2\beta_1$, and at higher shear stresses the platelet attachment is carried out by the GPIb/IX/V interaction with vWF, serving as an intermediary between the receptor and collagen. The consistent increase in the platelet adhesion with increasing shear stresses in QD-treated whole blood indicates that platelet adhesion on collagen forms a more stable platelet aggregate. The results observed in platelet adhesion studies utilising fibrinogen coated channels showed a shear stress dependent increase in platelet adhesion. An increase in the number of aggregates was observed with shear stress rates up to 30 dynes/cm^2 in contrast to higher stress rates. This could be due to the formation of smaller aggregates in lower shear stress conditions and large aggregates in high shear stress rates. These results show that platelets adhere to fibrinogen-coated surfaces under high wall shear stress rates. This is in contrast to an earlier study which demonstrated disaggregation of platelets from fibrinogen when shear force was increased from 12 dynes/cm^2 to 68 dynes/cm^2 (Ikeda et al., 1991). In studies with vWF, the platelet adhesion from untreated whole blood to the protein was almost the same with all the shear stress conditions. This could be due the characteristics of the protein used to coat the channels. The vWF used here was purified (Thrombosis and Hemostasis group, IMM) from commercially available Hemate-P (Factor VIII + high-molecular-weight vWF multimers) by size exclusion column (hence partially pure). However, with whole blood treated with QDs, the platelet adhesion and the number of aggregates increased with increasing shear stress rates. This demonstrates that the QDs induce activation of platelet integrin GPIIb-IIIa (results in the sections 3.2.1 to 3.2.3), and vWF multimers in the channels supported platelet aggregation more effectively than vWF monomers, as described previously (Ikeda et al., 1991). These results show that when high shear stresses are applied

to platelets, vWF binds to GPIIb-IIIa complex, and this binding contributes substantially to direct shear stress-induced platelet aggregate formation (Goto et al., 1995, McCrary et al., 1995).

With all the three proteins studied, compared to untreated whole blood, treatment of whole blood with QDs decreased both the platelet adhesion and the number of aggregates in the channels. This effect could be due to the association of QD-activated platelets with leukocytes (P-selectin induced platelet leukocyte aggregation (Faraday et al., 2001)), red blood cells and plasma proteins forming large aggregates, unable to attach to the proteins coated channels. Studies with QD-treated whole blood also showed an increase in the adhesion of platelets and number of platelet aggregates with increasing shear stress rates. This could be due to the QD-induced surface expression of P-selectin and activation of GPIIb-IIIa (demonstrated in previous sections), events involved in the stability of the platelet aggregates (Merten and Thiagarajan, 2000).

Silica and magnetite-based NPs are well tolerated by human platelets. However, platelets are susceptible to the aggregating effects of QDs. The results suggest that QD-mediated platelet aggregation is likely to be mediated by the activation of surface bound integrin GPIIb-IIIa, and involves surface expression of P-selectin and GPIIb-IIIa receptors, and release of MMP-2, as shown by aggregometry, TEM, flow cytometry, confocal microscopy, and gelatin zymography experiments. Understanding the mechanisms of nanoparticle interaction with the platelets is important. More experimental evidence is required to translate these data into a predicted response in human patients. This will tease out the pathways involved in activation of platelets induced by nano-sized particles, which could help in designing more efficient anticoagulant regiments.

The information gathered in this study indicates that small, negatively charged QDs could be utilized in designing specific integrin-targeting nanoconstructs which could be used as coagulation–modifying drugs. The extremely small size will enable them to provide a large surface area for surface modification and to be excreted by the kidneys. Given the ability of interaction with plasma proteins, they must be studied *in vitro* prior to *in vivo* applications. Ultimately, patient's individual coagulation status has to be monitored even if the drugs are not intended to modify blood clotting mechanisms.

Chapter 4

Interaction of QDs with human plasma

Chapter 4

4.1 Introduction

Nanoparticles are being introduced in all kind of every day products including tooth pastes and sunscreens. Due to their small size, NPs have distinct properties compared to the bulk form of the same materials, and these properties are rapidly revolutionizing many areas of medicine and technology. Nanoparticles are rapidly being developed as probes in biological systems, and are also being investigated for numerous medical applications. They are showing potential as an emerging class of carriers for drug delivery, but at the same time it has become appreciated that the NPs can interact with the biological systems and organisms in ways that are really not expected on the basis of their chemistry alone. Nanoparticles are so biologically active because of their size similarity with small protein molecules and organelles. It is increasingly accepted that adsorption of proteins and other biomolecules from biological fluids modifies the surfaces of NPs, leading to a biomolecular interface organization that may be loosely divided into "hard" and "soft" coronas with "long" and "short" typical exchange times respectively (Monopoli et al., 2011). Typically the bare surface of the particle is covered by several biomolecules, including a select group of proteins drawn from the biological medium. This protein layer is stable for longer time and can impact particle uptake and trafficking inside the cells. What the biological cell, organ, or barrier actually "sees" when interacting with a nanoparticle dispersed in biological medium likely matters more than the bare material properties of the particle itself. The extent of nanoparticle biodistribution, efficacy and toxicity is determined by the association of blood proteins with drug delivery systems. Understanding the mechanisms of nanoparticle interaction with the body milieu could be instrumental in designing strategies to prevent the toxicity and premature clearance. A significant increase in biomedical applications of nanomaterials and their potential toxicity demands versatile analytical techniques to determine protein-nanoparticle interactions.

Numerous studies to analyse the mechanisms and compositions of protein corona on NPs have been done (Blunk et al., 1993, Allemann et al., 1997, Gessner et al., 2003, Lundqvist et al., 2004) (Cedervall et al., 2007b, Lynch et al., 2007, Lundqvist et al., 2008, Dobrovolskaia et al., 2009b). NPs of various sizes (large: e.g. polymer, liposomes, and iron oxide; small: e.g. gold, silica, titanium, and single wall carbon nanotubes) have been utilized (Karmali and Simberg, 2011). The smallest nanoparticle used so far is 6-7 nm silica

particles (Lundqvist et al., 2004, Karmali and Simberg, 2011). QDs are emerging as a potential candidate for biomedical applications. Even though QDs are not approved for *in vivo* applications in humans, they are suitable for *in vitro* imaging of cells and tissues. QDs are a suitable model candidate for studying nanoparticle-protein interactions. Detailed studies have not been done so far to examine the proteins interacting with QDs. The study of nanoparticle protein complex includes rigorous washing steps intended to remove thousands of unbound proteins from NPs. At the same time, there is a risk of over purifying the sample and consequently losing weakly bound proteins. The challenge is to use non-perturbing methods that do not disrupt the protein-particle complex or induce additional protein binding.

Chapter 3 described the influence of plasma on the effect of negatively charged CdTe QDs on platelet function. The aggregometry results showed that, the presence of plasma (platelet rich plasma) abrogated platelet activation compared to 'washed' platelets (without plasma). This instigated a study to ascertain the possible plasma proteins associated with the QDs. Therefore, the aim of this part of the study was to investigate the interaction of human plasma proteins with QDs.

To achieve this aim, the specific objectives were:

1. Investigation of interaction of QDs preincubated in plasma or albumin on washed platelets.
2. Optimization of 1D native gel electrophoretic conditions for resolution of proteins.
3. Separation of proteins by gel electrophoresis.
4. Identification of proteins by Mass Spectrometry.

4.2 Results

4.2.1 Effect of QDs pre-incubated with human plasma or albumin on washed platelets

The presence of plasma in platelet rich plasma (PRP) preparations caused reduction of platelet activation in previous experiments (Chapter 3, section 3.2.1). This concept was further investigated by studying the interaction of QDs preincubated in human plasma on washed platelets, before proceeding to isolation of nanoparticle associated proteins. 3 or 5 µM of negatively charged 4.6 nm QDs were incubated in undiluted human plasma for twenty minutes at room temperature before aggregometry studies. QDs preincubated in human albumin, the most abundant protein in human plasma, were also investigated with washed platelets for aggregatory response. Aggregometry results were shown in Figure 4.1. QDs incubated in albumin did not cause significant difference in the platelet aggregation compared to QDs alone (Figure 4.1A). However, plasma-incubated QDs caused significant reduction of platelet aggregation compared to platelets treated with untreated QDs (Figure 4.1B).
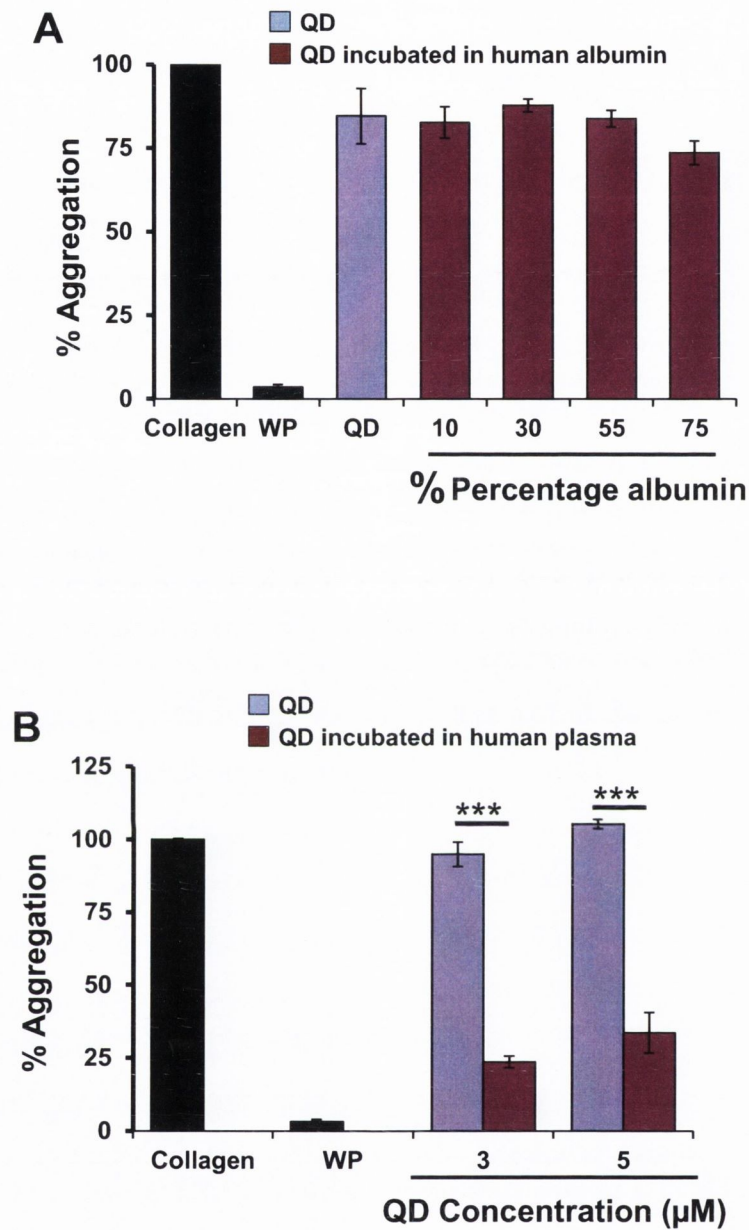
Figure 4.1: Effect of human albumin or plasma incubated negatively charged 4.6nm CdTe QDs on platelet function. Washed platelets were treated with untreated negatively charged 4.6nm QDs [3μM (A), 3 or 5μM (B)] or QDs incubated with human albumin (A) or human plasma (B) in the optical aggregometer. Collagen induced aggregation was used as positive control and untreated platelets (WP) were taken as negative control. Platelet aggregation with WP was recorded. Experiments were repeated with the samples from five healthy donors. Data are mean ± SEM of five independent experiments. *** p < 0.001 (ANOVA with Bonferroni posttests).

4.2.2 Optimization of electrophoretic conditions for resolution of proteins

Human blood was collected from healthy human volunteers. Plasma samples were obtained from citrated blood by centrifuging at 900 RCF for 10 minutes, and stored in a -80 $^{\circ}$C freezer until time of use. Before use, the plasma was thawed and centrifuged at 13000 RPM for 5 minutes. Since the 3μM concentration caused maximum aggregation of washed platelets in both the 2.5 and 5 nm CdTe QD category (refer section 3, Fig. 3.5b), the same concentration was used to investigate QD-plasma protein interactions. Electrophoresis was performed with various dilutions of human plasma for optimal resolution of proteins (Figure 4.2). The gels were then treated with fixation solution (see appendix 4) and incubation solution (see appendix 4). After staining the protein bands with colloidal Coomassie blue, the protein bands became visible. The proteins resolved well with 1:50 diluted plasma (Figure 4.2D) and, hence, the same dilution was used for all the subsequent experiments.
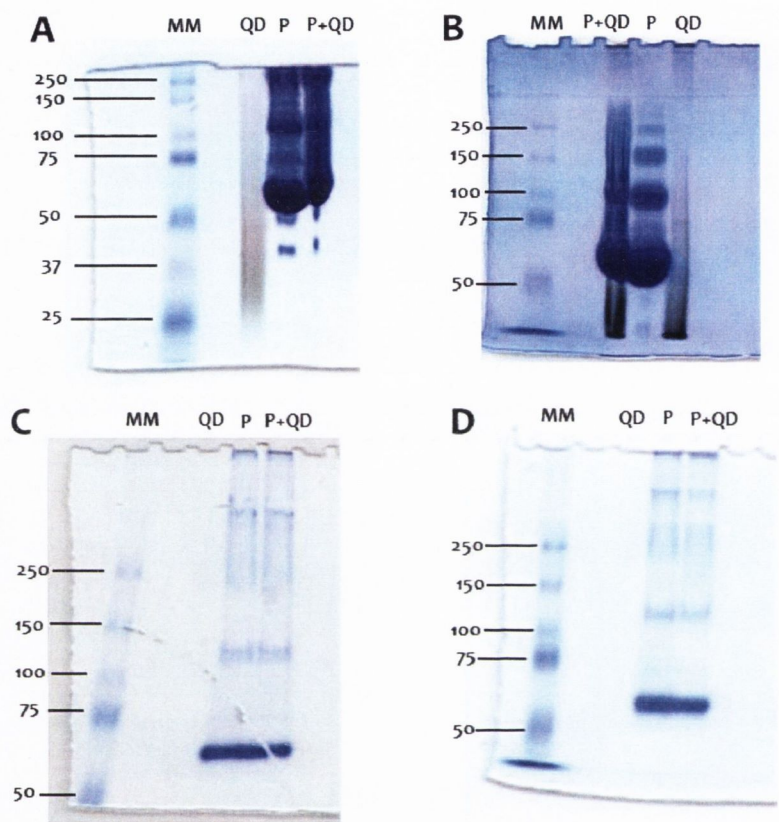
Figure 4.2: Colloidal Coomassie blue stained protein bands. Bands from undiluted (A), 10 times (B), 20 times (C), and 50 times (D) diluted human plasma were shown. QD, Quantum dots; P, plasma; P+QD, QDs incubated in human albumin; MM, molecular marker with corresponding molecular weight.

4.2.3 Gel electrophoresis of nanoparticle-binding proteins

Studies have shown that the nanoparticle–protein binding reached equilibrium within 5 min and remained constant over 4 h (Deng et al., 2011). Hence nanoparticles (negatively charged 2.7 or 4.9 nm QDs) were incubated with diluted human plasma at 37 °C for 20 minutes. Plasma without NPs, and QDs incubated in 10% human albumin were used as a negative control. Proteins were then separated by gel electrophoresis. The gels were then imaged under ultra violet light confirm the electrophoretic mobility of QDs (Figure 4.3a, 4.3b). The gels were then treated with fixation solution (see appendix 4) and incubation solution (see appendix 4). After staining the gels with colloidal Coomassie blue, the protein bands of interest (Figure 4.4a, 4.4b) were subjected to mass spectrometry analysis.
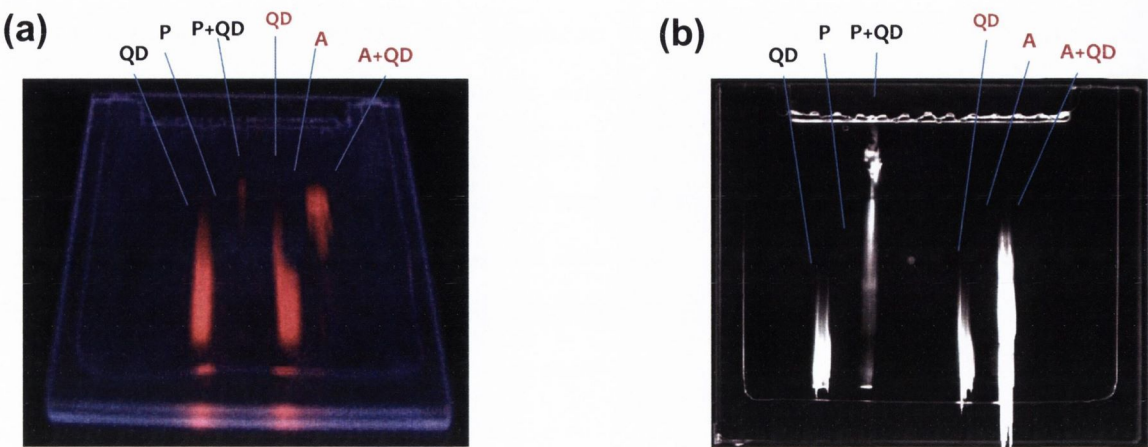
Figure 4.3: Ultra violet illuminated images of electrophoresis gels with GelDoc system. Electrophoretic mobility of 4.9 nm QDs (a) with undiluted plasma or 2.7 nm QDs (b) with 50times diluted plasma were shown. P+QD represent QDs incubated with plasma. QDs by themselves (QD), plasma (P), albumin (A), and albumin incubated QDs (A+QD) were run as controls.
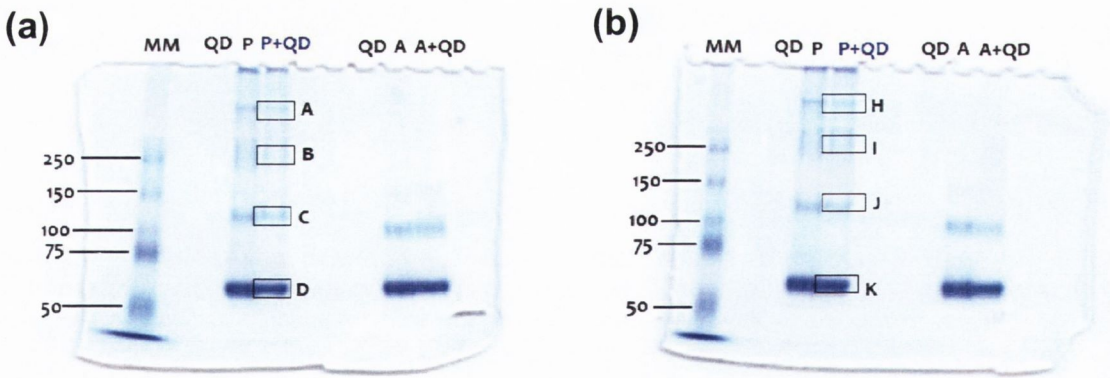
Figure 4.4: Gel electrophoresis of plasma incubated QDs. Coomassie blue stained protein bands of 2.7 (a) or 4.9 nm (b) CdTe QDs incubated in human plasma (P+QD) were shown. Quantum dots (QD) by themselves, plasma (P), albumin (A), and QDs incubated in human albumin (A+QD) were run as controls. Bands of interest (rectangular boxes) from 2.7 (A to D) or 4.9 nm (H to K) CdTe QDs were shown. MM represents molecular marker with corresponding molecular weight.

4.2.4 Identification of QD-interacting proteins by mass spectrometry

Proteins were first separated by gel electrophoresis and the bands of interest were excised from the gel. Protein bands were then analysed using mass spectrometry as described in materials and methods (section 2.7). All the detected proteins were grouped according to their function. The protein groups associated with 2.7 and 4.9 nm CdTe QDs are shown in Figure 4.5 and Figure 4.6 respectively. The known normal values (%) of relevant plasma proteins for this study are shown in Figure 4.7. The proteins associated with both the particles are grouped according to their function and are listed in Table 4.1. Table 4.2 shows a general comparison of the proteins associated with each particle type, which is derived from the complete proteomics data (protein name, Mascot score, peptides matched from each band) presented in appendix 2 and 3. (Mascot is a proprietary identification program available from Matrix Science. It performs mass spectrometry data analysis through a statistical evaluation of matches between observed and projected peptide fragments rather than cross correlation). The data shows that the 2.7 nm QDs are associated with more protein groups in spite of equal amounts of proteins being detected with both particle types. Immunoglobulin fractions constitute the bulk of detected proteins with both the QDs. However, 4.9 nm QDs re associated with more immunoglobulin fractions than 2.7 nm QDs. The functional importance of each of the associated proteins will be discussed further in the thesis.
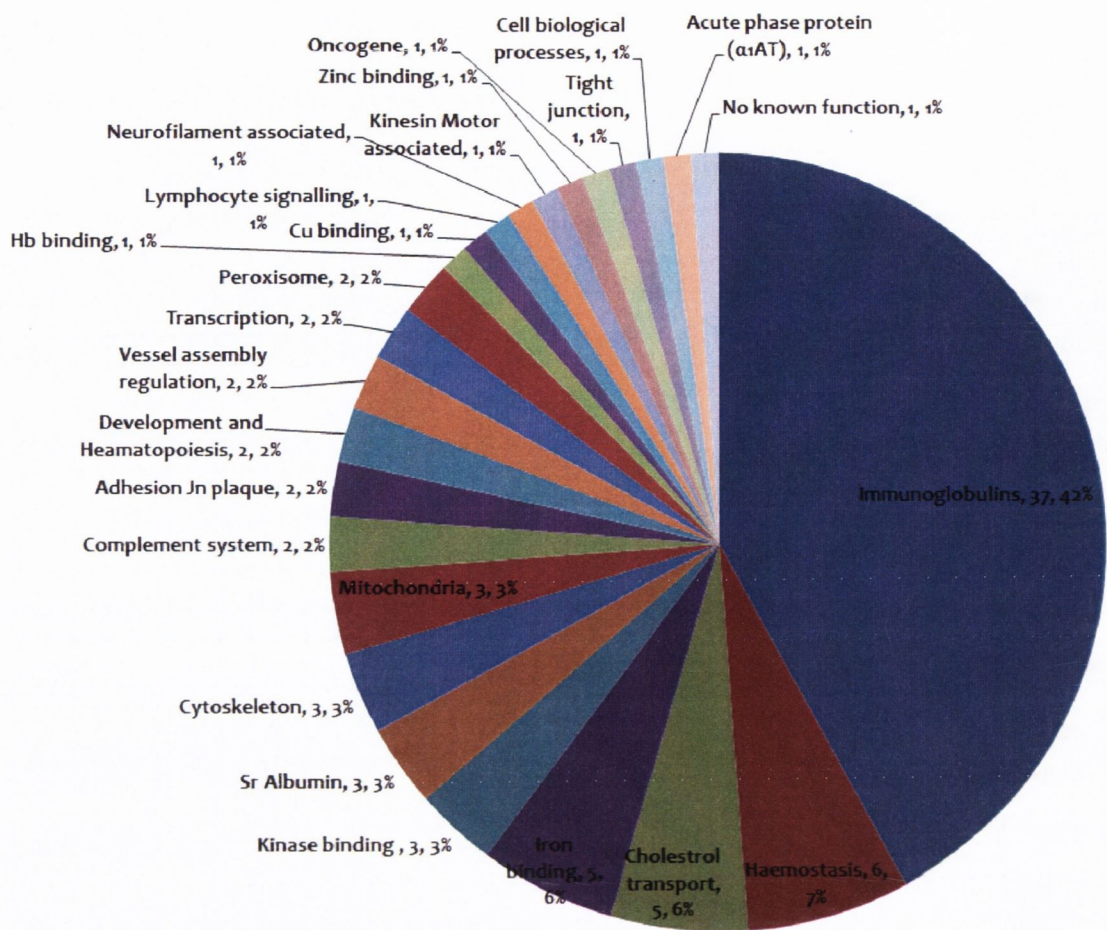
Figure 4.5: Negatively charged 2.7 nm (-20 mV) CdTe QD associated protein groups. The name, number of proteins, and the percentage value (name, number, %) of each protein group were shown. The total number of proteins identified is 88. Total number of protein groups according to their function is 25.
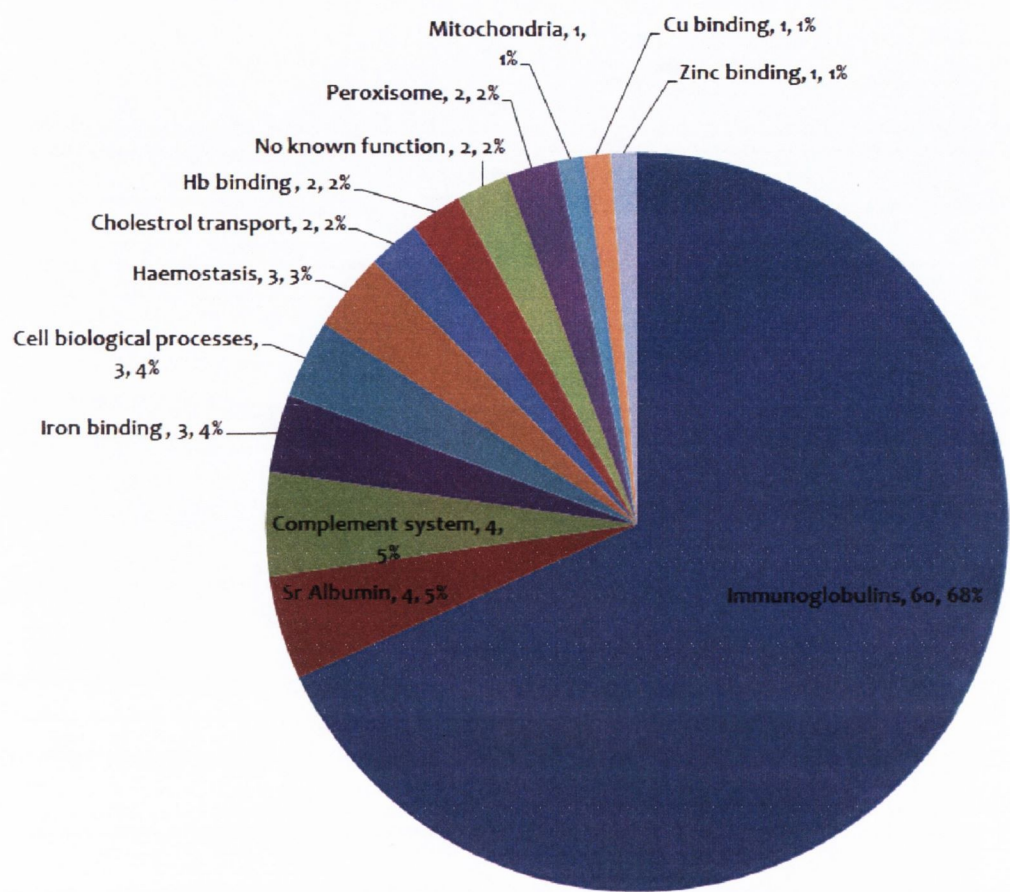
Figure 4.6: Negatively charged 4.9 nm (-40 mV) CdTe QD associated protein groups. The name, number of proteins, and the percentage value (name, number, %) of each protein group were shown. The total number of proteins identified is 88. Total number of protein groups according to their function is 13.
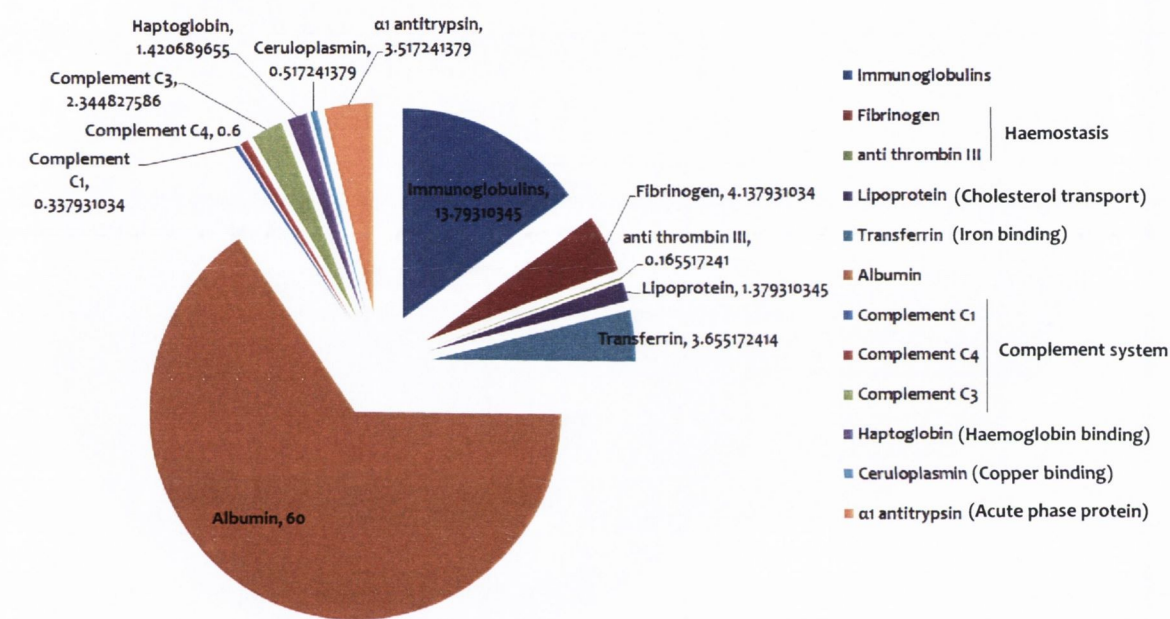
Figure 4.7: Percentage values of relevant proteins in healthy human plasma. Normal concentrations range of relevant plasma proteins was obtained from the literature. Percentage values calculated against the mean total serum protein (6.25 mg/dl).

Table 4.1: Negatively charged CdTe QD associated proteins grouped according to their function

1. Immunoglobulins	**Immunoglobulin fractions**
	Ig G_1 H Nie
	Ig G
	Ig G kappa chain
	Ig A_1 Burr
	Ig M – chain A, Fab fragment of monoclonal Ig M cold agglutinin
	Ig E heavy chain
	Ig gamma heavy chain
	Ig gamma-3 constant region
	Ig gamma-3 constant heavy chain
	Ig gamma-4 chain C region
	Ig kappa heavy chain
	Ig kappa light chain
	Ig kappa light chain VLJ region
	Ig kappa light chain variable region
	Ig kappa chain V – VIII region
	Ig kappa chain NIG93 precursor
	Ig kappa chain variable region
	Ig lamda heavy chain
	Ig lamda light chain variable region
	Ig lamda light chain VLJ region
	Ig lamda chain precursor
	Ig lamda-3 surrogate light chain
	Ig heavy chain constant region
	Ig heavy chain
	Ig heavy chain V region
	Ig heavy chain V- III region
	Ig heavy chain variable region
	Ig light chain variable region
	Bence Jones proteins
	Ig lamda NIG51
	Antibodies
	Monoclonal
	Fab fragment of a human monoclonal antibody A5b7

		Anti-HIV
		  • anti-HIV GP120 Ig heavy chain
		  • Chain H - HIV1 neutralizing antibody 2f5
		  • Chain H – anti-HIV1 Fab 447-52d in cx with V_3 peptide
		  • Chain L – HIV1 GP 120 core complexed with Cd4 and a neutralizing antibody
		Anti-TNFα: light-chain Fab fragment
		Anti-tetanus toxoid: Ig heavy chain variable region
		Anti-P185(receptor for macrophage stimulating protein): chain B of antigen binding domain of anti P185
		Anti-Hepatitis B: Ig heavy chain against hepatitis surface antigen
		Anti-Ent. Histolytica: Ig gamma heavy chain

2.	**Albumin**	albumin precursor albumin
3.	**Cholesterol transport**	pro apolipoprotein apolipoprotein lipoprotein Glu I ABC A13
4.	**Iron binding**	transferrin serotransferrin precursor hemopexin precursor lactoferrin
5.	**Hemostasis associated proteins**	fibrinogen α α fibrinogen precursor β fibrinogen precursor fibrinogen γ chain heparin cofactor II precursor factor VII active site antithrombin III $α_2$ macroglobulin (protease inhibitor)
6.	**Kinase binding**	leucine rich repeat kinase citron-Rho interacting kinase Serine/threonine protein kinase
7.	**Cytoskeleton associated proteins**	supervillin nesprin plectin

8.	**Peroxisome associated proteins**	peroxisome biogenesis factor (2.5nm QD) PEX1PQ261Ter (5nm QD)
9.	**Mitochondria associated proteins**	S-AKAP-84 (2.5nm QD) ALR (2.5nm QD) NADH ubiquinone oxidoreductase (5nm QD)
10.	**Complement system associated proteins**	Complement component C_3 (2.5 and 5 nm QD) Complement component C_4B (2.5 and 5 nm QD) Complement factor B (5nm QD)
11.	**Adhesion junction plaque associated proteins**	bullous phemphigoid antigen dystonin
12.	**Development and hematopoiesis associated proteins**	Myeloid lymphoid leukaemia variant G protein pathway suppressor 1
13.	**Vessel assembly associated proteins**	GTPase activating protein Extracellular glycoprotein EMILIN-2 precursor
14.	**Haemoglobin binding**	haptoglobin isoform 1 preproprotein (2.5 and 5 nm QD) haptoglobin (5nm QD)
15.	**Copper binding**	ceruloplasmin (2.5 and 5 nm QD)
16.	**No known function**	IGH@ protein (2.5 and 5 nm QD) FLJ00385 (5nm QD)
17.	**Lymphocyte signaling associated protein**	CD45
18.	**Neurofilament associated protein**	Heavy neurofilament subunit
19.	**Kinesin motor associated protein**	Kinesin superfamily protein KIF1B
20.	**Zinc binding**	PHD finger protein (2.5nm QD) KIAA0853 (5nm QD)
21.	**Oncogene**	oncogene
22.	**Tight junction associated protein**	symplekin
23.	**Cell biological processes associated proteins**	Inter-α trypsin inhibitor heavy chain (2.5 and 5 nm QD) Trypsin inhibitor (5nm QD)
24.	**Acute phase protein**	Chain A, α_1 anti-trypsin
25.	**Transcription associated proteins**	Transcription factor Absent small and homeotic disks protein 1

homolog (ASH1)

Table 4.2: A general comparison of proteins associated with each particle type

Protein groups	2.7nm QD	4.9nm QD
Immunoglobulins		
Ig G	+	+
Ig A	+	+
Ig M	-	+
Ig E	+	+
immunoglobulin gamma heavy chain	+	+
gamma 3 immunoglobulin constant heavy chain	+	+
Ig kappa chain precursor	+	-
immunoglobulin kappa heavy chain	+	+
immunoglobulin kappa light chain	+	+
immunoglobulin kappa light chain VLJ region	+	+
immunoglobulin kappa chain variable region	+	+
Ig kappa chain V-III region Precursor	+	+
Ig lambda chain precursor	+	+
immunoglobulin lambda heavy chain	+	+
immunoglobulin lambda-3 surrogate light chain	+	+
immunoglobulin lambda light chain VLJ region	-	+
immunoglobulin lambda light chain variable region	-	+
immunoglobulin heavy chain constant region	+	+
immunoglobulin heavy chain variable region	+	+
immunoglobulin heavy chain	+	+
immunoglobulin light chain variable region	-	+
Monoclonal Antibody	+	+
protein NIG64 *lambda,Bence-Jones*	+	+
anti-HIV-1	+	+
Antigen-Binding Domains of *Anti-P185*	+	+
anti-tetanus toxoid immunoglobulin heavy chain variable region	+	+
anti TNF-alpha antibody light-chain Fab fragment	+	-
anti-HBs antibody heavy chain	-	+
anti-Entamoeba histolytica immunoglobulin gamma heavy chain	-	+
Albumin		
serum albumin precursor	+	-
serum albumin	+	+
Cholesterol transport		
proapolipoprotein	+	+
lipoprotein Gln I	+	+
ABC3	+	-
apolipoprotein A-1	+	-

ABC A13	+	-
Iron binding		
serotransferrin precursor	+	+
hemopexin precursor	+	+
Transferrin	+	+
Human Transferrin Receptor-Transferrin Complex	+	-
lactoferrin	+	-
Haemostasis		
alpha-2-macroglobulin precursor	+	+
fibrinogen alphaA	+	-
beta-fibrinogen precursor	+	-
alpha-fibrinogen precursor	+	-
fibrinogen gamma chain	+	-
heparin cofactor II precursor	+	-
factor VII active site	-	+
Human Antithrombin III Complex	-	+
Kinase binding		
leucine-rich repeat kinase 2	+	-
citron Rho-interacting kinase	+	-
receptor-interacting serine/threonine-protein kinase	+	-
Cytoskeleton		
supervillin	+	-
nesprin-1	+	-
plectin	+	-
Peroxisome		
peroxisome biogenesis factor 1	+	-
Pex1pQ261Ter	-	+
Mitochondria		
S-AKAP84	+	-
ALR	+	-
NADH:ubiquinone oxidoreductase 51-kD subunit	-	+
Complement system		
complement C3 precursor	+	+
complement C4B precursor	+	+
complement component C3	-	+
complement factor B	-	+
Adhesion junction		
bullous pemphigoid antigen 1 isoform 1eA precursor	+	-
dystonin	+	-
Development and haematopoiesis		
myeloid/lymphoid or mixed-lineage leukaemia 2 variant	+	-
Gps1	+	-
Vessel assembly regulation		
GTPase activating protein	+	-

extracellular glycoprotein EMILIN-2 precursor	+	-
Haemoglobin binding		
haptoglobin isoform 1 preproprotein	+	+
haptoglobin	-	+
Copper binding		
ceruloplasmin	+	+
No known function		
IGH@ protein	+	+
FLJ00385 protein	-	+
Lymphocyte signalling		
Cd45	+	-
Neurofilament		
heavy neurofilament subunit	+	-
Kinesin Motor associated		
kinesin superfamily protein KIF1B	+	-
Zinc binding		
PHD finger protein 3	+	-
KIAA0853 protein	-	+
Oncogene		
oncogene	+	-
Tight junction		
symplekin	+	-
Cell biological process		
inter-alpha-trypsin inhibitor family	+	+
trypsin inhibitor	-	+
Acute phase protein		
Alpha-1-Antitrypsin	+	-
Transcription		
transcription factor	+	-
ASH1	+	-

+: associated; -: not associated

4.3 Discussion

The rapidly developing field of nanomedicine pursues the use of NPs in biomedical applications. Nanomedical approaches, many of which are designed for systemic administration, have the potential for interactions with plasma proteins. This protein adsorbed nanoparticle interacts with cells in the circulatory system including platelets. Aggregometry results clearly showed that the QDs preincubated in plasma caused significant reduction in platelet aggregation compared to QDs preincubated in albumin. The reason for this discrepancy could be due to the size of the interacting proteins compared to the size of the QDs. Albumin is described as an ellipsoid molecule of 15 nm in length and 3.8 nm in diameter (Gekle, 1998). The size is much larger than QD, and will not be able to form the classical protein "corona". This could lead to albumin being partially attached to particles, or its surface being decorated by QDs, or albumin being able to form protein corona around sufficiently large QD aggregates. The association of smaller biomolecules in plasma with the particles could be the reason for the significant reduction of aggregation found with QDs preincubated in plasma. On the basis of observations obtained in aggregometry studies, it was decided to investigate more closely the plasma proteins interacting with QDs. The interaction of proteins with solid surfaces is a fundamental phenomenon with implications for nanotechnology, biomaterials and biotechnological processes (Gray, 2004). The adsorbed plasma protein patterns depend on the physico-chemical characteristics of the nanoparticle surface and are regarded as a key factor for its *in vivo* behaviour. The purpose of this study was to isolate the proteins associated with the QDs utilizing a non-perturbing method, so native gel electrophoresis was used. Unlike SDS-PAGE type electrophoresis, native gel electrophoresis does not use a charged denaturing agent (SDS, a detergent wraps around the polypeptide backbone contributing a negative charge thereby making the intrinsic charge of the polypeptide negligible). The proteins being separated therefore differ in molecular mass and intrinsic charge, and experience different electrophoretic forces dependent on the ratio of the two. In this study the effect of size and surface charge on QD-plasma protein interactions was investigated. Protein adsorption on two different QD types [negatively charged 2.7 nm (-20 mV) or 4.9 nm (-40mV)] was investigated using gel electrophoresis and mass spectrometry. QDs were incubated with human plasma for twenty minutes and subjected to native gel

electrophoresis. UV examination of the gels after electrophoresis showed a difference in the migratory pattern. The QDs in the QD-plasma mixture were seen throughout the column indicating their attachment to the resolving proteins. After fixing and staining the gels, selected bands were excised and the proteins trypsin digested before detection by mass spectrometry. That is, it is peptides from the protein amino acid sequence that are detected.

The proteins associated with both the particles are grouped according to their function (Tables 4.1, 4.2). This is a useful manner to understand the relationship of physiochemical properties of nanoparticle to the overall profile of the proteins associated. The major part of the detected proteins consists of immunoglobulins (Ig), albumin, complement components, fibrinogen and apolipoprotein A (apo-A) as shown previously (Gessner et al., 2002, Gessner et al., 2003, Gessner et al., 2000, Lundqvist et al., 2008), (Cedervall et al., 2007a, Cedervall et al., 2007b, Hellstrand et al., 2009, Nagayama et al., 2007). Other groups identified according to their function are proteins associated with haemostasis, iron binding, copper binding, zinc binding, and haemoglobin binding. However, there are quite significant groups of proteins identified with 2.7nm QDs, like proteins associated with cytoskeleton, kinase binding, peroxisome, mitochondria, kinesin motor, adhesion junction, tight junction, development and haematopoiesis, vessel assembly regulation, neurofilament, lymphocyte signalling, acute phase reaction, oncogene, and transcription.

Even minor difference in QD property is sufficient to influence the protein adsorption portfolio which is sufficient to cause a change in the (potential) biological impact. The proteins associated with two different sized and negatively charged CdTe particles have ~50% homology between them suggesting that the size and charge are more important than the molecular composition. The observed differences could have resulted from one or a combination of the key functional properties such as size and surface charge of QDs. The zeta potential of 2.7 nm QD (-20 mV) is much lower compared to the 4.7 nm QD (-40 mV), indicating that the charge could have played a role in protein adsorption. This conforms with the findings of the previous studies; the plasma protein associations with the NPs will be size (Dobrovolskaia et al., 2009b, Karmali and Simberg, 2011, Lacerda et al., 2010, Lynch et al., 2007, Pedersen et al., 2010) and/or charge dependent (Bradley et al., 1998, Chonn et al., 1992, Cullis et al., 1998, Gessner et al., 2002, Gessner et

al., 2003, Kamps and Scherphof, 1998, Karmali and Simberg, 2011, Oku et al., 1996). Therefore, one may expect different biological impacts, not just from the direct consequence of nanoparticle surface characteristics, but from the implicit interactions from the corona.

The major groups of proteins identified are Ig fractions with different forms of the constant regions and the variable regions of immunoglobulins. Interestingly, the 4.9 nm QDs are associated with a large number of immunoglobulins (68%) compared to the 2.7 nm QDs (42%). The great variability due to size and charge is intriguing. An antibody, also known as an immunoglobulin, is a large Y-shaped protein used by the immune system to identify and neutralize foreign objects such as bacteria and viruses. The antibody recognizes a unique part of the foreign target, termed an antigen. Immunoglobulins of the type identified on the particles are involved in many processes from immunity response to allergic reaction and anaphylactic shock. IgG is involved in transport across the placenta, and in the process of opsonization for presentation to macrophage. IgA is an antibody that plays a critical role in mucosal immunity. IgM, the physically largest antibody in the human circulatory system, is a basic antibody that is produced by B cells. It is the primary antibody against A and B antigens on red blood cells. IgE is a class of antibody that has been found only in mammals. It plays an important role in allergy, and is especially associated with type 1 hypersensitivity (Lundqvist et al., 2008). The binding of a specific antibody (Ig) to the surface of QDs (QD-Ig complex) could be utilized to tag a microbe or an infected cell for attack by other parts of immune system, or can neutralize it directly by blocking a part of a microbe that is essential for its invasion or survival. Albumin is detected with both particle types. It is the main protein of plasma, 60% of total plasma protein (Figure 40), and it binds water, cations (calcium, sodium and potassium), fatty acids, hormones, bilirubin and drugs. Its main function is to regulate the colloidal osmotic pressure. Albumin, along with other proteins such as immunoglobulins and complement system components are thought to be important in the clearance process of NP (Dobrovolskaia et al., 2008). The other group identified was the proteins associated with cholesterol transport. Apolipoproteins are involved in the transportation of lipids and cholesterol in the bloodstream (Anderson and Anderson, 2002) and, as such, are expected to greatly affect the intracellular trafficking, fate, and transport of NP in cells and animals.

Studies have shown that apolipoproteins are associated with NPs of different materials and different sizes (Cedervall et al., 2007a). The apolipoproteins were detected in both the particles studied. In contrast, ABC protein involved in pulmonary surfactant production, by transporting cholesterol is associated with only with 2.7 nm QDs. Apolipoprotein A-I is the major protein component of HDL. It has been reported that apo A-I is a significant component of the protein layer adsorbed from blood or plasma to a variety of biomaterial surfaces, including hydrophobic/hydrophilic polymers, and liposomes (Cornelius et al., 2002). It is being suggested that apolipoprotein A-I and/or HDL deposition may be an important event in blood-biomaterial interactions generally (Cornelius et al., 2002). It is yet to be determined whether the association of apo A-1 with QDs results from the uptake of free protein or HDL particles.

Proteins associated with complement system, a key part of the innate immune response, was the other group identified. These proteins were detected in both the particle types. Studies have shown that addition of citrate to the plasma (while plasma separation) may elevate adsorption of complement owing to the possible inactivation of complement cascade, and complement components plays an important role in opsonization of NPs (Allemann et al., 1997). Complement proteins are a group of proteins linked to each other in a biochemical cascade which "complements" cell-mediated and humoral immunity in removing pathogens from the body. Activation of complement proteins by the NPs will result in altered bio-distribution in the form of rapid clearance from the systemic circulation via complement receptor-mediated phagocytosis by mononuclear cells (Dobrovolskaia et al., 2008). Therefore, NPs designed for systemic administration should be tested for their tendency to activate the complement system. If significant activation of the complement occurs, its surface properties must be tuned to decrease these interactions to an acceptable level. Previous studies have proved that charged NPs activate complement more efficiently than their neutral counterparts (Dobrovolskaia et al., 2008). Our study shows 4.9 nm QDs (-40mV) is associated with more complement proteins than 2.7 nm QDs (-20 mV). This suggests that the association of complements with the NPs increases in direct proportion to the increase in negative surface charge. Acute phase proteins (not presented as a group in Table) like α1 anti trypsin and fibrinogen were associated with 2.7 nm particles, while complement factors were associated with both the particles. These observations might

suggest the activation of differing inflammatory responses by the particles of different size and surface charge. Another group found concerns the proteins involved in haemostasis. As can be seen in the table, majority of the coagulation system proteins are associated with 2.7 nm QDs. The 4.9 nm QDs have a different profile of associated proteins when it comes to molecules involved in coagulation process. Fibrinogen is the major protein of this group. Fibrinogen (factor I) is a soluble plasma glycoprotein, synthesised by the liver, that is converted by thrombin into fibrin during blood coagulation. Fibrinogen binds to the integrin receptors, αIIbβ3, on activated platelets, one receptor at each end of the fibrinogen molecule, thereby acting as a bridge to link platelets together in order to bring about platelet aggregation. Fibrin fibrils entangle blood cells and plasma, helping to increase the mass of the blood clot at the site of damage. Fibrin can interact with several cell types, including endothelial cells, smooth muscle cells, fibroblasts, leukocytes and keratinocytes. Coagulation factors VII and heparin cofactor II (coagulation factor that inhibits factor IIa) are also identified with the QDs. Therefore, QD binding to proteins involved in coagulation could influence haemostatic mechanisms. Of note, previous data in this study (chapter 3) showed that the QDs did not induce human platelet activation in the presence of plasma. Since the QD-protein binding study was done in static conditions, and anticoagulants were used while collecting blood samples from volunteers, the degree to which this reflects the protein corona in vivo is yet to be investigated. However, the results are suggestive of different coagulation profiles.

Proteins related to zinc transport are associated with both the particles. This essential element is of established importance in mammals, and deficiency restricts growth and normal development. Of the total plasma zinc concentration of 12-25 µmol/l, over 90% is associated with albumin, <10% with alpha-2 macroglobulin, and a small amount, <1%, complexed to amino acids and other low molecular weight species. A protein related to haemoglobin (haptoglobin) transport is associated with both the particles. Haptoglobin (Hp) is an acute phase protein, increased in the presence of acute inflammatory process, tissue necrosis or malignancy, synthesized in the liver that binds free haemoglobin (Hb) irreversibly, preventing Hb-induced oxidative damage in the vascular system and possible renal damage as a consequence of haemoglobin excretion. The hapto-haemoglobin complexes, as well free haptoglobin itself, also play significant roles in the iron storage

(Tsai-Mu and et al., 2011). This haemoglobin binding property could also be exploited for developing a nanocarrier for haemoglobin, for example in treatment of thrombosis oxygen deprived pathologies (Chauvierre et al., 2004). Proteins related to iron (lactoferrin, transferrin), and copper (ceruloplasmin) transport are associated with both the particles. Studies have shown that lactoferrin, and ceruloplasmin derivatized (a technique which transforms a chemical compound into a product of similar chemical structure) superparamagnetic NPs were attached to human fibroblast's cell membrane, most likely to the cell expressed receptors, and were not endocytosed. Hence, ceruloplasmin bound to QDs would make them adher to cell surface and not being endocytosed. Confinement of NPs to the cell surface would provide a route that might allow removal of the particles from the cells after an appropriate residence time (Gupta and Gupta, 2005). Mitochondria related proteins, associated with ATP synthesis, were isolated with both the particles. Inter-α-trypsin inhibitor (cell biological processes group protein) acts as a carrier of hyaluronan which is essential for cellular biological processes, and peroxisome associated proteins, critical for normal development of mammalian brains and lungs, are found with both the QDs.

Some proteins are different to 2.7 nm QD-coronas. Kinase binding proteins represent one of the groups. Protein kinases are one of the largest families of evolutionary related proteins. The binding of QDs to these proteins could interfere in regulation of phosphorylation or cytokinesis or apoptosis. Cytoskeleton associated proteins constitute the next group, and are involved in regulation of filament dynamics and cell migration. Proteins involved in gene regulation during early development and haematopoiesis, and vessel assembly are also detected. Further, adhesion junction and tight junction plaque associated proteins, the defect of which could lead to degenerative disorders are detected. Proteins with distinct biological roles like lymphocyte signalling, and neurofilament, kinesin motor, oncogene, and transcription associated proteins are also identified. These few unique proteins identified could play a crucial role in a wide range of cellular processes, including protein synthesis, metabolism, regulation of membrane receptors and channels, cell division, apoptosis, and reorganization of the cytoskeletal architecture. Therefore, the binding of QDs could influence downstream signalling pathways of these proteins. The observed variations in associated proteins between QDs suggest that different

particles could activate different pathways. The proteomic data shows that the binding of highly abundant proteins to particles are independent of QD size and surface charge. However, a whole range of less abundant proteins with unique roles were also isolated. As in cases of biological NPs like LDL and HDL where single or few copies of surface-expressed proteins dominate the biological impacts (Lundqvist et al., 2008), the presence of these proteins could be highly significant. The adsorption of specific group of proteins in 2.7 nm QD coronas could be due the NP size and surface properties. This mechanism could be further analysed by molecular modelling studies encompassing computational techniques and protein structure libraries.

Just as the protein binding profile is influenced by the nanoparticle properties, the biodistribution of NPs is influenced by the binding profile. Protein binding can cause a change in nanoparticle size and surface charge (Dutta et al., 2007, Moghimi et al., 2001). Protein binding is one of the key factors postulated to influence biodistribution (Dutta et al., 2007, Gessner et al., 2002, Goppert and Muller, 2005a), along with size and surface chemistry of the nanoparticle. The knowledge of this "cause and effect" relationship helps to understand the biodistribution of NPs. Specific proteins associated with nanoparticle can have a direct impact on particle internalization and biodistribution (Moghimi et al., 2001, Owens and Peppas, 2006, Patel and Moghimi, 1998). Studies have shown that binding of opsonins (blood serum proteins that signal cells to ingest the particles) such as IgG, complement factors, and fibrinogen promotes macrophages of the reticuloendothelial system (RES) to phagocytose and remove particles (Goppert and Muller, 2005a, Leroux et al., 1995, Owens and Peppas, 2006). These particles are said to rapidly sequester in the RES organs and concentrate in liver and spleen (Illum et al., 1987, Panagi et al., 2001). On the other hand, circulation time in the blood is said to be prolonged by dys-opsonins, naturally occurring substances known to inhibit phagocytic ingestion, such as albumin (Goppert and Muller, 2005a, Moghimi et al., 1993, Ogawara et al., 2004). In vitro studies done with serum have shown that, an increase in the amount of IgG and C3 adsorbed on the surface of NPs over time was directly proportional to an increase in uptake by primary cultured Kupffer cells (Nagayama et al., 2007). Albumin is one of the prominent plasma proteins that bind to NPs when they come in contact with plasma, which makes it as a logical choice for binding to NPs. Binding to albumin, a 60-kDa cell surface glycoprotein,

mediates albumin transcytosis and uptake into endothelial cells, which further signals the rest of the cascade to internalize albumin and albumin bound particles (Desai et al., 2006, Hawkins et al., 2008, John et al., 2003, Vogel et al., 2001). IgA and ApoA-1 attachment to NPs were shown to increase the uptake of NPs by hepatocytes and brain endothelial cells (Kreuter et al., 2007, Kreuter et al., 2002, Michaelis et al., 2006). Studies have shown that polysorbate 80 coated NPs adsorb apolipoprotein E from blood plasma. The particles then seem to mimic low density lipoprotein (LDL) particles and could interact with the LDL receptor leading to their uptake by the brain endothelial cells. After this the drug may be released in these cells and diffuse into the brain parenchyma or the particles may be transcytosed (Kreuter, 2001). The benefits and disadvantages of protein binding to NPs are still debated. It is useful in some cases to have these proteins in nanoparticle-associated form as the nanoparticle could be targeted to a particular area of the body. For example, NPs bound to certain apolipoproteins could be distributed across the blood brain barrier into the brain (Goppert and Muller, 2003, Goppert and Muller, 2005b, Kreuter, 2001, Olivier, 2005). However, a rapid uptake and clearance by RES has also been shown for the particles bound to these proteins, a negative effect for someone attempting to increase circulation and retention time of NPs in the body (Owens and Peppas, 2006). Studies have shown that covalent binding of apolipoproteins (Apo A-1, Apo E3, or Apo B-100) to albumin NPs significantly facilitated transport of a bound model drug, loperamide, across BBB as opposed to controls (loperamide alone or NPs without apolipoproteins attached) (Kreuter et al., 2007). A study with polysorbate 80-coated PBCA NPs, which preferentially adsorbed Apo E, showed that drugs having poor brain diffusion such as doxorubicin, tubocurarines, and dalargin, were also able to be delivered across BBB (Alyautdin et al., 1998, Gulyaev et al., 1999, Kreuter et al., 1995, Olivier, 2005, Steiniger et al., 2004).

Therefore, it could be stated that the adsorbed proteins determine the biological activity, *in vivo* organ distribution, and subcellular localization of nanomaterials. Furthermore, an effective size cut-off (10 nm) of the glomerular filtration apparatus determines the clearance of nanotechnology-derived constructs. This knowledge and understanding will establish rational approaches in developing targeted biomedical applications, including intravascular imaging and drug delivery.

Chapter 5

Interaction of nanoparticles with human endothelial cells

Chapter 5

5.1 Introduction

Nanotechnology is defined as 'the understanding and control of matter at dimensions of roughly 1-100 nanometers'. There are different classes of NPs available for biomedical applications. Inorganic, biocompatible, porous ceramic NPs such as silica can be used in cancer therapy (Cherian et al., 2000). Other properties such as water dispersity, resistance to microbial attack and swelling, and easily modifiable surface makes them an attractive candidate for nanomedicine. However, these particles are non-biodegradable, as they can accumulate in the cells. QDs have been used successfully in solar energy conversion, lasers, light emitting diodes, and display devices (Alivisatos et al., 2002, Bulovic et al., 2002, Huffaker et al., 1998, Likharev, 1999). For biological applications, QDs must be surface-passivated with other materials allowing dispersion and preventing leakage of the toxic heavy metals (Weng and Ren, 2006). QDs are also successfully utilized in biomedicine fields as labelling agents for imaging biological molecules, cells and even tissues (Resch-Genger et al., 2008), or to trace drug molecules in live organisms (Bagalkot et al., 2007, Manabe et al., 2006). Superparamagnetic iron oxide particles have a variety of applications in molecular and cellular imaging (Corot et al., 2006). They are being used as contrast agents in magnetic resonance imaging (Saini et al., 1995) and magnetically mediated hyperthermia (Moroz et al., 2002) in treatment of cancers.

There is a rising concern about the possible interactions of particles with living cells at the nanoscale. Engineered nanoconstructs designed for systemic administration have the potential to interact with the vascular microenvironment. Interestingly, NPs in the trachea (30 nm gold NPs) and alveoli (carbon NPs <100 nm) could gain access to the systemic circulation by avoiding the normal phagocytic defences of respiratory system (Berry et al., 1977, Nemmar et al., 2002a). NPs, as novel bioimaging and drug delivery agents, are generally introduced into vascular system by injection, and thus directly exposed to vascular endothelial cells.

Endothelial cells line the entire vascular system, from heart to the capillary beds. They reduce the turbulence of the flow of blood and allow the fluid to be pumped farther. They sense and integrate hemodynamic and hormonal stimuli (Vanhoutte, 1989). Mechanical forces are important modulators of cellular function in many tissues and are particularly important in the cardiovascular system. The endothelium, by virtue of its

unique location in the vessel wall, responds rapidly and sensitively to the mechanical conditions created by blood flow and the cardiac cycle. EC recognize shear stress and cyclic strain as mechanical stimuli, and transmit the signal into the interior of the cells, thereby triggering a variety of cellular responses that involve alterations in cell morphology, cell function, and gene expression (Ando and Yamamoto, 2011). Impaired EC responses to shear stress and cyclic strain lead to vascular diseases, including hypertension, thrombosis, and atherosclerosis (Ando and Yamamoto, 2009).

Endothelium can be targeted with NPs in order to deliver drug and/or gene therapy for a variety of pathological conditions in the vascular system because of its large population and proximity to blood flow (Davda and Labhasetwar, 2002, Omolola Eniola and Hammer, 2005). However, the mechanisms of cellular uptake of NPs can vary. The functionalized NPs could be internalized by one of the two main pathways; phagocytosis or pinocytosis (i.e., clarithrin-, caveolae-mediated, macropinocytosis and other clarithrin- and caveolae- independent endocytosis) (Hillaireau and Couvreur, 2009). Studies performed with CdSe/ZnS QDs (28.2 nm) on human epidermal keratinocytes showed that QDs with a carboxylic acid surface coating were recognized by lipid rafts but not by clathrin or caveolae, and were internalized into early endosomes and then transferred to late endosomes or lysosomes. QDs also induced more actin filaments formation in the cytoplasm (Zhang and Monteiro-Riviere, 2009). Lipid rafts are known to be involved in the formation of macropinosomes. Therefore, NP endocytosis by cells not only depends on the size of the particle, but also the surface coating and charge.

Investigators have studied the effects of NPs such as carbon black (Yamawaki and Iwai, 2006b), 45 nm silver (Rosas-Hernández et al., 2009), metal oxides (20-70 nm ZnO, 20-60 nm Y_2O_3 and 45 nm Fe_2O_3) (Gojova et al., 2007), 100 nm MgO (Ge et al., 2011), 14-335 nm silica (Napierska et al., 2009), 3.36 nm QD (Yan et al., 2011) and polymer NPs (mean hydrodynamic diameter of 321 nm) (Davda and Labhasetwar, 2002) on endothelial cells under static conditions. No comprehensive study evaluating the interaction of engineered NPs on endothelial cells under varying flow conditions is currently available. Therefore, the interactions of QDs and silica NPs with endothelial cells under regulated shear stress conditions were investigated in this study. In addition, the cytotoxic effect of QD, silica, silica coated magnetite and citrate stabilized magnetite on cultured endothelial

139

cells was also evaluated. Since 2.5-5 nm CdTe QDs and 5, 9 or 51nm silica- and magnetite-based NPs were investigated for their interaction with platelet function, particles with similar size and surface properties were used for this study. Negatively charged 2.6 and 4.9 nm CdTe QDs, 50 nm fluorescent silica, 5 nm silica, 51 nm silica coated magnetite and 9 nm citrate stabilized magnetite NPs, and a human umbilical vein cell line (HUVEC) were utilized. HUVEC were treated with TNF-α to simulate activated endothelium or with surfactant (Triton X-100) to increase cell permeability. The aim of this part of the study was to investigate the interaction of NPs with HUVEC under static and flow conditions.

To achieve this aim, the specific objectives were:

1. Study of nanoparticle uptake by normal and activated (TNF-α) endothelial cells under physiological shear stress conditions using Cellix™ biochips.

2. Comparative analysis of nanoparticle uptake by intact and membrane-compromised (surfactant-exposed) HUVEC.

3. Characterization of nanoparticle localization in endothelial cells under static and shear stress conditions using confocal microscopy.

4. Examination of HUVEC morphology using confocal and atomic force microscopy.

5. Investigation of the cytotoxicity of NPs on HUVEC using high content analysis platform (IN Cell Analyzer 1000).

5.2 Results

5.2.1 Nanoparticles uptake by live HUVEC under controlled shear stress conditions.

Cultured endothelium was used as a model of vascular transport for characterizing uptake or association of NPs with endothelial cells (Davda and Labhasetwar, 2002, Ehrenberg et al., 2009). Endothelium shows expression or upregulation of a number of adhesion molecules such as selectins (E, L and P), PECAM, VCAM and ICAM in response to TNF-α (a pro-inflammatory cytokine) (Littler et al., 1997). Quantitative detection of NPs in biological systems (i.e., cells, tissues and organs) is becoming a vital part of nanotoxicological and nanomedical studies (Elsaesser et al., 2011). Therefore to determine the uptake of NPs by HUVEC, we utilized Cellix^{TM} microfluidic platform to expose cells to different NPs under various shear stress conditions, and employed fluorescence microscopy and the High Content Analysis software (IN Cell investigator software) to detect and quantify the nanoparticle cellular uptake.

HUVEC were grown on gelatin coated acrylic substrates and an optically transparent chip containing two semi-circular channels was placed on top of the substrate to create channels resembling human capillaries. NPs suspended in PBS were run over the unactivated or activated endothelial cells for 20 minutes under shear stress rates of 0.5, 1 or 5 dynes/cm^2 using a nanopump. Uptake of negatively charged 2.9 or 4.6 nm CdTe QDs and 50 nm fluorescent silica NPs were examined in three independent experiments. In each experiment, images of 3 fields were taken in each channel for each shear stress and fluorescence intensity quantified. Since 3μM concentration induced maximal aggregation of washed platelets (refer section 3.2.1), the same concentration was chosen for experiments with QDs. In case of silica NPs, a better fluorescence was observed with 200μg/ml concentration in our optimization studies. Hence, the same concentration of 200μg/ml was used for experiments with fluorescent silica particles.

The quantitative data for 2.9 nm QD, 4.6 nm QD and 50 nm silica NPs are shown in Figures 5.1, Figure 5.2 and Figure 5.3 respectively. Results observed with 2.9 nm QD showed a decreased uptake of QD with increasing shear stress rates. The QD uptake by unactivated endothelial cells was significantly lower in 5 dynes/cm^2 compared to 0.5 dynes/cm^2. In studies with 4.6 nm QD, a significant decrease in the QD uptake by unactivated HUVEC was observed at 5 dynes/cm^2 compared to 0.5 dynes/cm^2. In cells

exposed to 50 nm fluorescent silica NPs, the uptake by unactivated HUVEC was significantly lower at 5 dynes/cm^2 compared to 0.5 dynes/cm^2. However, no significant difference in the uptake was detected (2 way ANOVA) between unactivated and activated cells in all the NPs types studied.
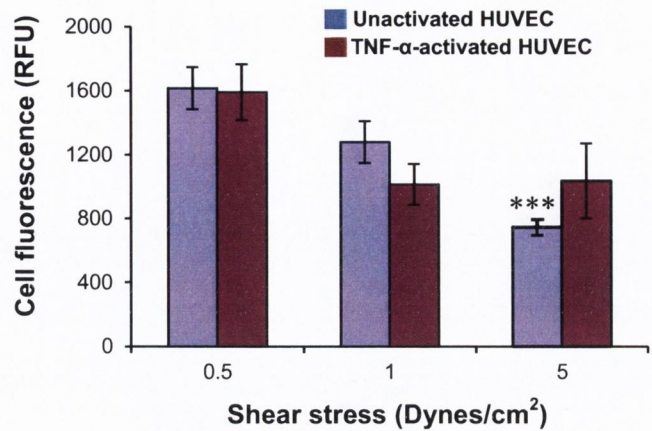
Figure 5.1: Uptake of negatively charged 2.9 nm (-32 mV) QDs by live HUVEC under controlled shear stress conditions. HUVEC were grown on gelatin coated Cellix biochips. Optically transparent PDMS chips were applied over intact HUVEC grown on Cellix biochips, thereby creating two channels. Negatively charged 2.9 nm QDs (3μM) re-suspended in PBS were run over unactivated or activated (TNF-α @10 ng/ml for 12 h) HUVEC under 0.5, 1 or 5 Dynes/cm^2 shear stresses for 20 minutes. Cellular uptake of NPs was judged by the overall cell fluorescence intensity (y-axis, relative fluorescence units). Data represents mean ± SEM of three independent experiments. ***p <0.001 vs. unactivated HUVEC at 0.5 Dynes/cm^2 (ANOVA with Dunnett's).
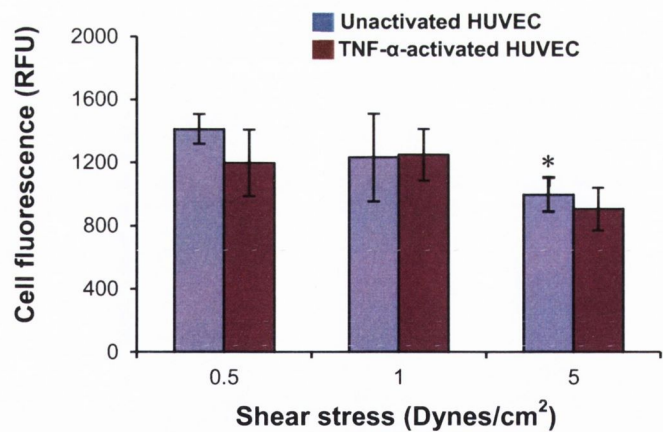
Figure 5.2: Uptake of negatively charged 4.6 nm (-60 mV) QDs by HUVEC under controlled shear stress conditions. HUVEC were grown on gelatin coated Cellix biochips. Optically transparent PDMS chips were applied over intact HUVEC grown on Cellix biochips, thereby creating two channels. Negatively charged 4.6 nm QDs (3μM) re-suspended in PBS were run over unactivated or activated (TNF-α @10 ng/ml for 12 h) HUVEC under 0.5, 1 or 5 Dynes/cm^2 shear stresses for 20 minutes. Cellular uptake of NPs was judged by the overall cell fluorescence intensity (y-axis, relative fluorescence units). Data represents mean ± SEM of three independent experiments. *p <0.05 vs. unactivated HUVEC at 0.5 Dynes/cm^2 (ANOVA with Dunnett's).
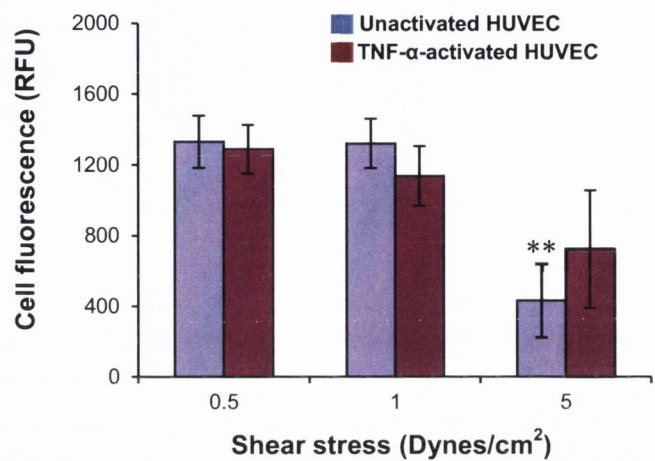
Figure 5.3: Uptake of negatively charged 50 nm (-42.2 mV) red fluorescent silica NPs by HUVEC under controlled shear stress conditions. HUVEC were grown on gelatin coated Cellix biochips. Optically transparent PDMS chips were applied over intact HUVEC grown on Cellix biochips, thereby creating two channels. Negatively charged 50 nm silica NPs (200µg/ml) re-suspended in PBS were run over unactivated or activated (TNF-α @10 ng/ml for 12 h) HUVEC under 0.5, 1 or 5 Dynes/cm^2 shear stresses for 20 minutes. Cellular uptake of NPs was judged by the overall cell fluorescence intensity (y-axis, relative fluorescence units). Data represents mean ± SEM of three independent experiments. **p <0.01 vs. unactivated HUVEC at 0.5 Dynes/cm^2 (ANOVA with Dunnett's).

5.2.2 Optimization of surfactant (Triton X-100) concentrations for permeabilizing live HUVEC.

Nonionic surfactants are widely used in biology for protein extraction from cells, as stabilizing and denaturing agents, and as membrane permeabilizing agents. Triton X-100 (Triton X) is one of the most widely used detergents for lysing cells to extract protein and other cellular organelles or to permeabilize the living cell membrane for transfection (Koley and Bard, 2010). However, cell death occurs if large amounts of detergents are added or if subjected to prolonged exposure to Triton X (Benoit et al., 1988, Borner et al., 1994). The polar head group of the Triton-X molecule disrupts the hydrogen bonding present within the cell's lipid bilayer, leading to the destruction of the compactness and integrity of the lipid membrane. The insertion of surfactant's polar head group into the lipid bilayer begins at low concentrations and causes disruption of cellular structure and eventual over-permeabilization of the cell membrane at concentrations above the critical micelle (aggregation of surfactant molecules) concentration. Introduction of hydrophilic species without damaging cells is difficult because cell viability is extremely sensitive within a narrow range of surfactant concentrations, especially near LD50 (The median lethal dose of a substance, or the amount required to kill 50% of a given test population) (Koley and Bard, 2010). Therefore, optimization of the concentration of Triton X to be employed on cultured live HUVEC was carried out.

HUVEC cells were cultured in 8 chamber slides. Cells were exposed to medium containing 0.001%, 0.01%, 0.1% or 0.5% Triton X for I hour at 37^0C. Cells not exposed to Triton X were taken as control. After fixing and staining (actin and nucleus), the cells were analyzed by confocal microscopy. The effect of 0.001%, 0.01%, 0.1% or 0.5% Triton X on live HUVEC is shown in Figure 5.4. As seen in Figure 5.4, exposure to 0.001% Triton X did not significantly alter the actin cytoskeleton of the cells compared to controls (No Triton X). However, cells exposed to 0.01%, 0.1% or 0.5% Triton X showed significant disruption of actin cytoskeleton compared to untreated cells.
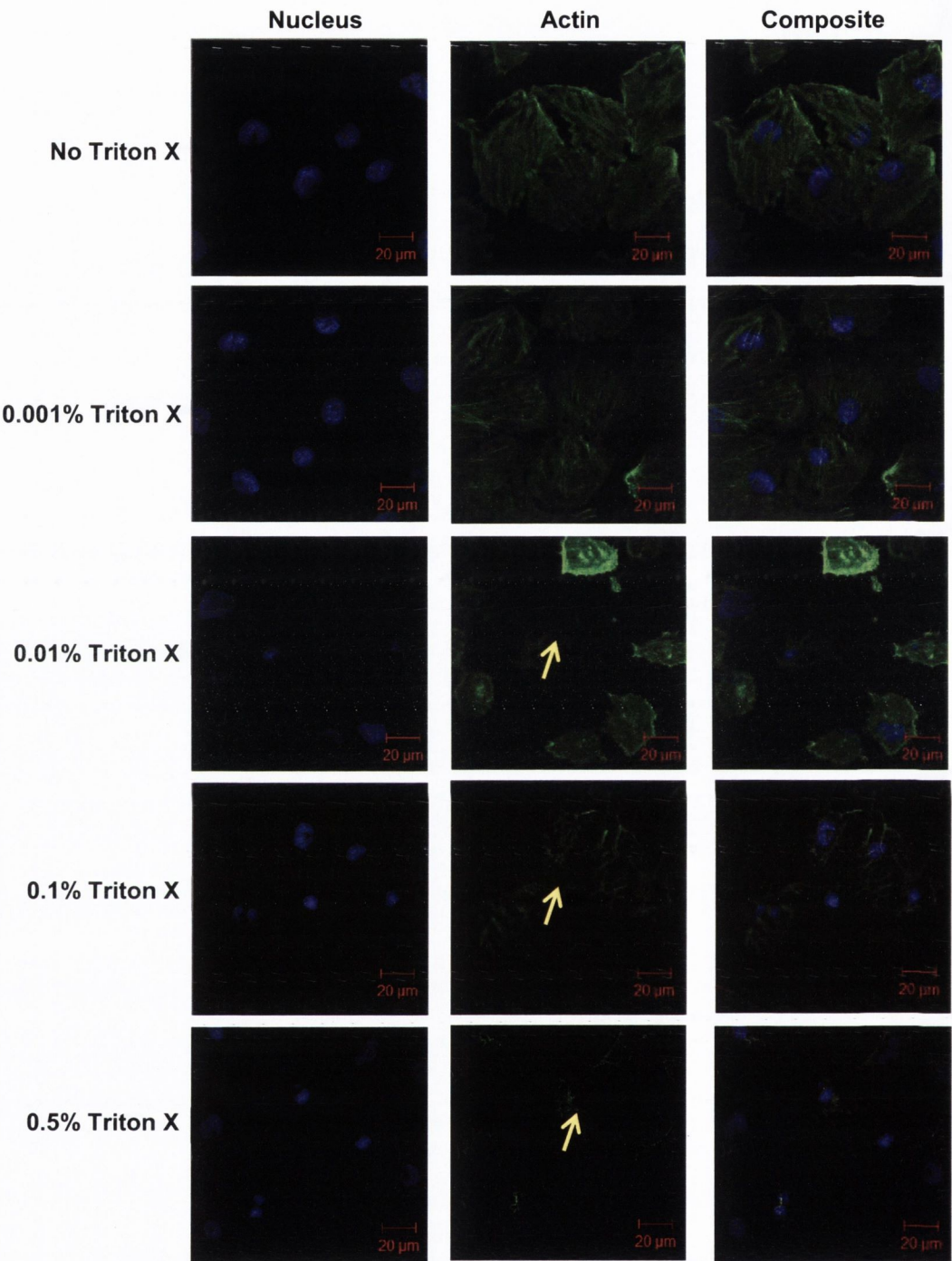
Figure 5.4: Effect of Triton X on actin cytoskeleton of live HUVEC. HUVEC were grown on 8 chamber slides. After the cells reached 80% confluence, live cells were treated with 0.001%, 0.01%, 0.1% or 0.5% Triton X in cell culture medium for 1 hour at 37^{0}C. Cells not treated with Triton X were taken as control. After fixation and staining (actin-red, nucleus-blue) the chambers were removed and cells covered with a glass cover slip using mounting medium and left at 4 degrees overnight. Confocal images (maximal projection) are shown. Images are representative of three independent experiments. Arrows: disrupted actin.

5.2.3 Characterization of nanoparticle localization in human endothelial cells under static and shear stress conditions.

NPs with certain surface functionalization have predictable cellular localization or molecular targets (nuclear localizing signal, antibody conjugates, etc.) (Alivisatos et al., 2005, Alivisatos, 2004, Smith et al., 2006). Multiple studies addressed the mechanism of interaction and distribution of nonfunctionalized NPs with human cells. There is evidence that negatively (Jaiswal et al., 2003) and positively (Duan and Nie, 2007, Knight and Serrano, 2006) charged QDs can be endocytosed and even penetrate the nucleus (Ryman-Rasmussen et al., 2007). A systematic study of the mechanism of interaction of nonfunctionalized CdTe and CdSe/ZnS QDs with a panel of live human cells of different origin (macrophages, vascular endothelium, upper and lower gastrointestinal epithelium) has demonstrated that the nonfunctionalized QDs exploit the cell's active transport machineries for delivery to specific intranuclear destinations (Nabiev et al., 2007). Investigators have studied the intracellular distribution of CdTe QDs on macrophage and lung epithelial cell lines, and showed that each cell line displays its own cut-off size thresholds reflecting cell-type-determined cytoplasmic and nuclear pore penetration specificity (Williams et al., 2009). Studies have shown that unmodified negatively charged CdTe QDs showed rapid accumulation in nucleus and nucleoli of living human cells and suggested that such strong tropism towards histones could be mediated by charge-related properties of the macromolecules presented in the nuclear compartments (Conroy et al., 2008). A recent study has found that conjugation of 100-nm polystyrene NPs with glycocalicin (the extracellular segment of GPIbα) significantly increased the particle adhesion on P-selectin-coated surfaces, and cellular uptake of NPs by activated endothelial cells under physiological flow conditions (Lin et al., 2010). No comprehensive study has been done on the distribution of QDs and silica NPs in human endothelial cells under physiological flow conditions. Therefore, the distribution of negatively charged 2.5 or 5 nm QDs and 50 nm fluorescent silica particles in HUVEC cells exposed to static or controlled shear stress conditions for 20 minutes was studied using Cellix^{TM} microfluidic platform.

For this study, two channels, resembling human capillaries, were created on top of HUVEC grown substrate as described in the methods. It has been shown that mild

detergent treatment (0.0094% Triton X) preserves cell viability but increases membrane penetration capacity of NPs (Williams et al., 2009). In addition, the same authors found that fixing and permeabilizing the cells prior to addition of QDs eliminates any cell-membrane-associated effects due to active QD uptake mechanisms but leaves the putative physical subcellular barriers intact. Therefore, endothelial cells were exposed to 0.001% Triton X for 1 h or fixed/permiabilized with 0.5% Triton X (3 min) before the experiments. Cells were then exposed to NPs under static condition or at a shear stress rate of 0.5 dynes/cm^2. Endothelial cells exposed to NPs under static conditions were used as controls. Negatively charged 2.5 and 5 nm CdTe QDs and 50 nm fluorescent silica NPs were used in the same concentrations as before. Following exposure to NPs, cells on the acrylic substrate were fixed and stained for the actin and nucleus. After washing, the acrylic substrate with cells was mounted on a glass slide and covered with a glass coverslip using a mounting medium. The slides were then analysed by confocal microscopy.

Figure 5.5 shows confocal images (maximal projection) of HUVEC exposed to 2.5 nm CdTe QDs under static and shear stress conditions. In un-permeabilized (not treated with Triton X) cells, shear stress significantly increased the uptake of QDs compared to cells not exposed to shear stress. The QD uptake was significantly increased when permeabilized (treated with 0.001% Triton X) cells are exposed under shear stress of 0.5 dynes/cm^2 compared to cells exposed to QDs under static conditions. With fixed and permeabilized cells (Fixed + treated with 0.5% Triton X), there was a significant uptake of QDs in both static and shear stress conditions. Under static conditions, there was no uptake of QDs in both permeabilised and non permeabilised live HUVEC. The key advantage of confocal microscopy is the possibility to obtain images of planes at various depths within the sample (known as Z-stacks) . Figure 5.6 shows one of the images from the Z-stack (single slice) of endothelial cells of showing QD uptake. Under flow conditions, QDs were found localized in the cytoplasm (near the nucleus) of both cells unexposed to detergent (a) and cells exposed to 0.001% Triton X (b). However, when fixed and permeabilized cells were exposed to QDs under static (c) and shear stress (d) conditions, QDs were found distributed in both the cytoplasm and the nucleus.

Figure 5.7 shows confocal images (maximal projection) of HUVEC exposed to 5 nm CdTe QDs under static and shear stress conditions. In unpermeabilized (not treated with

Triton X) cells, shear stress significantly increased the uptake of QDs compared to cells not exposed to shear stress. The QD uptake was significantly increased when permeabilized (treated with 0.001% Triton X) cells were exposed kept at a shear stress of 0.5 dynes/cm^2 compared to cells exposed to QDs under static conditions. In studies with fixed and permeabilized cells treated with 0.5% Triton X, there was a significant uptake of QDs in both static and shear stress conditions. Under static conditions, there was no uptake of QDs in both permeabilised and non permeabilised live HUVEC. Figure 5.8 shows one of the images from the Z-stack (single slice) obtained from endothelial cells showing QD uptake. Under flow conditions, QDs were found localized in the cytoplasm (near the nucleus) of both intact cells (a) and the cells exposed to 0.001% Triton X (b). However, when fixed and permeabilized cells were exposed to QDs under static (c) conditions the particles were found to be concentrated in the perinuclear region, and under shear stress (d) conditions, the QDs were found to be more uniformly distributed in the cytoplasm.

Figure 5.9 shows confocal images (maximal projection) of HUVEC exposed to 50 nm silica NPs under static and shear stress conditions. In unpermeabilized (not treated with Triton X) cells, shear stress significantly increased the uptake of NPs compared to cells not exposed to shear stress. The nanoparticle uptake was significantly increased when permeabilized (treated with 0.001% Triton X) cells were exposed under shear stress of 0.5 dynes/cm^2 compared to cells exposed to NPs under static conditions. In studies with fixed and permeabilized cells (Fixed + treated with 0.5% Triton X), shear stress caused a significant increase in nanoparticle uptake compared to cells not exposed to shear stress. Figure 5.10 shows one of the images from the Z stacks obtained from endothelial cells illustrating nanoparticle uptake. Under flow conditions, NPs were found associated with the outer membrane in both the intact cells (a) and cells treated with 0.001% Triton X (b). However, when fixed and permeabilized cells were exposed to NPs under static (c) conditions there was no uptake of NPs, whereas under shear stress (d) conditions NPs were found to be distributed in the cytoplasm.
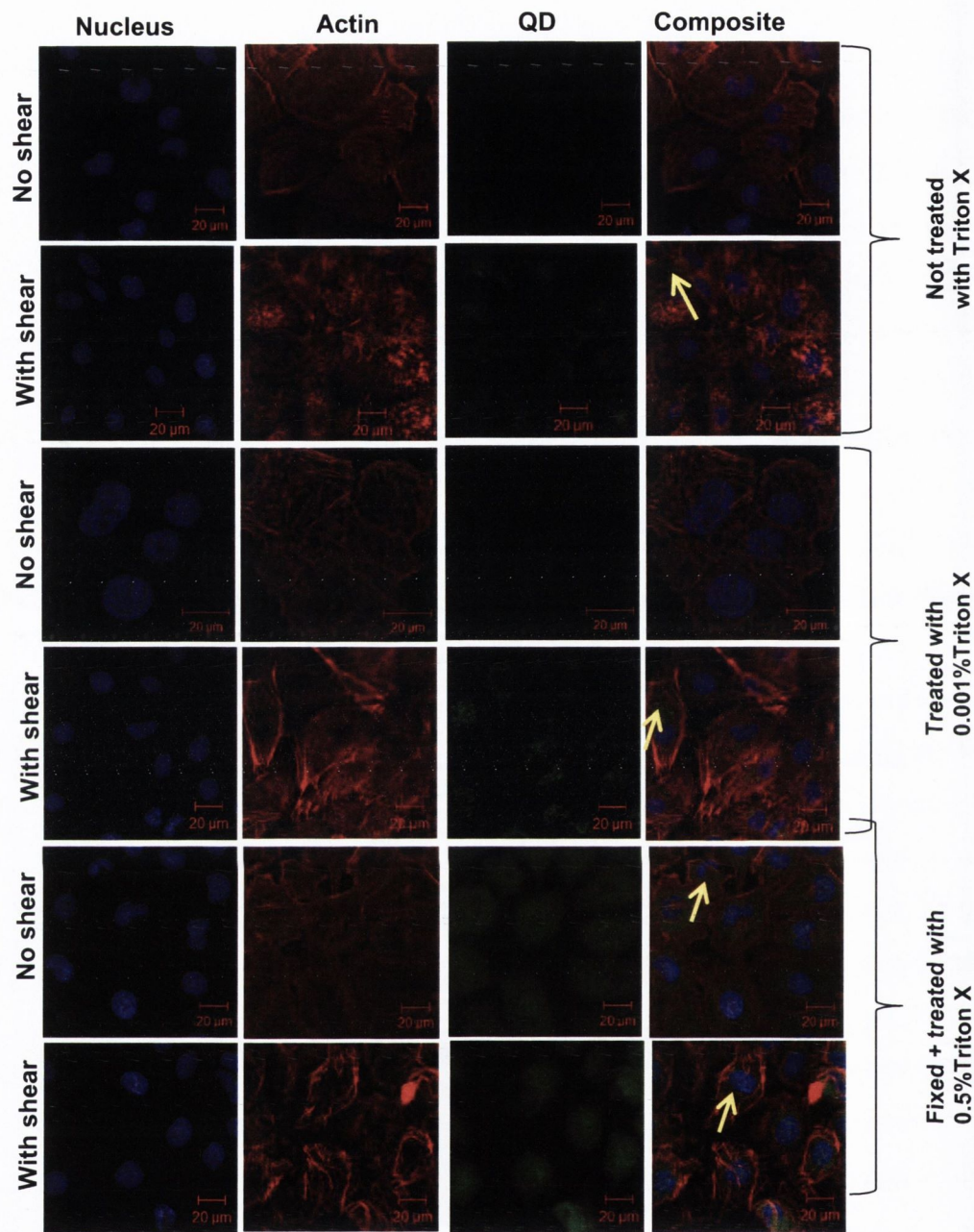
Figure 5.5: Uptake of negatively charged 2.5 nm CdTe QDs by HUVEC. HUVEC were grown on gelatin coated Cellix Vena EC biochips. Optically transparent PDMS chip containing two semi-circular channels were applied over HUVEC grown on acrylic substrates, thereby creating two channels. Negatively charged 2.5 nm QDs suspended in PBS were run over HUVEC at 0.5 Dynes/cm^2 shear stress for 20 minutes under various conditions as indicated. After removing the PDMS chips, biochips were fixed and stained (actin-red, nucleus-blue). The cells were covered with a glass cover slip using mounting medium and left at 4^{0}C overnight. Samples were then analysed using confocal microscopy. Uptake of QDs between HUVEC exposed (With shear) or not exposed (No shear) to shear was compared. Confocal images (maximal projection) are shown. Images are representative of three independent experiments. Arrows: location of 2.5 nm QDs.
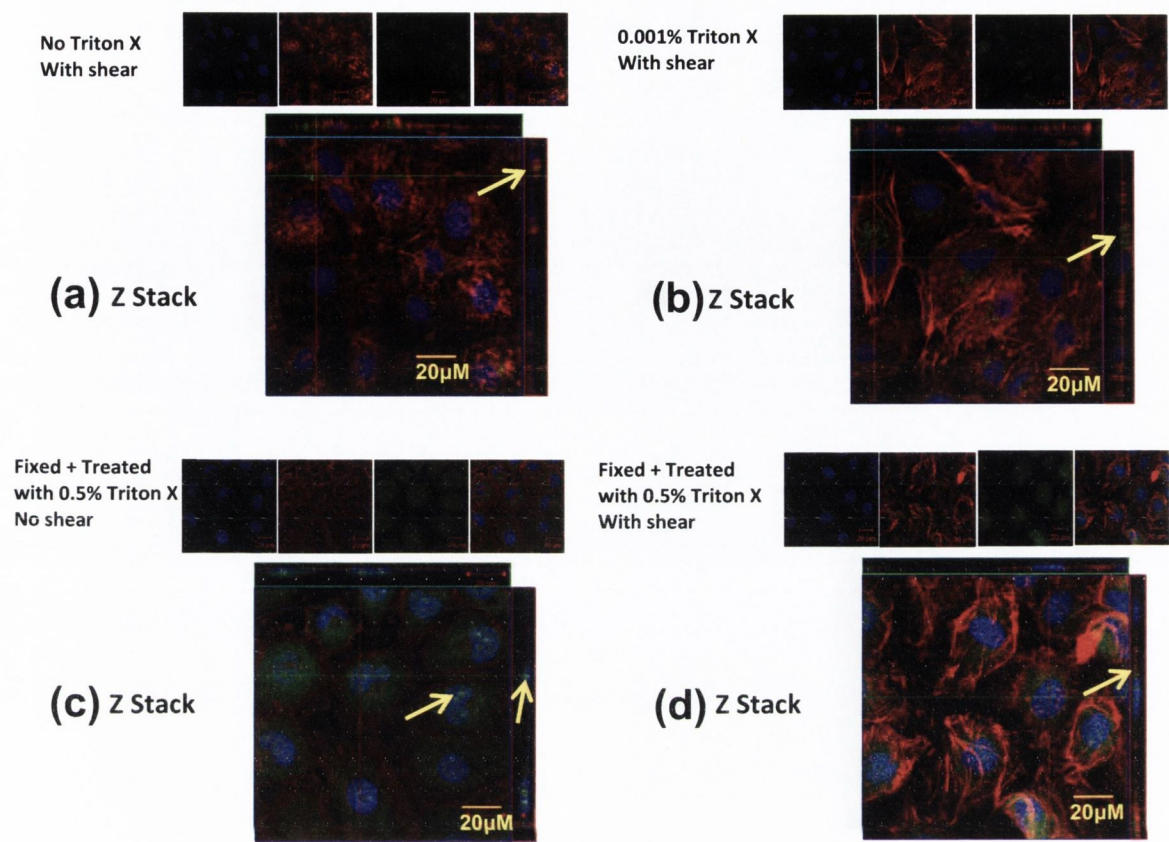
Figure 5.6: Localization of negatively charged 2.5 nm CdTe QDs in HUVEC. HUVEC were exposed to QDs under various conditions. Z-stack (single slice) images of HUVEC showing uptake of QDs in the following conditions. (a) Z-stack showing intra-cytoplasmic localization of QDs in cells which are not treated with Triton X and exposed to QDs under shear conditions; (b): Z-stack showing intra-cytoplasmic localization of QDs in cells which are treated with 0.001% Triton X and exposed to QDs under shear conditions; (c): Z-stack showing both intra-cytoplasmic and intra-nuclear localization of QDs in cells which are fixed with 2%PFA, treated with 0.5% Triton X and exposed to QDs under static conditions; (d): Z-stack showing both intra-cytoplasmic and intra-nuclear localization of QDs in cells which are fixed with 2%PFA, treated with 0.5% Triton X and exposed to QDs under shear conditions. Images are representative of three independent experiments. Arrows: location of 2.5 nm QDs

Figure 5.7: Uptake of negatively charged 5 nm CdTe QDs by HUVEC. HUVEC were grown on gelatin coated Cellix Vena EC biochips. Optically transparent PDMS chip containing two semi-circular channels were applied over HUVEC grown on acrylic substrates, thereby creating two channels. Negatively charged 5 nm QDs suspended in PBS were run over HUVEC at 0.5 Dynes/cm^2 shear stress for 20 minutes under various conditions as indicated. After removing the PDMS chips, biochips were fixed and stained (actin-red, nucleus-blue). The cells were covered with a glass cover slip using mounting medium and left at 4^{0}C overnight. Samples were then analysed using confocal microscopy. Uptake of QDs between HUVEC exposed (With shear) or not exposed (No shear) to shear was compared. Confocal images (maximal projection) are shown. Images are representative of three independent experiments. Arrows: location of 5 nm QDs
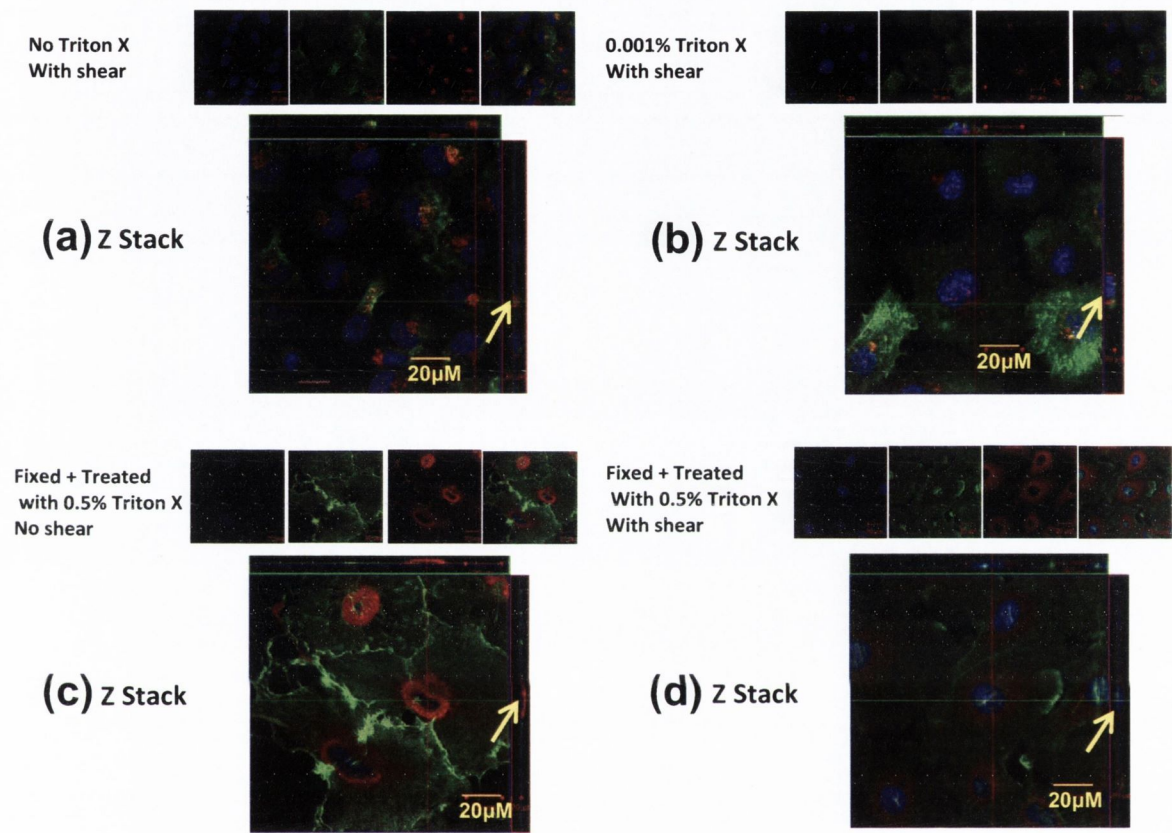
Figure 5.8: Localization of negatively charged 5 nm CdTe QDs in HUVEC. HUVEC were exposed to QDs under various conditions. Z-stack (single slice) images of HUVEC showing uptake of QDs in the following conditions. (a) Z-stack showing intra-cytoplasmic localization of QDs in cells which are not treated with Triton X and exposed to QDs under shear conditions; (b): Z-stack showing intra-cytoplasmic localization of QDs in cells which are treated with 0.001% Triton X and exposed to QDs under shear conditions; (c): Z- stack showing peri-nuclear localization of QDs in cells which are fixed with 2%PFA, treated with 0.5% Triton X and exposed to QDs under static conditions; (d): Z-stack showing intra-cytoplasmic localization of QDs in cells which are fixed with 2%PFA, treated with 0.5% Triton X and exposed to QDs under shear conditions. Images are representative of three independent experiments. Arrows: location of 5 nm QDs.
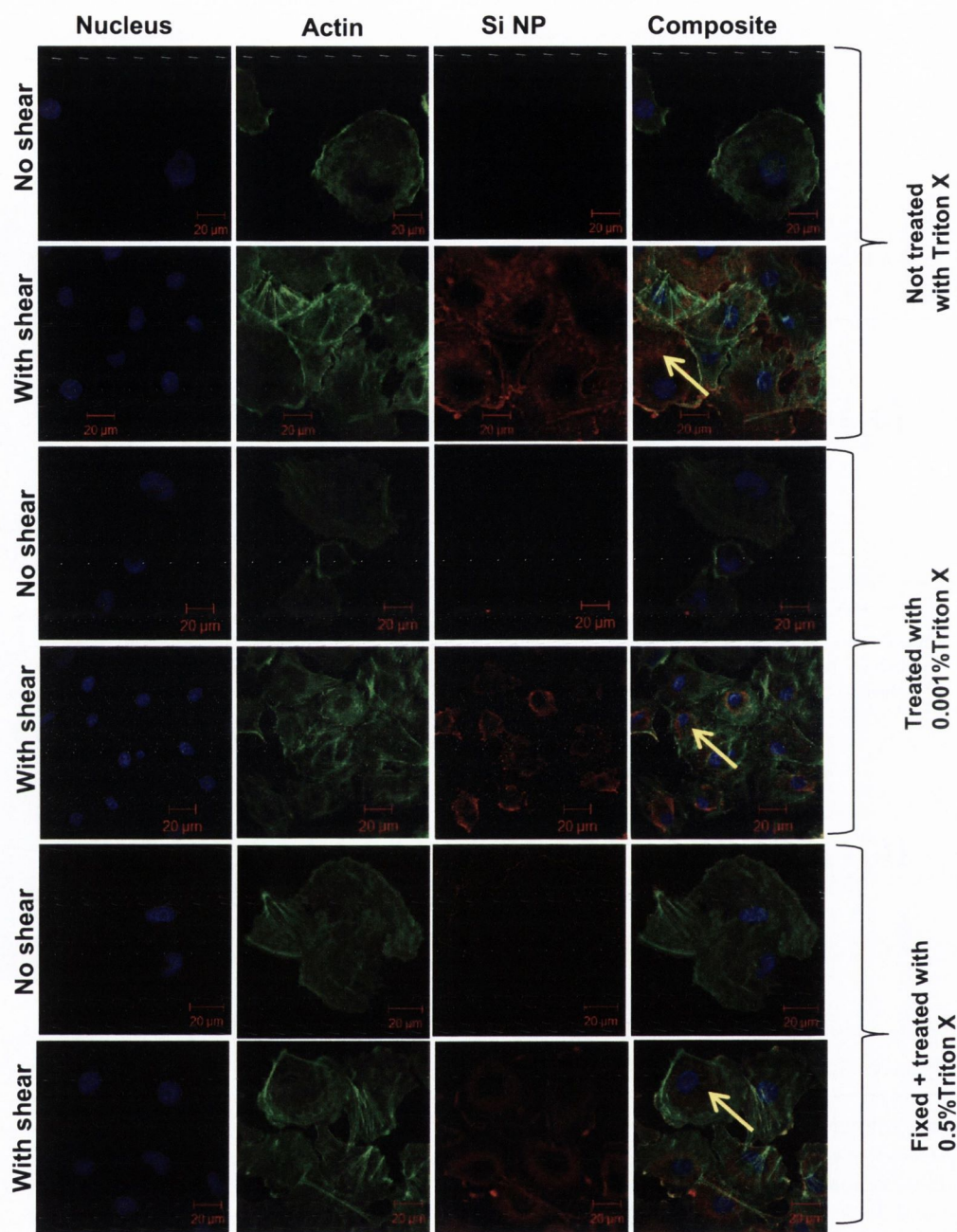
Figure 5.9: Uptake of negatively charged 50 nm fluorescent silica NPs by HUVEC. HUVEC were grown on gelatin coated Cellix biochips. Optically transparent PDMS chip containing two semi-circular channels were applied over HUVEC grown on acrylic substrates, thereby creating two channels. Negatively charged 50nm silica NPs suspended in PBS were run over HUVEC at 0.5 Dynes/cm^2 shear stress for 20 minutes under various conditions as indicated. After removing the PDMS chips, biochips were fixed and stained (actin-red, nucleus-blue). The cells were covered with a glass cover slip using mounting medium and left at 4^{0}C overnight. Samples were then analysed using confocal microscopy. Uptake of QDs between HUVEC exposed (With shear) or not exposed (No shear) to shear was compared. Confocal images (maximal projection) are shown. Images are representative of three independent experiments. Arrows: location of 50 nm silica NPs.
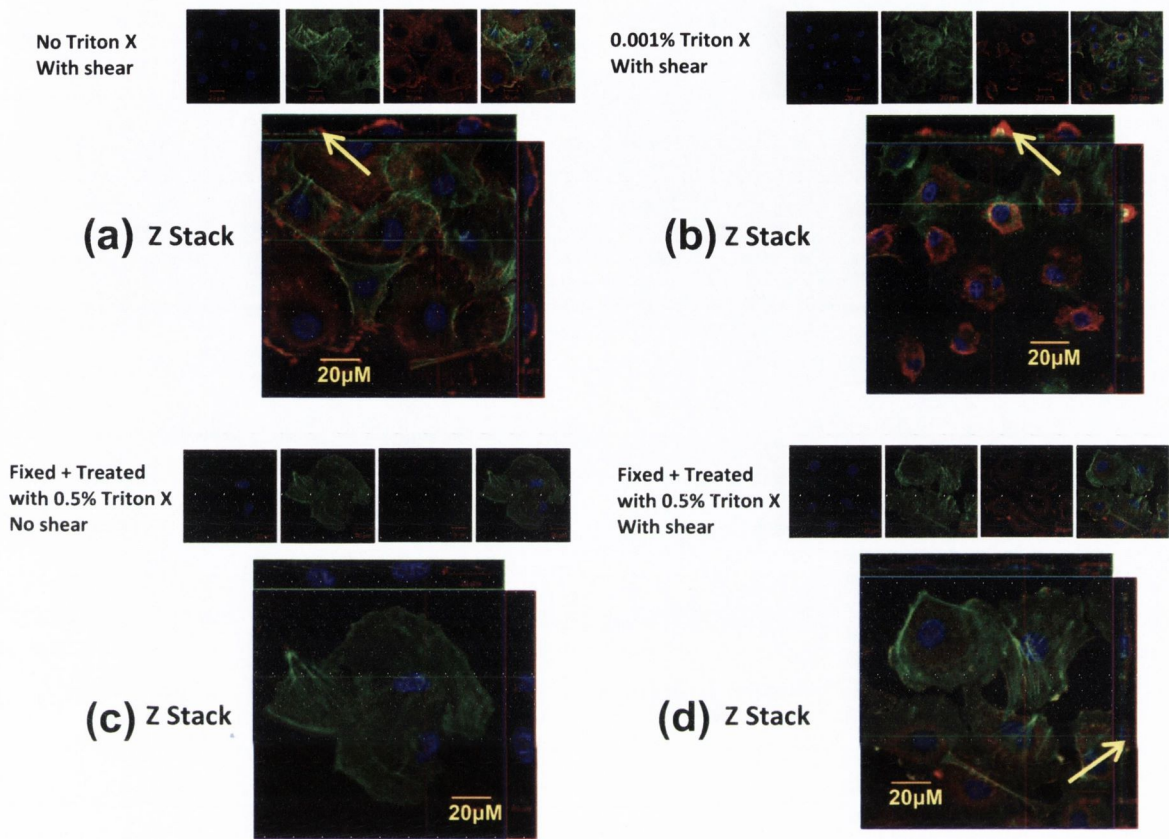
Figure 5.10: Localization of negatively charged 50 nm fluorescent silica NPs in HUVEC. HUVEC are exposed to silica NPs under various conditions. Z-stack (single slice) images shows HUVEC associated with nanoparticles under following conditions. (a) Z stack showing surface localization of NPs in cells which are not treated with Triton X and exposed to NPs under shear conditions; (b): Z stack showing surface localization of NPs in cells which are treated with 0.001% Triton X and exposed to NPs under shear conditions; (c): Z stack showing absence of NPs association in cells which are fixed with 2%PFA, treated with 0.5% Triton X and exposed to NPs under static conditions; (d): Z stack showing intra-cytoplasmic localization of NPs in cells which are fixed with 2%PFA, treated with 0.5% Triton X and exposed to NPs under shear conditions. Images are representative of three independent experiments. Arrows: location of 50 nm silica NPs.

5.2.4 Effect of shear stress on HUVEC cell morphology

Vascular endothelial cells are continuously exposed to hemodynamic forces of the flowing blood inside the blood vessel. It has been well established that wall shear stress is an important determinant of endothelial cell structure, function and gene expression (Reneman et al., 2006). Previous studies have demonstrated that the sub-confluent endothelial cultures undergo a time dependent change in cell shape when exposed to a laminar shear stress of 5-10 dynes/cm^2 (Dewey et al., 1981).

Studies have been done in flow systems such as cone-and plate device (Davies et al., 1986, Dewey et al., 1981, Franke et al., 1984), parallel plate chamber (Frangos et al., 1985, Levesque and Nerem, 1985, Shen et al., 1992) or flow tube (Dull and Davies, 1991, Olesen et al., 1988). Here the endothelial cells grown on acrylic biochips were exposed to a shear stress of 0.5 dynes/cm^2 in a microfluidic platform. The cells on the chips were fixed/stained (actin-red, nucleus-blue) for confocal microscopy studies. For atomic force microscopy (AFM) studies, the cells were either fixed and left in PBS (for wet phase) or dehydrated with ascending grades of ethanol (for dry phase). Detailed characterization of surface topography of the cell in response to fluid forces has been inaccessible until the advent of the AFM (Binnig et al., 1986). The AFM, which raster-scans a sample past a sharp stylus tracking the surface undulations, can image samples in a fluid environment. AFM has been used to image hard surfaces with atomic resolution (Ohnesorge and Binnig, 1993), biologic molecules bound to a surface (Butt et al., 1990, Hoh et al., 1991, Lal et al., 1993, Lal and Yu, 1993, Yang et al., 1993), and both fixed and living cells (Henderson et al., 1992, Horber et al., 1992, Kasas et al., 1993, Radmacher et al., 1992). In the present study, we utilized AFM to image the surface topography of fixed endothelial cells after being subjected to shear stress, and confocal microscopy to visualize actin cytoskeleton.

The confocal images (maximal projection) of cells are shown in Figure 5.11. The cells exposed to shear stress (b) showed a notable difference in the actin cytoskeleton compared to the cells unexposed to shear stress (a).

Images of endothelial cells taken by AFM are shown in Figure 5.12. As shown in dry phase images (a), HUVEC not exposed to shear stress did not show membrane ruffling or stress fibers. However, HUVEC exposed to 0.5 dynes/cm^2 induced formation of

membrane ruffling and stress fibers. The findings were consistent with the liquid phase AFM data (b), with an exception that stress fibers were less prominent in the latter case.
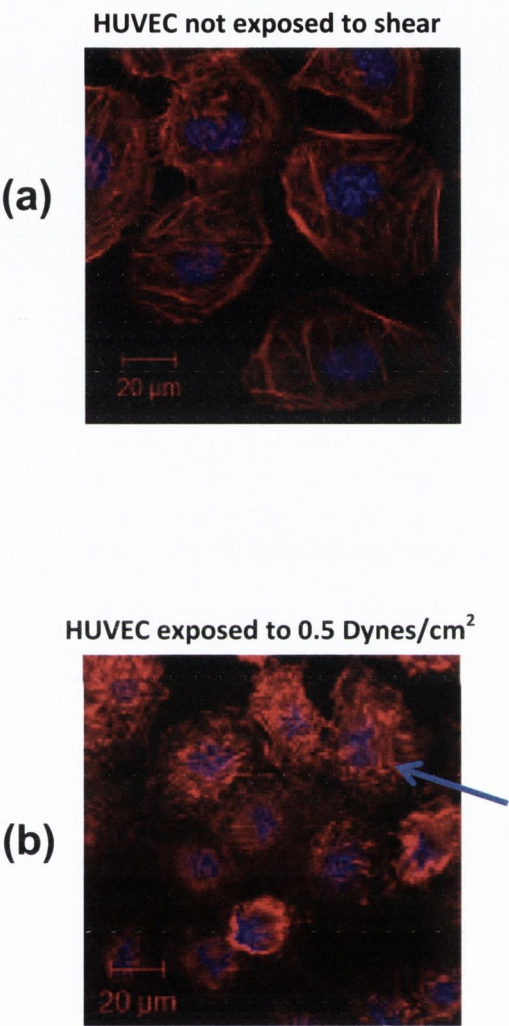
Figure 5.11: Shear induced cytoskeletal reorganization. HUVEC were grown on gelatin coated Cellix biochips. Optically transparent PDMS chip containing two semi-circular channels were applied over HUVEC grown on acrylic substrates, thereby creating two channels. HUVEC not exposed to shear were taken as controls (a). PBS without QDs was run over HUVEC at a shear stress of 0.5 Dynes/cm^2 for 20 minutes (b). After fixation and staining (actin-red, nucleus-blue) membrane morphology was studied by confocal microscopy. Images are representative of three independent experiments and show shear induced cytoskeletal (actin) reorganisation (arrow).

(a) AFM images in Dry phase

HUVEC not exposed to shear

HUVEC exposed to 0.5 Dynes/cm²
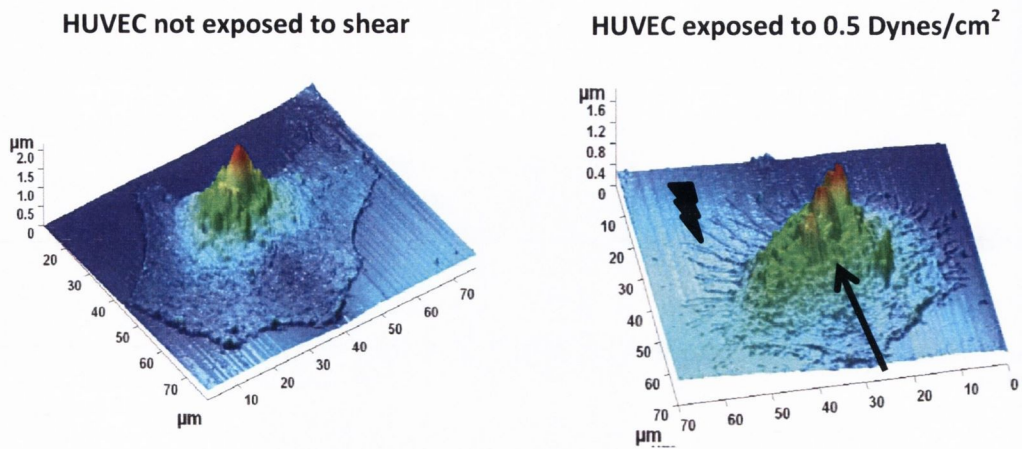
(b) AFM images in liquid phase

HUVEC not exposed to shear

HUVEC exposed to 0.5 Dynes/cm²
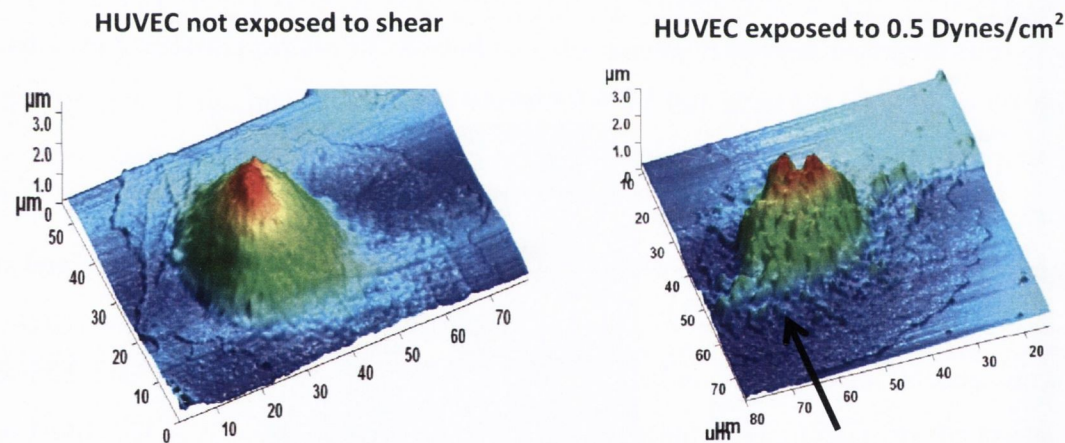
Figure 5.12: Shear induced changes in membrane topography. HUVEC were grown on gelatin coated Cellix biochips. Optically transparent PDMS chip containing two semi-circular channels were applied over HUVEC grown on acrylic substrates, thereby creating two channels. PBS without QDs was run over HUVEC at a shear stress of 0.5 Dynes/cm² for 20 minutes. HUVEC not exposed to shear taken as controls. After fixing the cells with glutaraldehyde, the cells were either dehydrated with ascending grades of ethanol for dry phase imaging (a) or left in PBS for liquid phase (b) imaging. The changes in membrane morphology were studied by atomic force microscopy (AFM). AFM images of HUVEC are shown. Images are representative of three independent experiments and show shear induced membrane ruffling (arrows) and actin stress fibres (lightning bolt).

5.2.5 Cytotoxic effects of nanoparticles on HUVEC cells

Nanomaterials have the potential for widespread application in biology and medicine. There are many routes for nanomaterials into human body. Once NPs entered into blood by inhalation or injection, it is inevitable that endothelial cells have a direct contact with these particles. Therefore, it is necessary to evaluate toxic effects of these NPs on endothelial cells. Traditionally, MTT (3-(4, 5-dimethylthiazol-2-yl)-2, 5-diphenyl-2h-tetrazolium bromide) or proliferation assay (determines cell survival) and lactate dehydrogenase assay (indicates cytotoxic damage) were used to evaluate the cytotoxic effects of NPs. Many studies have been performed to evaluate the cytotoxic effects of various NPs such as carbon black (Yamawaki and Iwai, 2006b), 45 nm silver (Rosas-Hernández et al., 2009), metal oxides (20-70 nm ZnO, 20-60 nm Y_2O_3 and 45 nm Fe_2O_3) (Gojova et al., 2007), 100 nm MgO (Ge et al., 2011), 14-335 nm silica (Napierska et al., 2009), 3.36 nm QDs (Yan et al., 2011) on endothelial cells. In toxicity studies with nanomaterials, the dye compounds used as reporters may interact with NPs causing significant interference with the assay performance, for instance due to fluorescence shift (Worle-Knirsch et al., 2006). A cell-based high content screening (HCS) assay operating on the principle of fully automated fluorescence microscopy was introduced recently as a modern drug discovery tool (Perlman et al., 2004). This technology assists the research and industry in understanding complex cellular processes in disease pathogenesis, drug target validation and drug lead identification (Mohamed et al., 2008, Mohamed et al., 2011). HCS assays are becoming an indispensable approach in studying the cytotoxicity of nanomaterials because they permit multiplexing of key reporter parameters such as cell viability, permeability, membrane potential and lysosomal mass (Mohamed et al., 2011). Therefore, in this study, we employed high content analysis platform to investigate the potential vascular endothelial toxicity of negatively charged 5 nm silica, 50 nm silica (fluorescent), 51 nm silica coated magnetite, 9 nm citrate stabilized magnetite NPs and TGA-capped 2.7 or 4.6 nm CdTe QDs on HUVEC in vitro in static conditions.

For this study, HUVEC cells were grown in 96 well plates. Cells were then treated with 1, 3 or 5μM concentrations of negatively charged silica, silica coated magnetite, and citrate stabilized magnetite for 20 min, 4 h, 8 h or 24 h. In the case of QDs, since 3μM concentration was used in QD uptake (refer section 5.2.1) and localization (refer section

5.2.3) studies, endothelial cells were treated with the same concentration of CdTe QDs for 20 min, 4 h, 8 h or 24 h. For experiments with fluorescent silica NPs, 50, 100, 200 or 400µg/ml concentrations were used. Untreated cells were taken as negative control. Cells were also treated with 3µM positively charged CdTe QDs and taken as an additional comparative control. After fixing and staining (actin and nucleus), the plates were analysed using high content analysis platform (IN Cell Analyzer 1000) and the viable cell number was quantified.

The results of the cytotoxicity analysis of negatively charged 5 nm silica NPs on HUVEC are shown in Figure 5.13. No significant difference in the cell count was observed with 3 or 5µM concentrations. However, a significant reduction in cell numbers was noted with 1 µM concentration at 4 h. In studies with negatively charged 51 nm silica coated magnetite NPs (Figure 5.14), 1 µM caused a significant reduction in cell number at 4 h compared to untreated cells. However, negatively charged 9 nm citrate stabilized magnetite NPs (Figure 5.15) did not show any significant difference in cell numbers compared to controls in all the concentrations used. Results obtained from endothelial cells treated with 3µM of negatively charged 2.7 nm CdTe QDs are shown in Figure 5.16. There was no significant difference in cell number for up to 8 h compared to controls. However, a significant reduction in cell number was observed at 24 h. The influence of negatively charged 4.6 nm CdTe QDs on endothelial cell viability is shown in Figure 5.17. A significant reduction in cell number was observed with at 20 min, 4 h, 8 h and 24 h. The cytotoxic effects of negatively charged 50 nm fluorescent silica NPs on HUVEC are shown in Figure 5.18. No significant difference in cell number was noted with 50, 100 and 200 µg/ml concentrations. However, at 4 h, there was a significant reduction in cell number with 400 µg/ml concentration compared to untreated cells.
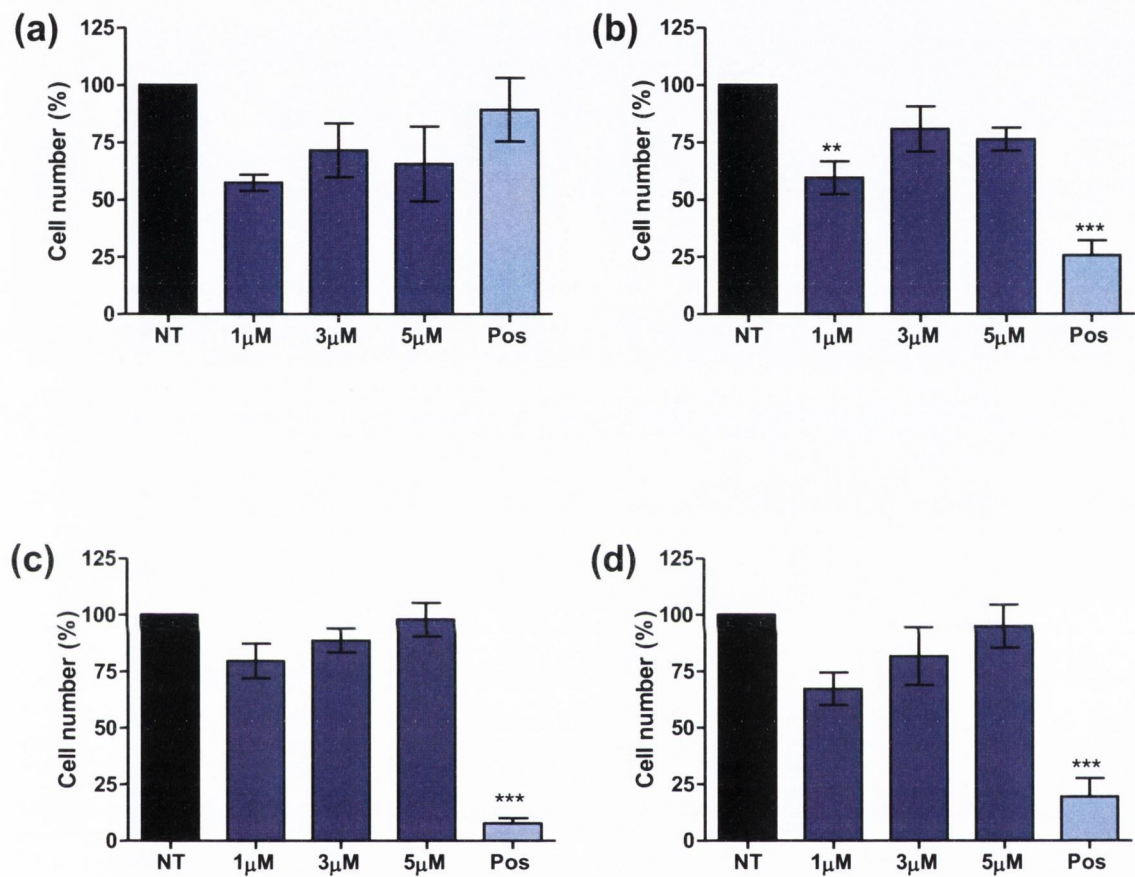
Figure 5.13: Cytotoxic effects of negatively charged 5 nm silica NPs nanoparticles on HUVEC cells. HUVEC grown in 96 well plates were treated with various concentrations of negatively charged 5 nm silica NPs or 3μM positively charged QDs (Pos) for 20 min (a), 4 h (b), 8 h(c) or 24 h (d). Viable cell number was quantified using IN Cell analyzer 1000 automated microscope. Data are mean ± SEM of three independent experiments performed in triplicate. NT, no treatment. **p < 0.01, ***p < 0.001 vs. NT (ANOVA with Dunnett's).
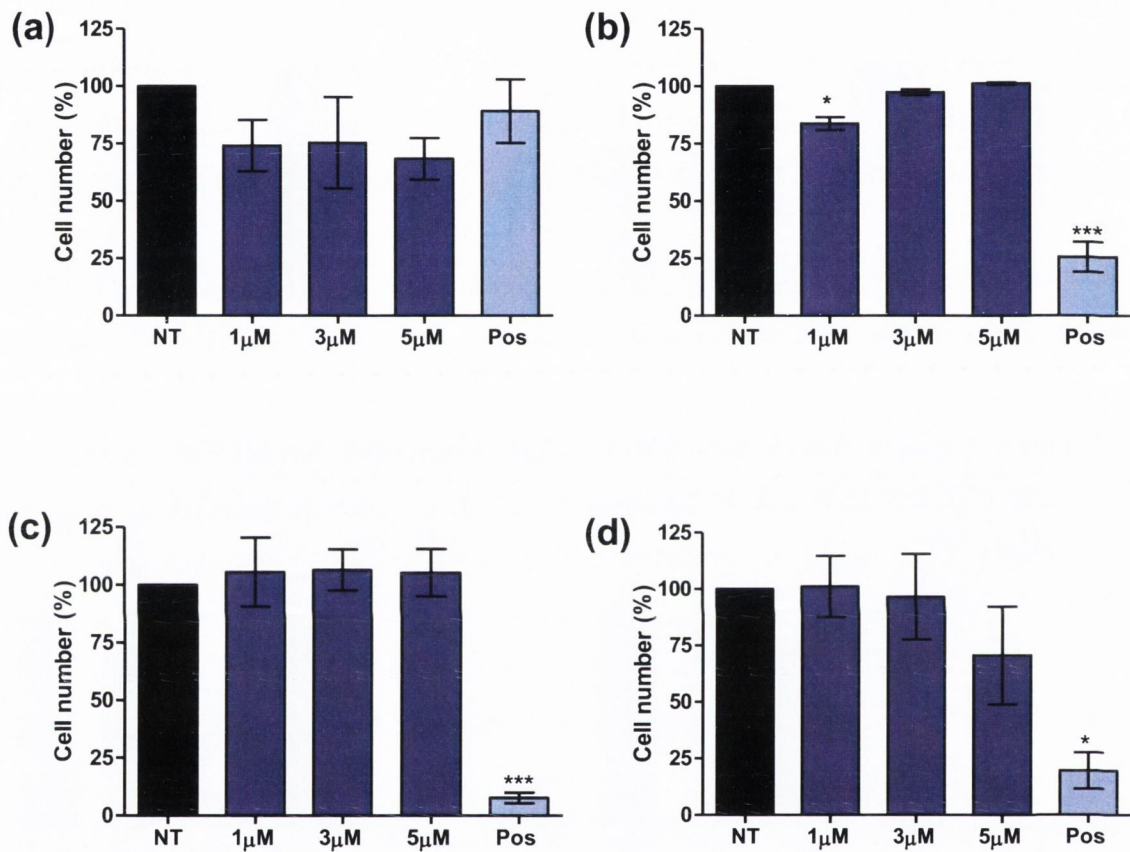
Figure 5.14: Cytotoxic effects of negatively charged 51 nm silica coated magnetite NPs on HUVEC cells. HUVEC grown in 96 well plates were treated with various concentartions of negatively charged 51 nm silica coated magnetite NPs or 3μM positively charged QDs (Pos) for 20 min (a), 4 h (b), 8 h (c) or 24 h (d). Viable cell number was quantified using INCell analyzer 1000 automated microscope. Data are mean ± SEM of three independent experiments performed in triplicate. NT, no treatment. *p < 0.05, ***p < 0.001vs. NT (ANOVA with Dunnett's).
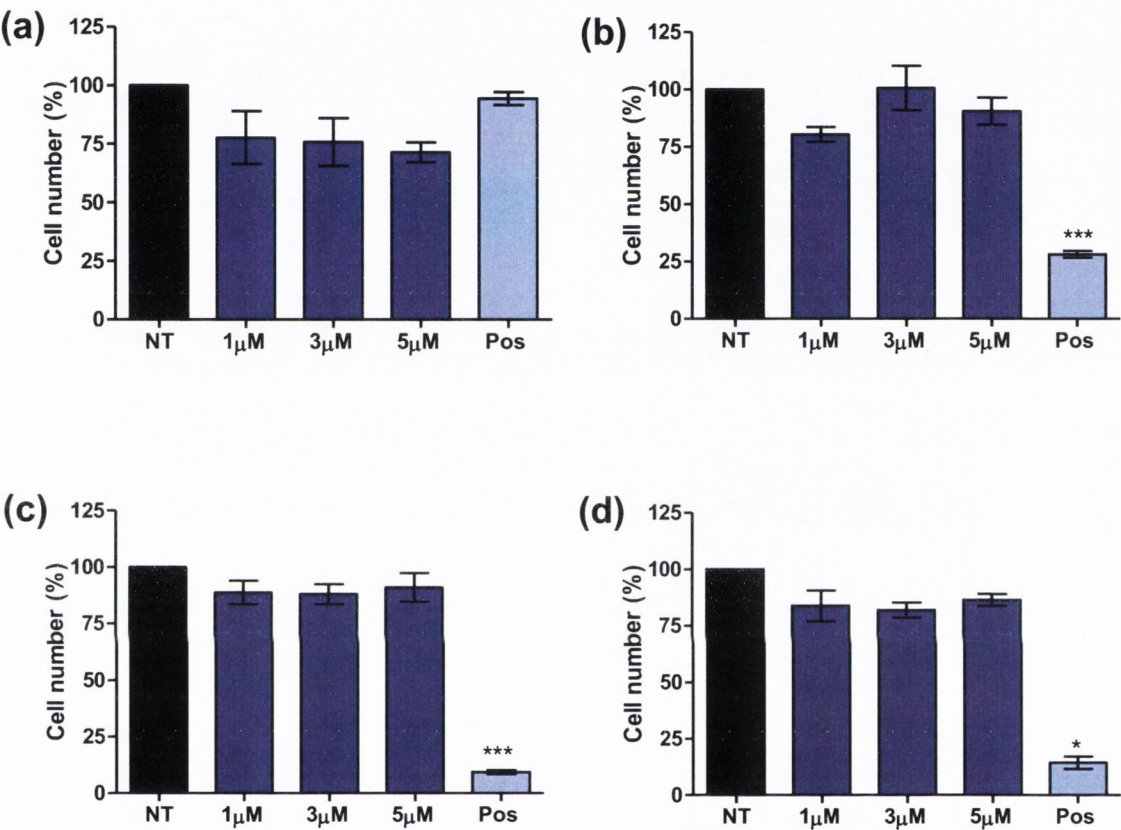
Figure 5.15: Cytotoxic effects of negatively charged 9 nm citrate stabilized magnetite NPs on HUVEC cells. HUVEC grown in 96 well plates were treated with negatively charged 9 nm citrate stabilized magnetite NPs or 3μM positively charged QDs (Pos) for 20 min (a), 4 h (b), 8 h (c) or 24 h (d). Viable cell number was quantified using INCell analyzer 1000 automated microscope. Data are mean ± SEM of three independent experiments performed in triplicate. NT, no treatment. *p < 0.05, ***p < 0.001vs. NT (ANOVA with Dunnett's).
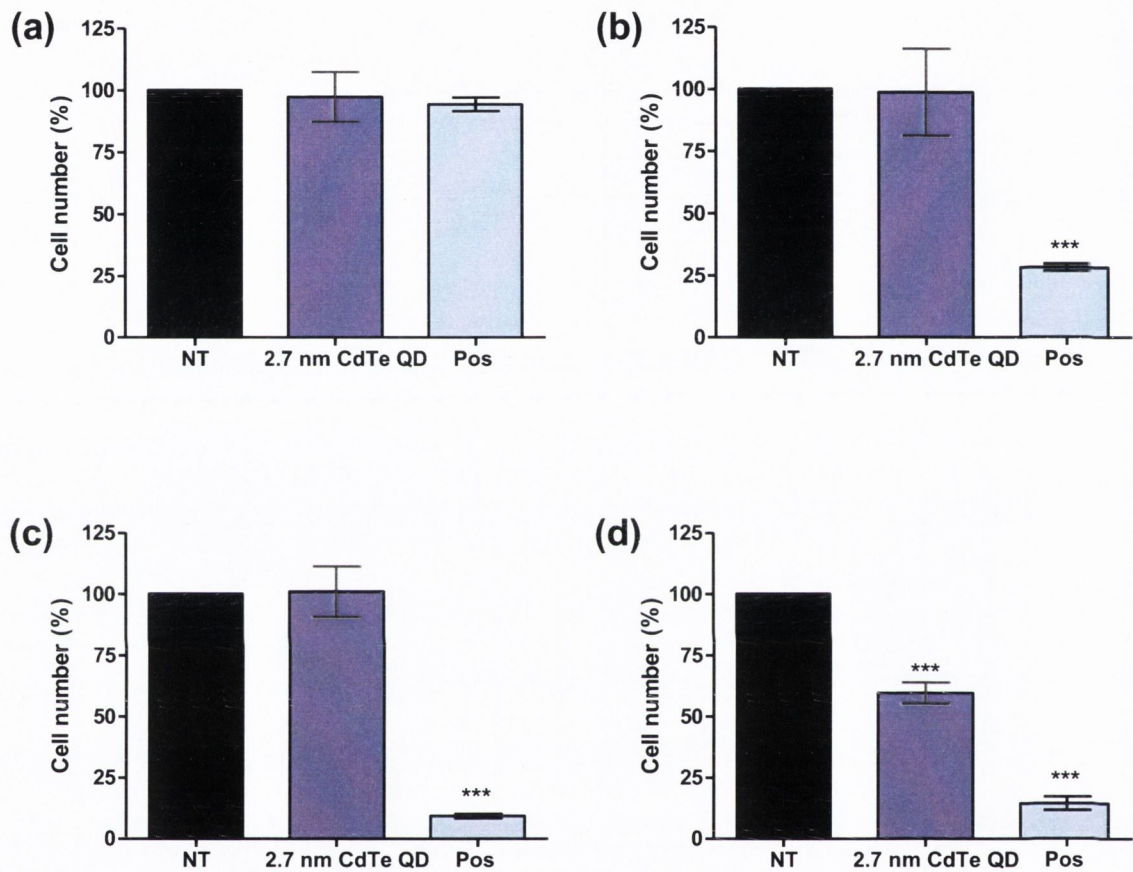
Figure 5.16: Cytotoxic effects of negatively charged 2.7 nm CdTe QDs on HUVEC cells. HUVEC grown in 96 well plates were treated with negatively charged 2.7 nm CdTe QDs or 3μM postively charged QDs (Pos) for 20 min (a), 4 h (b), 8 h (c) or 24 h (d). Viable cell number was quantified using INCell analyzer 1000 automated microscope. Data are mean ± SEM of three independent experiments performed in triplicate. NT, no treatment. ***$p < 0.001$ vs. NT (ANOVA with Dunnett's).

Figure 5.17: Cytotoxic effects of negatively charged 4.6 nm CdTe QDs on HUVEC cells. HUVEC grown in 96 well plates were treated with negatively charged 4.6 nm CdTe QDs or 3µM positively charged QDs (Pos) for 20 min (a), 4 h (b), 8 h (c) or 24 h (d). Viable cell number was quantified using INCell analyzer 1000 automated microscope. Data are mean ± SEM of three independent experiments performed in triplicate. NT, no treatment. ***p < 0.001 vs. NT (ANOVA with Dunnett's).
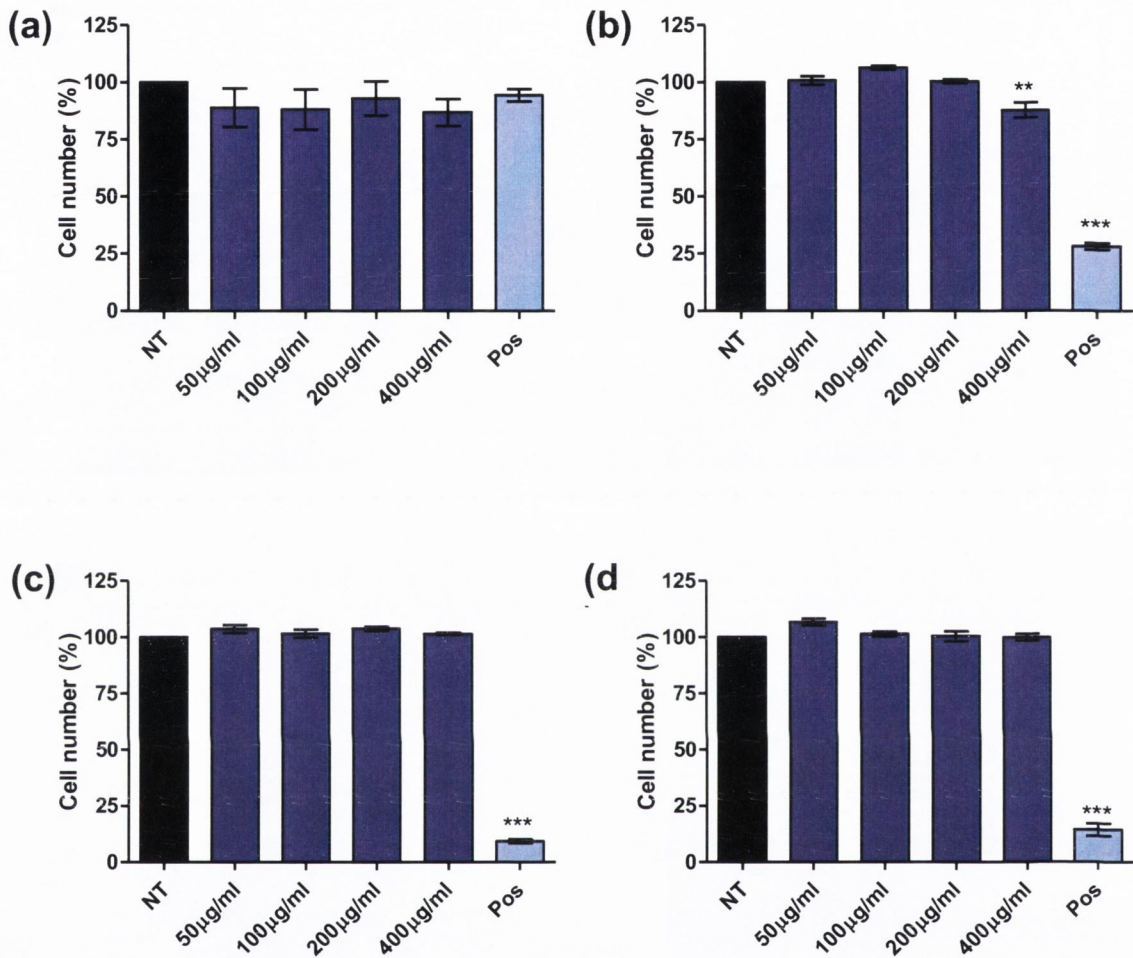
Figure 5.18: Cytotoxic effects of negatively charged 50 nm fluorescent silica NPs on HUVEC cells. HUVEC grown in 96 well plates were treated with negatively charged 50 nm fluorescent silica NPs or 3μM positively charged QDs (Pos) for 20 min (a), 4 h (b), 8 h (c) or 24 h (d). Viable cell number was quantified using INCell analyzer 1000 automated microscope. Data are mean ± SEM of three independent experiments performed in triplicate. NT, no treatment. **p < 0.01, ***p < 0.001 vs. NT (ANOVA with Dunnett's).

5.3 Discussion

Endothelial cells form the interior layer of the entire vascular system. Endothelial cells in vivo are constantly exposed to hemodynamic forces and they sense and respond to them. In humans, the mean shear stress varies between 0.5 to 7.6 dynes/cm^2 in veins, 3 to 7 dynes/cm^2 in the peripheral arteries (e.g. brachial, femoral artery), and between 10 to 15 dynes/cm^2 in the central arteries (e.g. carotid artery). Endothelial cells respond to shear stress by alterations in cell morphology, cell function and gene expression. Because of its proximity to blood flow, vascular endothelium could be targeted by nanoparticle-based therapeutic applications. Systemically administered nanomedicine based therapies have the potential to interact with vascular endothelial cells.

Researchers have been focusing on targeting the endothelium with NPs in order to deliver therapeutic agents such as drugs and/or genes for a variety of vascular pathologies (Davda and Labhasetwar, 2002, Kuldo et al., 2005, Omolola Eniola and Hammer, 2005, Yao et al., 1991). Since endothelium has specific and highly regulated expression of selectins (E, L and P) and other cell adhesion molecules (PECAM, VCAM and ICAM) (Littler et al., 1997), site-specific delivery of therapeutics to the vascular endothelium could be achieved. Platelets bind to activated endothelial cells through the interaction between platelet glycoprotein Ibα (GP Ibα) and P-selectin on activated endothelial cells. Studies have found that conjugation of 100 nm polystyrene NPs with glycocalicin (the extracellular segment of GP Ibα) mimics platelets, and significantly increased the particle adhesion on P-selectin-coated surfaces and cellular uptake of NPs by activated endothelial cells under physiological flow conditions (Lin et al., 2010). Investigators have also described leukocyte-mimetic targeting of endothelium via two receptors, selectin and intercellular cell adhesion molecule-1 (ICAM-1). Biodegradable, poly (lactic-co-glycolic acid) (PLGA) microspheres were co-functionalized with a selectin ligand and an antibody against ICAM-1. The NPs firmly adhered to the substrate only under flow, mimicking the multi-step *in vivo* leukocyte adhesion in inflammation (Omolola Eniola and Hammer, 2005). This study has demonstrated that the live endothelial cells uptake negatively charged CdTe QDs and fluorescent silica particles under flow conditions. It also showed that the uptake was the maximum at a lower shear stress rate of 0.5 dynes/cm^2. The activation of cells with TNF-α, simulating an inflamed endothelium (Schreyer et al., 1996), showed no difference in the

uptake of NPs. This could indicate that the nanoparticle uptake was independent of adhesion molecules [selectins (E, L and P), PECAM, VCAM and ICAM] expressed by activated (artificially-inflamed) endothelium at least at the size range not exceeding 50 nm as demonstrated in our study. Therefore, the possible role of adhesion molecules in the uptake of larger particles has to be investigated in the future. However, the results have shown that negatively charged 2.9 and 4.6 nm CdTe QDs, and negatively charged 50 nm fluorescent silica NPs could be utilized to target both the normal and activated endothelium. In addition, maximal accumulation of NPs could be achieved if the shear stress of the vascular segment of interest could be maintained at 0.5 dynes/cm^2. The reduction of shear stress rates commonly happens in the dilated vessels in the inflammatory sites. This physical phenomenon could be exploited for selective NPs delivery to such vascular compartments. Furthermore the NPs could be bio-functionalized with adhesion molecule ligands to mimic leukocytes or platelets to achieve more efficient targeting of endothelium.

Triton X-100 is one of the most widely used non-ionic detergents in biology. Cells have been exposed to non-ionic surfactants to permeabilize cell membrane for transfection (Koley and Bard, 2010) or to study nanoparticle localization pattern. Indeed, studies have demonstrated that cells exposed to mild detergent (0.0094%) treatment preserves cell viability and did not significantly alter the ultimate QD localization patterns in macrophage and lung epithelial cell types (Williams et al., 2009). Observations made in this study also suggest that HUVEC could be exposed to mild detergent treatment with 0.001% Triton X-100 for up to 1 hour. Treatment of HUVEC with TNF-α, a physiological pro-inflammatory mediator, simulates an inflamed endothelium. Endothelial cells are inflamed and have increased permeability in certain disease conditions such as atherosclerosis (Schreyer et al., 1996, Tedgui and Mallat, 2006). Therefore, the use of TNF-α (simulates inflamed endothelium) and Triton X-100 (alters membrane permeability) on endothelial cells could to some extent represent an *in vitro* model for atherosclerosis.

Systemically administered bio-functionalized NPs would unavoidably interact with the vascular microenvironment. The distribution of luminescent NPs in human endothelial cell line, which is one of the important cellular components of the microvasculature, was studied. Live cells were exposed to NPs under static and physiological shear stress

conditions. Nanoparticle distribution was further analysed by exposing the live cells to a mild detergent treatment with 0.001% Triton X-100. Such treatment increases membrane penetration capacity for NPs but preserves cell viability (Williams et al., 2009). The cells are also fixed and permeabilized before exposing them to NPs under static and flow conditions. The above step eliminates cell-membrane-associated nanoparticle uptake mechanisms, but preserves the putative physical subcellular barriers (Williams et al., 2009).

The NP uptake in live cells was studied over a time period of 20 minutes under static and shear stress conditions. The negatively charged 2.5 and 5 nm CdTe QDs did not enter the live endothelial cells under static conditions but penetrated the cells under flow conditions. Treatment with detergent did not significantly alter the uptake of QDs in live cells. Our findings observed under static conditions are similar to the results of a previous study performed with negatively charged 2.1 and 3.4 nm CdTe QDs on vascular endothelial cells (Nabiev et al., 2007). However, this study clearly indicates that the shear stress is critical for QD intake by live cells, and enhancement of membrane permeability per se does not influence QD transport mechanisms.

The nuclear pore allows biomolecules of diameter less than 9 nm by passive diffusion (Choi et al., 2007) while active transport is required for molecules of greater size up to approximately 39 nm (Pante and Kann, 2002). However, the effective size of the nuclear pore to function as a barrier for nanomaterial transport across the nuclear membrane is yet to be determined. Large aggregated particles may be prevented from entry through the pores, but single QD should be getting through. A selective transport barrier could be formed by many proteins that line the inner surface of nuclear pore complex (Alber et al., 2007). Therefore, while the potential mechanism for QD uptake is passive diffusion, the same mechanism can no longer be applied when the particles are strongly charged. In this current study, QDs of both sizes entered the cytoplasm of live cells within 20 minutes of exposure to shear stress, but not into the nucleus. This could be attributed to the interaction of QDs with the cytoplasmic proteins forming a "protein corona", which gives a different biological identity and may determine the subcellular localization of QDs. Both the 2.5 and 5 nm QDs were localized near the nucleus. It could be presumed that the QDs are originally trapped in endocytic vesicles and are subsequently transported by molecular motors along microtubule tracks to the perinuclear area. QDs could be

accumulated in cytoplasmic organelle(s). Indeed, 100 nm gold NPs have found to be accumulated in the mitochondria and endoplasmic reticulum in the cytoplasm of cardiac myocytes (Sathuluri et al., 2011), and 13 nm gold NPs were shown to be localized with endoplasmic reticulum and Golgi apparatus in melanoma cells (Chang et al., 2008).

However, in experiments with fixed and permeabilized endothelial cells, the QDs entered the cells both under static and flow conditions. Fixation of cells with paraformaldehyde and permeabilization of cell plasma membrane with Triton X-100 prior to addition of QDs ensures that the barriers to particle localization were mainly a function of size. Fixed cells could be referred to as cells irreversibly "frozen" at a certain stage of their life cycle (Williams et al., 2009). Although they represent a different system compared to living cells, they preserve their key morphological and structural features. Both the QDs were accumulated in the cytoplasm, but the smaller, green-fluorescence-emitting 2.5 nm QD penetrated the nucleus. This would indicate that the permeabilization did not affect the particles infiltrating the outer cell membrane, while the size of the particles determined the entry through nuclear membrane. The leading mechanism for nuclear localization could be due to the strong tropism of negatively charged CdTe QDs to positively charged histone-enriched compartments in the nucleus and the nucleolus in a process involving endocytosis, active cytoplasmic transport, and nucleocytoplasmic exchange via the nuclear pore complex (Conroy et al., 2008). The findings in this study additionally confirm that contrary to the passive diffusion mechanisms operating in fixed/permeabilized cells, active transport processes are functioning at the level of nuclear gate entry in live endothelial cells (Nabiev et al., 2007). The larger, red-fluorescence-emitting CdTe QDs (5 nm in diameter) had concentrated at the perinuclear region in fixed/permeabilized cells. This could suggest that the QDs are strongly bound to the components around the nucleus. This is in agreement with previous studies with QDs in epithelial cells (Jaiswal et al., 2004, Williams et al., 2009). This indicates that even in the case of paralyzed nuclear transport machinery (fixed cells), a size-specific cut-off band at approximately 3.8-4 nm still holds true for nuclear pore, despite the forced permeabilization of the cell membrane (Nabiev et al., 2007). The results in this study are similar to previous studies done under static conditions with CdTe QDs on macrophage-like THP-1 cell line demonstrating accumulation of 2.1 nm QDs in the nucleus and 3.4 nm QDs in the cytoplasm (Nabiev et al., 2007).

The results obtained with negatively charged 50 nm fluorescent silica NPs showed that in static conditions the particles did not infiltrate into the cytoplasm of both live and fixed/permeabilized cells. However, under flow conditions, the particles are cell-membrane-bound in live cells and intra-cytoplasmic in fixed/permeabilized cells. It would seem that the inability of the silica particles to penetrate the live plasma membrane in spite of shear stress could be due to the sheer size of the particles. However, previous studies performed with BSA-coated NPs (varying from 20 to 100 nm in diameter) on endothelial cells have demonstrated caveolae-mediated nanoparticle uptake, and also showed that caveolae could accommodate up to 100 nm diameter NPs, a size larger than the diameter of typical caveolae, suggesting compliant property of caveolae (Wang et al., 2009). Therefore, it could be suggested here that the fluorescent rhodamine molecules attached to the silica particles could have played a role in preventing their uptake by the live cells. Of note, our confocal microscopy studies with negatively charged 50 nm fluorescent silica particles (section 5.2.4) did not show membrane ruffling. Membrane ruffling (also known as cell ruffling) is the formation of a motile cell surface that contains a meshwork of newly polymerized actin filaments. The ruffling of membranes and/or cytoskeletal rearrangement is thought to be controlled by a group of enzymes known as vasodilator-stimulated phosphoprotein (Price and Brindle, 2000), Rac 1and Rho GTPases (Ishida et al., 1997). In addition, the particles were not able to penetrate into the live cells. Internalization studies carried out with fluorescently labelled Ebolavirus-like particles (80-100 nm in diameter) in renal epithelial cells have demonstrated that the plasma membrane ruffling accelerated the internalization of macropinosomes (macropinocytosis-specific endosomes) (Nanbo et al., 2010). Furthermore, lipid rafts (microdomains that are enriched in sphingolipids and cholesterol, found in the plasma membrane) have been implicated in macropinosome formation by the finding that cholesterol depletion inhibits both membrane ruffling and macropinocytosis (Kirkham and Parton, 2005). Lipid rafts provide a platform for the assembly of receptors, adaptors, regulators, and other downstream proteins as a signaling complex, and may be joined with caveolae. Endocytosis of various membrane receptors may also occur via lipid rafts (Nichols, 2003). CdSe QDs were recognised by lipid rafts and QDs have been shown to induce more actin formation in the cytoplasm (Zhang and Monteiro-Riviere, 2009). In this study, silica NPs did not induce more actin filament

formation compared to controls. Therefore, it could be suggested that QDs induce formation of membrane ruffles there-by aiding in particle uptake. The mechanism by which the fluorescent-tagged silica particles inhibit the formation of membrane ruffling is yet to be defined. However, it could be suggested that membrane ruffling plays a critical role in the uptake of particles in live cells.

A significant change in the cytoskeleton (actin filament) rearrangement was noticed in the cells exposed to shear stress compared to cells under static conditions. This instigated us to study the membrane morphology in close details. The endothelial actin filament skeleton responds to fluid shear stress by formation of stress fibers (Franke et al., 1984), and these actin bundles are probably a functionally important mechanism that protects the endothelium from hydrodynamic injury and detachment (Wong et al., 1983). Bundles of 6- to 7-nm microfilaments were also formed in the cytoplasm to combat wall shear stress (Masuda et al., 1985). Endothelial cells are known to form membrane ruffling in the process of transducing mechanical force into biological responses (Ishida et al., 1997). Confocal microscopy and atomic force microscopy (AFM) techniques were used to characterize the changes in morphology of endothelial cells. Confocal laser scanning microscopy is a technique for obtaining high-resolution optical images with depth selectivity, and the key feature of confocal microscopy is its ability to acquire in-focus images from selected depths. AFM has been increasingly used recently to address problems of biomedical relevance. AFM has the advantage of being able to operate in air and fluid under physiological conditions, which has allowed biologically relevant applications, such as studying cell-surface morphology and the cytoskeleton (Haupt et al., 2006).

This study has demonstrated shear stress (0.5 dynes/cm^2 for 20 minutes) induced cytoskeletal rearrangement in human cultured endothelial cell lines. Confocal images showed a distinctly different staining pattern of reorganized actin filaments in the cells exposed to shear stress compared to the control cells. The actin stress fibers and membrane ruffling were visualized in explicit details by AFM images. Previous authors have demonstrated the development of stress fibers on cultured endothelial cells after being subjected to a unidirectional shear stress of 12 dynes/cm^2 for 24 h in a cone-and-plate device (Barbee et al., 1994). However, they did not notice membrane ruffling on the surface of the cells. This indicates that the persistence or transience of membrane ruffling in in

vitro experiments may depend on the duration of exposure to shear stress. In addition, the different system used in our study (microfluidic platform) could be the reason for the development of stress fibers at a much shorter duration. Previous studies have demonstrated that endothelial progenitor cells became elongated and orient their long axis in the direction of flow when exposed to shear stress of 0.1 to 2.5 dynes/cm^2 in a disk-type flow loading device for 24 hours (Yamamoto et al., 2003). These morphological changes were also observed in mature endothelial cells, such as HUVEC and bovine aortic endothelial cells (exposed to a maximum of 34 dynes/cm^2 for up to 45 hours in flow circuits) (Dewey, 1984, Eskin et al., 1984). Changes in cell shape and orientation were not observed in this study. The reason for this discrepancy could be either due to the flow system used in our study or the shorter exposure time to shear stress conditions.

The cytotoxic effects of various particles on human endothelial cells were studied utilizing high content analysis platform (IN Cell Analyzer 1000). In previous studies, using lactate dehydrogenase and proliferation assays, investigators have demonstrated that carbon black causes cytotoxic injury and inhibition of cell growth (Yamawaki and Iwai, 2006b). MTT assay on HUVEC treated with 100 nm MgO NPs did not detect cytotoxicity in low concentrations (<200µg/ml). However, the growth rate was compromised in higher concentration (>500 µg/ml) (Ge et al., 2011).

Silica NPs, because of their ease of production and relatively low cost, have found widespread application for biosensors, catalyst supports, drug carriers and gene delivery (Tan et al., 2004). Toxicity studies performed with silica NPs (diameter of 14-, 15-, 16-, 19-, 60-, 104-, and 335-nm) on endothelial cell survival (assessed by MTT assay) have demonstrated that smaller particles showed significantly higher toxicity than the bigger ones (Napierska et al., 2009). High content analysis data shows that negatively charged 5 nm silica, 50 nm fluorescent silica and 51 nm silica coated magnetite were tolerated well for up to 24 h by the endothelial cells. However, at 1µM concentration, the 5 nm silica particles caused a decrease in cell number compared to cells grown with higher concentration of NPs. This could be due to the increased production of nitric oxide (implicated in endothelial cell proliferation) (Ziche and Morbidelli, 2000) by silica particles. A similar response was observed in coronary endothelial cells on treatment with 45 nm silver particles (Rosas-Hernández et al., 2009).

Superparamagnetic iron oxide NPs are a promising candidate for cell tracking, cell targeted drug delivery and contrast agents for MR imaging (Gupta et al., 2007, Islam and Harisinghani, 2009, Sajja et al., 2009, Xie et al., 2009). In addition, they can be utilized in magnetically mediated hyperthermia in treatment of cancers (Barry, 2008, Gupta and Gupta, 2005, Le Renard et al., 2009). Citric acid is commonly used for stabilizing and functionalizing iron oxide NPs for biomedical applications (Hajdú et al., 2008). Cell viability assays [assessed by MTT assay] carried out with citrate-stabilized iron oxide particles (approximate core size of 38±8.14 nm and cells were treated at a concentration from 0.1 to 20 mM) showed that the cell viability decreased with increasing iron concentration (Wu et al., 2010). Gojova *et al.* studied the effects of metal oxides such as 20-70 nm ZnO, 20-60 nm Y_2O_3 and 45 nm Fe_2O_3 on vascular endothelium and found that Fe_2O_3 did not have any cytotoxic effects(Gojova et al., 2007). However, ZnO caused considerable cell death at concentrations above 10µg/ml. Our studies show that citrate stabilized magnetite NPs were well tolerated by the endothelial cells. In fact, an increase in the endothelial cell number was noticed in treatment with citrate stab magnetite NPs. This could be due to the increased adsorption of nutrient proteins from the medium on the surface of citrate stabilized magnetite NPs, similar to previous studies done with citrate-coated gold NPs (Brewer et al., 2005) or increased endothelial nitric oxide production (Ziche and Morbidelli, 2000) by magnetite particles.

Semiconductor QDs are quickly becoming a critical diagnostic tool for discerning cellular function at the molecular level (Rosenthal et al., 2011). Yan et al. studied effects of negatively charged 3.36 nm mercaptosuccinic acid-capped CdTe QDs on cell viability [assessed by MTT assay] of human vascular endothelial cells. It was found that the TC50 value (concentration of CdTe QDs causing 50% cell death) was at 24.06 nM, indicating the remarkable endothelial toxicity of CdTe QDs (Yan et al., 2011). In our studies, 3µM of negatively charged 4.6 nm QDs caused a significant decrease in cell number at all the time points studied. The cell death could be due to QD-generated singlet oxygen species (Samia et al., 2003) leading to detrimental autophagic cell death as well as necrosis (Liu and Sun, 2010, Stern et al., 2008, Yamawaki and Iwai, 2006a) or QD-activated intrinsic mitochondrial apoptotic pathways (Yan et al., 2011). The 2.7 nm QDs were well tolerated by the endothelial cells at 3µM concentration for up to four hours. This warrants further

studies with different concentrations. However, data suggests that smaller QDs can be utilized for short term targeting of endothelium, and needs surface passivation if intended for long-term observations with live cells. Understanding the mechanism of QD-induced endothelial toxicity will enable researchers to design more biocompatible QDs.

In all our data with various particles, a transient decrease in cell number was observed within 20 min. This could be attributed to the interactions between the charged particles and the cell membrane (Tsuneda et al., 2003), resulting in a transient detachment of cells from the growth surface.

In conclusion, this study has demonstrated that shear stress is critical in both inflamed and non-inflamed endothelial cells for uptake of NPs and the uptake is maximal at a lower shear stress rate. The findings also provide strong evidence that formation of membrane ruffles may aid in endocytosis of the NPs. The cytotoxicity data in this study indicates that silica- and magnetite-based NPs were well tolerated by endothelial cells, and smaller QDs were not toxic for up to 8 hours. One can expect that bio-functionalized NPs would be targeted to the endothelial plasma membrane or the cytoplasm. This could have two-fold implications. Firstly, the NPs could be utilized for drug delivery in vascular compartment with a given shear stress inside, e.g. 0.5 dynes/cm^2 as in post-capillary venules and veins. Secondly, co-administration of vaso-active drugs (to reduce shear stress) with functionalized NPs will facilitate uptake of NPs for selective delivery in inflammation related conditions and atherosclerosis.

Chapter 6

General discussion and future work

The ultimate goal for translational research in medicine is the design and development of new therapeutic strategies with high efficacy and minimal side effects and diagnostic methods of high specificity and sensitivity. Nanomedicine represents an innovative and growing field with potentially unlimited prospects in the fields of diagnostics, therapeutics and regenerative medicine. Bio-functionalized nanoparticle-based systems have an immense potential in various application fields such as drug delivery, imaging, tissue engineering and coatings for implants.

Advances in nano-biotechnology have led to a dramatic increase in the development of nanomedicines for a variety of diseases. Some nanomedicines have already been tested in mice and are awaiting human trials, e.g. using gold nanoshells to help diagnose and treat cancer, and using liposomes as vaccine adjuvants and as vehicles for drug transport (Mozafari, 2006). Tumour-targeted nanomedicines, which enhance tumoural drug levels are being approved for the treatment of various cancers such as breast, lung, kidney, liver, ovary, prostate, melanoma, non-Hodgkin's lymphoma etc. (Lammers et al., 2008). Two superparamagnetic iron oxide agents, composed of nano-sized iron oxide crystals coated with dextran or carboxydextran, are clinically approved as MRI contrast agents, namely: ferumoxides (Feridex in the USA, Endorem in Europe), and ferucarbotran (Resovist) (Wang, 2011). Biodegradable small polymer rods [goserelin (Zoladex)] and polymer microparticles [leuprolide (Leupron Depot)] made from polylactide-co-glycolide, entrapping leutinizing hormone releasing hormone analogues, are common treatments for prostate cancer (Duncan, 2006). Another biodegradable polymeric implant [discs containing the alkylating agent bis(2-chloroethyl)nitrosourea], carmustine (Gliadel), is used to treat a type of brain cancer (glioblastoma multiforme) (Brem et al., 1995, Westphal et al., 2003). The first therapeutic nanoparticle [albumin-entrapped paclitaxel (Abraxane)] (Duncan, 2006, Kattan et al., 1992) was approved in 2005 as a treatment for metastatic breast cancer. Recently reports have suggested the exciting possibility of conjugating QDs (superior fluorescent properties with less photobleaching compared with conventional chromophores) to carbon nanotubes (allotropes of carbon in a honeycomb-like lattice) to exploit their novel attributes in the domain of cancer theranostics (diagnostics and therapy) (Tan et al., 2011). QDs may be used in the future for locating tumours in patients and in the near term for performing diagnostic tests in samples. However, National Renewable Energy

Laboratory (i.e. NERL, a national laboratory of U.S. department of energy) researchers have been working to develop QDs composed of silicon, which are believed to be less toxic than the cadmium containing QDs. Medical gauze incorporated with aluminosilicate NPs which help the blood to clot faster in open wounds is being developed by a company called Z-Medica.

6.1 Cardinal findings from this thesis

This thesis investigates the effects of a panel of nanomaterials including negatively or positively charged CdTe QDs, negatively charged SiO_2, Fe_2O_3, silica coated magnetite and citrate stabilized magnetite NPs on human platelets. The data presented in chapter 3 clearly demonstrate that silica and magnetite based NPs did not activate platelets. This could be attributed to the chemically inert nature of the particles, and these particles could be considered as potential candidates while designing nanomedicines targeting the coagulation system. We have found that engineered CdTe QDs caused activation of washed platelets. This was further confirmed by the detection of surface-expressed platelet activation markers P-selectin and GPIIb-IIIa, and the release of a pro-coagulant enzyme MMP-2 from QD-activated platelets. Since there is evidence that the surface charge of NPs such as latex, poly(D,L-lactide-co-glycolide) (PLGA) and chitosan may determine the degree and mechanism of platelet activation (Li et al., 2009, McGuinnes et al., 2011, Miyamoto et al., 1989), it was found necessary to study the influence of negative charge on the surface of CdTe QDs on platelet function. For this purpose, measurement of the zeta potential of QD-treated platelets was carried out. The results obtained suggest that the negative surface charge of QD per se was not involved in the mechanism of activation of platelets. To further characterize the mechanism of QD-induced platelet activation, platelet aggregates were studied at the ultra-structural level. The ultramicroscopic examinations done in this study clearly demonstrated the association of QDs on platelet membranes. With the gathered information, it could be hypothesized that the platelet aggregation could be mediated by the membrane-bound QDs, likely through the activation of GPIIb-IIIa integrins, thereby triggering the outside-in signalling cascades.

The platelet aggregometry assays carried out with PRP at static conditions clearly showed that the presence of plasma abrogated QD-induced platelet aggregation. This could be due to the adsorption of plasma protein complexes on the QD surface resulting in

formation of a protein "corona" which determines the biological identity of the particle. This possibility was further analysed by studying the effects of plasma-treated QDs on washed platelets. The results showed that the plasma-incubated QDs caused significantly lower activation of platelets. This finding strongly indicates the possibility of binding of plasma proteins to the surface of QDs providing thereby a certain degree of surface passivation. It should be noted that the studies performed to investigate the influence of QDs on platelets (PRP) under controlled shear stress conditions (Q-Sense Quartz Crystal Microbalance) showed platelet activation even in the presence of plasma. Further studies need to be carried out in vivo to clarify the physiological significance of these observations.

The aggregometry studies performed with PRP clearly demonstrated that the plasma proteins inhibit the ability of CdTe QDs to activate platelets. On the basis of the results obtained from aggregometry studies, more investigations were carried out to characterize the plasma proteins interacting with the negatively charged QDs. It was found necessary to optimize the dilution of human plasma to yield well resolved proteins in 1D native gel electrophoresis. The proteins associated with the two differently sized and charged QDs had a ~50% homology between them. The data obtained from this study clearly indicates that functional properties such as size and surface charge play a more critical role than the molecular composition. A number of haemostasis-associated proteins were detected in the QD-enriched protein bands. This explains the decreased platelet aggregation observed in PRP samples treated with QDs.

In this study, investigation of interactions of negatively charged QDs and fluorescent silica NPs on endothelial cells under controlled shear stress conditions were carried out. In addition, cytotoxic effects of QDs and silica and magnetite-based NPs on cultured endothelial cells were also evaluated. Endothelial cells exposed to cytokines and mild non-ionic detergents could to some extent represent an *in vitro* equivalent for inflamed and membrane compromised cells in conditions such as atherosclerosis (Schreyer et al., 1996, Tedgui and Mallat, 2006). It was found that shear stress played a critical role in the uptake of NPs in both normal and artificially-inflamed (activated with TNF-α) endothelial cells and maximal accumulation of NPs occurred at a lower shear stress rate. This study clearly indicated that the uptake of NPs not exceeding 50 nm in diameter was independent of adhesion molecules (selectins, PECAM, VCAM and ICAM). It was also observed that

the exposure of live HUVEC to mild detergents (Triton X-100) did not significantly alter the nanoparticle uptake under moderate shear stress conditions implemented in our studies. This study clearly demonstrated that shear stress induced membrane ruffling and cytoplasmic localization of the QDs in live endothelial cells. In fixed and permeabilized cells, only the smaller QDs were found localized in the nucleus which confirms the existence of active transport and barrier cut-off mechanisms operating at the level of nuclear pores in live endothelial cells. In experiments performed with silica NPs, membrane ruffling was not observed and silica particles did not enter the cytoplasm. Therefore, it could be suggested that the formation of membrane ruffles aids nanoparticle uptake. In addition, this study demonstrated that the silica and magnetite-based particles were not cytotoxic to the endothelial cells at the range of concentrations used in our experiments. The observed data also showed that the smaller QDs were tolerated by the HUVEC for up to 8 h.

In conclusion, this study has demonstrated that the silica and magnetite-based NPs exhibit a high level of biocompatibility with platelets and endothelial cells. In addition, this study has contributed to understanding of the mechanism of QD-associated platelet activation. QDs induce activation of platelets by binding to surface integrin GPIIb-IIIa, thereby initiating the outside-in signaling. We established that the presence of plasma inhibits QD-induced platelet aggregation due to the adsorption of plasma proteins on the surface of QDs. We were able to for the first time to demonstrate that shear stress is critical in both the normal and artificially-inflamed endothelial cells for uptake of QDs and silica NPs. Our findings suggest that membrane ruffle formation aids in the endocytosis of particles. The NPs and their drug conjugates therefore may be potentially used for short term targeting of endothelial plasma membrane or the cytoplasm provided the shear stress is maintained at 0.5 dynes/cm^2, for e.g. as in post capillary venules.

6.2 Opportunities for nanoparticle-based therapeutics

According to World Health Organization estimates, ischemic heart disease (myocardial infarction) and cerebrovascular disease (stroke), primarily due to the formation of blood clots in the microvasculature, are the two leading causes of mortality worldwide and account for well over 20% of all deaths (Kim and Johnston, 2011). Despite increased research activities in developing NPs, existing literature shows far fewer nanomedicines being developed to target the microvasculature. Platelets and vascular endothelial cells, important components of microvaculature, are involved in many disease states such as coagulation disorders, inflammation, atherosclerosis and tumour metastasis. Therefore, it is imperative to develop nanoparticle based therapeutic agents for such diseases. Platelets play a critical role in thrombotic disorders such as myocardial infarction, ischemic stroke, arterial and venous thrombosis, and pulmonary embolism. Disorders of platelet function could lead to bleeding disorders such as Bernard-Soulier syndrome (deficiency of GPIb) and Glanzmann thrombasthenia (deficiency of GPIIb-IIIa). Disseminated intravascular coagulation or consumptive coagulopathy, a pathological activation of coagulation cascade in response to the release of tissue factor from injured lungs, brain or placenta, results in consumption of platelets leading to microvascular or macrovascular thrombosis with life threatening complications such as multiple organ failure and death. Vascular endothelial cells provide a phospholipid surface for platelet aggregation and are also involved in inflammation and atherosclerosis.

Overall results presented in this thesis clearly indicate that QDs, silica and magnetite-based NPs could be considered in the designing of nanomedicines targeting the microvasculature. Magnetite NPs could be utilized as contrast agents and silica NPs could be used for attaching drugs. Hence, silica coated magnetite NPs could be utilized as a dual modular system for site-specific imaging and drug delivery in life threatening thrombotic disorders such as stroke, myocardial infarction, arterial and venous thrombosis, and pulmonary embolism. Systemically administered magnetic NPs, functionalized with anti-coagulants, could be concentrated at the thrombotic vessels by application of a magnetic field. Tumour cells are known to induce platelet activation for metastasis of cancers (Medina et al., 2006). Therefore, magnetic NPs functionalized with cancer-specific ligands could be utilized for targeting various tumours. If placed in an alternating magnetic field of

well-chosen amplitude and frequency, the particles would increase the tumor temperature and kill the tumour cells by necrosis. QDs, which have distinct optical properties, also have the ability to induce coagulation by activating platelets. Angiogenesis plays a critical role in the growth of tumours. Nanocomposites made of QDs (platelet-activating) and magnetite [functionalized with NGR tripeptide ligand to target CD13 receptor expressed in angiogenic endothelium of tumours (Simnick et al., 2011)] could be employed for both imaging and reducing blood supply to tumours, thereby depriving tumour cells of oxygen and nutrients.

The high surface to volume ratio of NP increases their tendency to bind to opsonins leading to phagocytosis by reticuloendothelial system (RES) macrophages (Segat et al., 2011). Attachment of polymers has been widely used to decrease the amount of proteins bound to NPs, and addition of poly (ethylene glycol) (PEG), called "PEGylation", is the most common and preferred method of "masking" NPs from immune recognition (Aggarwal et al., 2009). PEGylation has been shown to decrease nanoparticle interaction with blood proteins and avoid recognition by RES, thereby prolonging blood circulation (stealth effect) (Gref et al., 2000, Kim et al., 2007, Lemarchand et al., 2006, Peracchia et al., 1999). It has also been shown that PEGylation of cytotoxic PHDCA NPs decreased protein binding, increased blood circulation time, and decreased cytotoxicity (Peracchia et al., 1999). Utilizing a PEG coating, QDs could serve as an effective platform with the ability to incorporate a variety of targeting, therapeutic or imaging ligands. Therefore, biocompatible QDs could be further functionalized with specific ligands to target and treat damaged blood vessels in acute emergencies such as polytrauma, ruptured aneurysm and post-partum hemorrhage. Furthermore, the QDs can be attached with glycoprotein receptors such as GPIb or GPIIb-IIIa to mimic platelets in treating bleeding disorders such as Bernard-Soulier syndrome and Glanzmann thrombasthenia. In addition, PEGylated nanocomposites functionalized with ICAM-1and P-selectin, and loaded with drugs such antibiotics, hypolipideamic agents, aspirin and thrombolytics can be made to mimic leukocytes to target endothelial cells in conditions such as inflammation and atherosclerosis.

In general, the NPs studied here could be modified as multifunctional nano-agents for potential application in various fields of clinical medicine such as drug delivery,

detection and treatment of thrombotic disorders and cancers, diagnostic vascular imaging, molecular imaging of angiogenesis and as contrast agents for cardiovascular medical imaging. Furthermore, nanoparticle systemic accumulation and toxicity could be possibly reduced if the diameter of the functionalized nanoparticle is below the renal cut-off of 10 nm (Choi et al., 2011).

6.3 Future directions

6.3.1 Influence of nanoparticles on flow induced platelet adhesion on cultured endothelial cells

During this thesis, the influence of QDs on flow induced platelet adhesion on artificially-inflamed (with TNF-α) endothelial cells was also investigated using whole blood. It was needed to optimize the concentration of DiOC6 (a live membrane stain used for staining the platelets), so that only the platelets and not the endothelial cells were stained. For this purpose, whole blood pre-treated with 0.125 or 0.25 or 0.5 or 1μM DiOC6 was run over the cultured endothelial cells (activated with TNF-α) at a shear stress rate of 5 dynes/cm^2. It was found that the DiOC6 also stained the endothelial cells in all the concentrations used (refer Appendix 1). The staining of endothelial cells interfered in the quantification of the platelets adhered on them. Therefore, in the future, specific immunofluorescence staining of platelet ligands (e.g. CD 61 or CD 41) will be performed and the influence of various NPs on flow induced platelet adhesion on activated endothelial cells will be carried out. In addition, platelet adhesion on cultured endothelial cells exposed to cytokines (TNF-α) and mild detergents (Triton X-100), which provides an in vitro model closely resembling atherosclerosis, will be performed. Furthermore, a direct physical injury (e.g. a scratch) to the cultured human endothelial monolayer will represent an in vitro model for the study of vascular injury. Platelet adhesion to damaged endothelium and the effect of functionalized (for e.g. anti-platelet drugs) NPs on platelet adhesion will be studied under flow conditions.

6.3.2 Endothelial cell targeting with functionalized nanoparticles under controlled shear stress conditions

Functionalization of NPs is indeed the first and perhaps foremost step towards nano-scale drug delivery systems (Bhaskar et al., 2010). Functionalization facilitates targeted delivery

of these NPs to various cell types, bioimaging, gene delivery, drug delivery and other therapeutic and diagnostic applications. This study has showed that silica and magnetite-based NPs did not activate platelets and are not cytotoxic to the endothelial cells. Next, the NPs will be functionalized with PEG (PEGylation mask them from immune recognition, decreases the nanoparticle interactions with opsonins and avoids recognition by RES, thereby prolonging blood circulation). NPs will be subsequently functionalized with antibodies against specific endothelial cell ligands (e.g. VCAM, ICAM etc.) and fluorescent-tagged drug molecules to target artificially-inflamed (with TNF-α) endothelial cells.

6.3.3 Quantitative Structure-Activity Relationship (QSARS)

Quantitative structure–activity relationship (QSAR) models are regression models (for prediction and forecasting) used in the chemical and biological sciences and engineering. Nanomaterials possess distinct physicochemical properties in comparison to their micron-sized counterparts. The NPs surface characteristics and high surface area to mass ratio makes them potentially toxic to biological systems. The knowledge and understanding of the relationships between the physicochemical properties of the nano systems and their *in vivo* behaviour is essential for designing nanomedicines which are safe and effective. QSAR methods help to establish such relationships, although modelling the behaviour of nanomaterials requires new ideas and applications to account for the novel properties of this group of compounds (Burello and Worth, 2011). Indeed, QSAR has been proven to be very useful in pharmaceutical industry and many important medicines such as penicillin, sulfamethoxazole and captopril were optimized in the past following this approach (Braiuca et al., 2006, DePriest et al., 1993, Johnson et al., 1998). Nanomaterials, possessing structural and behavioural heterogeneity, require theoretically and experimentally derived descriptors for QSAR modelling. Therefore, research should focus on both aspects of a QSAR study: the generation of nanospecific theoretical descriptors and experimental test data (Burello and Worth, 2011).

6.4 Societal implications

Nanomedicine may significantly improve life span and quality of life. This would lead to an increase in the population of elderly people, which might lead to many consequences

such as changes in pension or health insurance schemes or an increase in the retirement age. Another example would be in medical care: nanotech-based treatments may be initially expensive, hence only the very rich would access them. Other undesirable consequences include environmental pollution, especially from bulk applications of nanomaterials, such as the 'Silver Nano' platform for using silver NPs as an antibacterial agent, nanoparticle-based (ZnO, TiO_2 etc.) transparent sunscreens, and carbon nanotubes for stain-resistant textiles. One such example is the silver NPs, used in the socks to reduce foot odour, being released in the wash and destroying the beneficial bacteria which are important for breaking down organic matter in waste treatment plants or farms. Therefore, to take full advantage of this new technology-based medical treatments, the entire medical, scientific and technology community must involve all participants, including the general public, policy makers and socio-economic experts; creatively envision the future; set broad, realistic goals; and work together to facilitate societal benefits.

References

References

Freitas R.A. Jr. Nanomedicine, Volume 1: Basic Capabilities. 1999, Landes Bioscience.
http://en.wikipedia.org/wiki/Blood_plasma.
http://en.wikipedia.org/wiki/Blood_proteins.
http://en.wikipedia.org/wiki/Cell_nucleus#Nuclear_envelope_and_pores.
http://en.wikipedia.org/wiki/Confocal_laser_scanning_microscopy#cite_ref-
     Pawley_2006_0-0.
http://phycomp.technion.ac.il/~anastasy/thesis/node10.html.
http://www.clinam.org.
http://www.trace-elements.org.uk/zinc1.htm.
http://www.uniprot.org/uniprot/Q99758.
http://www.vitaldiagnostics.com/PackInserts/specificProteins/TF_HAPTO_04_.pdf.
Nanospectra Biosciences, Inc. - Publications.
     http://www.nanospectra.com/clinicians/spublications.html.
ADEREM, A. & UNDERHILL, D. M. 1999. Mechanisms of phagocytosis in macrophages.
     Annu Rev of Immunol, 17, 593-623.
AGEMY, L., SUGAHARA, K. N., KOTAMRAJU, V. R., GUJRATY, K., GIRARD, O.
     M., KONO, Y., MATTREY, R. F., PARK, J. H., SAILOR, M. J., JIMENEZ, A. I.,
     CATIVIELA, C., ZANUY, D., SAYAGO, F. J., ALEMAN, C., NUSSINOV, R. &
     RUOSLAHTI, E. 2010. Nanoparticle-induced vascular blockade in human prostate
     cancer. *Blood,* 116, 2847-56.
AGGARWAL, P., HALL, J. B., MCLELAND, C. B., DOBROVOLSKAIA, M. A. &
     MCNEIL, S. E. 2009. Nanoparticle interaction with plasma proteins as it relates to
     particle biodistribution, biocompatibility and therapeutic efficacy. *Adv Drug Deliv
     Rev,* 61, 428-437.
AKERMAN, M. E., CHAN, W. C., LAAKKONEN, P., BHATIA, S. N. & RUOSLAHTI,
     E. 2002. Nanocrystal targeting in vivo. *Proc Natl Acad Sci U S A,* 99, 12617-21.
ALBER, F., DOKUDOVSKAYA, S., VEENHOFF, L. M., ZHANG, W., KIPPER, J.,
     DEVOS, D., SUPRAPTO, A., KARNI-SCHMIDT, O., WILLIAMS, R., CHAIT, B.
     T., ROUT, M. P. & SALI, A. 2007. Determining the architectures of
     macromolecular assemblies. *Nature,* 450, 683-94.
ALEXIS, F., PRIDGEN, E., MOLNAR, L. K. & FAROKHZAD, O. C. 2008. Factors
     affecting the clearance and biodistribution of polymeric nanoparticles. *Mol Pharm,*
     5, 505-15.
ALIVISATOS, A. P. 2000. Biomineralization. Naturally aligned nanocrystals. *Science,*
     289, 736-7.
ALIVISATOS, A. P., GU, W. & LARABELL, C. 2005. Quantum dots as cellular probes.
     Annu Rev Biomed Eng, 7, 55-76.
ALIVISATOS, A. P., HUYNH, W. U. & DITTMER, J. J. 2002. Hybrid nanorod-polymer
     solar cells. *Science,* 295, 2425-2427.
ALIVISATOS, P. 2004. The use of nanocrystals in biological detection. *Nat Biotechnol,*
     22, 47-52.
ALLEMANN, E., GRAVEL, P., LEROUX, J. C., BALANT, L. & GURNY, R. 1997.
     Kinetics of blood component adsorption on poly(D,L-lactic acid) nanoparticles:
     evidence of complement C3 component involvement. *J Biomed Mater Res,* 37, 229-
     34.
ALMEIDA, J. P. M., CHEN, A. L., FOSTER, A. & DREZEK, R. 2011. In vivo
     biodistribution of nanoparticles. *Nanomedicine,* 6, 815-835.

ALYAUTDIN, R. N., TEZIKOV, E. B., RAMGE, P., KHARKEVICH, D. A., BEGLEY, D. J. & KREUTER, J. 1998. Significant entry of tubocurarine into the brain of rats by adsorption to polysorbate 80-coated polybutylcyanoacrylate nanoparticles: an in situ brain perfusion study. *J Microencapsul,* 15, 67-74.

ANDERSON, N. L. & ANDERSON, N. G. 2002. The human plasma proteome: history, character, and diagnostic prospects. *Mol Cell Proteomics,* 1, 845-67.

ANDERSON, N. L., POLANSKI, M., PIEPER, R., GATLIN, T., TIRUMALAI, R. S., CONRADS, T. P., VEENSTRA, T. D., ADKINS, J. N., POUNDS, J. G., FAGAN, R. & LOBLEY, A. 2004. The human plasma proteome: a nonredundant list developed by combination of four separate sources. *Mol Cell Proteomics,* 3, 311-26.

ANDO, J. & YAMAMOTO, K. 2009. Vascular mechanobiology: endothelial cell responses to fluid shear stress. *Circ J,* 73, 1983-92.

ANDO, J. & YAMAMOTO, K. 2011. Effects of Shear Stress and Stretch on Endothelial Function. *Antioxid Redox Signal,* 15, 1389-403.

ANDREWS, R. K. & BERNDT, M. C. 2004. Platelet physiology and thrombosis. *Thromb Res,* 114, 447-53.

ARIMA, Y., KAWAGOE, M., TODA, M. & IWATA, H. 2009. Complement activation by polymers carrying hydroxyl groups. *ACS Appl Mater Interfaces,* 1, 2400-7.

AZZAZY, H. M. & MANSOUR, M. M. 2009. In vitro diagnostic prospects of nanoparticles. *Clin Chim Acta,* 403, 1-8.

AZZAZY, H. M., MANSOUR, M. M. & KAZMIERCZAK, S. C. 2007. From diagnostics to therapy: prospects of quantum dots. *Clin Biochem,* 40, 917-27.

BAGALKOT, V., ZHANG, L., LEVY-NISSENBAUM, E., JON, S., KANTOFF, P. W., LANGER, R. & FAROKHZAD, O. C. 2007. Quantum dot-aptamer conjugates for synchronous cancer imaging, therapy, and sensing of drug delivery based on bi-fluorescence resonance energy transfer. *Nano Lett,* 7, 3065-70.

BAILEY, R. E. & NIE, S. 2003. Alloyed semiconductor quantum dots: tuning the optical properties without changing the particle size. *J Am Chem Soc,* 125, 7100-6.

BAKKER, E. N., VERSLUIS, J. P., SIPKEMA, P., VANTEEFFELEN, J. W., ROLF, T. M., SPAAN, J. A. & VANBAVEL, E. 2003. Differential structural adaptation to haemodynamics along single rat cremaster arterioles. *J Physiol,* 548, 549-55.

BARBEE, K., DAVIES, P. & LAL, R. 1994. Shear stress-induced reorganization of the surface topography of living endothelial cells imaged by atomic force microscopy. *Circ Res,* 74, 163-171.

BARRY, S. E. 2008. Challenges in the development of magnetic particles for therapeutic applications. *Int J Hyperthermia,* 24, 451-66.

BARUA, S. & REGE, K. 2009. Cancer-Cell-Phenotype-Dependent Differential Intracellular Trafficking of Unconjugated Quantum Dots. *Small,* 5, 370-376.

BARUCH, D., DENIS, C., MARTEAUX, C., SCHOEVAERT, D., COULOMBEL, L & MEYER, D. 1991. Role of von Willebrand factor associated to extracellular matrices in platelet adhesion. *Blood,* 77, 519-27.

BEHRENS, I., PENA, A. I., ALONSO, M. J. & KISSEL, T. 2002. Comparative uptake studies of bioadhesive and non-bioadhesive nanoparticles in human intestinal cell lines and rats: the effect of mucus on particle adsorption and transport. *Pharm Res,* 19, 1185-93.

BELTING, M., SANDGREN, S. & WITTRUP, A. 2005. Nuclear delivery of macromolecules: barriers and carriers. *Adv Drug Deliv Rev,* 57, 505-27.

BENOIT, J., CORMIER, M. & WEPIERRE, J. 1988. Comparative effects of four surfactants on growth, contraction and adhesion of cultured human fibroblasts. *Cell Biol Toxicol,* 4, 111-22.

BENTOLILA, L. A., EBENSTEIN, Y. & WEISS, S. 2009. Quantum Dots for In Vivo Small-Animal Imaging. *J Nucl Med,* 50, 493-496.

BERCELI, S. A., WARTY, V. S., SHEPPECK, R. A., MANDARINO, W. A., TANKSALE, S. K. & BOROVETZ, H. S. 1990. Hemodynamics and low density lipoprotein metabolism. Rates of low density lipoprotein incorporation and degradation along medial and lateral walls of the rabbit aorto-iliac bifurcation. *Arteriosclerosis,* 10, 686-94.

BERK, B. C., CORSON, M. A., PETERSON, T. E. & TSENG, H. 1995. Protein kinases as mediators of fluid shear stress stimulated signal transduction in endothelial cells: a hypothesis for calcium-dependent and calcium-independent events activated by flow. *J Biomech,* 28, 1439-50.

BERRY, J. P., ARNOUX, B., STANISLAS, G., GALLE, P. & CHRETIEN, J. 1977. A microanalytic study of particles transport across the alveoli: role of blood platelets. *Biomedicine,* 27, 354-7.

BERTORELLE, F., WILHELM, C., ROGER, J., GAZEAU, F., MENAGER, C. & CABUIL, V. 2006. Fluorescence-modified superparamagnetic nanoparticles: intracellular uptake and use in cellular imaging. *Langmuir,* 22, 5385-5391.

BHASKAR, S., TIAN, F., STOEGER, T., KREYLING, W., DE LA FUENTE, J. M., GRAZU, V., BORM, P., ESTRADA, G., NTZIACHRISTOS, V. & RAZANSKY, D. 2010. Multifunctional Nanocarriers for diagnostics, drug delivery and targeted treatment across blood-brain barrier: perspectives on tracking and neuroimaging. *Part Fibre Toxicol,* 7, 3.

BHATT, A. D. 1997. Endothelins and anti-endothelins. *J Assoc Physicians India,* 45, 868-72.

BINNIG, G., QUATE, C. F. & GERBER, C. 1986. Atomic force microscope. *Phys Rev Lett,* 56, 930-933.

BISWAS, P., CELLA, L. N., KANG, S. H., MULCHANDANI, A., YATES, M. V. & CHEN, W. 2011. A quantum-dot based protein module for in vivo monitoring of protease activity through fluorescence resonance energy transfer. *Chem Commun (Camb),* 47, 5259-61.

BLAIR, P. & FLAUMENHAFT, R. 2009. Platelet alpha-granules: basic biology and clinical correlates. *Blood Rev,* 23, 177-89.

BLUNK, T., HOCHSTRASSER, D. F., SANCHEZ, J. C., MULLER, B. W. & MULLER, R. H. 1993. Colloidal carriers for intravenous drug targeting: plasma protein adsorption patterns on surface-modified latex particles evaluated by two-dimensional polyacrylamide gel electrophoresis. *Electrophoresis,* 14, 1382-7.

BORN, G. V. 1962. Aggregation of blood platelets by adenosine diphosphate and its reversal. *Nature,* 194, 927-9.

BORN, G. V. 1966. Effects of adenosine diphosphate (ADP) and related substances on the adhesiveness of platelets in vitro and in vivo. *Br J Haematol,* 12, 37-8.

BORNER, M. M., SCHNEIDER, E., PIRNIA, F., SARTOR, O., TREPEL, J. B. & MYERS, C. E. 1994. The detergent Triton X-100 induces a death pattern in human carcinoma cell lines that resembles cytotoxic lymphocyte-induced apoptosis. *FEBS Lett,* 353, 129-32.

References

BRADLEY, A. J., DEVINE, D. V., ANSELL, S. M., JANZEN, J. & BROOKS, D. E. 1998. Inhibition of liposome-induced complement activation by incorporated poly(ethylene glycol)-lipids. *Arch Biochem Biophys,* 357, 185-94.

BRAIUCA, P., BOSCAROL, L., EBERT, C., LINDA, P. & GARDOSSI, L. 2006. 3D-QSAR applied to the quantitative prediction of penicillin G amidase selectivity. *Advanced Synthesis & Catalysis,* 348, 773-780.

BREM, H., PIANTADOSI, S., BURGER, P. C., WALKER, M., SELKER, R., VICK, N. A., BLACK, K., SISTI, M., BREM, S., MOHR, G. & ET AL. 1995. Placebo-controlled trial of safety and efficacy of intraoperative controlled delivery by biodegradable polymers of chemotherapy for recurrent gliomas. The Polymer-brain Tumor Treatment Group. *Lancet,* 345, 1008-12.

BREWER, S. H., GLOMM, W. R., JOHNSON, M. C., KNAG, M. K. & FRANZEN, S. 2005. Probing BSA binding to citrate-coated gold nanoparticles and surfaces. *Langmuir,* 21, 9303-7.

BROOK, R. D., FRANKLIN, B., CASCIO, W., HONG, Y., HOWARD, G., LIPSETT, M., LUEPKER, R., MITTLEMAN, M., SAMET, J., SMITH, S. C., JR. & TAGER, I. 2004. Air pollution and cardiovascular disease: a statement for healthcare professionals from the Expert Panel on Population and Prevention Science of the American Heart Association. *Circulation,* 109, 2655-71.

BROWN, C. H., 3RD, LEVERETT, L. B., LEWIS, C. W., ALFREY, C. P., JR. & HELLUMS, J. D. 1975. Morphological, biochemical, and functional changes in human platelets subjected to shear stress. *J Lab Clin Med,* 86, 462-71.

BUGA, G. M., GOLD, M. E., FUKUTO, J. M. & IGNARRO, L. J. 1991. Shear stress-induced release of nitric oxide from endothelial cells grown on beads. *Hypertension,* 17, 187-93.

BULOVIC, V., COE, S., WOO, W. K. & BAWENDI, M. 2002. Electroluminescence from single monolayers of nanocrystals in molecular organic devices. *Nature,* 420, 800-803.

BURELLO, E. & WORTH, A. P. 2011. QSAR modeling of nanomaterials. *Wiley Interdisciplinary Reviews-Nanomedicine and Nanobiotechnology,* 3, 298-306.

BUTLER, P. J., NORWICH, G., WEINBAUM, S. & CHIEN, S. 2001. Shear stress induces a time- and position-dependent increase in endothelial cell membrane fluidity. *Am J Physiol Cell Physiol,* 280, C962-9.

BUTT, H. J., DOWNING, K. H. & HANSMA, P. K. 1990. Imaging the membrane protein bacteriorhodopsin with the atomic force microscope. *Biophys J,* 58, 1473-80.

BUXTON, D. B., LEE, S. C., WICKLINE, S. A. & FERRARI, M. 2003. Recommendations of the National Heart, Lung, and Blood Institute Nanotechnology Working Group. *Circulation,* 108, 2737-42.

CARUTHERS, S. D., WICKLINE, S. A. & LANZA, G. M. 2007. Nanotechnological applications in medicine. *Curr Opin Biotechnol,* 18, 26-30.

CEDERVALL, T., LYNCH, I., FOY, M., BERGGARD, T., DONNELLY, S. C., CAGNEY, G., LINSE, S. & DAWSON, K. A. 2007a. Detailed identification of plasma proteins adsorbed on copolymer nanoparticles. *Angew Chem Int Ed Engl,* 46, 5754-6.

CEDERVALL, T., LYNCH, I., LINDMAN, S., BERGGARD, T., THULIN, E., NILSSON, H., DAWSON, K. A. & LINSE, S. 2007b. Understanding the nanoparticle-protein

corona using methods to quantify exchange rates and affinities of proteins for nanoparticles. *Proc Natl Acad Sci U S A,* 104, 2050-5.

CEVC, G., SCHÄTZLEIN, A. & RICHARDSEN, H. 2002. Ultradeformable lipid vesicles can penetrate the skin and other semi-permeable barriers unfragmented. Evidence from double label CLSM experiments and direct size measurements. *Biochimica et Biophysica Acta (BBA) - Biomembranes,* 1564, 21-30.

CHANG, J. C. & ROSENTHAL, S. J. 2011. Real-time quantum dot tracking of single proteins. *Methods Mol Biol,* 726, 51-62.

CHANG, M.-Y., SHIAU, A.-L., CHEN, Y.-H., CHANG, C.-J., CHEN, H. H. W. & WU, C.-L. 2008. Increased apoptotic potential and dose-enhancing effect of gold nanoparticles in combination with single-dose clinical electron beams on tumor-bearing mice. *Cancer Sci,* 99, 1479-1484.

CHAUVIERRE, C., MARDEN, M. C., VAUTHIER, C., LABARRE, D., COUVREUR, P. & LECLERC, L. 2004. Heparin coated poly(alkylcyanoacrylate) nanoparticles coupled to hemoglobin: a new oxygen carrier. *Biomaterials,* 25, 3081-3086.

CHEN, C. S., ANAYA, J. M., ZHANG, S., SPURGIN, J., CHUANG, C. Y., XU, C., MIAO, A. J., CHEN, E. Y., SCHWEHR, K. A., JIANG, Y., QUIGG, A., SANTSCHI, P. H. & CHIN, W. C. 2011. Effects of engineered nanoparticles on the assembly of exopolymeric substances from phytoplankton. *PLoS One,* 6, e21865.

CHEN, J., SAEKI, F., WILEY, B. J., CANG, H., COBB, M. J., LI, Z. Y., AU, L., ZHANG, H., KIMMEY, M. B., LI, X. & XIA, Y. 2005. Gold nanocages: bioconjugation and their potential use as optical imaging contrast agents. *Nano Lett,* 5, 473-7.

CHEN, Z., MENG, H., XING, G., CHEN, C., ZHAO, Y., JIA, G., WANG, T., YUAN, H., YE, C., ZHAO, F., CHAI, Z., ZHU, C., FANG, X., MA, B. & WAN, L. 2006. Acute toxicological effects of copper nanoparticles in vivo. *Toxicol Lett,* 163, 109-20.

CHERIAN, A. K., RANA, A. C. & JAIN, S. K. 2000. Self-assembled carbohydrate-stabilized ceramic nanoparticles for the parenteral delivery of insulin. *Drug Dev Ind Pharm,* 26, 459-63.

CHO, J. H., KO, S. G., AHN, Y. K., SONG, K. C. & CHOI, E. J. 2009. Preparation of biopolymer-coated magnetite nanoparticles for magnetic resonance image contrast agent. *J Nanosci Nanotechnol,* 9, 779-82.

CHO, S. J., MAYSINGER, D., JAIN, M., RODER, B., HACKBARTH, S. & WINNIK, F. M. 2007. Long-term exposure to CdTe quantum dots causes functional impairments in live cells. *Langmuir : the ACS journal of surfaces and colloids,* 23, 1974-80.

CHOI, C. H., ZUCKERMAN, J. E., WEBSTER, P. & DAVIS, M. E. 2011. Targeting kidney mesangium by nanoparticles of defined size. *Proc Natl Acad Sci U S A,* 108, 6656-61.

CHOI, H. S., LIU, W., MISRA, P., TANAKA, E., ZIMMER, J. P., ITTY IPE, B., BAWENDI, M. G. & FRANGIONI, J. V. 2007. Renal clearance of quantum dots. *Nat Biotechnol,* 25, 1165-70.

CHONN, A., SEMPLE, S. C. & CULLIS, P. R. 1992. Association of blood proteins with large unilamellar liposomes in vivo. Relation to circulation lifetimes. *J Biol Chem,* 267, 18759-65.

CHUN, Y. W. & WEBSTER, T. J. 2009. The role of nanomedicine in growing tissues. *Ann Biomed Eng,* 37, 2034-47.

CLAPP, A. R., GOLDMAN, E. R. & MATTOUSSI, H. 2006. Capping of CdSe-ZnS quantum dots with DHLA and subsequent conjugation with proteins. *Nat Protoc,* 1, 1258-66.

COLLER, B. S. 1995. Blockade of platelet GPIIb/IIIa receptors as an antithrombotic strategy. *Circulation,* 92, 2373-80.

CONNER, S. D. & SCHMID, S. L. 2003. Regulated portals of entry into the cell. *Nature,* 422, 37-44.

CONROY, J., BYRNE, S. J., GUN'KO, Y. K., RAKOVICH, Y. P., DONEGAN, J. F., DAVIES, A., KELLEHER, D. & VOLKOV, Y. 2008. CdTe nanoparticles display tropism to core histones and histone-rich cell organelles. *Small,* 4, 2006-15.

CONTAG, C. H. & ROSS, B. D. 2002. It's not just about anatomy: in vivo bioluminescence imaging as an eyepiece into biology. *J Magn Reson Imaging,* 16, 378-87.

CORNELIUS, R. M., ARCHAMBAULT, J. & BRASH, J. L. 2002. Identification of apolipoprotein A-I as a major adsorbate on biomaterial surfaces after blood or plasma contact. *Biomaterials,* 23, 3583-7.

COROT, C., ROBERT, P., IDEE, J. M. & PORT, M. 2006. Recent advances in iron oxide nanocrystal technology for medical imaging. *Adv Drug Deliv Rev,* 58, 1471-504.

CORSON, M. A., JAMES, N. L., LATTA, S. E., NEREM, R. M., BERK, B. C. & HARRISON, D. G. 1996. Phosphorylation of endothelial nitric oxide synthase in response to fluid shear stress. *Circ Res,* 79, 984-91.

CRAMER, E. M., SAVIDGE, G. F., VAINCHENKER, W., BERNDT, M. C., PIDARD, D., CAEN, J. P., MASSE, J. M. & BRETON-GORIUS, J. 1990. Alpha-granule pool of glycoprotein IIb-IIIa in normal and pathologic platelets and megakaryocytes. *Blood,* 75, 1220-7.

CULLIS, P. R., CHONN, A. & SEMPLE, S. C. 1998. Interactions of liposomes and lipid-based carrier systems with blood proteins: Relation to clearance behaviour in vivo. *Adv Drug Deliv Rev,* 32, 3-17.

CUNNINGHAM, K. S. & GOTLIEB, A. I. 2005. The role of shear stress in the pathogenesis of atherosclerosis. *Lab Invest,* 85, 9-23.

CYBULSKY, M. I. & GIMBRONE, M. A., JR. 1991. Endothelial expression of a mononuclear leukocyte adhesion molecule during atherogenesis. *Science,* 251, 788-91.

DAMMERS, R., STIFFT, F., TORDOIR, J. H., HAMELEERS, J. M., HOEKS, A. P. & KITSLAAR, P. J. 2003. Shear stress depends on vascular territory: comparison between common carotid and brachial artery. *J Appl Physiol,* 94, 485-9.

DANGARIA, J. H. & BUTLER, P. J. 2007. Macrorheology and adaptive microrheology of endothelial cells subjected to fluid shear stress. *Am J Physiol Cell Physiol,* 293, C1568-75.

DARDIK, A., LIU, A. & BALLERMANN, B. J. 1999. Chronic in vitro shear stress stimulates endothelial cell retention on prosthetic vascular grafts and reduces subsequent in vivo neointimal thickness. *J Vasc Surg,* 29, 157-67.

DAUSEND, J., MUSYANOVYCH, A., DASS, M., WALTHER, P., SCHREZENMEIER, H., LANDFESTER, K. & MAILANDER, V. 2008. Uptake mechanism of oppositely charged fluorescent nanoparticles in HeLa cells. *Macromolecular bioscience,* 8, 1135-43.

DAVDA, J. & LABHASETWAR, V. 2002. Characterization of nanoparticle uptake by endothelial cells. *Int J Pharm,* 233, 51-59.

DAVIE, E. W., FUJIKAWA, K. & KISIEL, W. 1991. The coagulation cascade: initiation, maintenance, and regulation. *Biochemistry,* 30, 10363-70.

DAVIES, P. F. 1995. Flow-mediated endothelial mechanotransduction. *Physiol Rev,* 75, 519-60.

DAVIES, P. F., REMUZZI, A., GORDON, E. J., DEWEY, C. F., JR. & GIMBRONE, M. A., JR. 1986. Turbulent fluid shear stress induces vascular endothelial cell turnover in vitro. *Proc Natl Acad Sci U S A,* 83, 2114-7.

DE GROOT, P. C., POELKENS, F., KOOIJMAN, M. & HOPMAN, M. T. 2004. Preserved flow-mediated dilation in the inactive legs of spinal cord-injured individuals. *Am J Physiol Heart Circ Physiol,* 287, H374-80.

DE KONINCK, P., LABRECQUE, S., HEYES, C. D. & WISEMAN, P. W. 2007. Probing synaptic signaling with quantum dots. *HFSP Journal,* 1, 5-10.

DELL'ORCO, D., LUNDQVIST, M., OSLAKOVIC, C., CEDERVALL, T. & LINSE, S. 2010. Modeling the time evolution of the nanoparticle-protein corona in a body fluid. *PLoS One,* 5, e10949.

DENG, X., MAROIS, Y., HOW, T., MERHI, Y., KING, M., GUIDOIN, R. & KARINO, T. 1995. Luminal surface concentration of lipoprotein (LDL) and its effect on the wall uptake of cholesterol by canine carotid arteries. *J Vasc Surg,* 21, 135-45.

DENG, Z. J., LIANG, M., MONTEIRO, M., TOTH, I. & MINCHIN, R. F. 2011. Nanoparticle-induced unfolding of fibrinogen promotes Mac-1 receptor activation and inflammation. *Nat Nano,* 6, 39-44.

DEPRIEST, S. A., MAYER, D., NAYLOR, C. B. & MARSHALL, G. R. 1993. 3D-QSAR of angiotensin-converting enzyme and thermolysin inhibitors: a comparison of CoMFA models based on deduced and experimentally determined active site geometries. *Journal of the American Chemical Society,* 115, 5372-5384.

DESAI, N., TRIEU, V., YAO, Z., LOUIE, L., CI, S., YANG, A., TAO, C., DE, T., BEALS, B., DYKES, D., NOKER, P., YAO, R., LABAO, E., HAWKINS, M. & SOON-SHIONG, P. 2006. Increased antitumor activity, intratumor paclitaxel concentrations, and endothelial cell transport of cremophor-free, albumin-bound paclitaxel, ABI-007, compared with cremophor-based paclitaxel. *Clin Cancer Res,* 12, 1317-24.

DESJARDINS, M. 2003. ER-mediated phagocytosis: a new membrane for new functions. *Nat Rev Immunol,* 3, 280-91.

DEWEY, C. F., JR. 1984. Effects of fluid flow on living vascular cells. *J Biomech Eng,* 106, 31-5.

DEWEY, C. F., JR., BUSSOLARI, S. R., GIMBRONE, M. A., JR. & DAVIES, P. F. 1981. The dynamic response of vascular endothelial cells to fluid shear stress. *J Biomech Eng,* 103, 177-85.

DIAMOND, S. L., SHAREFKIN, J. B., DIEFFENBACH, C., FRASIER-SCOTT, K., MCINTIRE, L. V. & ESKIN, S. G. 1990. Tissue plasminogen activator messenger RNA levels increase in cultured human endothelial cells exposed to laminar shear stress. *J Cell Physiol,* 143, 364-71.

DIEDERICHS, J. E. 1996. Plasma protein adsorption patterns on liposomes: establishment of analytical procedure. *Electrophoresis,* 17, 607-11.

DIMMELER, S., HAENDELER, J., RIPPMANN, V., NEHLS, M. & ZEIHER, A. M. 1996. Shear stress inhibits apoptosis of human endothelial cells. *FEBS Lett,* 399, 71-4.

DOBROVOLSKAIA, M. A., AGGARWAL, P., HALL, J. B. & MCNEIL, S. E. 2008. Preclinical studies to understand nanoparticle interaction with the immune system and its potential effects on nanoparticle biodistribution. *Mol Pharm,* 5, 487-95.

DOBROVOLSKAIA, M. A., GERMOLEC, D. R. & WEAVER, J. L. 2009a. Evaluation of nanoparticle immunotoxicity. *Nature nanotechnology,* 4, 411-4.

DOBROVOLSKAIA, M. A. & MCNEIL, S. E. 2007. Immunological properties of engineered nanomaterials. *Nat Nanotechnol,* 2, 469-78.

DOBROVOLSKAIA, M. A., PATRI, A. K., ZHENG, J., CLOGSTON, J. D., AYUB, N., AGGARWAL, P., NEUN, B. W., HALL, J. B. & MCNEIL, S. E. 2009b. Interaction of colloidal gold nanoparticles with human blood: effects on particle size and analysis of plasma protein binding profiles. *Nanomedicine,* 5, 106-17.

DONALDSON, K., STONE, V., SEATON, A. & MACNEE, W. 2001. Ambient particle inhalation and the cardiovascular system: potential mechanisms. *Environ Health Perspect,* 109 Suppl 4, 523-7.

DUAN, H. & NIE, S. 2007. Cell-penetrating quantum dots based on multivalent and endosome-disrupting surface coatings. *J Am Chem Soc,* 129, 3333-8.

DUBERTRET, B., SKOURIDES, P., NORRIS, D. J., NOIREAUX, V., BRIVANLOU, A. H. & LIBCHABER, A. 2002. In vivo imaging of quantum dots encapsulated in phospholipid micelles. *Science,* 298, 1759-62.

DULL, R. O. & DAVIES, P. F. 1991. Flow modulation of agonist (ATP)-response (Ca2+) coupling in vascular endothelial cells. *Am J Physiol,* 261, H149-54.

DUNCAN, R. 2006. Polymer conjugates as anticancer nanomedicines. *Nat Rev Cancer,* 6, 688-701.

DUTTA, D., SUNDARAM, S. K., TEEGUARDEN, J. G., RILEY, B. J., FIFIELD, L. S., JACOBS, J. M., ADDLEMAN, S. R., KAYSEN, G. A., MOUDGIL, B. M. & WEBER, T. J. 2007. Adsorbed proteins influence the biological activity and molecular targeting of nanomaterials. *Toxicol Sci,* 100, 303-15.

EDGAR, R., MCKINSTRY, M., HWANG, J., OPPENHEIM, A. B., FEKETE, R. A., GIULIAN, G., MERRIL, C., NAGASHIMA, K. & ADHYA, S. 2006. High-sensitivity bacterial detection using biotin-tagged phage and quantum-dot nanocomplexes. *Proc Natl Acad Sci U S A,* 103, 4841-5.

EHRENBERG, M. S., FRIEDMAN, A. E., FINKELSTEIN, J. N., OBERDÖRSTER, G. & MCGRATH, J. L. 2009. The influence of protein adsorption on nanoparticle association with cultured endothelial cells. *Biomaterials,* 30, 603-610.

ELSAESSER, A., BARNES, C. A., MCKERR, G., SALVATI, A., LYNCH, I., DAWSON, K. A. & HOWARD, C. V. 2011. Quantification of nanoparticle uptake by cells using an unbiased sampling method and electron microscopy. *Nanomedicine (Lond),* 6, 1189-98.

ENDENBURG, S. C., HANTGAN, R. R., LINDEBOOM-BLOKZIJL, L., LANKHOF, H., JEROME, W. G., LEWIS, J. C., SIXMA, J. J. & DE GROOT, P. G. 1995. On the role of von Willebrand factor in promoting platelet adhesion to fibrin in flowing blood. *Blood,* 86, 4158-65.

ESCOFFRE, J. M., TEISSIE, J. & ROLS, M. P. 2010. Gene transfer: how can the biological barriers be overcome? *J Membr Biol,* 236, 61-74.

ESCOLAR, G., LEISTIKOW, E. & WHITE, J. G. 1989. The fate of the open canalicular system in surface and suspension-activated platelets. *Blood,* 74, 1983-8.

ESKIN, S. G., IVES, C. L., MCINTIRE, L. V. & NAVARRO, L. T. 1984. Response of cultured endothelial cells to steady flow. *Microvasc Res,* 28, 87-94.

ESMON, C. T. 2000. Regulation of blood coagulation. *Biochim Biophys Acta,* 1477, 349-60.

ESMON, C. T. 2005. Coagulation inhibitors in inflammation. *Biochem Soc Trans,* 33, 401-5.

ESTEBANELL, E., DIAZ-RICART, M., LOZANO, M., MAZZARA, R., ESCOLAR, G. & ORDINAS, A. 1998. Cytoskeletal reorganization after preparation of platelet concentrates, using the buffy coat method, and during their storage. *Haematologica,* 83, 112-7.

EUROPEAN, C. 2006. The appropriateness of existing methodologies to assess the potential risks associated with engineered and adventitious products of nanotechnologies *Scientific Committee on Emerging and Newly Identified Health Risks (SCENIHR)/002/05.*

FALCINELLI, E., GUGLIELMINI, G., TORTI, M. & GRESELE, P. 2005. Intraplatelet signaling mechanisms of the priming effect of matrix metalloproteinase-2 on platelet aggregation. *J Thromb Haemost,* 3, 2526-35.

FARADAY, N., SCHARPF, R. B., DODD-O, J. M., MARTINEZ, E. A., ROSENFELD, B. A. & DORMAN, T. 2001. Leukocytes can enhance platelet-mediated aggregation and thromboxane release via interaction of P-selectin glycoprotein ligand 1 with P-selectin. *Anesthesiology,* 94, 145-51.

FERNANDEZ-PATRON, C., MARTINEZ-CUESTA, M. A., SALAS, E., SAWICKI, G., WOZNIAK, M., RADOMSKI, M. W. & DAVIDGE, S. T. 1999. Differential regulation of platelet aggregation by matrix metalloproteinases-9 and -2. *Thromb Haemost,* 82, 1730-5.

FLEMING, I., BAUERSACHS, J. & BUSSE, R. 1997. Calcium-dependent and calcium-independent activation of the endothelial NO synthase. *J Vasc Res,* 34, 165-74.

FORAKER, A. B., WALCZAK, R. J., COHEN, M. H., BOIARSKI, T. A., GROVE, C. F. & SWAAN, P. W. 2003. Microfabricated porous silicon particles enhance paracellular delivery of insulin across intestinal Caco-2 cell monolayers. *Pharm Res,* 20, 110-6.

FOX, J. E. 1993a. The platelet cytoskeleton. *Thromb Haemost,* 70, 884-93.

FOX, J. E. 1993b. Regulation of platelet function by the cytoskeleton. *Adv Exp Med Biol,* 344, 175-85.

FOX, J. E. 1994. Transmembrane signaling across the platelet integrin glycoprotein IIb-IIIa. *Ann N Y Acad Sci,* 714, 75-87.

FOX, J. E., LIPFERT, L., CLARK, E. A., REYNOLDS, C. C., AUSTIN, C. D. & BRUGGE, J. S. 1993. On the role of the platelet membrane skeleton in mediating signal transduction. Association of GP IIb-IIIa, pp60c-src, pp62c-yes, and the p21ras GTPase-activating protein with the membrane skeleton. *J Biol Chem,* 268, 25973-84.

FRANGIONI, J. V., KIM, S. W., OHNISHI, S., KIM, S. & BAWENDI, M. G. 2007. Sentinel lymph node mapping with type-II quantum dots. *Methods Mol Biol,* 374, 147-59.

FRANGOS, J. A., ESKIN, S. G., MCINTIRE, L. V. & IVES, C. L. 1985. Flow effects on prostacyclin production by cultured human endothelial cells. *Science,* 227, 1477-9.

FRANKE, R. P., GRAFE, M., SCHNITTLER, H., SEIFFGE, D., MITTERMAYER, C. & DRENCKHAHN, D. 1984. Induction of human vascular endothelial stress fibres by fluid shear stress. *Nature,* 307, 648-9.

FREITAS, J. R. A. 2005a. What is nanomedicine? *Nanomedicine: Nanotechnology, Biology and Medicine,* 1, 2-9.

FREITAS, R. A. 2005b. Current Status of Nanomedicine and Medical Nanorobotics. *Journal of Computational and Theoretical Nanoscience,* 2, 1-25.

FRY, D. L., HERDERICK, E. E. & JOHNSON, D. K. 1993. Local intimal-medial uptakes of 125I-albumin, 125I-LDL, and parenteral Evans blue dye protein complex along the aortas of normocholesterolemic minipigs as predictors of subsequent hypercholesterolemic atherogenesis. *Arterioscler Thromb,* 13, 1193-204.

FURCHGOTT, R. F. & ZAWADZKI, J. V. 1980. The obligatory role of endothelial cells in the relaxation of arterial smooth muscle by acetylcholine. *Nature,* 288, 373-6.

GAO, X., CHAN, W. C. & NIE, S. 2002. Quantum-dot nanocrystals for ultrasensitive biological labeling and multicolor optical encoding. *J Biomed Opt,* 7, 532-7.

GAO, X., CUI, Y., LEVENSON, R. M., CHUNG, L. W. & NIE, S. 2004. In vivo cancer targeting and imaging with semiconductor quantum dots. *Nat Biotechnol,* 22, 969-76.

GAO, X. & NIE, S. 2003. Molecular profiling of single cells and tissue specimens with quantum dots. *Trends Biotechnol,* 21, 371-3.

GAO, X. & NIE, S. 2004. Quantum dot-encoded mesoporous beads with high brightness and uniformity: rapid readout using flow cytometry. *Anal Chem,* 76, 2406-10.

GARLANDA, C. & DEJANA, E. 1997. Heterogeneity of endothelial cells. Specific markers. *Arterioscler Thromb Vasc Biol,* 17, 1193-202.

GE, S., WANG, G., SHEN, Y., ZHANG, Q., JIA, D., WANG, H., DONG, Q. & YIN, T. 2011. Cytotoxic effects of MgO nanoparticles on human umbilical vein endothelial cells in vitro. *IET Nanobiotechnol,* 5, 36.

GEKLE, M. 1998. Renal Proximal Tubular Albumin Reabsorption: Daily Prevention of Albuminuria. *Physiology,* 13, 5-11.

GESSNER, A., LIESKE, A., PAULKE, B. & MULLER, R. 2002. Influence of surface charge density on protein adsorption on polymeric nanoparticles: analysis by two-dimensional electrophoresis. *Eur J Pharm Biopharm,* 54, 165-70.

GESSNER, A., LIESKE, A., PAULKE, B. R. & MULLER, R. H. 2003. Functional groups on polystyrene model nanoparticles: influence on protein adsorption. *J Biomed Mater Res A,* 65, 319-26.

GESSNER, A., WAICZ, R., LIESKE, A., PAULKE, B., MADER, K. & MULLER, R. H. 2000. Nanoparticles with decreasing surface hydrophobicities: influence on plasma protein adsorption. *Int J Pharm,* 196, 245-9.

GEYS, J., NEMMAR, A., VERBEKEN, E., SMOLDERS, E., RATOI, M., HOYLAERTS, M. F., NEMERY, B. & HOET, P. H. 2008. Acute toxicity and prothrombotic effects of quantum dots: impact of surface charge. *Environ Health Perspect,* 116, 1607-13.

GIBBS-FLOURNOY, E. A., BROMBERG, P. A., HOFER, T. P., SAMET, J. M. & ZUCKER, R. M. 2011. Darkfield-confocal microscopy detection of nanoscale particle internalization by human lung cells. *Part Fibre Toxicol,* 8, 2.

GIDDENS, D. P., ZARINS, C. K. & GLAGOV, S. 1993. The role of fluid mechanics in the localization and detection of atherosclerosis. *J Biomech Eng,* 115, 588-94.

GINSBERG, M. H., LOFTUS, J. C. & PLOW, E. F. 1988. Cytoadhesins, integrins, and platelets. *Thromb Haemost,* 59, 1-6.

GINSBERG, M. H., XIAOPING, D., O'TOOLE, T. E., LOFTUS, J. C. & PLOW, E. F. 1993. Platelet integrins. *Thromb Haemost,* 70, 87-93.

GIRARD, P. R. & NEREM, R. M. 1995. Shear stress modulates endothelial cell morphology and F-actin organization through the regulation of focal adhesion-associated proteins. *J Cell Physiol,* 163, 179-93.

GLYNN, M. F., MOVAT, H. Z., MURPHY, E. A. & MUSTARD, J. F. 1965. Study of Platelet Adhesiveness and Aggregation, with Latex Particles. *J Lab Clin Med,* 65, 179-201.

GOJOVA, A., GUO, B., KOTA, R. S., RUTLEDGE, J. C., KENNEDY, I. M. & BARAKAT, A. I. 2007. Induction of inflammation in vascular endothelial cells by metal oxide nanoparticles: effect of particle composition. *Environ Health Perspect,* 115, 403-9.

GOLDMAN, E. R., BALIGHIAN, E. D., MATTOUSSI, H., KUNO, M. K., MAURO, J. M., TRAN, P. T. & ANDERSON, G. P. 2002. Avidin: a natural bridge for quantum dot-antibody conjugates. *J Am Chem Soc,* 124, 6378-82.

GOLDMAN, E. R., CLAPP, A. R., ANDERSON, G. P., UYEDA, H. T., MAURO, J. M., MEDINTZ, I. L. & MATTOUSSI, H. 2004. Multiplexed toxin analysis using four colors of quantum dot fluororeagents. *Anal Chem,* 76, 684-8.

GOLDMAN, E. R., MEDINTZ, I. L. & MATTOUSSI, H. 2006. Luminescent quantum dots in immunoassays. *Anal Bioanal Chem,* 384, 560-3.

GOPPERT, T. M. & MULLER, R. H. 2003. Plasma protein adsorption of Tween 80- and poloxamer 188-stabilized solid lipid nanoparticles. *J Drug Target,* 11, 225-31.

GOPPERT, T. M. & MULLER, R. H. 2005a. Adsorption kinetics of plasma proteins on solid lipid nanoparticles for drug targeting. *Int J Pharm,* 302, 172-86.

GOPPERT, T. M. & MULLER, R. H. 2005b. Polysorbate-stabilized solid lipid nanoparticles as colloidal carriers for intravenous targeting of drugs to the brain: comparison of plasma protein adsorption patterns. *J Drug Target,* 13, 179-87.

GORBET, M. B. & SEFTON, M. V. 2004. Biomaterial-associated thrombosis: roles of coagulation factors, complement, platelets and leukocytes. *Biomaterials,* 25, 5681-703.

GOTO, S., SALOMON, D. R., IKEDA, Y. & RUGGERI, Z. M. 1995. Characterization of the unique mechanism mediating the shear-dependent binding of soluble von Willebrand factor to platelets. *J Biol Chem,* 270, 23352-61.

GRABOWSKI, E. F., JAFFE, E. A. & WEKSLER, B. B. 1985. Prostacyclin production by cultured endothelial cell monolayers exposed to step increases in shear stress. *J Lab Clin Med,* 105, 36-43.

GRAY, J. J. 2004. The interaction of proteins with solid surfaces. *Curr Opin Struct Biol,* 14, 110-5.

GREF, R., LUCK, M., QUELLEC, P., MARCHAND, M., DELLACHERIE, E., HARNISCH, S., BLUNK, T. & MULLER, R. H. 2000. 'Stealth' corona-core nanoparticles surface modified by polyethylene glycol (PEG): influences of the corona (PEG chain length and surface density) and of the core composition on

phagocytic uptake and plasma protein adsorption. *Colloids Surf B Biointerfaces,* 18, 301-313.

GU, H., XU, K., YANG, Z., CHANG, C. K. & XU, B. 2005. Synthesis and cellular uptake of porphyrin decorated iron oxide nanoparticles-a potential candidate for bimodal anticancer therapy. *Chem. Comm.,* 4270-4272.

GULYAEV, A. E., GELPERINA, S. E., SKIDAN, I. N., ANTROPOV, A. S., KIVMAN, G. Y. & KREUTER, J. 1999. Significant transport of doxorubicin into the brain with polysorbate 80-coated nanoparticles. *Pharm Res,* 16, 1564-9.

GUO, S., LI, D., ZHANG, L., LI, J. & WANG, E. 2009. Monodisperse mesoporous superparamagnetic single-crystal magnetite nanoparticles for drug delivery. *Biomaterials,* 30, 1881-9.

GUPTA, A. K. & GUPTA, M. 2005. Synthesis and surface engineering of iron oxide nanoparticles for biomedical applications. *Biomaterials,* 26, 3995-4021.

GUPTA, A. K., NAREGALKAR, R. R., VAIDYA, V. D. & GUPTA, M. 2007. Recent advances on surface engineering of magnetic iron oxide nanoparticles and their biomedical applications. *Nanomedicine (Lond),* 2, 23-39.

HAIDEKKER, M. A., L'HEUREUX, N. & FRANGOS, J. A. 2000. Fluid shear stress increases membrane fluidity in endothelial cells: a study with DCVJ fluorescence. *Am J Physiol Heart Circ Physiol,* 278, H1401-6.

HAJDÚ, A., TOMBÁCZ, E., ILLÉS, E., BICA, D. & VÉKÁS, L. 2008. Magnetite Nanoparticles Stabilized Under Physiological Conditions for Biomedical Application. . *Colloids for Nano- and Biotechnology.* Springer Berlin / Heidelberg.

HAJJAR, K. A. 1995. Cellular receptors in the regulation of plasmin generation. *Thromb Haemost,* 74, 294-301.

HALBREICH, A., ROGER, J., PONS, J. N., GELDWERTH, D., DA SILVA, M. F., ROUDIER, M. & BACRI, J. C. 1998. Biomedical applications of maghemite ferrofluid. *Biochimie,* 80, 379-90.

HAMBURGER, S. A. & MCEVER, R. P. 1990. GMP-140 mediates adhesion of stimulated platelets to neutrophils. *Blood,* 75, 550-4.

HAMILTON, K. K., JI, Z., ROLLINS, S., STEWART, B. H. & SIMS, P. J. 1990. Regulatory control of the terminal complement proteins at the surface of human endothelial cells: neutralization of a C5b-9 inhibitor by antibody to CD59. *Blood,* 76, 2572-7.

HAN, J. & ULEVITCH, R. J. 2005. Limiting inflammatory responses during activation of innate immunity. *Nat Immunol,* 6, 1198-205.

HAN, M., GAO, X., SU, J. Z. & NIE, S. 2001. Quantum-dot-tagged microbeads for multiplexed optical coding of biomolecules. *Nat Biotechnol,* 19, 631-5.

HANTGAN, R. R., ENDENBURG, S. C., CAVERO, I., MARGUERIE, G., UZAN, A., SIXMA, J. J. & DE GROOT, P. G. 1992. Inhibition of platelet adhesion to fibrin(ogen) in flowing whole blood by Arg-Gly-Asp and fibrinogen gamma-chain carboxy terminal peptides. *Thromb Haemost,* 68, 694-700.

HANTGAN, R. R., HINDRIKS, G., TAYLOR, R. G., SIXMA, J. J. & DE GROOT, P. G. 1990. Glycoprotein Ib, von Willebrand factor, and glycoprotein IIb:IIIa are all involved in platelet adhesion to fibrin in flowing whole blood. *Blood,* 76, 345-53.

HARDMAN, R. 2006. A toxicologic review of quantum dots: toxicity depends on physicochemical and environmental factors. *Environmental health perspectives,* 114, 165-72.

References

HARUSH-FRENKEL, O., DEBOTTON, N., BENITA, S. & ALTSCHULER, Y. 2007. Targeting of nanoparticles to the clathrin-mediated endocytic pathway. *Biochem Biophys Res Commun,* 353, 26-32.

HAUPT, B. J., PELLING, A. E. & HORTON, M. A. 2006. Integrated confocal and scanning probe microscopy for biomedical research. *Scientific World Journal,* 6, 1609-18.

HAWKINS, M. J., SOON-SHIONG, P. & DESAI, N. 2008. Protein nanoparticles as drug carriers in clinical medicine. *Adv Drug Deliv Rev,* 60, 876-85.

HE, Q., SHI, J., CHEN, F., ZHU, M. & ZHANG, L. 2010. An anticancer drug delivery system based on surfactant-templated mesoporous silica nanoparticles. *Biomaterials,* 31, 3335-46.

HELLSTRAND, E., LYNCH, I., ANDERSSON, A., DRAKENBERG, T., DAHLBACK, B., DAWSON, K. A., LINSE, S. & CEDERVALL, T. 2009. Complete high-density lipoproteins in nanoparticle corona. *FEBS J,* 276, 3372-81.

HELMLINGER, G., BERK, B. C. & NEREM, R. M. 1995. Calcium responses of endothelial cell monolayers subjected to pulsatile and steady laminar flow differ. *Am J Physiol,* 269, C367-75.

HENDERSON, E., HAYDON, P. G. & SAKAGUCHI, D. S. 1992. Actin filament dynamics in living glial cells imaged by atomic force microscopy. *Science,* 257, 1944-6.

HILLAIREAU, H. & COUVREUR, P. 2009. Nanocarriers' entry into the cell: relevance to drug delivery. *Cell Mol Life Sci,* 66, 2873-96.

HOEKS, A. P., SAMIJO, S. K., BRANDS, P. J. & RENEMAN, R. S. 1995. Noninvasive determination of shear-rate distribution across the arterial lumen. *Hypertension,* 26, 26-33.

HOFHEINZ, R. D., GNAD-VOGT, S. U., BEYER, U. & HOCHHAUS, A. 2005. Liposomal encapsulated anti-cancer drugs. *Anti-cancer drugs,* 16, 691-707.

HOH, J. H., LAL, R., JOHN, S. A., REVEL, J. P. & ARNSDORF, M. F. 1991. Atomic force microscopy and dissection of gap junctions. *Science,* 253, 1405-8.

HORBER, J. K., HABERLE, W., OHNESORGE, F., BINNIG, G., LIEBICH, H. G., CZERNY, C. P., MAHNEL, H. & MAYR, A. 1992. Investigation of living cells in the nanometer regime with the scanning force microscope. *Scanning Microsc,* 6, 919-29; discussion 929-30.

HUFFAKER, D. L., PARK, G., ZOU, Z., SHCHEKIN, O. B. & DEPPE, D. G. 1998. 1.3 mu m room-temperature GaAs-based quantum-dot laser. *Applied Physics Letters,* 73, 2564-2566.

IKEDA, Y., HANDA, M., KAWANO, K., KAMATA, T., MURATA, M., ARAKI, Y., ANBO, H., KAWAI, Y., WATANABE, K., ITAGAKI, I. & ET AL. 1991. The role of von Willebrand factor and fibrinogen in platelet aggregation under varying shear stress. *J Clin Invest,* 87, 1234-40.

ILLUM, L., DAVIS, S. S., MULLER, R. H., MAK, E. & WEST, P. 1987. The organ distribution and circulation time of intravenously injected colloidal carriers sterically stabilized with a block copolymer--poloxamine 908. *Life Sci,* 40, 367-74.

IMBERTI, B., MORIGI, M., ZOJA, C., ANGIOLETTI, S., ABBATE, M., REMUZZI, A. & REMUZZI, G. 2000. Shear stress-induced cytoskeleton rearrangement mediates NF-kappaB-dependent endothelial expression of ICAM-1. *Microvasc Res,* 60, 182-8.

ISENBERG, W. M., MCEVER, R. P., PHILLIPS, D. R., SHUMAN, M. A. & BAINTON, D. F. 1987. The platelet fibrinogen receptor: an immunogold-surface replica study of agonist-induced ligand binding and receptor clustering. *J Cell Biol,* 104, 1655-63.

ISHIDA, T., TAKAHASHI, M., CORSON, M. A. & BERK, B. C. 1997. Fluid shear stress-mediated signal transduction: how do endothelial cells transduce mechanical force into biological responses? *Ann N Y Acad Sci,* 811, 12-23; discussion 23-4.

ISLAM, T. & HARISINGHANI, M. G. 2009. Overview of nanoparticle use in cancer imaging. *Cancer Biomark,* 5, 61-7.

ITO, A., HIBINO, E., KOBAYASHI, C., TERASAKI, H., KAGAMI, H., UEDA, M., KOBAYASHI, T. & HONDA, H. 2005. Construction and delivery of tissue-engineered human retinal pigment epithelial cell sheets, using magnetite nanoparticles and magnetic force. *Tissue Eng,* 11, 489-96.

ITO, A., HONDA, H. & KOBAYASHI, T. 2006. Cancer immunotherapy based on intracellular hyperthermia using magnetite nanoparticles: a novel concept of "heat-controlled necrosis" with heat shock protein expression. *Cancer Immunol Immunother,* 55, 320-8.

ITO, A., TANAKA, K., HONDA, H., ABE, S., YAMAGUCHI, H. & KOBAYASHI, T. 2003. Complete regression of mouse mammary carcinoma with a size greater than 15 mm by frequent repeated hyperthermia using magnetite nanoparticles. *J Biosci Bioeng,* 96, 364-9.

JAFFE, E. A., HOYER, L. W. & NACHMAN, R. L. 1974. Synthesis of von Willebrand factor by cultured human endothelial cells. *Proc Natl Acad Sci U S A,* 71, 1906-9.

JAIN, K. K. 2007. Applications of nanobiotechnology in clinical diagnostics. *Clin Chem,* 53, 2002-9.

JAIN, R. K. & STYLIANOPOULOS, T. 2010. Delivering nanomedicine to solid tumors. *Nat Rev Clin Oncol,* 7, 653-64.

JAISWAL, J. K., GOLDMAN, E. R., MATTOUSSI, H. & SIMON, S. M. 2004. Use of quantum dots for live cell imaging. *Nat Methods,* 1, 73-8.

JAISWAL, J. K., MATTOUSSI, H., MAURO, J. M. & SIMON, S. M. 2003. Long-term multiple color imaging of live cells using quantum dot bioconjugates. *Nat Biotechnol,* 21, 47-51.

JANSSENS, S. P., SHIMOUCHI, A., QUERTERMOUS, T., BLOCH, D. B. & BLOCH, K. D. 1992. Cloning and expression of a cDNA encoding human endothelium-derived relaxing factor/nitric oxide synthase. *J Biol Chem,* 267, 14519-22.

JEFFERIS, R. & KUMARARATNE, D. S. 1990. Selective IgG subclass deficiency: quantification and clinical relevance. *Clin Exp Immunol,* 81, 357-67.

JESTY, J., BELTRAMI, E. & WILLEMS, G. 1993. Mathematical analysis of a proteolytic positive-feedback loop: dependence of lag time and enzyme yields on the initial conditions and kinetic parameters. *Biochemistry,* 32, 6266-74.

JIANG, W., PAPA, E., FISCHER, H., MARDYANI, S. & CHAN, W. C. 2004. Semiconductor quantum dots as contrast agents for whole animal imaging. *Trends Biotechnol,* 22, 607-9.

JOHN, T. A., VOGEL, S. M., TIRUPPATHI, C., MALIK, A. B. & MINSHALL, R. D. 2003. Quantitative analysis of albumin uptake and transport in the rat microvessel endothelial monolayer. *Am J Physiol Lung Cell Mol Physiol,* 284, L187-96.

JOHNSON, T., KHAN, I. A., AVERY, M. A., GRANT, J. & MESHNICK, S. R. 1998. Quantitative structure-activity relationship studies of a series of sulfa drugs as

inhibitors of Pneumocystis carinii dihydropteroate synthetase. *Antimicrobial agents and chemotherapy,* 42, 1454-8.

JOSEPH, J. E., HARRISON, P., MACKIE, I. J. & MACHIN, S. J. 1998. Platelet activation markers and the primary antiphospholipid syndrome (PAPS). *Lupus,* 7 Suppl 2, S48-51.

KAISER, D., FREYBERG, M. A. & FRIEDL, P. 1997. Lack of hemodynamic forces triggers apoptosis in vascular endothelial cells. *Biochem Biophys Res Commun,* 231, 586-90.

KAKISIS, J. D., LIAPIS, C. D. & SUMPIO, B. E. 2004. Effects of cyclic strain on vascular cells. *Endothelium,* 11, 17-28.

KAMIYA, A., BUKHARI, R. & TOGAWA, T. 1984. Adaptive regulation of wall shear stress optimizing vascular tree function. *Bull Math Biol,* 46, 127-37.

KAMIYA, A. & TOGAWA, T. 1980. Adaptive regulation of wall shear stress to flow change in the canine carotid artery. *Am J Physiol,* 239, H14-21.

KAMPS, J. A. & SCHERPHOF, G. L. 1998. Receptor versus non-receptor mediated clearance of liposomes. *Adv Drug Deliv Rev,* 32, 81-97.

KANASEKI, T. & KADOTA, K. 1969. The "vesicle in a basket". A morphological study of the coated vesicle isolated from the nerve endings of the guinea pig brain, with special reference to the mechanism of membrane movements. *J cell biol,* 42, 202-20.

KANWAR, Y. S. & FARQUHAR, M. G. 1979. Presence of heparan sulfate in the glomerular basement membrane. *Proc Natl Acad Sci U S A,* 76, 1303-7.

KARMALI, P. P. & SIMBERG, D. 2011. Interactions of nanoparticles with plasma proteins: implication on clearance and toxicity of drug delivery systems. *Expert Opin Drug Deliv,* 8, 343-357.

KASAS, S., GOTZOS, V. & CELIO, M. R. 1993. Observation of living cells using the atomic force microscope. *Biophys J,* 64, 539-44.

KASCHE, V., DE BOER, M., LAZO, C. & GAD, M. 2003. Direct observation of intraparticle equilibration and the rate-limiting step in adsorption of proteins in chromatographic adsorbents with confocal laser scanning microscopy. *J Chromatogr B Analyt Technol Biomed Life Sci,* 790, 115-29.

KATTAN, J., DROZ, J. P., COUVREUR, P., MARINO, J. P., BOUTAN-LAROZE, A., ROUGIER, P., BRAULT, P., VRANCKX, H., GROGNET, J. M., MORGE, X. & ET AL. 1992. Phase I clinical trial and pharmacokinetic evaluation of doxorubicin carried by polyisohexylcyanoacrylate nanoparticles. *Invest New Drugs,* 10, 191-9.

KAUF, A. C., HOUGH, S. M. & BOWDITCH, R. D. 2001. Recognition of fibronectin by the platelet integrin alpha IIb beta 3 involves an extended interface with multiple electrostatic interactions. *Biochemistry,* 40, 9159-66.

KAWAI, Y., MATSUMOTO, Y., IKEDA, Y. & WATANABE, K. 1997. [Regulation of antithrombogenicity in endothelium by hemodynamic forces]. *Rinsho Byori,* 45, 315-20.

KIM, A. S. & JOHNSTON, S. C. 2011. Global Variation in the Relative Burden of Stroke and Ischemic Heart Disease / Clinical Perspective. *Circulation,* 124, 314-323.

KIM, D. K., ZHANG, Y., KEHR, J., KLASON, T., BJELKE, B. & MUHAMMED, M. 2001. Characterization and MRI study of surfactant-coated superparamagnetic nanoparticles administered into the rat brain. *J. Magn. Magn. Mater.,* 225, 256-261.

KIM, H. R., ANDRIEUX, K., DELOMENIE, C., CHACUN, H., APPEL, M., DESMAELE, D., TARAN, F., GEORGIN, D., COUVREUR, P. & TAVERNA, M. 2007. Analysis of plasma protein adsorption onto PEGylated nanoparticles by complementary methods: 2-DE, CE and Protein Lab-on-chip system. *Electrophoresis,* 28, 2252-61.

KIM, J., KIM, H. S., LEE, N., KIM, T., KIM, H., YU, T., SONG, I. C., MOON, W. K. & HYEON, T. 2008. Multifunctional uniform nanoparticles composed of a magnetite nanocrystal core and a mesoporous silica shell for magnetic resonance and fluorescence imaging and for drug delivery. *Angew Chem Int Ed Engl,* 47, 8438-41.

KIM, S., LIM, Y. T., SOLTESZ, E. G., DE GRAND, A. M., LEE, J., NAKAYAMA, A., PARKER, J. A., MIHALJEVIC, T., LAURENCE, R. G., DOR, D. M., COHN, L. H., BAWENDI, M. G. & FRANGIONI, J. V. 2004. Near-infrared fluorescent type II quantum dots for sentinel lymph node mapping. *Nat Biotechnol,* 22, 93-7.

KIM, S. W., ZIMMER, J. P., OHNISHI, S., TRACY, J. B., FRANGIONI, J. V. & BAWENDI, M. G. 2005. Engineering InAs(x)P(1-x)/InP/ZnSe III-V alloyed core/shell quantum dots for the near-infrared. *J Am Chem Soc,* 127, 10526-32.

KIRKHAM, M. & PARTON, R. G. 2005. Clathrin-independent endocytosis: New insights into caveolae and non-caveolar lipid raft carriers. *Biochimica et Biophysica Acta (BBA) - Mol Cell Res,* 1745, 273-286.

KLEIN, J. 2007. Probing the interactions of proteins and nanoparticles. *PNAS,* 104, 2029-2030.

KLOSTRANEC, J. & CHAN, C. W. 2006. Quantum Dots in Biological and Biomedical Research: Recent progress and Present Challenges. *Adv Mat,* 18, 1953.

KNEUER, C., SAMETI, M., BAKOWSKY, U., SCHIESTEL, T., SCHIRRA, H., SCHMIDT, H. & LEHR, C. M. 2000a. A nonviral DNA delivery system based on surface modified silica-nanoparticles can efficiently transfect cells in vitro. *Bioconjug Chem,* 11, 926-32.

KNEUER, C., SAMETI, M., HALTNER, E. G., SCHIESTEL, T., SCHIRRA, H., SCHMIDT, H. & LEHR, C. M. 2000b. Silica nanoparticles modified with aminosilanes as carriers for plasmid DNA. *Int J Pharm,* 196, 257-61.

KNIGHT, V. B. & SERRANO, E. E. 2006. Tissue and species differences in the application of quantum dots as probes for biomolecular targets in the inner ear and kidney. *IEEE Trans Nanobioscience,* 5, 251-62.

KOBAYASHI, H., KAWAMOTO, S., BRECHBIEL, M. W., BERNARDO, M., SATO, N., WALDMANN, T. A., TAGAYA, Y. & CHOYKE, P. L. 2005. Detection of lymph node involvement in hematologic malignancies using micromagnetic resonance lymphangiography with a gadolinum-labeled dendrimer nanoparticle. *Neoplasia,* 7, 984-91.

KOHLER, N., SUN, C., WANG, J. & ZHANG, M. 2005. Methotrexate-modified superparamagnetic nanoparticles and their intracellular uptake into human cancer cells. *Langmuir,* 21, 8858-64.

KOLEY, D. & BARD, A. J. 2010. Triton X-100 concentration effects on membrane permeability of a single HeLa cell by scanning electrochemical microscopy (SECM). *PNAS,* 107, 16783-16787.

KOOLE, R., VAN SCHOONEVELD, M. M., HILHORST, J., CASTERMANS, K., CORMODE, D. P., STRIJKERS, G. J., DE MELLO DONEGA, C., VANMAEKELBERGH, D., GRIFFIOEN, A. W., NICOLAY, K., FAYAD, Z. A.,

MEIJERINK, A. & MULDER, W. J. 2008. Paramagnetic lipid-coated silica nanoparticles with a fluorescent quantum dot core: a new contrast agent platform for multimodality imaging. *Bioconjug Chem,* 19, 2471-9.

KORNET, L., HOEKS, A. P., LAMBREGTS, J. & RENEMAN, R. S. 1999. In the femoral artery bifurcation, differences in mean wall shear stress within subjects are associated with different intima-media thicknesses. *Arterioscler Thromb Vasc Biol,* 19, 2933-9.

KOZIARA, J., OH, J., AKERS, W., FERRARIS, S. & MUMPER, R. 2005a. Blood Compatibility of Cetyl Alcohol/Polysorbate-Based Nanoparticles. *Pharm Res,* 22, 1821-1828.

KOZIARA, J. M., OH, J. J., AKERS, W. S., FERRARIS, S. P. & MUMPER, R. J. 2005b. Blood compatibility of cetyl alcohol/polysorbate-based nanoparticles. *Pharm Res,* 22, 1821-8.

KRAISS, L. W., RAINES, E. W., WILCOX, J. N., SEIFERT, R. A., BARRETT, T. B., KIRKMAN, T. R., HART, C. E., BOWEN-POPE, D. F., ROSS, R. & CLOWES, A. W. 1993. Regional expression of the platelet-derived growth factor and its receptors in a primate graft model of vessel wall assembly. *J Clin Invest,* 92, 338-48.

KRALJ, M. & PAVELIC, K. 2003. Medicine on a small scale. *EMBO Rep,* 4, 1008-12.

KREUTER, J. 2001. Nanoparticulate systems for brain delivery of drugs. *Adv Drug Deliv Rev,* 47, 65-81.

KREUTER, J., ALYAUTDIN, R. N., KHARKEVICH, D. A. & IVANOV, A. A. 1995. Passage of peptides through the blood-brain barrier with colloidal polymer particles (nanoparticles). *Brain Res,* 674, 171-4.

KREUTER, J., HEKMATARA, T., DREIS, S., VOGEL, T., GELPERINA, S. & LANGER, K. 2007. Covalent attachment of apolipoprotein A-I and apolipoprotein B-100 to albumin nanoparticles enables drug transport into the brain. *J Control Release,* 118, 54-8.

KREUTER, J., SHAMENKOV, D., PETROV, V., RAMGE, P., CYCHUTEK, K., KOCH-BRANDT, C. & ALYAUTDIN, R. 2002. Apolipoprotein-mediated transport of nanoparticle-bound drugs across the blood-brain barrier. *J Drug Target,* 10, 317-25.

KREYLING, W. G., SEMMLER, M., ERBE, F., MAYER, P., TAKENAKA, S., SCHULZ, H., OBERDORSTER, G. & ZIESENIS, A. 2002. Translocation of ultrafine insoluble iridium particles from lung epithelium to extrapulmonary organs is size dependent but very low. *J Toxicol Environ Health A,* 65, 1513-30.

KROLL, M. H., HELLUMS, J. D., MCINTIRE, L. V., SCHAFER, A. I. & MOAKE, J. L. 1996. Platelets and shear stress. *Blood,* 88, 1525-41.

KU, D. N., GIDDENS, D. P., ZARINS, C. K. & GLAGOV, S. 1985. Pulsatile flow and atherosclerosis in the human carotid bifurcation. Positive correlation between plaque location and low oscillating shear stress. *Arteriosclerosis,* 5, 293-302.

KUCHAN, M. J. & FRANGOS, J. A. 1994. Role of calcium and calmodulin in flow-induced nitric oxide production in endothelial cells. *Am J Physiol,* 266, C628-36.

KULDO, J. M., OGAWARA, K. I., WERNER, N., ASGEIRSDOTTIR, S. A., KAMPS, J. A., KOK, R. J. & MOLEMA, G. 2005. Molecular pathways of endothelial cell activation for (targeted) pharmacological intervention of chronic inflammatory diseases. *Curr Vasc Pharmacol,* 3, 11-39.

KUMAGAI, M., KANO, M. R., MORISHITA, Y., OTA, M., IMAI, Y., NISHIYAMA, N., SEKINO, M., UENO, S., MIYAZONO, K. & KATAOKA, K. 2009. Enhanced

magnetic resonance imaging of experimental pancreatic tumor in vivo by block copolymer-coated magnetite nanoparticles with TGF-beta inhibitor. *J Control Release,* 140, 306-11.

KUROKI, Y., HONMA, T., CHIBA, H., SANO, H., SAITOH, M., OGASAWARA, Y., SOHMA, H. & AKINO, T. 1997. A novel type of binding specificity to phospholipids for rat mannose-binding proteins isolated from serum and liver. *FEBS Lett,* 414, 387-92.

L'AZOU, B., JORLY, J., ON, D., SELLIER, E., MOISAN, F., FLEURY-FEITH, J., CAMBAR, J., BROCHARD, P. & OHAYON-COURTES, C. 2008. In vitro effects of nanoparticles on renal cells. *Part Fibre Toxicol,* 5, 22.

LABARRE, D., VAUTHIER, C., CHAUVIERRE, C., PETRI, B., MULLER, R. & CHEHIMI, M. M. 2005. Interactions of blood proteins with poly(isobutylcyanoacrylate) nanoparticles decorated with a polysaccharidic brush. *Biomaterials,* 26, 5075-84.

LACERDA, S. H., PARK, J. J., MEUSE, C., PRISTINSKI, D., BECKER, M. L., KARIM, A. & DOUGLAS, J. F. 2010. Interaction of gold nanoparticles with common human blood proteins. *ACS Nano,* 4, 365-79.

LAHDENKARI, A. T., LOUNATMAA, K., PATRAKKA, J., HOLMBERG, C., WARTIOVAARA, J., KESTILA, M., KOSKIMIES, O. & JALANKO, H. 2004. Podocytes are firmly attached to glomerular basement membrane in kidneys with heavy proteinuria. *J Am Soc Nephrol,* 15, 2611-8.

LAL, R., KIM, H., GARAVITO, R. M. & ARNSDORF, M. F. 1993. Imaging of reconstituted biological channels at molecular resolution by atomic force microscopy. *Am J Physiol,* 265, C851-6.

LAL, R. & YU, L. 1993. Atomic force microscopy of cloned nicotinic acetylcholine receptor expressed in Xenopus oocytes. *Proc Natl Acad Sci U S A,* 90, 7280-4.

LAMMERS, T., HENNINK, W. E. & STORM, G. 2008. Tumour-targeted nanomedicines: principles and practice. *Br J Cancer,* 99, 392-397.

LANGILLE, B. L. & ADAMSON, S. L. 1981. Relationship between blood flow direction and endothelial cell orientation at arterial branch sites in rabbits and mice. *Circ Res,* 48, 481-8.

LANGILLE, B. L., GRAHAM, J. J., KIM, D. & GOTLIEB, A. I. 1991. Dynamics of shear-induced redistribution of F-actin in endothelial cells in vivo. *Arterioscler Thromb,* 11, 1814-20.

LARSEN, E., CELI, A., GILBERT, G. E., FURIE, B. C., ERBAN, J. K., BONFANTI, R., WAGNER, D. D. & FURIE, B. 1989. PADGEM protein: a receptor that mediates the interaction of activated platelets with neutrophils and monocytes. *Cell,* 59, 305-12.

LE RENARD, P. E., BUCHEGGER, F., PETRI-FINK, A., BOSMAN, F., RUFENACHT, D., HOFMANN, H., DOELKER, E. & JORDAN, O. 2009. Local moderate magnetically induced hyperthermia using an implant formed in situ in a mouse tumor model. *Int J Hyperthermia,* 25, 229-39.

LEE, J. E., LEE, N., KIM, H., KIM, J., CHOI, S. H., KIM, J. H., KIM, T., SONG, I. C., PARK, S. P., MOON, W. K. & HYEON, T. 2010. Uniform mesoporous dye-doped silica nanoparticles decorated with multiple magnetite nanocrystals for simultaneous enhanced magnetic resonance imaging, fluorescence imaging, and drug delivery. *J Am Chem Soc,* 132, 552-7.

LEE, J. S., PANORCHAN, P., HALE, C. M., KHATAU, S. B., KOLE, T. P., TSENG, Y. & WIRTZ, D. 2006. Ballistic intracellular nanorheology reveals ROCK-hard cytoplasmic stiffening response to fluid flow. *J Cell Sci,* 119, 1760-8.

LEMARCHAND, C., GREF, R., PASSIRANI, C., GARCION, E., PETRI, B., MULLER, R., COSTANTINI, D. & COUVREUR, P. 2006. Influence of polysaccharide coating on the interactions of nanoparticles with biological systems. *Biomaterials,* 27, 108-18.

LEROUX, J. C., DE JAEGHERE, F., ANNER, B., DOELKER, E. & GURNY, R. 1995. An investigation on the role of plasma and serum opsonins on the internalization of biodegradable poly(D,L-lactic acid) nanoparticles by human monocytes. *Life Sci,* 57, 695-703.

LEVESQUE, M. J. & NEREM, R. M. 1985. The elongation and orientation of cultured endothelial cells in response to shear stress. *J Biomech Eng,* 107, 341-7.

LEVY, L., SAHOO, Y., KIM, K. S., BERGEY, E. J. & PRASAD, P. N. 2002. Nanochemistry: synthesis and characterization of multifunctional nanoclinics for biological applications. *Chem. Mater.,* 14, 3715-3721.

LI, X., RADOMSKI, A., CORRIGAN, O. I., TAJBER, L., DE SOUSA MENEZES, F., ENDTER, S., MEDINA, C. & RADOMSKI, M. W. 2009. Platelet compatibility of PLGA, chitosan and PLGA-chitosan nanoparticles. *Nanomedicine (Lond),* 4, 735-46.

LI, Z. Z., WEN, L. X., SHAO, L. & CHEN, J. F. 2004. Fabrication of porous hollow silica nanoparticles and their applications in drug release control. *J Control Release,* 98, 245-54.

LIKHAREV, K. K. 1999. Single-electron devices and their applications. *P IEEE,* 87, 606-632.

LIN, A., SABNIS, A., KONA, S., NATTAMA, S., PATEL, H., DONG, J. F. & NGUYEN, K. T. 2010. Shear-regulated uptake of nanoparticles by endothelial cells and development of endothelial-targeting nanoparticles. *J Biomed Mater Res A,* 93, 833-42.

LINDMAN, S., LYNCH, I., THULIN, E., NILSSON, H., DAWSON, K. A. & LINSE, S. 2007. Systematic investigation of the thermodynamics of HSA adsorption to N-iso-propylacrylamide/N-tert-butylacrylamide copolymer nanoparticles. Effects of particle size and hydrophobicity. *Nano Lett,* 7, 914-20.

LIPOWSKY, H. H., KOVALCHECK, S. & ZWEIFACH, B. W. 1978. The distribution of blood rheological parameters in the microvasculature of cat mesentery. *Circ Res,* 43, 738-49.

LITTLER, A. J., BUCKLEY, C. D., WORDSWORTH, P., COLLINS, I., MARTINSON, J. & SIMMONS, D. L. 1997. A distinct profile of six soluble adhesion molecules (ICAM-1, ICAM-3, VCAM-1, E-selectin, L-selectin and P-selectin) in rheumatoid arthritis. *Rheumatology,* 36, 164-169.

LIU, X. & SUN, J. 2010. Endothelial cells dysfunction induced by silica nanoparticles through oxidative stress via JNK/P53 and NF-kappaB pathways. *Biomaterials,* 31, 8198-209.

LOPES-MARTINS, R., CATELLI, M., ARAUJO, C., ESTATO, V., CORDEIRO, R. & TIBIRICA, E. 1996. Pharmacological evidence of a role for platelet activating factor as a modulator of vasomotor tone and blood pressure. *Eur J Pharmacol,* 308, 287-94.

LOVRIC, J., BAZZI, H. S., CUIE, Y., FORTIN, G. R., WINNIK, F. M. & MAYSINGER, D. 2005. Differences in subcellular distribution and toxicity of green and red emitting CdTe quantum dots. *J Mol Med,* 83, 377-85.

LU, H., YI, G., ZHAO, S., CHEN, D., GUO, L.-H. & CHENG, J. 2004. Synthesis and characterization of multi-functional nanoparticles possessing magnetic, up-conversion fluorescence and bio-affinity properties. *J. Mater. Chem.,* 14, 1336-1341.

LU, J., LIONG, M., ZINK, J. I. & TAMANOI, F. 2007. Mesoporous silica nanoparticles as a delivery system for hydrophobic anticancer drugs. *Small,* 3, 1341-6.

LUCK, M., PAULKE, B. R., SCHRODER, W., BLUNK, T. & MULLER, R. H. 1998. Analysis of plasma protein adsorption on polymeric nanoparticles with different surface characteristics. *J Biomed Mater Res,* 39, 478-85.

LUFT, F. C., ARONOFF, G. R., EVAN, A. P., CONNORS, B. A., BLASE, D. K. & GATTONE, V. H. 1982. Effects of moxalactam and cefotaxime on rabbit renal tissue. *Antimicrob Agents Chemother,* 21, 830-5.

LUNDQVIST, M., SETHSON, I. & JONSSON, B. H. 2004. Protein adsorption onto silica nanoparticles: conformational changes depend on the particles' curvature and the protein stability. *Langmuir,* 20, 10639-47.

LUNDQVIST, M., STIGLER, J., ELIA, G., LYNCH, I., CEDERVALL, T. & DAWSON, K. A. 2008. Nanoparticle size and surface properties determine the protein corona with possible implications for biological impacts. *Proc Natl Acad Sci U S A,* 105, 14265-70.

LUNGU, A. O., JIN, Z. G., YAMAWAKI, H., TANIMOTO, T., WONG, C. & BERK, B. C. 2004. Cyclosporin A inhibits flow-mediated activation of endothelial nitric-oxide synthase by altering cholesterol content in caveolae. *J Biol Chem,* 279, 48794-800.

LUSCHER, T. F. & BARTON, M. 1997. Biology of the endothelium. *Clin Cardiol,* 20, II-3-10.

LYNCH, I., CEDERVALL, T., LUNDQVIST, M., CABALEIRO-LAGO, C., LINSE, S. & DAWSON, K. A. 2007. The nanoparticle-protein complex as a biological entity; a complex fluids and surface science challenge for the 21st century. *Adv Colloid Interface Sci,* 134-135, 167-74.

LYNCH, I., DAWSON, K. A. & LINSE, S. 2006a. Detecting Cryptic Epitopes Created by Nanoparticles. *Sci. STKE,* 2006, pe14-.

LYNCH, I., DAWSON, K. A. & LINSE, S. 2006b. Detecting cryptic epitopes created by nanoparticles. *Sci STKE,* 2006, pe14.

MAILANDER, V., LORENZ, M. R., HOLZAPFEL, V., MUSYANOVYCH, A., FUCHS, K., WIESNETH, M., WALTHER, P., LANDFESTER, K. & SCHREZENMEIER, H. 2008. Carboxylated superparamagnetic iron oxide particles label cells intracellularly without transfection agents. *Mol Imaging Biol,* 10, 138-46.

MALEK, A. M. & IZUMO, S. 1996. Mechanism of endothelial cell shape change and cytoskeletal remodeling in response to fluid shear stress. *J Cell Sci,* 109 (Pt 4), 713-26.

MALEK, A. M., JACKMAN, R., ROSENBERG, R. D. & IZUMO, S. 1994. Endothelial expression of thrombomodulin is reversibly regulated by fluid shear stress. *Circ Res,* 74, 852-60.

MANABE, N., HOSHINO, A., LIANG, Y. Q., GOTO, T., KATO, N. & YAMAMOTO, K. 2006. Quantum dot as a drug tracer in vivo. *IEEE Trans Nanobioscience,* 5, 263-7.

MANOLOVA, V., FLACE, A., BAUER, M., SCHWARZ, K., SAUDAN, P. & BACHMANN, M. F. 2008. Nanoparticles target distinct dendritic cell populations according to their size. *Eur J Immunol,* 38, 1404-13.

MARSH, M. & HELENIUS, A. 2006. Virus entry: open sesame. *Cell,* 124, 729-40.

MARTIN, C. R. & KOHLI, P. 2003. The emerging field of nanotube biotechnology. *Nat Rev Drug Discov,* 2, 29-37.

MARTINEZ, A., SALAS, E., RADOMSKI, A. & RADOMSKI, M. W. 2001. Matrix metalloproteinase-2 in platelet adhesion to fibrinogen: interactions with nitric oxide. *Med Sci Monit,* 7, 646-51.

MASUDA, H., SHOZAWA, T., HOSODA, S., KANDA, M. & KAMIYA, A. 1985. Cytoplasmic microfilaments in endothelial cells of flow loaded canine carotid arteries. *Heart Vessels,* 1, 65-9.

MAXFIELD, F. R. & MCGRAW, T. E. 2004. Endocytic recycling. *Nat Rev Mol Cell Biol,* 5, 121-32.

MAYOR, S. & PAGANO, R. E. 2007. Pathways of clathrin-independent endocytosis. *Nat Rev Mol Cell Biol,* 8, 603-12.

MAYSINGER, D., LOVRIC, J., EISENBERG, A. & SAVIC, R. 2007. Fate of micelles and quantum dots in cells. *Eur J Pharm Biopharm,* 65, 270-81.

MCCRARY, J. K., NOLASCO, L. H., HELLUMS, J. D., KROLL, M. H., TURNER, N. A. & MOAKE, J. L. 1995. Direct demonstration of radiolabeled von Willebrand factor binding to platelet glycoprotein Ib and IIb-IIIa in the presence of shear stress. *Ann Biomed Eng,* 23, 787-93.

MCGUIGAN, A. P. & SEFTON, M. V. 2007a. The influence of biomaterials on endothelial cell thrombogenicity. *Biomaterials,* 28, 2547-2571.

MCGUIGAN, A. P. & SEFTON, M. V. 2007b. The influence of biomaterials on endothelial cell thrombogenicity. *Biomaterials,* 28, 2547-71.

MCGUINNES, C., DUFFIN, R., BROWN, S., N, L. M., MEGSON, I. L., MACNEE, W., JOHNSTON, S., LU, S. L., TRAN, L., LI, R., WANG, X., NEWBY, D. E. & DONALDSON, K. 2011. Surface derivatization state of polystyrene latex nanoparticles determines both their potency and their mechanism of causing human platelet aggregation in vitro. *Toxicol Sci,* 119, 359-68.

MCINTYRE, T. M., ZIMMERMAN, G. A., SATOH, K. & PRESCOTT, S. M. 1985. Cultured endothelial cells synthesize both platelet-activating factor and prostacyclin in response to histamine, bradykinin, and adenosine triphosphate. *J Clin Invest,* 76, 271-80.

MEDINA, C., JURASZ, P., SANTOS-MARTINEZ, M. J., JEONG, S. S., MITSKY, T., CHEN, R. & RADOMSKI, M. W. 2006. Platelet Aggregation-Induced by Caco-2 Cells: Regulation by Matrix Metalloproteinase-2 and Adenosine Diphosphate. *J Pharmacol Exp Ther,* 317, 739-745.

MEDINTZ, I. L., CLAPP, A. R., MATTOUSSI, H., GOLDMAN, E. R., FISHER, B. & MAURO, J. M. 2003. Self-assembled nanoscale biosensors based on quantum dot FRET donors. *Nat Mater,* 2, 630-8.

MERTEN, M. & THIAGARAJAN, P. 2000. P-Selectin Expression on Platelets Determines Size and Stability of Platelet Aggregates. *Circulation,* 102, 1931-1936.

MICHAELIS, K., HOFFMANN, M. M., DREIS, S., HERBERT, E., ALYAUTDIN, R. N., MICHAELIS, M., KREUTER, J. & LANGER, K. 2006. Covalent linkage of

apolipoprotein e to albumin nanoparticles strongly enhances drug transport into the brain. *J Pharmacol Exp Ther,* 317, 1246-53.

MIKHAYLOVA, M., KIM, D. K., BERRY, C. C., ZAGORODNI, A., TOPRAK, M., CURTIS, A. S. G. & MUHAMMED, M. 2004. BSA immobilization on amine-functionalized superparamagnetic iron oxide nanoparticles. *Chem. Mater.,* 16, 2344-2354.

MIYAMOTO, M., SASAKAWA, S., OZAWA, T., KAWAGUCHI, H. & OHTSUKA, Y. 1989. Platelet aggregation induced by latex particles. I. Effects of size, surface potential and hydrophobicity of particles. *Biomaterials,* 10, 251-7.

MIYAMOTO, M., SASAKAWA, S., OZAWA, T., KAWAGUCHI, H. & OHTSUKA, Y. 1990. Mechanisms of blood coagulation induced by latex particles and the roles of blood cells. *Biomaterials,* 11, 385-8.

MOAKE, J. L., TURNER, N. A., STATHOPOULOS, N. A., NOLASCO, L. & HELLUMS, J. D. 1988. Shear-induced platelet aggregation can be mediated by vWF released from platelets, as well as by exogenous large or unusually large vWF multimers, requires adenosine diphosphate, and is resistant to aspirin. *Blood,* 71, 1366-74.

MOGHIMI, S. M., HUNTER, A. C. & MURRAY, J. C. 2001. Long-circulating and target-specific nanoparticles: theory to practice. *Pharmacol Rev,* 53, 283-318.

MOGHIMI, S. M., HUNTER, A. C. & MURRAY, J. C. 2005. Nanomedicine: current status and future prospects. *FASEB J,* 19, 311-30.

MOGHIMI, S. M., MUIR, I. S., ILLUM, L., DAVIS, S. S. & KOLB-BACHOFEN, V. 1993. Coating particles with a block co-polymer (poloxamine-908) suppresses opsonization but permits the activity of dysopsonins in the serum. *Biochim Biophys Acta,* 1179, 157-65.

MOHAMED, B. M., FELGHERY, C. & WILLIAMS, C. 2008. The use of Cellomics to study enterocyte cytoskeletal proteins in coeliac disease patients. *Cent Eur J Biol,* 3, 258-267.

MOHAMED, B. M., VERMA, N. K., PRINA-MELLO, A., WILLIAMS, Y., DAVIES, A. M., BAKOS, G., TORMEY, L., EDWARDS, C., HANRAHAN, J., SALVATI, A., LYNCH, I., DAWSON, K., KELLEHER, D. & VOLKOV, Y. 2011. Activation of stress-related signalling pathway in human cells upon SiO2 nanoparticles exposure as an early indicator of cytotoxicity. *J Nanobiotechnology,* 9, 29.

MONOPOLI, M. P., WALCZYK, D., CAMPBELL, A., ELIA, G., LYNCH, I., BOMBELLI, F. B. & DAWSON, K. A. 2011. Physical-chemical aspects of protein corona: relevance to in vitro and in vivo biological impacts of nanoparticles. *J Am Chem Soc,* 133, 2525-34.

MOROZ, P., JONES, S. K. & GRAY, B. N. 2002. Magnetically mediated hyperthermia: current status and future directions. *Int J Hyperthermia,* 18, 267-84.

MOVAT, H. Z., WEISER, W. J., GLYNN, M. F. & MUSTARD, J. F. 1965. Platelet phagocytosis and aggregation. *J Cell Biol,* 27, 531-43.

MOZAFARI, M. R. 2006. Nanocarrier Technologies: Frontiers of Nanotherapy. *Springer,* Chapters 1 and 2: 10-11, 25-34.

MUKHERJEE, S., GHOSH, R. N. & MAXFIELD, F. R. 1997. Endocytosis. *Physiol Rev,* 77, 759-803.

MULLER, R. H., RUHL, D., LUCK, M. & PAULKE, B. R. 1997. Influence of fluorescent labelling of polystyrene particles on phagocytic uptake, surface hydrophobicity, and plasma protein adsorption. *Pharm Res,* 14, 18-24.

MURRAY, C. D. 1926. The Physiological Principle of Minimum Work: II. Oxygen Exchange in Capillaries. *PNAS,* 12, 299-304.

MUTHUSAMY, B., HANUMANTHU, G., SURESH, S., REKHA, B., SRINIVAS, D., KARTHICK, L., VRUSHABENDRA, B. M., SHARMA, S., MISHRA, G., CHATTERJEE, P., MANGALA, K. S., SHIVASHANKAR, H. N., CHANDRIKA, K. N., DESHPANDE, N., SURESH, M., KANNABIRAN, N., NIRANJAN, V., NALLI, A., PRASAD, T. S., ARUN, K. S., REDDY, R., CHANDRAN, S., JADHAV, T., JULIE, D., MAHESH, M., JOHN, S. L., PALVANKAR, K., SUDHIR, D., BALA, P., RASHMI, N. S., VISHNUPRIYA, G., DHAR, K., RESHMA, S., CHAERKADY, R., GANDHI, T. K., HARSHA, H. C., MOHAN, S. S., DESHPANDE, K. S., SARKER, M. & PANDEY, A. 2005. Plasma Proteome Database as a resource for proteomics research. *Proteomics,* 5, 3531-6.

NABIEV, I., MITCHELL, S., DAVIES, A., WILLIAMS, Y., KELLEHER, D., MOORE, R., GUN'KO, Y. K., BYRNE, S., RAKOVICH, Y. P., DONEGAN, J. F., SUKHANOVA, A., CONROY, J., COTTELL, D., GAPONIK, N., ROGACH, A. & VOLKOV, Y. 2007. Nonfunctionalized nanocrystals can exploit a cell's active transport machinery delivering them to specific nuclear and cytoplasmic compartments. *Nano Lett,* 7, 3452-61.

NAGAYAMA, S., OGAWARA, K., FUKUOKA, Y., HIGAKI, K. & KIMURA, T. 2007. Time-dependent changes in opsonin amount associated on nanoparticles alter their hepatic uptake characteristics. *Int J Pharm,* 342, 215-21.

NAKAMURA, M., SHONO, M. & ISHIMURA, K. 2007. Synthesis, characterization, and biological applications of multifluorescent silica nanoparticles. *Anal Chem,* 79, 6507-14.

NANBO, A., IMAI, M., WATANABE, S., NODA, T., TAKAHASHI, K., NEUMANN, G., HALFMANN, P. & KAWAOKA, Y. 2010. Ebolavirus Is Internalized into Host Cells <italic>via</italic> Macropinocytosis in a Viral Glycoprotein-Dependent Manner. *PLoS Pathog,* 6, e1001121.

NAPIERSKA, D., THOMASSEN, L. C., RABOLLI, V., LISON, D., GONZALEZ, L., KIRSCH-VOLDERS, M., MARTENS, J. A. & HOET, P. H. 2009. Size-dependent cytotoxicity of monodisperse silica nanoparticles in human endothelial cells. *Small,* 5, 846-53.

NEEDLEMAN, P., MONCADA, S., BUNTING, S., VANE, J. R., HAMBERG, M. & SAMUELSSON, B. 1976. Identification of an enzyme in platelet microsomes which generates thromboxane A2 from prostaglandin endoperoxides. *Nature,* 261, 558-60.

NEGRI, V., CERPA, A., LOPEZ-LARRUBIA, P., NIETO-CHARQUES, L., CERDAN, S. & BALLESTEROS, P. 2010. Nanotubular Paramagnetic Probes as Contrast Agents for Magnetic Resonance Imaging Based on the Diffusion Tensor. *Angew Chem Int Ed Engl.*

NEL, A., XIA, T., MADLER, L. & LI, N. 2006. Toxic potential of materials at the nanolevel. *Science,* 311, 622-7.

NEL, A. E., MADLER, L., VELEGOL, D., XIA, T., HOEK, E. M. V., SOMASUNDARAN, P., KLAESSIG, F., CASTRANOVA, V. & THOMPSON, M.

2009. Understanding biophysicochemical interactions at the nano-bio interface. *Nat Mater,* 8, 543-557.

NEMMAR, A., HOET, P. H., DINSDALE, D., VERMYLEN, J., HOYLAERTS, M. F. & NEMERY, B. 2003a. Diesel exhaust particles in lung acutely enhance experimental peripheral thrombosis. *Circulation,* 107, 1202-8.

NEMMAR, A., HOET, P. H., VANQUICKENBORNE, B., DINSDALE, D., THOMEER, M., HOYLAERTS, M. F., VANBILLOEN, H., MORTELMANS, L. & NEMERY, B. 2002a. Passage of inhaled particles into the blood circulation in humans. *Circulation,* 105, 411-4.

NEMMAR, A., HOET, P. H., VERMYLEN, J., NEMERY, B. & HOYLAERTS, M. F. 2004. Pharmacological stabilization of mast cells abrogates late thrombotic events induced by diesel exhaust particles in hamsters. *Circulation,* 110, 1670-7.

NEMMAR, A., HOYLAERTS, M. F., HOET, P. H., DINSDALE, D., SMITH, T., XU, H., VERMYLEN, J. & NEMERY, B. 2002b. Ultrafine particles affect experimental thrombosis in an in vivo hamster model. *Am J Respir Crit Care Med,* 166, 998-1004.

NEMMAR, A., HOYLAERTS, M. F., HOET, P. H., VERMYLEN, J. & NEMERY, B. 2003b. Size effect of intratracheally instilled particles on pulmonary inflammation and vascular thrombosis. *Toxicol Appl Pharmacol,* 186, 38-45.

NEMMAR, A., NEMERY, B., HOET, P. H., VAN ROOIJEN, N. & HOYLAERTS, M. F. 2005. Silica particles enhance peripheral thrombosis: key role of lung macrophage-neutrophil cross-talk. *Am J Respir Crit Care Med,* 171, 872-9.

NEMMAR, A., NEMERY, B., HOET, P. H., VERMYLEN, J. & HOYLAERTS, M. F. 2003c. Pulmonary inflammation and thrombogenicity caused by diesel particles in hamsters: role of histamine. *Am J Respir Crit Care Med,* 168, 1366-72.

NEREM, R. M., ALEXANDER, R. W., CHAPPEL, D. C., MEDFORD, R. M., VARNER, S. E. & TAYLOR, W. R. 1998. The Study of the Influence of Flow on Vascular Endothelial Biology. *Am J Med Sci,* 316, 169-175.

NICHOLS, B. 2003. Caveosomes and endocytosis of lipid rafts. *J Cell Sci,* 116, 4707-14.

NIEKERK, V. & FOURIE, M. H. 2004. Ultrafine particles: Aggrevating exposure factor?

NIESSEN, J., JEDLITSCHKY, G., GREINACHER, A. & KROEMER, H. K. 2010. Isolation of platelet granules. *Curr Protoc Cell Biol,* Chapter 3, Unit 3.35.

NISHIDA, K., HARRISON, D. G., NAVAS, J. P., FISHER, A. A., DOCKERY, S. P., UEMATSU, M., NEREM, R. M., ALEXANDER, R. W. & MURPHY, T. J. 1992. Molecular cloning and characterization of the constitutive bovine aortic endothelial cell nitric oxide synthase. *J Clin Invest,* 90, 2092-6.

OBERDORSTER, G., SHARP, Z., ATUDOREI, V., ELDER, A., GELEIN, R., LUNTS, A., KREYLING, W. & COX, C. 2002. Extrapulmonary translocation of ultrafine carbon particles following whole-body inhalation exposure of rats. *J Toxicol Environ Health A,* 65, 1531-43.

OGAWA, S., OTA, Z., SHIKATA, K., HIRONAKA, K., HAYASHI, Y., OTA, K., KUSHIRO, M., MIYATAKE, N., KISHIMOTO, N. & MAKINO, H. 1999. High-resolution ultrastructural comparison of renal glomerular and tubular basement membranes. *Am J Nephrol,* 19, 686-93.

OGAWARA, K., FURUMOTO, K., NAGAYAMA, S., MINATO, K., HIGAKI, K., KAI, T. & KIMURA, T. 2004. Pre-coating with serum albumin reduces receptor-

mediated hepatic disposition of polystyrene nanosphere: implications for rational design of nanoparticles. *J Control Release,* 100, 451-5.

OHNESORGE, F. & BINNIG, G. 1993. True atomic resolution by atomic force microscopy through repulsive and attractive forces. *Science,* 260, 1451-6.

OHNO, M., COOKE, J. P., DZAU, V. J. & GIBBONS, G. H. 1995. Fluid shear stress induces endothelial transforming growth factor beta-1 transcription and production. Modulation by potassium channel blockade. *J Clin Invest,* 95, 1363-9.

OKU, N., TOKUDOME, Y., NAMBA, Y., SAITO, N., ENDO, M., HASEGAWA, Y., KAWAI, M., TSUKADA, H. & OKADA, S. 1996. Effect of serum protein binding on real-time trafficking of liposomes with different charges analyzed by positron emission tomography. *Biochim Biophys Acta,* 1280, 149-54.

OKUDA, K., YAMAMIYA, K., KAWASE, T., MIZUNO, H., UEDA, M. & YOSHIE, H. 2009. Treatment of human infrabony periodontal defects by grafting human cultured periosteum sheets combined with platelet-rich plasma and porous hydroxyapatite granules: case series. *J Int Acad Periodontol,* 11, 206-13.

OLESEN, S. P., CLAPHAM, D. E. & DAVIES, P. F. 1988. Haemodynamic shear stress activates a K+ current in vascular endothelial cells. *Nature,* 331, 168-70.

OLIVIER, J. C. 2005. Drug transport to brain with targeted nanoparticles. *NeuroRx,* 2, 108-19.

OLSON, J. D., ZALESKI, A., HERRMANN, D. & FLOOD, P. A. 1989. Adhesion of platelets to purified solid-phase von Willebrand factor: effects of wall shear rate, ADP, thrombin, and ristocetin. *J Lab Clin Med,* 114, 6-18.

OMOLOLA ENIOLA, A. & HAMMER, D. A. 2005. In vitro characterization of leukocyte mimetic for targeting therapeutics to the endothelium using two receptors. *Biomaterials,* 26, 7136-44.

ORTEGA MATEO, A. & DE ARTINANO, A. A. 1997. Highlights on endothelins: a review. *Pharmacol Res,* 36, 339-51.

OSAKA, T., NAKANISHI, T., SHANMUGAM, S., TAKAHAMA, S. & ZHANG, H. 2009. Effect of surface charge of magnetite nanoparticles on their internalization into breast cancer and umbilical vein endothelial cells. *Colloids Surf B Biointerfaces,* 71, 325-30.

OW, H., LARSON, D. R., SRIVASTAVA, M., BAIRD, B. A., WEBB, W. W. & WIESNER, U. 2005. Bright and stable core-shell fluorescent silica nanoparticles. *Nano Lett,* 5, 113-7.

OWENS, D. E., 3RD & PEPPAS, N. A. 2006. Opsonization, biodistribution, and pharmacokinetics of polymeric nanoparticles. *Int J Pharm,* 307, 93-102.

PALMER, R. M., ASHTON, D. S. & MONCADA, S. 1988. Vascular endothelial cells synthesize nitric oxide from L-arginine. *Nature,* 333, 664-6.

PANAGI, Z., BELETSI, A., EVANGELATOS, G., LIVANIOU, E., ITHAKISSIOS, D. S. & AVGOUSTAKIS, K. 2001. Effect of dose on the biodistribution and pharmacokinetics of PLGA and PLGA-mPEG nanoparticles. *Int J Pharm,* 221, 143-52.

PANTE, N. & KANN, M. 2002. Nuclear pore complex is able to transport macromolecules with diameters of about 39 nm. *Mol Biol Cell,* 13, 425-34.

PARK, H., GO, Y. M., ST JOHN, P. L., MALAND, M. C., LISANTI, M. P., ABRAHAMSON, D. R. & JO, H. 1998. Plasma membrane cholesterol is a key

molecule in shear stress-dependent activation of extracellular signal-regulated kinase. *J Biol Chem,* 273, 32304-11.

PATEL, D., KELL, A., SIMARD, B., DENG, J., XIANG, B., LIN, H.-Y., GRUWEL, M. & TIAN, G. 2010. Cu2+-labeled, SPION loaded porous silica nanoparticles for cell labeling and multifunctional imaging probes. *Biomaterials,* 31, 2866-2873.

PATEL, H. M. & MOGHIMI, S. M. 1998. Serum-mediated recognition of liposomes by phagocytic cells of the reticuloendothelial system - The concept of tissue specificity. *Adv Drug Deliv Rev,* 32, 45-60.

PATHAK, S., CHOI, S. K., ARNHEIM, N. & THOMPSON, M. E. 2001. Hydroxylated quantum dots as luminescent probes for in situ hybridization. *J Am Chem Soc,* 123, 4103-4.

PEARSON, J. D. 1999. Endothelial cell function and thrombosis. *Baillieres Best Pract Res Clin Haematol,* 12, 329-41.

PEDERSEN, M. B., ZHOU, X., LARSEN, E. K., SORENSEN, U. S., KJEMS, J., NYGAARD, J. V., NYENGAARD, J. R., MEYER, R. L., BOESEN, T. & VORUP-JENSEN, T. 2010. Curvature of synthetic and natural surfaces is an important target feature in classical pathway complement activation. *J Immunol,* 184, 1931-45.

PERACCHIA, M. T., FATTAL, E., DESMAELE, D., BESNARD, M., NOEL, J. P., GOMIS, J. M., APPEL, M., D'ANGELO, J. & COUVREUR, P. 1999. Stealth PEGylated polycyanoacrylate nanoparticles for intravenous administration and splenic targeting. *J Control Release,* 60, 121-8.

PERLMAN, Z. E., SLACK, M. D., FENG, Y., MITCHISON, T. J., WU, L. F. & ALTSCHULER, S. J. 2004. Multidimensional drug profiling by automated microscopy. *Science,* 306, 1194-8.

PERRIN-COCON, L. A., MARCHE, P. N. & VILLIERS, C. L. 1999. Purification of intracellular compartments involved in antigen processing: a new method based on magnetic sorting. *Biochem. J.,* 338 (Pt 1), 123-30.

PETERSON, D. M., STATHOPOULOS, N. A., GIORGIO, T. D., HELLUMS, J. D. & MOAKE, J. L. 1987. Shear-induced platelet aggregation requires von Willebrand factor and platelet membrane glycoproteins Ib and IIb-IIIa. *Blood,* 69, 625-8.

PINAUD, F., KING, D., MOORE, H. P. & WEISS, S. 2004. Bioactivation and cell targeting of semiconductor CdSe/ZnS nanocrystals with phytochelatin-related peptides. *J Am Chem Soc,* 126, 6115-23.

PLOW, E. F. & MA, Y.-Q. 2007. Inside-out, outside-in: what's the difference? *Blood,* 109, 3128-3129.

POHL, U., HOLTZ, J., BUSSE, R. & BASSENGE, E. 1986. Crucial role of endothelium in the vasodilator response to increased flow in vivo. *Hypertension,* 8, 37-44.

PRICE, C. J. & BRINDLE, N. P. 2000. Vasodilator-stimulated phosphoprotein is involved in stress-fiber and membrane ruffle formation in endothelial cells. *Arterioscler Thromb Vasc Biol,* 20, 2051-6.

PRIES, A. R., SECOMB, T. W. & GAEHTGENS, P. 1995. Design principles of vascular beds. *Circ Res,* 77, 1017-23.

PROUD, D. 2008. The pulmonary epithelium in health and disease.

QHOBOSHEANE, M., SANTRA, S., ZHANG, P. & TAN, W. 2001. Biochemically functionalized silica nanoparticles. *Analyst,* 126, 1274-8.

QHOBOSHEANE, M., ZHANG, P. & TAN, W. 2004. Assembly of silica nanoparticles for two-dimensional nanomaterials. *J Nanosci Nanotechnol,* 4, 635-40.

QU, B., CHU, X., SHEN, G. & YU, R. 2008. A novel electrochemical immunosensor based on colabeled silica nanoparticles for determination of total prostate specific antigen in human serum. *Talanta,* 76, 785-90.

RABILLOUD, T. 2002. Two-dimensional gel electrophoresis in proteomics: old, old fashioned, but it still climbs up the mountains. *Proteomics,* 2, 3-10.

RABINOVITCH, M. 1995. Professional and non-professional phagocytes: an introduction. *Trends Cell Biol,* 5, 85-7.

RACUCIU, M., CREANGA, D. E. & AIRINEI, A. 2006. Citric-acid-coated magnetite nanoparticles for biological applications. *Eur Phys J E Soft Matter,* 21, 117-21.

RADMACHER, M., TILLAMNN, R. W., FRITZ, M. & GAUB, H. E. 1992. From molecules to cells: imaging soft samples with the atomic force microscope. *Science,* 257, 1900-5.

RADOMSKI, A., JURASZ, P., ALONSO-ESCOLANO, D., DREWS, M., MORANDI, M., MALINSKI, T. & RADOMSKI, M. W. 2005. Nanoparticle-induced platelet aggregation and vascular thrombosis. *Br J Pharmacol,* 146, 882-93.

RADOMSKI, A., JURASZ, P., SANDERS, E. J., OVERALL, C. M., BIGG, H. F., EDWARDS, D. R. & RADOMSKI, M. W. 2002. Identification, regulation and role of tissue inhibitor of metalloproteinases-4 (TIMP-4) in human platelets. *Br J Pharmacol,* 137, 1330-8.

RADOMSKI, A., STEWART, M. W., JURASZ, P. & RADOMSKI, M. W. 2001. Pharmacological characteristics of solid-phase von Willebrand factor in human platelets. *Br J Pharmacol,* 134, 1013-20.

RADOMSKI, M. & MONCADA, S. 1983. An improved method for washing of human platelets with prostacyclin. *Thromb Res,* 30, 383-9.

RENEMAN, R. S., ARTS, T. & HOEKS, A. P. 2006. Wall shear stress--an important determinant of endothelial cell function and structure--in the arterial system in vivo. Discrepancies with theory. *J Vasc Res,* 43, 251-69.

RENEMAN, R. S. & HOEKS, A. P. 2008. Wall shear stress as measured in vivo: consequences for the design of the arterial system. *Med Biol Eng Comput,* 46, 499-507.

RESCH-GENGER, U., GRABOLLE, M., CAVALIERE-JARICOT, S., NITSCHKE, R. & NANN, T. 2008. Quantum dots versus organic dyes as fluorescent labels. *Nat Methods,* 5, 763-75.

RESNICK, N., COLLINS, T., ATKINSON, W., BONTHRON, D. T., DEWEY, C. F., JR. & GIMBRONE, M. A., JR. 1993. Platelet-derived growth factor B chain promoter contains a cis-acting fluid shear-stress-responsive element. *Proc Natl Acad Sci U S A,* 90, 4591-5.

ROBERT, A., FREITAS, JR. 1999. Nanomedicine, Volume 1: Basic capabilities.

ROSAS-HERNÁNDEZ, H., JIMÉNEZ-BADILLO, S., MARTÍNEZ-CUEVAS, P. P., GRACIA-ESPINO, E., TERRONES, H., TERRONES, M., HUSSAIN, S. M., ALI, S. F. & GONZÁLEZ, C. 2009. Effects of 45-nm silver nanoparticles on coronary endothelial cells and isolated rat aortic rings. *Toxicology Letters,* 191, 305-313.

ROSENTHAL, S. J., CHANG, J. C., KOVTUN, O., MCBRIDE, J. R. & TOMLINSON, I. D. 2011. Biocompatible Quantum Dots for Biological Applications. *J chembiol,* 18, 10-24.

ROSENTHAL, S. J., TOMLINSON, I., ADKINS, E. M., SCHROETER, S., ADAMS, S., SWAFFORD, L., MCBRIDE, J., WANG, Y., DEFELICE, L. J. & BLAKELY, R.

D. 2002. Targeting cell surface receptors with ligand-conjugated nanocrystals. *J Am Chem Soc,* 124, 4586-94.

ROSS, R. 1993. The pathogenesis of atherosclerosis: a perspective for the 1990s. *Nature,* 362, 801-9.

RUBANYI, G. M., ROMERO, J. C. & VANHOUTTE, P. M. 1986. Flow-induced release of endothelium-derived relaxing factor. *Am J Physiol,* 250, H1145-9.

RYMAN-RASMUSSEN, J. P., RIVIERE, J. E. & MONTEIRO-RIVIERE, N. A. 2007. Surface coatings determine cytotoxicity and irritation potential of quantum dot nanoparticles in epidermal keratinocytes. *J Invest Dermatol,* 127, 143-53.

SADLER, J. E. 1998. Biochemistry and genetics of von Willebrand factor. *Annu Rev Biochem,* 67, 395-424.

SAHLI, H., TAPON-BRETAUDIERE, J., FISCHER, A. M., STERNBERG, C., SPENLEHAUER, G., VERRECCHIA, T. & LABARRE, D. 1997. Interactions of poly(lactic acid) and poly(lactic acid-co-ethylene oxide) nanoparticles with the plasma factors of the coagulation system. *Biomaterials,* 18, 281-8.

SAINI, S., EDELMAN, R. R., SHARMA, P., LI, W., MAYO-SMITH, W., SLATER, G. J., EISENBERG, P. J. & HAHN, P. F. 1995. Blood-pool MR contrast material for detection and characterization of focal hepatic lesions: initial clinical experience with ultrasmall superparamagnetic iron oxide (AMI-227). *Am J Roentgenol,* 164, 1147-52.

SAJJA, H. K., EAST, M. P., MAO, H., WANG, Y. A., NIE, S. & YANG, L. 2009. Development of multifunctional nanoparticles for targeted drug delivery and noninvasive imaging of therapeutic effect. *Curr Drug Discov Technol,* 6, 43-51.

SAKARIASSEN, K. S., NIEVELSTEIN, P. F., COLLER, B. S. & SIXMA, J. J. 1986. The role of platelet membrane glycoproteins Ib and IIb-IIIa in platelet adherence to human artery subendothelium. *Br J Haematol,* 63, 681-91.

SALVADOR-MORALES, C., FLAHAUT, E., SIM, E., SLOAN, J., GREEN, M. L. & SIM, R. B. 2006. Complement activation and protein adsorption by carbon nanotubes. *Mol Immunol,* 43, 193-201.

SALVI, S., BLOMBERG, A., RUDELL, B., KELLY, F., SANDSTROM, T., HOLGATE, S. T. & FREW, A. 1999. Acute inflammatory responses in the airways and peripheral blood after short-term exposure to diesel exhaust in healthy human volunteers. *Am J Respir Crit Care Med,* 159, 702-9.

SAMIA, A. C., CHEN, X. & BURDA, C. 2003. Semiconductor quantum dots for photodynamic therapy. *J Am Chem Soc,* 125, 15736-7.

SAMIJO, S. K., WILLIGERS, J. M., BARKHUYSEN, R., KITSLAAR, P. J., RENEMAN, R. S., BRANDS, P. J. & HOEKS, A. P. 1998. Wall shear stress in the human common carotid artery as function of age and gender. *Cardiovasc Res,* 39, 515-22.

SANHAI, W. R., SAKAMOTO, J. H., CANADY, R. & FERRARI, M. 2008. Seven challenges for nanomedicine. *Nat Nanotechnol,* 3, 242-4.

SANTRA, S., WANG, K., TAPEC, R. & TAN, W. 2001a. Development of novel dye-doped silica nanoparticles for biomarker application. *J Biomed Opt,* 6, 160-6.

SANTRA, S., ZHANG, P., WANG, K., TAPEC, R. & TAN, W. 2001b. Conjugation of biomolecules with luminophore-doped silica nanoparticles for photostable biomarkers. *Anal Chem,* 73, 4988-93.

SARIN, H. 2010. Physiologic upper limits of pore size of different blood capillary types and another perspective on the dual pore theory of microvascular permeability. *Journal of Angiogenesis Research,* 2, 14.

SATHULURI, R. R., YOSHIKAWA, H., SHIMIZU, E., SAITO, M. & TAMIYA, E. 2011. Gold Nanoparticle-Based Surface-Enhanced Raman Scattering for Noninvasive Molecular Probing of Embryonic Stem Cell Differentiation. *PLoS One,* 6, e22802.

SATO, M., LEVESQUE, M. J. & NEREM, R. M. 1987. Micropipette aspiration of cultured bovine aortic endothelial cells exposed to shear stress. *Arteriosclerosis,* 7, 276-86.

SAWICKI, G., SALAS, E., MURAT, J., MISZTA-LANE, H. & RADOMSKI, M. W. 1997. Release of gelatinase A during platelet activation mediates aggregation. *Nature,* 386, 616-9.

SAWICKI, G., SANDERS, E. J., SALAS, E., WOZNIAK, M., RODRIGO, J. & RADOMSKI, M. W. 1998. Localization and translocation of MMP-2 during aggregation of human platelets. *Thromb Haemost,* 80, 836-9.

SCHLEEF, R. R., BEVILACQUA, M. P., SAWDEY, M., GIMBRONE, M. A., JR. & LOSKUTOFF, D. J. 1988. Cytokine activation of vascular endothelium. Effects on tissue-type plasminogen activator and type 1 plasminogen activator inhibitor. *J Biol Chem,* 263, 5797-803.

SCHMIDT-TRUCKSASS, A., SCHMID, A., BRUNNER, C., SCHERER, N., ZACH, G., KEUL, J. & HUONKER, M. 2000. Arterial properties of the carotid and femoral artery in endurance-trained and paraplegic subjects. *J Appl Physiol,* 89, 1956-63.

SCHREYER, S. A., PESCHON, J. J. & LEBOEUF, R. C. 1996. Accelerated atherosclerosis in mice lacking tumor necrosis factor receptor p55. *J Biol Chem,* 271, 26174-8.

SCHWENKE, D. C. & CAREW, T. E. 1988. Quantification in vivo of increased LDL content and rate of LDL degradation in normal rabbit aorta occurring at sites susceptible to early atherosclerotic lesions. *Circ Res,* 62, 699-710.

SEATON, A., SOUTAR, A., CRAWFORD, V., ELTON, R., MCNERLAN, S., CHERRIE, J., WATT, M., AGIUS, R. & STOUT, R. 1999. Particulate air pollution and the blood. *Thorax,* 54, 1027-32.

SEGAT, D., TAVANO, R., DONINI, M., SELVESTREL, F., RIO-ECHEVARRIA, I., ROJNIK, M., KOCBEK, P., KOS, J., IRATNI, S., SHEGLMANN, D., MANCIN, F., DUSI, S. & PAPINI, E. 2011. Proinflammatory effects of bare and PEGylated ORMOSIL-, PLGA- and SUV-NPs on monocytes and PMNs and their modulation by f-MLP. *Nanomedicine (Lond),* 6, 1027-46.

SESSA, W. C., HARRISON, J. K., BARBER, C. M., ZENG, D., DURIEUX, M. E., D'ANGELO, D. D., LYNCH, K. R. & PEACH, M. J. 1992. Molecular cloning and expression of a cDNA encoding endothelial cell nitric oxide synthase. *J Biol Chem,* 267, 15274-6.

SHAREFKIN, J. B., DIAMOND, S. L., ESKIN, S. G., MCINTIRE, L. V. & DIEFFENBACH, C. W. 1991. Fluid flow decreases preproendothelin mRNA levels and suppresses endothelin-1 peptide release in cultured human endothelial cells. *J Vasc Surg,* 14, 1-9.

SHEN, J., LUSCINSKAS, F. W., CONNOLLY, A., DEWEY, C. F., JR. & GIMBRONE, M. A., JR. 1992. Fluid shear stress modulates cytosolic free calcium in vascular endothelial cells. *Am J Physiol,* 262, C384-90.

SHEU, J. R., FONG, T. H., LIU, C. M., SHEN, M. Y., CHEN, T. L., CHANG, Y., LU, M. S. & HSIAO, G. 2004. Expression of matrix metalloproteinase-9 in human platelets: regulation of platelet activation in in vitro and in vivo studies. *Br J Pharmacol,* 143, 193-201.

SHIMIZU, K., ITO, A., ARINOBE, M., MURASE, Y., IWATA, Y., NARITA, Y., KAGAMI, H., UEDA, M. & HONDA, H. 2007. Effective cell-seeding technique using magnetite nanoparticles and magnetic force onto decellularized blood vessels for vascular tissue engineering. *J Biosci Bioeng,* 103, 472-8.

SHRIVASTAVA, S., BERA, T., SINGH, S. K., SINGH, G., RAMACHANDRARAO, P. & DASH, D. 2009. Characterization of antiplatelet properties of silver nanoparticles. *ACS Nano,* 3, 1357-64.

SIMBERG, D., PARK, J. H., KARMALI, P. P., ZHANG, W. M., MERKULOV, S., MCCRAE, K., BHATIA, S. N., SAILOR, M. & RUOSLAHTI, E. 2009. Differential proteomics analysis of the surface heterogeneity of dextran iron oxide nanoparticles and the implications for their in vivo clearance. *Biomaterials,* 30, 3926-33.

SIMNICK, A. J., AMIRAM, M., LIU, W., HANNA, G., DEWHIRST, M. W., KONTOS, C. D. & CHILKOTI, A. 2011. In vivo tumor targeting by a NGR-decorated micelle of a recombinant diblock copolypeptide. *J Cont Rel,* 155, 144-151.

SIMON, A. C., FLAUD, P. & LEVENSON, J. 1990. Non-invasive evaluation of segmental pressure drop and resistance in large arteries in humans based on a Poiseuille model of intra-arterial velocity distribution. *Cardiovasc Res,* 24, 623-6.

SIMOVIC, S., HUI, H., SONG, Y., DAVEY, A. K., RADES, T. & PRESTIDGE, C. A. 2010. An oral delivery system for indomethicin engineered from cationic lipid emulsions and silica nanoparticles. *J Control Release,* 143, 367-73.

SIXMA, J. J., SAKARIASSEN, K. S., BEESER-VISSER, N. H., OTTENHOF-ROVERS, M. & BOLHUIS, P. A. 1984. Adhesion of platelets to human artery subendothelium: effect of factor VIII-von Willebrand factor of various multimeric composition. *Blood,* 63, 128-39.

SLOWING, II, VIVERO-ESCOTO, J. L., WU, C. W. & LIN, V. S. 2008. Mesoporous silica nanoparticles as controlled release drug delivery and gene transfection carriers. *Adv Drug Deliv Rev,* 60, 1278-88.

SLUPSKY, J. R., KALBAS, M., WILLUWEIT, A., HENN, V., KROCZEK, R. A. & MULLER-BERGHAUS, G. 1998. Activated platelets induce tissue factor expression on human umbilical vein endothelial cells by ligation of CD40. *Thromb Haemost,* 80, 1008-14.

SMITH, A. M., DUAN, H., MOHS, A. M. & NIE, S. 2008. Bioconjugated quantum dots for in vivo molecular and cellular imaging. *Adv Drug Deliv Rev,* 60, 1226-40.

SMITH, A. M., RUAN, G., RHYNER, M. N. & NIE, S. 2006. Engineering luminescent quantum dots for in vivo molecular and cellular imaging. *Ann Biomed Eng,* 34, 3-14.

SO, M. K., XU, C., LOENING, A. M., GAMBHIR, S. S. & RAO, J. 2006. Self-illuminating quantum dot conjugates for in vivo imaging. *Nat Biotechnol,* 24, 339-43.

SPRAGUE, E. A., STEINBACH, B. L., NEREM, R. M. & SCHWARTZ, C. J. 1987. Influence of a laminar steady-state fluid-imposed wall shear stress on the binding,

internalization, and degradation of low-density lipoproteins by cultured arterial endothelium. *Circulation,* 76, 648-56.

STAMLER, J., MENDELSOHN, M. E., AMARANTE, P., SMICK, D., ANDON, N., DAVIES, P. F., COOKE, J. P. & LOSCALZO, J. 1989. N-acetylcysteine potentiates platelet inhibition by endothelium-derived relaxing factor. *Circ Res,* 65, 789-95.

STEINIGER, S. C., KREUTER, J., KHALANSKY, A. S., SKIDAN, I. N., BOBRUSKIN, A. I., SMIRNOVA, Z. S., SEVERIN, S. E., UHL, R., KOCK, M., GEIGER, K. D. & GELPERINA, S. E. 2004. Chemotherapy of glioblastoma in rats using doxorubicin-loaded nanoparticles. *Int J Cancer,* 109, 759-67.

STEL, H. V., SAKARIASSEN, K. S., DE GROOT, P. G., VAN MOURIK, J. A. & SIXMA, J. J. 1985. Von Willebrand factor in the vessel wall mediates platelet adherence. *Blood,* 65, 85-90.

STENBECK, G. & HORTON, M. A. 2004. Endocytic trafficking in actively resorbing osteoclasts. *J Cell Sci,* 117, 827-36.

STERN, S. T. & MCNEIL, S. E. 2008. Nanotechnology Safety Concerns Revisited. *Toxicol Sci,* 101, 4-21.

STERN, S. T., ZOLNIK, B. S., MCLELAND, C. B., CLOGSTON, J., ZHENG, J. & MCNEIL, S. E. 2008. Induction of autophagy in porcine kidney cells by quantum dots: a common cellular response to nanomaterials? *Toxicol Sci,* 106, 140-52.

STEVENS, K. N., CRESPO-BIEL, O., VAN DEN BOSCH, E. E., DIAS, A. A., KNETSCH, M. L., ALDENHOFF, Y. B., VAN DER VEEN, F. H., MAESSEN, J. G., STOBBERINGH, E. E. & KOOLE, L. H. 2009a. The relationship between the antimicrobial effect of catheter coatings containing silver nanoparticles and the coagulation of contacting blood. *Biomaterials,* 30, 3682-90.

STEVENS, K. N., KNETSCH, M. L., SEN, A., SAMBHY, V. & KOOLE, L. H. 2009b. Disruption and Activation of Blood Platelets in Contact with an Antimicrobial Composite Coating Consisting of a Pyridinium Polymer and AgBr Nanoparticles. *ACS Appl Mater Interfaces,* 1, 2049-2054.

STEVENS, K. N. J., CRESPO-BIEL, O., VAN DEN BOSCH, E. E. M., DIAS, A. A., KNETSCH, M. L. W., ALDENHOFF, Y. B. J., VAN DER VEEN, F. H., MAESSEN, J. G., STOBBERINGH, E. E. & KOOLE, L. H. 2009c. The relationship between the antimicrobial effect of catheter coatings containing silver nanoparticles and the coagulation of contacting blood. *Biomaterials,* 30, 3682-3690.

STROEV, P. V., HOSKINS, P. R. & EASSON, W. J. 2007. Distribution of wall shear rate throughout the arterial tree: A case study. *Atherosclerosis,* 191, 276-280.

STRONY, J., BEAUDOIN, A., BRANDS, D. & ADELMAN, B. 1993. Analysis of shear stress and hemodynamic factors in a model of coronary artery stenosis and thrombosis. *Am J Physiol,* 265, H1787-96.

STRONY, J., PHILLIPS, M., BRANDS, D., MOAKE, J. & ADELMAN, B. 1990. Aurintricarboxylic acid in a canine model of coronary artery thrombosis. *Circulation,* 81, 1106-14.

SUKHANOVA, A., SUSHA, A. S., BEK, A., MAYILO, S., ROGACH, A. L., FELDMANN, J., OLEINIKOV, V., REVEIL, B., DONVITO, B., COHEN, J. H. & NABIEV, I. 2007. Nanocrystal-encoded fluorescent microbeads for proteomics: antibody profiling and diagnostics of autoimmune diseases. *Nano Lett,* 7, 2322-7.

SUN, D. H., TRINDADE, M. C., NAKASHIMA, Y., MALONEY, W. J., GOODMAN, S. B., SCHURMAN, D. J. & SMITH, R. L. 2003. Human serum opsonization of orthopedic biomaterial particles: protein-binding and monocyte/macrophage activation in vitro. *J Biomed Mater Res A,* 65, 290-8.

SUWA, T., HOGG, J. C., QUINLAN, K. B., OHGAMI, A., VINCENT, R. & VAN EEDEN, S. F. 2002. Particulate air pollution induces progression of atherosclerosis. *J Am Coll Cardiol,* 39, 935-42.

SWANSON, J. A. & WATTS, C. 1995. Macropinocytosis. *Trends Cell Biol,* 5, 424-8.

TAKADA, Y., SHINKAI, F., KONDO, S., YAMAMOTO, S., TSUBOI, H., KORENAGA, R. & ANDO, J. 1994. Fluid shear stress increases the expression of thrombomodulin by cultured human endothelial cells. *Biochem Biophys Res Commun,* 205, 1345-52.

TALLURY, P., PAYTON, K. & SANTRA, S. 2008. Silica-based multimodal/multifunctional nanoparticles for bioimaging and biosensing applications. *Nanomedicine (Lond),* 3, 579-92.

TAN, A., YILDIRIMER, L., RAJADAS, J., DE LA PENA, H., PASTORIN, G. & SEIFALIAN, A. 2011. Quantum dots and carbon nanotubes in oncology: a review on emerging theranostic applications in nanomedicine. *Nanomedicine (Lond),* 6, 1101-14.

TAN, W., WANG, K., HE, X., ZHAO, X. J., DRAKE, T., WANG, L. & BAGWE, R. P. 2004. Bionanotechnology based on silica nanoparticles. *Med Res Rev,* 24, 621-38.

TANGELDER, G. J., SLAAF, D. W., ARTS, T. & RENEMAN, R. S. 1988. Wall shear rate in arterioles in vivo: least estimates from platelet velocity profiles. *Am J Physiol,* 254, H1059-64.

TAPEC, R., ZHAO, X. J. & TAN, W. 2002. Development of organic dye-doped silica nanoparticles for bioanalysis and biosensors. *J Nanosci Nanotechnol,* 2, 405-9.

TEDESCO, F., FISCHETTI, F., PAUSA, M., DOBRINA, A., SIM, R. B. & DAHA, M. R. 1999. Complement-endothelial cell interactions: pathophysiological implications. *Mol Immunol,* 36, 261-8.

TEDGUI, A. & MALLAT, Z. 2006. Cytokines in Atherosclerosis: Pathogenic and Regulatory Pathways. *Physiol Rev,* 86, 515-581.

TRAUB, O. & BERK, B. C. 1998. Laminar Shear Stress : Mechanisms by Which Endothelial Cells Transduce an Atheroprotective Force. *Arterioscler Thromb Vasc Biol,* 18, 677-685.

TSAI-MU, C. & ET AL. 2011. Human haptoglobin phenotypes and concentration determination by nanogold-enhanced electrochemical impedance spectroscopy. *Nanotechnology,* 22, 245105.

TSUNEDA, S., AIKAWA, H., HAYASHI, H., YUASA, A. & HIRATA, A. 2003. Extracellular polymeric substances responsible for bacterial adhesion onto solid surface. *FEMS Microbiol Lett,* 223, 287-92.

UNFRIED, K., SYDLIK, U., BIERHALS, K., WEISSENBERG, A. & ABEL, J. 2008. Carbon nanoparticle-induced lung epithelial cell proliferation is mediated by receptor-dependent Akt activation. *Am J Physiol Lung Cell Mol Physiol,* 294, L358-67.

VANHOUTTE, P. M. 1989. Endothelium and control of vascular function. State of the Art lecture. *Hypertension,* 13, 658-67.

VOGEL, S. M., MINSHALL, R. D., PILIPOVIC, M., TIRUPPATHI, C. & MALIK, A. B. 2001. Albumin uptake and transcytosis in endothelial cells in vivo induced by albumin-binding protein. *Am J Physiol Lung Cell Mol Physiol,* 281, L1512-22.

VOURA, E. B., JAISWAL, J. K., MATTOUSSI, H. & SIMON, S. M. 2004. Tracking metastatic tumor cell extravasation with quantum dot nanocrystals and fluorescence emission-scanning microscopy. *Nat Med,* 10, 993-8.

VROMAN, L., ADAMS, A. L., FISCHER, G. C. & MUNOZ, P. C. 1980. Interaction of high molecular weight kininogen, factor XII, and fibrinogen in plasma at interfaces. *Blood,* 55, 156-9.

WALCZYK, D., BOMBELLI, F. B., MONOPOLI, M. P., LYNCH, I. & DAWSON, K. A. 2010. What the cell "sees" in bionanoscience. *J Am Chem Soc,* 132, 5761-8.

WANG, N., BUTLER, J. P. & INGBER, D. E. 1993. Mechanotransduction across the cell surface and through the cytoskeleton. *Science,* 260, 1124-7.

WANG, Y.-X. J. 2011. Superparamagnetic iron oxide based MRI contrast agents: current status of clinical application. *Quant Imaging Med Surg,* 1, 35-40.

WANG, Z., TIRUPPATHI, C., MINSHALL, R. D. & MALIK, A. B. 2009. Size and Dynamics of Caveolae Studied Using Nanoparticles in Living Endothelial Cells. *ACS Nano,* 3, 4110-4116.

WECHEZAK, A. R., VIGGERS, R. F. & SAUVAGE, L. R. 1985. Fibronectin and F-actin redistribution in cultured endothelial cells exposed to shear stress. *Lab Invest,* 53, 639-47.

WEINBAUM, S. & CHIEN, S. 1993. Lipid transport aspects of atherogenesis. *J Biomech Eng,* 115, 602-10.

WEISS, H. J., BAUMGARTNER, H. R., TSCHOPP, T. B., TURITTO, V. T. & COHEN, D. 1978a. Correction by factor VIII of the impaired platelet adhesion to subendothelium in von Willebrand disease. *Blood,* 51, 267-79.

WEISS, H. J., ROGERS, J. & BRAND, H. 1973. Defective ristocetin-induced platelet aggregation in von Willebrand's disease and its correction by factor VIII. *J Clin Invest,* 52, 2697-707.

WEISS, H. J., TURITTO, V. T. & BAUMGARTNER, H. R. 1978b. Effect of shear rate on platelet interaction with subendothelium in citrated and native blood. I. Shear rate--dependent decrease of adhesion in von Willebrand's disease and the Bernard-Soulier syndrome. *J Lab Clin Med,* 92, 750-64.

WEISS, H. J., TURITTO, V. T. & BAUMGARTNER, H. R. 1986. Platelet adhesion and thrombus formation on subendothelium in platelets deficient in glycoproteins IIb-IIIa, Ib, and storage granules. *Blood,* 67, 322-30.

WEISSLEDER, R. 2001. A clearer vision for in vivo imaging. *Nat Biotechnol,* 19, 316-7.

WEISSLEDER, R. 2002. Scaling down imaging: molecular mapping of cancer in mice. *Nat Rev Cancer,* 2, 11-8.

WEISSLEDER, R., ELIZONDO, G., WITTENBERG, J., LEE, A. S., JOSEPHSON, L. & BRADY, T. J. 1990. Ultrasmall superparamagnetic iron oxide: an intravenous contrast agent for assessing lymph nodes with MR imaging. *Radiology,* 175, 494-8.

WEISSLEDER, R., TUNG, C. H., MAHMOOD, U. & BOGDANOV, A., JR. 1999. In vivo imaging of tumors with protease-activated near-infrared fluorescent probes. *Nat Biotechnol,* 17, 375-8.

WENG, J. & REN, J. 2006. Luminescent quantum dots: a very attractive and promising tool in biomedicine. *Curr Med Chem,* 13, 897-909.

WESTPHAL, M., HILT, D. C., BORTEY, E., DELAVAULT, P., OLIVARES, R., WARNKE, P. C., WHITTLE, I. R., JAASKELAINEN, J. & RAM, Z. 2003. A phase 3 trial of local chemotherapy with biodegradable carmustine (BCNU) wafers (Gliadel wafers) in patients with primary malignant glioma. *Neuro Oncol,* 5, 79-88.

WHITE, J. G. & BURRIS, S. M. 1984. Morphometry of platelet internal contraction. *Am J Pathol,* 115, 412-7.

WIKLUND, O., CAREW, T. E. & STEINBERG, D. 1985. Role of the low density lipoprotein receptor in penetration of low density lipoprotein into rabbit aortic wall. *Arteriosclerosis,* 5, 135-41.

WILLIAMS, Y., SUKHANOVA, A., NOWOSTAWSKA, M., DAVIES, A. M., MITCHELL, S., OLEINIKOV, V., GUN'KO, Y., NABIEV, I., KELLEHER, D. & VOLKOV, Y. 2009. Probing cell-type-specific intracellular nanoscale barriers using size-tuned quantum dots. *Small,* 5, 2581-8.

WINTER, P. M., MORAWSKI, A. M., CARUTHERS, S. D., FUHRHOP, R. W., ZHANG, H., WILLIAMS, T. A., ALLEN, J. S., LACY, E. K., ROBERTSON, J. D., LANZA, G. M. & WICKLINE, S. A. 2003. Molecular Imaging of Angiogenesis in Early-Stage Atherosclerosis With {alpha}v{beta}3-Integrin-Targeted Nanoparticles. *Circulation,* 108, 2270-2274.

WIWANITKIT, V., SEREEMASPUN, A. & ROJANATHANES, R. 2009. Gold nanoparticles and a microscopic view of platelets: a preliminary observation. *Cardiovasc J Afr,* 20, 141-2.

WONG, A. J., POLLARD, T. D. & HERMAN, I. M. 1983. Actin filament stress fibers in vascular endothelial cells in vivo. *Science,* 219, 867-9.

WORLE-KNIRSCH, J. M., PULSKAMP, K. & KRUG, H. F. 2006. Oops they did it again! Carbon nanotubes hoax scientists in viability assays. *Nano Lett,* 6, 1261-8.

WU, P., HE, X., WANG, K., TAN, W., MA, D., YANG, W. & HE, C. 2008a. Imaging breast cancer cells and tissues using peptide-labeled fluorescent silica nanoparticles. *J Nanosci Nanotechnol,* 8, 2483-7.

WU, P. C., SU, C. H., CHENG, F. Y., WENG, J. C., CHEN, J. H., TSAI, T. L., YEH, C. S., SU, W. C., HWU, J. R., TZENG, Y. & SHIEH, D. B. 2008b. Modularly assembled magnetite nanoparticles enhance in vivo targeting for magnetic resonance cancer imaging. *Bioconjug Chem,* 19, 1972-9.

WU, S. P., RINGGAARD, S., OYRE, S., HANSEN, M. S., RASMUS, S. & PEDERSEN, E. M. 2004. Wall shear rates differ between the normal carotid, femoral, and brachial arteries: An in vivo MRI study. *JMRI,* 19, 188-193.

WU, X., LIU, H., LIU, J., HALEY, K. N., TREADWAY, J. A., LARSON, J. P., GE, N., PEALE, F. & BRUCHEZ, M. P. 2003. Immunofluorescent labeling of cancer marker Her2 and other cellular targets with semiconductor quantum dots. *Nat Biotechnol,* 21, 41-6.

WU, X., TAN, Y., MAO, H. & ZHANG, M. 2010. Toxic effects of iron oxide nanoparticles on human umbilical vein endothelial cells. *Int J Nanomedicine,* 5, 385-99.

XIANG, S. D., SCHOLZEN, A., MINIGO, G., DAVID, C., APOSTOLOPOULOS, V, MOTTRAM, P. L. & PLEBANSKI, M. 2006. Pathogen recognition and development of particulate vaccines: does size matter? *Methods,* 40, 1-9.

XIE, J., HUANG, J., LI, X., SUN, S. & CHEN, X. 2009. Iron oxide nanoparticle platform for biomedical applications. *Curr Med Chem,* 16, 1278-94.

XIE, M., LIU, H. H., CHEN, P., ZHANG, Z. L., WANG, X. H., XIE, Z. X., DU, Y. M., PAN, B. Q. & PANG, D. W. 2005. CdSe/ZnS-labeled carboxymethyl chitosan as a bioprobe for live cell imaging. *Chem Commun (Camb)*, 5518-20.

YAMAMOTO, K., TAKAHASHI, T., ASAHARA, T., OHURA, N., SOKABE, T., KAMIYA, A. & ANDO, J. 2003. Proliferation, differentiation, and tube formation by endothelial progenitor cells in response to shear stress. *J Appl Physiol,* 95, 2081-8.

YAMAWAKI, H. & IWAI, N. 2006a. Cytotoxicity of water-soluble fullerene in vascular endothelial cells. *Am J Physiol Cell Physiol,* 290, C1495-502.

YAMAWAKI, H. & IWAI, N. 2006b. Mechanisms underlying nano-sized air-pollution-mediated progression of atherosclerosis: carbon black causes cytotoxic injury/inflammation and inhibits cell growth in vascular endothelial cells. *Circ J,* 70, 129-40.

YAN, M., ZHANG, Y., XU, K., FU, T., QIN, H. & ZHENG, X. 2011. An in vitro study of vascular endothelial toxicity of CdTe quantum dots. *Toxicology,* 282, 94-103.

YANG, D., YANG, F., HU, J., LONG, J., WANG, C., FU, D. & NI, Q. 2009. Hydrophilic multi-walled carbon nanotubes decorated with magnetite nanoparticles as lymphatic targeted drug delivery vehicles. *Chem Commun (Camb)*, 4447-9.

YANG, J., TAMM, L. K., TILLACK, T. W. & SHAO, Z. 1993. New approach for atomic force microscopy of membrane proteins. The imaging of cholera toxin. *J Mol Biol,* 229, 286-90.

YAO, S. N., WILSON, J. M., NABEL, E. G., KURACHI, S., HACHIYA, H. L. & KURACHI, K. 1991. Expression of human factor IX in rat capillary endothelial cells: toward somatic gene therapy for hemophilia B. *Proc Natl Acad Sci U S A,* 88, 8101-5.

YIN, Y. & ALIVISATOS, A. P. 2005. Colloidal nanocrystal synthesis and the organic-inorganic interface. *Nature,* 437, 664-70.

ZAMIR, M. 2000. Steady Flow in Tubes. *The Physics of Pulsatile Flow.* Springer New York.

ZHANG, L. W. & MONTEIRO-RIVIERE, N. A. 2009. Mechanisms of Quantum Dot Nanoparticle Cellular Uptake. *Toxicol Sci,* 110, 138-155.

ZHAO, W., WANG, L. & TAN, W. 2007. Fluorescent nanoparticle for bacteria and DNA detection. *Adv Exp Med Biol,* 620, 129-35.

ZHU, L., ANG, S. & LIU, W. T. 2004. Quantum dots as a novel immunofluorescent detection system for Cryptosporidium parvum and Giardia lamblia. *Appl Environ Microbiol,* 70, 597-8.

ZICHE, M. & MORBIDELLI, L. 2000. Nitric oxide and angiogenesis. *J Neurooncol,* 50, 139-48.

ZIMMERMAN, G. A., MCINTYRE, T. M., MEHRA, M. & PRESCOTT, S. M. 1990. Endothelial cell-associated platelet-activating factor: a novel mechanism for signaling intercellular adhesion. *J Cell Biol,* 110, 529-40.

ZRAZHEVSKIY, P., SENA, M. & GAO, X. 2010. Designing multifunctional quantum dots for bioimaging, detection, and drug delivery. *Chem Soc Rev,* 39, 4326-4354.

Appendix 1
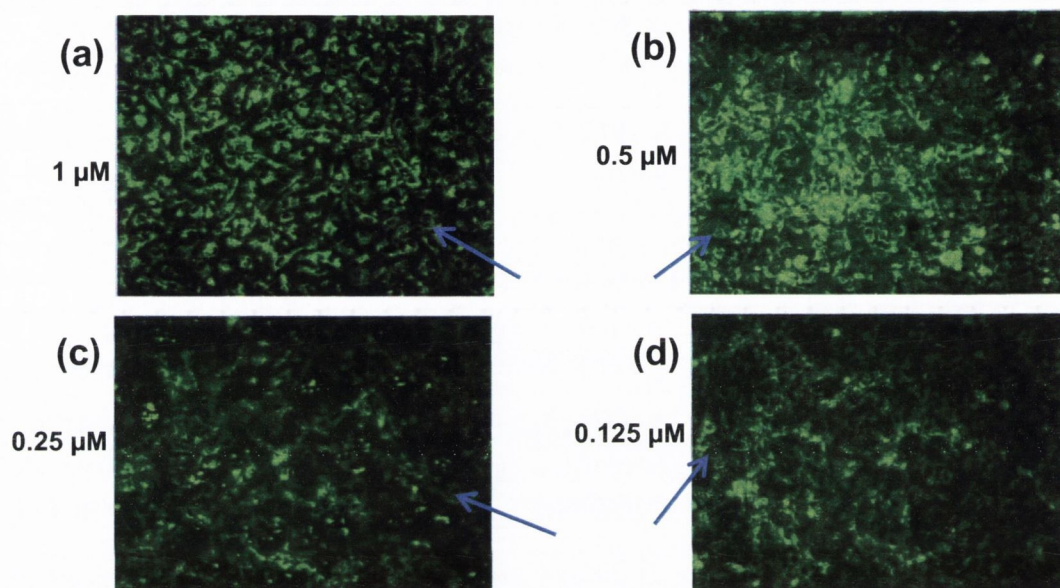
Optimization of DiOC6 staining: HUVEC were grown on gelatin coated acrylic substrates. An optically transparent PDMS chip (containing a semi channel) is applied over the cells to create a complete microchannel. Whole blood pre-treated with a live membrane stain, DiOC6 at 1 µM (a), 0.5 µM (b), 0.25 µM (c), or 0.125 µM (d) was run over the inflammed (TNF-α) endothelial cells through the artificially created microchannels. The cells were imaged using fluorescence microscope. Images are representative of three independent experiments. Arrows indicate endothelial cells stained by DiOC6.

Appendix 2

Mascot score and peptide matched for proteins associated with negatively charged 2.7 nm CdTe QDs

S.No	Group	Protein name	Mascot score	Queries matched
	Immunoglobulins	*Band A*		
1		Ig G1 H Nie	262	9
2		gamma 3 immunoglobulin constant heavy chain	234	7
3		immunoglobulin heavy chain constant region	234	6
4		Ig lambda chain	106	8
5		immunoglobulin heavy chain variable region	104	4
6		Chain B, Fab Fragment Of Engineered Human Monoclonal Antibody A5b7	96	3
7		immunoglobulin heavy chain variable region	89	3
8		immunoglobulin heavy chain	80	3
9		Full=Ig heavy chain V-III region HIL	63	2
10		Ig A1 Bur	52	2
		Band B		
11		Ig A1 Bur	291	9
12		Full=Ig gamma-4 chain C region	243	7
13		immunoglobulin kappa heavy chain	241	8
14		immunoglobulin gamma heavy chain	238	8
15		immunoglobulin heavy chain constant region	210	8
16		Chain L, Hiv-1 Gp120 Core Complexed With Cd4 And A Neutralizing Human Antibody	137	2
17		anti-HIV-1 gp120 immunoglobulin 48d heavy chain	126	3
18		Ig kappa chain NIG93 precursor	113	2
19		Ig lambda chain precursor	112	3
20		immunoglobulin heavy chain variable region	110	4
21		protein NIG64 lambda,Bence-Jones	109	3
22		immunoglobulin heavy chain variable region	110	4
23		anti TNF-alpha antibody light-chain Fab fragment	101	2
24		immunoglobulin heavy chain variable region	98	3
25		immunoglobulin kappa light chain VLJ region	98	2
26		Chain B, X-Ray Structures Of The Antigen-Binding Domains From Three Variants Of Humanized Anti-P185	95	3
27		Chain H, Crystal Structure Of Fab' From The Hiv-1 Neutralizing Antibody 2f5	92	7
28		immunoglobulin lambda-3 surrogate light chain	72	3

29		Full=Ig kappa chain V-III region NG9; Flags: Precursor	61	1
30		immunoglobulin kappa light chain	61	1
31		immunoglobulin kappa chain variable region	61	1
32		IgE heavy chain	53	2
33		anti-tetanus toxoid immunoglobulin heavy chain variable region	47	2
34		Full=Ig heavy chain V-III region HIL	45	1
35		immunoglobulin heavy chain variable and joining regions	44	2
36		immunoglobulin kappa light chain variable region	39	2
		Band C		
37		immunoglobulin kappa light chain variable region	42	1
	Albumin			
		Band B		
38		serum albumin precursor	409	15
		Band C		
39		serum albumin	847	18
		Band D		
40		serum albumin		
	Cholesterol transport			
		Band B		
41		ABC3	35	2
		Band C		
42		proapolipoprotein	237	9
43		lipoprotein Gln I	187	8
44		apolipoprotein A-1 A175P variant	61	3
45		ABC A13	40	4
	Iron binding			
		Band C		
46		serotransferrin precursor	2529	55
47		Transferrin	2290	52
48		hemopexin precursor	263	7
49		Chain E, Structure Of Human Transferrin Receptor-Transferrin Complex	208	5
50		lactoferrin	48	2
	Hemostasis			
		Band A		
51		alpha-2-macroglobulin precursor	1229	32
52		fibrinogen alphaA	154	4
53		beta-fibrinogen precursor	136	3
54		alpha-fibrinogen precursor	120	4

55		fibrinogen gamma chain	103	3
		Band C		
56		heparin cofactor II precursor	44	1
	Kinase binding			
		Band C		
57		leucine-rich repeat kinase 2	53	4
58		citron Rho-interacting kinase	51	5
59		receptor-interacting serine/threonine-protein kinase 2	40	1
	Cytoskeleton			
		Band A		
60		supervillin	36	2
		Band C		
61		nesprin-1	48	8
62		plectin	38	5
	Peroxisome			
		Band A		
63		peroxisome biogenesis factor 1	39	4
		Band C		
64		peroxisome biogenesis factor 1	48	3
	Mitochondria			
		Band A		
65		S-AKAP84	50	2
66		ALR	49	4
		Band C		
67		S-AKAP84	3	1
	Complement system			
		Band B		
68		complement C3 precursor	796	28
69		complement C4B precursor	252	7
	Adhesion junction plaque			
		Band A		
70		bullous pemphigoid antigen 1 isoform 1eA precursor	42	4
71		dystonin	42	5
	Development and hemotopoiesis			
		Band A		
72		myeloid/lymphoid or mixed-lineage leukemia 2 variant	41	3
		Band C		
73		Gps1	39	1

	Vessel assembly regulation			
		Band C		
74		GTPase activating protein	40	1
75		extracellular glycoprotein EMILIN-2 precursor	37	2
	Hemoglobin binding			
		Band C		
76		haptoglobin isoform 1 preproprotein	955	21
	Copper binding			
		Band C		
77		ceruloplasmin	586	13
	No Known function			
		Band B		
78		IGH@ protein	246	8
	Lymphocyte signalling			
		Band A		
79		Chain A, Crystal Structure Of The Tandem Phosphatase Domain Of Rptp Cd45	45	3
	Neurofilament associated			
		Band C		
80		heavy neurofilament subunit	95	3
	Kinesin motor associated			
		Band C		
81		kinesin superfamily protein KIF1B	37	3
	Zinc binding			
		Band C		
82		PHD finger protein 3	43	2
	Oncogene			
		Band C		
83		oncogene	48	2
	Tight Junction			
		Band C		
84		symplekin	40	2
	Cell biological process			
		Band C		
85		inter-alpha-trypsin inhibitor family heavy chain-related protein (IHRP)	48	2
	Acute phase protein			
		Band C		
86		Chain A, 2.0 Angstrom Structure Of Intact Alpha-1-Antitrypsin: A Canonical Template For Active Serp	39	1
	Transcription			

	associated protein	Band A		
87		transcription factor	35	1
		Band C		
88		ASH1	36	3

Appendix 3

Mascot score and peptide matched for proteins associated with negatively charged 4.9 nm CdTe QDs

S.No		Protein	Mascot score	Queries matched
	Immunoglobulins			
		Band H		
1		immunoglobulin lambda heavy chain	312	11
2		immunoglobulin kappa heavy chain	288	11
3		immunoglobulin gamma heavy chain	283	10
4		immunoglobulin heavy chain constant region	279	10
5		gamma 3 immunoglobulin constant heavy chain	256	10
6		IgG kappa chain	130	3
7		Ig A1 Bur	130	5
8		Chain L, Hiv-1 Gp120 Core Complexed With Cd4 And A Neutralizing Human Antibody	146	3
9		anti-HIV-1 gp120 immunoglobulin 48d heavy chain	126	3
10		immunoglobulin heavy chain variable region	118	3
11		Chain H, Crystal Structure Of Fab' From The Hiv-1 Neutralizing Antibody 2f5	116	4
12		immunoglobulin heavy chain	115	3
13		immunoglobulin heavy chain	106	4
14		Chain B, Fab Fragment Of Engineered Human Monoclonal Antibody A5b7	91	4
15		Ig lambda Sm L	60	2
16		immunoglobulin lambda light chain VLJ region	60	2
17		Full=Ig kappa chain V-III region NG9; Flags: Precursor	47	1
18		immunoglobulin kappa light chain	47	1
19		immunoglobulin kappa chain variable region	47	1
20		immunoglobulin kappa light chain variable region	47	1
		Band I		
21		IgG	417	12
22		anti-HBs antibody heavy chain	416	12
23		Ig A1 Bur	348	10
24		immunoglobulin heavy chain	341	10
25		immunoglobulin heavy chain	299	10
26		immunoglobulin heavy chain constant	292	11

		region		
27		IgG kappa chain	209	5
28		immunoglobulin kappa light chain VLJ region	207	5
29		Chain A, Crystal Structure Of The Fab Fragment Of A Human Monoclonal Igm Cold Agglutinin	201	5
30		Chain L, Hiv-1 Gp120 Core Complexed With Cd4 And A Neutralizing Human Antibody	200	5
31		immunoglobulin heavy chain, constant region	198	7
32		anti-HIV-1 gp120 immunoglobulin 48d heavy chain	151	3
33		Chain B, X-Ray Structures Of The Antigen-Binding Domains From Three Variants Of Humanized Anti-P185	135	3
34		immunoglobulin kappa light chain	134	3
35		anti-Entamoeba histolytica immunoglobulin gamma heavy chain	130	3
36		immunoglobulin heavy chain variable region	128	3
37		Chain H, Crystal Structure Analysis Of Anti-Hiv-1 Fab 447-52d In Complex With V3 Peptide	127	5
38		immunoglobulin heavy chain	122	3
39		immunoglobulin heavy chain variable region	120	3
40		Chain H, Crystal Structure Of Fab' From The Hiv-1 Neutralizing Antibody 2f5	120	4
41		immunoglobulin heavy chain variable region	120	4
42		Chain B, Fab Fragment Of Engineered Human Monoclonal Antibody A5b7	114	5
43		immunoglobulin heavy chain variable region	111	4
44		immunoglobulin heavy chain variable region	106	4
45		immunoglobulin light chain variable region	98	2
46		IgG heavy chain variable region	95	3
47		protein NIG64 lambda, Bence-Jones	91	4
48		Ig lambda chain precursor	81	4
49		protein NIG51 lambda, Bence-Jones	78	4
50		immunoglobulin lambda light chain VLJ region	75	4
51		Ig heavy chain V region - human	59	4
52		RecName: Full=Ig heavy chain V-III	56	2

		region HIL		
53		immunoglobulin light chain variable region	53	3
54		immunoglobulin light chain variable region	52	1
55		immunoglobulin lambda light chain variable region	40	2
56		IgE heavy chain	40	2
57		anti-tetanus toxoid immunoglobulin heavy chain variable region	39	2
58		immunoglobulin lambda light chain variable region	38	2
59		immunoglobulin heavy chain variable region	37	2
60		immunoglobulin heavy chain variable region	36	2
	Albumin			
		Band H		
61		serum albumin	497	14
		Band I		
62		serum albumin	614	19
		Band J		
63		serum albumin	791	19
		Band K		
64		serum albumin		
	Cholesterol transport			
		Band J		
65		proapolipoprotein	124	7
66		lipoprotein Gln I	124	7
	Iron binding			
		Band I		
67		hemopexin precursor	155	4
		Band J		
68		serotransferrin precursor	1886	46
69		Transferrin	1704	46
	Hemostasis			
		Band H		
70		alpha-2-macroglobulin precursor	1912	61
71		factor VII active site mutant immunoconjugate	169	8
		Band J		
72		Chain A, The Intact And Cleaved Human Antithrombin Iii Complex As A Model For Serpin-Proteinase Int	51	1

	Peroxisome			
		Band H		
73		Pex1pQ261Ter	42	2
		Band I		
74		Pex1pQ261Ter	37	2
	Complement system			
		Band H		
75		complement component C3	42	3
76		complement component C4B	36	1
		Band I		
77		complement component C3	108	3
78		complement factor B	56	2
	Mitochondria			
		Band J		
79		NADH:ubiquinone oxidoreductase 51-kD subunit	36	3
	Hemoglobin binding			
		Band J		
80		haptoglobin isoform 1 preproprotein	907	25
81		haptoglobin	858	24
	No known function			
		Band I		
82		IGH@ protein	422	12
83		FLJ00385 protein	273	10
	Copper binding			
		Band J		
84		ceruloplasmin	59	3
	Zinc binding			
		Band J		
85		KIAA0853 protein	43	2
	Cell biological process			
		Band H		
86		inter-alpha-trypsin inhibitor heavy chain ITIH1	63	1
		Band I		
87		trypsin inhibitor	139	4
88		inter-alpha-trypsin inhibitor heavy chain ITIH1	128	3

Appendices

Appendix 4

Acrylamide 30%

Acrylamide	30 g
N,N'methylenebisacrylamide	0.8 g

Add DH_2O up to 100 ml

*Filter 0.45 µm

Stacking Buffer (4x Tris HCl/SDS, pH 6.8)

Tris base	6.05 g
DH_2O	40 ml

Adjust to pH 6.8

Add DH_2O up to 100 ml

*Filter 0.45 µm

Add SDS 0.4 g

Store 4^0C

Resolving Buffer for Zymography (4x Tris HCl, pH 8.8)

Tris base	91 g
DH_2O	300 ml

Adjust to pH 8.8

Add DH_2O up to 500 ml

*Filter 0.45 µm

Store 4^0C

Tank Buffer (10x)

Tris base	30.2 g
Glycine	144 g
SDS	10 g
DH_2O	700 ml

Adjust pH to 8.3

Add DH_2O up to 1000 ml

232

2M Tris HCl pH 7.6 (for zymography buffer)

Tris base	242.28 g (2M)
DH_2O	500 ml
Adjust pH to 7.6	
Add DH_2O up to 1000 ml	

Zymography Buffer

2M Tris HCl	50 ml
NaCl	18 g
$CaCl_2$	1.47 g
NaN_3	1 g
Add DH_2O up to 2000 ml	

Staining Solution

Coomassie blue G-250	250 mg
Methanol	250 ml
Acetic acid	100 ml
DH_2O	650 ml

Distaining Solution

Methanol	40 ml
Acetic acid	80 ml
DH_2O	880 ml

Separating Gel for Zymography 8%	**(4 gels)**	**(2 gels)**
Acrylamide 30%	4 ml	2 ml
4x Tris pH 8.8 (resolving buffer)	3.75 ml	1.875 ml
Gelatin	1.5 ml	0.75 ml
DH_2O	5.75 ml	2.875 ml
Ammonium persulfate (APS) (0.1 g APS + 960 µl DH_2O)	50 µl	25 µl
TEMED	10 µl	5 µl

Appendices

Stacking Gel

Acrylamide 30%	650 µl
Stacking buffer	1250 µl
DH$_2$O	3000 µl
APS	25 µl
TEMED	5 µl

Sodium citrate 3.15%

Dissolve 15.75 g Sodium Citrate in 500 ml of ddH2O.
Filtrate (45um) and make 4 ml aliquots in 50 ml tubes
Freeze it

PGI2, prostacyclin

Prepare **Tris 1M**: pH 9
      Trizma base 40.3 g
      Tris HCl 26.4 g
      Dissolve in 500 ml of ddH2O, make 1 ml aliquots and freeze
      (-80C)

Add 1 ml 1M Tris, pH 9 to 1 mg PGI2 (1 vial) always on ice!!!
      Make 20ul aliquot and freeze (-80C)

Phosphate-Buffered saline PBS 1X

PBS tablets (Gibco)   5 g

Each 5 g tablet dissolved in 500 ml distilled water and sterilised by autoclaving.

Paraformaldehyde – fixation reagent (3%)

Paraformaldehyde	1.5 g
PBS	50 ml

While heating to dissolve paraformaldehyde we ensured not to exceed 56˚C, so as to avoid resulting reagent autofluorescence.

SDS-PAGE REAGENTS

Components of resolving gel solution for SDS-PAGE

Component	7% gel	8% gel	10 % gel	12 % gel
Distilled water	10.03 ml	9.37 ml	8.03 ml	6.7 ml
1.5 M Tris-HCl; pH 8.8	5 ml	5 ml	5 ml	5 ml
10 % w/v SDS	200 µl	200 µl	200 µl	200 µl
10 % w/v APS	200 µl	200 µl	200 µl	200 µl
TEMED	16 µl	11 µl	10 µl	10 µl
30 % Polyacrylamide	4.67 ml	5.33 ml	6.67 ml	8.0 ml
Total	**20 ml**	**20 ml**	**20 ml**	**20 ml**

Components of the stacking gel solution for SDS-PAGE

Component	5% gel
Distilled water	6.8 ml
1.5 M Tris-HCl; pH 8.8	1.25 ml
10 % w/v SDS	100 µl
10 % w/v APS	100 µl
TEMED	10 ml
30 % Polyacrylamide	1.7 ml
Total	**10 ml**

5X SDS-PAGE sample buffer (Laemmli sample buffer)

Tris-HCl (pH 6.8, stock solution 1M))	3.125 ml
SDS	1gm
Glycerol	5 ml
Bromophenol blue	1 mg

Add DH$_2$O up to 10 ml.

This solution was aliquoted into 1 ml and frozen at -20°C. β-mercaptoethanol was added fresh (50 μl/ 1ml of 5x sample buffer.

5x sample buffer was added to the protein sample to give a final concentration of 1X.

10X SDS-PAGE Running Buffer

Trizma base	30 g
Glycine	142 g
SDS	10 g

Dissolved in deionised water to final volume of 1 L.

Dilute 1:10 in deionised water before use.

Coomassie stain G-250 Fixation Solvent

Methanol	50 ml
Phosphoric acid (H$_3$PO$_4$; 85 % stock solution)	2 ml
Add DH$_2$O up to 100 ml	

Coomassie stain G-250 Incubation Solvent

Methanol	34 ml
Phosphoric acid (H$_3$PO$_4$; 85 % stock solution)	2 ml
Ammonium sulphate	17 ml
Add DH$_2$O up to 100 ml	

Coomassie stain solution

Coomassie R-250 was prepared by adding 0.25 g in a solution of 125 ml methanol, 100 ml dH$_2$O and 25 ml glacial acetic acid. Coomassie Blue G-250 was prepared by dissolving 0.25 g of powder in 20 ml of methanol and this was added to 1L incubation solvent buffer.

Coomassie Destain solution

Methanol	100 ml
Glacial Acetic Acid	100 ml
Distilled water	800 ml

10% Ammonium persulphate (APS)

APS	0.1 g
Deionised water	1.0 ml

Make up fresh before use.

A nanoscale resolution assay of flow-induced platelet microaggregation

Mikroagregacja płytek indukowana przepływem
– badanie w nanorozdzielczości

M.J. Santos-Martínez[1], C. Medina[1], A. Prina-Mello[2], J. Conroy[3], S.P. Samuels[3], Y. Volkov[2,3], M.W. Radomski[1,2]

[1]School of Pharmacy and Pharmaceutical Sciences, Panoz Institute, Trinity College Dublin, Dublin 2, Ireland
[2]Centre for Research on Adaptive Nanostructures and Nanodevices, Trinity College Dublin, Dublin 2, Ireland
[3]Department of Clinical Medicine, Institute of Molecular Medicine Trinity College Dublin, Dublin 8, Ireland

Redacted

E_4

E_4

E_4

Redacted

Redacted

v_{mean}

Redacted

Redacted

Redacted

Redacted

Redacted

Redacted

Redacted